Ultra High Performance Fibre Reinforced Concrete for Highway Bridge Applications

Thesis submitted in accordance with the requirements of the University of Liverpool for the degree of Doctor in Philosophy by

Aram Mohammad Tariq Hassan

June 2013

Acknowledgements

Firstly, I would like to express my sincere thanks and gratitude to my supervisor Dr S.W. Jones without his continued support and guidance this work would not be possible. I will always be in debt to Dr S.W. Jones for giving as much time needed for discussion and guidance. Sincere thanks are extended to Dr Z. Guan for his interest in this work and serving as second supervisor.

I would like to extend my thanks to Prof J. Bungey, Prof S. Millard, and Dr S. Barnett. Their advice and valuable time are greatly appreciated. Special thanks to all the technical staff in the Concrete Laboratory at the University of Liverpool and Queen's University Belfast.

This study was funded via an Engineering and Physical Science Research Council (EPSRC) grant. The financial support from EPSRC is gratefully acknowledged.

Finally, I would like to thank my family and friends, especially, my parents for their love, guidance and encouragement at all times.

Publications

Mahmud, G. H.Yang, Z. & **Hassan, A. M. T**. 2013. Experimental and Numerical Studies of Size Effects of Ultra High Performance Steel Fibre Reinforced Concrete (UHPFRC) Beams. Construction and Building Materials, 48**,** 1027-1034.

Hassan, A. M. T., & Jones, S. W. 2012. Non-destructive testing of ultra high performance fibre reinforced concrete (UHPFRC): A feasibility study for using ultrasonic and resonant frequency testing techniques. Construction and Building Materials, 35**,** 361-367.

Hassan, A. M. T., Jones, S. W. & Mahmud, G. H. 2012. Experimental test methods to determine the uniaxial tensile and compressive behaviour of ultra high performance fibre reinforced concrete (UHPFRC). Construction and Building Materials, 37**,** 874-882.

Mahmud, G., Yang, Z. & **Hassan, A.** 2012. An investigation on size effect for Ultra High Performance Steel Fibre Reinforced Concrete (UHPSFRC) Beams using Finite Element Method. The 20th Annual Conference on Computational Mechanics in Engineering. Manchester, UK. University of Manchester, 47-50.

Hassan. A., Ultra high performance fibre reinforced concrete (UHPFRC) for bridge deck applications, Oral presentation in Young Researchers' Conference (YRC), 15 March 2012, London, UK.

Abstract

It has been two decades since Ultra High Performance Fibre Reinforced Concrete (UHPFRC) has come to the market and, so far, it has been used in only a limited number of highway bridge structures. This is due to many unanswered questions related to its structural behaviour for highway bridge structures and its high initial cost. The lack of knowledge regarding the structural behaviour is down to unavailability of appropriate test methods for this special type of concrete which behaves differently compared to normal concrete. Furthermore, the current precast production contributes to its high initial cost significantly. Therefore, this study has investigated various aspects that are restricting the potential use of UHPFRC for highway bridge applications.

The investigation included extensive experimental studies and numerical modelling. In the experimental programme, various parameters ranging from material and mechanical properties, potential use of the concrete for cast in-situ applications to ductility behaviour were investigated. Furthermore, the numerical analyses were carried out to identify appropriate finite element models to predict the flexural and shear behaviour of the concrete.

In the experimental work, simple and reliable test methods for material characterisation were developed. The validity of two non-destructive testing methods in studying the elastic properties of the concrete was confirmed. From this, the UHPFRC constitutive material model was obtained and used in numerical modelling. The reliability of the test methods were established by performing numerous experimental tests and similar results obtained at all times. Furthermore, the suitability of the concrete for cast in-situ applications at various temperatures by monitoring the strength development from an early age (12 hours) up to 360 days were investigated. The results showed significant strength gain of the concrete in both compression and tension within 7 days when cured at temperatures similar to site conditions (20 and 30 ^{o}C). A phenomenon related to the 90 ^{o}C curing temperature in precast production was reported and showed to have caused loss of flexural strength and toughness of the concrete. In addition, for the first time, an effective test method for studying the punching shear strength of the concrete with minimal influence of flexural stress was developed and used successfully. The results

showed a reduced effective punching shear perimeter of UHPFRC slabs by half compared to normal concrete.

The numerical analyses were carried out using the Abaqus finite element software. In this study, the Concrete Damaged Plasticity (CDP) and Concrete Smeared Cracking (CSC) material models with minor modifications were used to simulate the flexural and shear behaviour of UHPFRC beam and slab specimens, respectively. The results obtained here were validated against experimental studies with good agreement. The CDP model was found to replicate the linear and nonlinear structural response of the concrete with better accuracies than the CSC model.

This study presents significant findings on the suitability of UHPFRC for structural applications with a lower initial cost compared to its current precast production. Furthermore, results obtained on its excellent structural behaviour in flexure and shear provides structural designers great confidence in using this concrete for highway bridge applications. The findings reported in this study contribute to the literature of UHPFRC significantly.

List of Abbreviations

BC	Brittle Cracking
CDP	Concrete Damaged Plasticity
CSC	Concrete Smeared Cracking
EVC	Electronic Vernier Calliper
FEA	Finite Element Analysis
GGBS	Ground Granulated Blast Furnace Slag
HSC	High Strength Concrete
LVDT	Linear Variable Displacement Transducer
PFA	Pulverised Fuel Ash
SF	Silica Fume
SFR	Steel Fibre Reinforced Concrete
UHPC	Ultra High Strength Concrete
UHPFRC	Ultra High Performance Fibre Reinforced Concrete
UPV	Ultrasonic Pulse Velocity

List of Symbols

A	basic control section in punching shear check
A_{cont}	basic control area in punching shear check
A_p	horizontally projected area of the punching shear failure surface
b	width of beam specimen
b_0	perimeter of critical shear surface
c	column diameter
D	loaded area in punching shear check
d	density of concrete
d	depth to centre of reinforcing steel
d	diameter of cylinder specimen
d	effective depth of a section in punching shear check
d_c	compressive degradation variable
d_g	maximum aggregate diameter in concrete
d_t	tensile degradation variable
E	dynamic modulus of elasticity
E	degraded elastic stiffness value
E^{el}	initial modulus of elasticity
E_{cm}	static modulus of elasticity
$E_{cm,r}$	static modulus of elasticity, resonant frequency test
$E_{d,u}$	dynamic modulus of elasticity, UPV surface transmission
E_{dr}	dynamic modulus of elasticity, resonant frequency transmission
E_0	initial modulus of elasticity
F	maximum tensile splitting load
f_{b0}	initial equibiaxial compressive yield stress
f_c', f_{cj} & f_{ck}	28 days cylinder compressive strength
f_{co}	initial uniaxial compressive yield stress
f_{ct}	tensile splitting strength
$f_{ct,\,flexure}$	flexural tensile cracking strength
$f_{ct,1}$	corrected first crack flexural tensile strength
f_{cu}	28 days cube compressive strength
G	shear modulus
G_f	fracture energy
h	height of a section

K	ratio of second stress invariant on tensile meridian to compressive meridian
K	fibre orientation
k	radius of gyration
$L\,\&\,l$	length of specimen
n	fundamental flexural frequency
P_u	ultimate flexural load
P_y	first cracking flexural load
r_{cont}	further control perimeter in punching shear check
T_b	flexural toughness
u_t^{ck}	cracking displacement
u_t^{pl}	cracking displacement at failure
u_{t0}	cracking displacement at loss of strength
u_{0t}^{el}	displacement at elastic strain
u_1	total displacement
u_1	basic control perimeter in punching shear check
V_f	volume fraction of fibers
V_p	compression wave velocity
$V_{p,d}$	direct compression wave velocity, UPV test for beam specimen
$V_{p,s}$	indirect compression wave velocity, UPV test for slab specimen
$V_{R,c}$	concrete contribution to punching shear strength
$V_{R,f}$	fibre contribution to punching shear strength
V_r	surface wave velocity
V_{rd}	ultimate punching shear load
V_s	shear wave velocity
w	critical shear crack opening
δ_{rd}	deflection at maximum punching shear load
δ_{tb}	deflection of l/150 in flexural test
δ_u	deflection at ultimate flexural load
δ_y	deflection at first crack flexural load
ε	flow potential eccentricity
ε_a	strain under upper loading compressive stress
ε_b	strain under basic compressive stress
ε_c	lateral strain under upper loading compressive stress
ε_c	compressive strain

$\varepsilon_{ck,f}$	first crack compressive strain
$\varepsilon_{ck,\max}$	compressive strain at maximum strength
$\tilde{\varepsilon}_c^{in}$	compressive inelastic strain
$\tilde{\varepsilon}_c^{pl}$	compressive plastic strain
ε_d	lateral strain under basic compressive stress
ε_t	tensile strain
$\varepsilon_{t,f}$	first crack tensile strain
$\varepsilon_{t,\max}$	tensile strain at maximum stress
$\tilde{\varepsilon}_t^{ck}$	cracking tensile strain
ε_{0c}^{el}	compressive elastic strain
ε_{0t}^{el}	elastic tensile strain
φ	dilation angle
μ	viscosity parameter
ν	static Poisson's ratio
ν_u	dynamic Poisson's ratio, surface transmission
ν_r	dynamic Poisson's ratio, UPV transmission
ρ	density of concrete
σ	compressive stress
σ_a	upper loading compressive stress
σ_b	basic compressive stress
σ_b	tensile flexural strength
$\bar{\sigma}_b$	flexural toughness factor
σ_c	compressive stress
$\sigma_{ck,f}$	first crack compressive stress
$\sigma_{ck,\max}$	maximum cylinder compressive stress
$\bar{\sigma}_c$	effective compressive stress
σ_f	fibre bridging stress
σ_t	tensile stress
$\sigma_{t,f}$	first crack tensile stress
$\sigma_{t,\max}$	maximum tensile stress
σ_t^u	ultimate tensile stress
σ_{t0}	failure tensile stress
$\bar{\sigma}_t$	effective tensile stress
ψ	rotation

Contents

Chapter I: Introduction

1.1 Introduction

For centuries, concrete has been used widely in structural applications, ranging from buildings to highway and offshore structures. The advantages include its high compressive strength, good fire resistance, low cost, and being readily moulded into virtually any required shape. However, concrete also has many disadvantages including its low tensile strength, low ductility, and high degree of variability.

Concrete is classified based on its compressive strength measured at a given age, usually 28 days. In the early 1970's, concrete mixes with compressive strength of 40 MPa or higher were known as high strength concrete (HSC). As the development of high-rise buildings and long-span bridges increased, concrete with compressive strength in a range of 60-100 MPa became available commercially. Unfortunately, improvements in compressive strength increase the brittleness of the concrete. Consequently, ultra high performance fibre reinforced concrete (UHPFRC) emerged and became available in construction under many different commercial names such as compact reinforced composite, reactive powder concrete, Ductal, and ultra high performance concrete (Andrade et al. 1996, Roux et al. 1996, Orange et al. 2000, Rossi 2000, Aarup 2007). These all have high binder contents with special blends of aggregate, and high volume of water reducing admixtures in their mix. The resulting concrete exhibits high compressive and tensile strength with significantly improved ductile behaviour (Yang and Diao 2009).

UHPFRC is a combination of HSC with compressive strengths in the range of 150-250 MPa and steel fibres with high tensile strengths in the range of 850-2000 MPa (Le 2008). The resultant composite will have significantly improved mechanical, ductility and durability properties compared to existing conventional and high strength concretes. The UHPFRC mix is designed to minimise some of the characteristic weaknesses that are inherent in normal concrete. The mix contains cement, silica fume, quartz sand, superplasticisers, admixtures, and steel fibres. The use of very fine powder components and removing coarse aggregate from the mix is designed to achieve high compaction,

enhance homogeneity and increase the bond strength between the mortar matrix and fibres' surfaces. Heat treatment of 90 ^{o}C after casting is usually applied to achieve rapid strength gain within 7 days. The inclusion of steel fibres is to improve the composite material's ductility and tensile properties.

One of the potential applications of this advanced construction material has been identified as a promising way to design slender, lighter and more durable structures (Aarup 2007, Leung 2009). To date, there have been several applications of UHPFRC around the globe, ranging from footbridges to architectural applications and a few short span highway bridges (Blais and Couture 1999, Vicenzino et al. 2005, Behloul and Batoz 2008, Graybeal 2008, Rebentrost and Wight 2008b). However, the structural application of UHPFRC is still not widespread considering its superior properties, this is due to: (i) high initial cost, (ii) industry's reluctance to adopt a new material whose properties are perceived to be not fully understood, and (iii) the lack of recognised design standards.

1.2 Scope

The scope of this study includes experimental investigations and numerical modelling. The experimental programme is focussed on determining the material properties of UHPFRC using conventional testing methods used for normal concrete. In some cases, the tests were modified or new test methods had to be developed to improve the accuracy of the results. Furthermore, the structural behaviour of small scale specimens was also investigated.

The experimental programme was conducted in two phases. The first phase was aimed at determining the material properties of the concrete and finding the constitutive material relationships. The test results of this phase were used in finite element simulations to predict the structural behaviour of beam and slab specimens prepared in the second phase. The finite element analyses were carried out using a software package called Abaqus (Abaqus theory manual 2010).

In the second phase, beam and notched slab specimens were cast and tested. The results were used to analyse various parameters of the concrete ranging from strength development at various curing ages and temperatures to the structural behaviour in shear and flexure. The results reported in this phase, provided valuable data for the validation of the finite element analysis and for potential future development of this concrete in construction. Overall, more than 700 specimens of cubes, cylinders, beams, and slabs were cast and tested in this study.

1.3 Objectives

This study aims to investigate the suitability of UHPFRC for highway bridge applications. Detailed experimental studies to understand the material and mechanical properties of UHPFRC in compression, tension, flexural and shear were investigated. This study was built upon previous research conducted at the University of Liverpool (Le 2008). More specifically, the main objectives are listed below:

1. Determine the material and mechanical properties of a specific UHPFRC mix using static and dynamic testing methods.
2. Investigate the effect of different curing temperatures on the strength development of the concrete in compression and flexure from early ages up to a year.
3. Finite element modelling to predict the structural behaviour of beam and notched slab specimens and verify the analysis experimentally.
4. Evaluate the applicability, economy and efficiency of UHPFRC for highway bridge applications compared to normal concrete.

Each of the objectives stated above will be explained in details in the following chapters of this PhD study.

1.4 Research Contribution

The major obstacles limiting the use of UHPFRC for highway bridge applications are high initial cost and the unfamiliarity of its structural behaviour for such structures. In

this study, experimental work was carried out to investigate possible solutions for both these obstacles.

One of the factors contributing to the high initial cost is the current production process of this type of concrete. Curing UHPFRC members for at least 48 hours in high temperatures of 90 ^{o}C in factories is very expensive. The high energy consumption and potential increase in the carbon footprint is substantial. Therefore, shifting the precast production to cast in-situ could reduce the cost of the concrete considerably. To date, numerous studies have reported the improved properties of the UHPFRC precast members. However, very few studies have considered investigating the concrete cured at temperatures lower than 90 ^{o}C, such as 10, 20 and 30 ^{o}C. These temperatures are typical of weather conditions for cast in-situ concrete applications. Studying the influence of these three temperatures on the development of the mechanical properties of the concrete was found to be important. Therefore, an extensive experimental investigation to monitor the strength development of the concrete in compression and flexure from one to 360 days was carried out. Results obtained from this study confirmed UHPFRC can gain acceptable construction strengths within days after casting. It can easily be used for cast in-situ applications for all three temperatures.

Furthermore, an investigation of the applicability of non-destructive testing methods to determine the elastic properties of UHPFRC structures was found to be useful for future highway bridge applications. Two non-destructive testing methods available for normal concrete were investigated for the concrete and results with a high degree of accuracy were obtained. This provides more confidence in promoting this concrete in construction. The findings from both investigations discussed above can contribute in reducing the cost of the concrete considerably.

For the structural behaviour of UHPFRC, studies on its punching shear strength appeared to be an important area of research since very little can be found in the literature. This is due to the difficulties associated in determining this parameter without the influence of flexural failure during testing. After several attempts, this study managed to present a novel test method that could capture the material's punching shear

strength with minimal flexural stress. The results obtained here were important in confirming the high punching shear capacity of the concrete and its potential use for highway bridge structures. Furthermore, material characterisation was carried out and used in finite element modelling to predict the structural behaviour of the concrete in flexure and punching shear with good accuracy. Overall, the results reported in this study can be used in producing cheaper UHPFRC members with better understanding of its structural behaviour in flexure and shear.

1.5 Thesis Organisation

This thesis is divided into nine chapters. Each chapter consists of a brief introduction describing the content of the work and a summary at the end. A brief summary of the content of each chapter is presented below.

Chapter 1 - Introduction: A brief introduction to UHPFRC, its properties, limitations and applications were included. The scope, objectives and significance of this study are presented.

Chapter 2 - Review of Literature: This chapter introduces the literature relevant to UHPFRC. Detailed summaries from its development to the constituents of the material, mixing, casting and production methods were presented. The influence of the mix proportions and curing regimes on the mechanical and durability properties were discussed. Furthermore, a review of the application and limitations of UHPFRC for structural designs, in particular, for highway bridge applications were discussed. Finally, a brief review of the finite element analysis for this material was included.

Chapter 3 - Material Characterisation: In this chapter, the efficiency of a number of conventional test methods used for the determination of the mechanical properties of normal concrete was assessed for UHPFRC and UHPC. Furthermore, new direct tests (uniaxial tensile and compressive tests) were developed to characterise the material properties of both concretes at different ages. From the results obtained, material properties of the concretes were determined, in particular, the tensile and compressive stress-strain relationship for this specific mix of UHPFRC. The results are vital and

required for formulating and calibrating any potential constitutive material model for the concrete for design purposes or FE modelling, i.e. Chapter 7.

Chapter 4 - Non-destructive Testing Methods for UHPFRC: This chapter summarises the investigation on the validity of two existing non-destructive testing methods used for normal concrete in determining the elastic properties of UHPFRC; these properties are the modulus of elasticity and Poisson's ratio. The testing methods are the ultrasonic pulse velocity and resonant frequency methods, which have been used successfully in the past for investigating various properties of normal concrete. In addition, a number of existing relevant empirical relationships to determine the modulus of elasticity of UHPFRC from its compressive strength were also studied. To validate the results obtained from the non-destructive tests and the empirical equations, static tests were also performed to determine the same properties.

Chapter 5 –UHPFRC Cast in-situ Application: In this chapter, an extensive experimental study was carried out to investigate the potential use of UHPFRC for cast in-situ applications. Cube and beam specimens were cured at 10, 20, 30 and 90 ^{o}C temperatures and tested in compression and flexure at various ages up to 360 days. Results from the three lower curing temperatures were compared to those obtained for 90 ^{o}C temperature. The three lower curing temperatures were used to replicate environmental conditions that may be typically encountered on construction sites, while 90 ^{o}C is applicable to precast construction. From this study, significance findings for each of the curing regimes were found, in particular, the effect of the 90 ^{o}C curing temperature on the flexural behaviour of the concrete. In addition, visual durability checks on the steel fibres in the concrete at various curing temperatures were also performed. The findings reported here, are believed to have significant beneficial cost and the environmental impact consequences on UHPFRC cast in-situ applications.

Chapter 6 - Punching Shear Strength: In this chapter, experimental investigation was carried out to study the punching shear capacity of thin UHPFRC slab specimens. For this, a sophisticated punching shear test was designed in which notched UHPFRC slab specimens with various notch diameters were tested. Results obtained here were used to

investigate various parameters ranging from punching shear load and angle, failure mode, failure behaviour to the value of the basic control perimeter of UHPFRC slab specimens under a high concentrated load.

Chapter 7 - Finite Element Modelling for UHPFRC: In this chapter, numerical study using Abaqus was carried out to examine the efficiency and limitation of two material models (the concrete smeared cracking (CSC) and the concrete damaged plasticity (CDP)) for predicting the flexural and shear behaviour of various UHPFRC specimens. Both models are originally developed for reinforced concrete members; however, with some modifications they were adapted here for UHPFRC. In this study, the concrete was modelled as a homogenous material and the physical presences of fibres were not feasible to model, and were ignored. The findings reported here were significant for the numerical investigation of this concrete.

Chapter 8 - UHPFRC for Highway Bridge Application: This chapter summarises the applicability of the concrete for highway bridge application based on the findings of the experimental and numerical studies presented in Chapter 3 to 7.

Chapter 9 - Conclusions and Recommendations: In this Chapter, the findings reported in the study are concluded and recommendation for future work is presented.

Chapter II: Review of Literature

2.1 Introduction

In this chapter, the historical development of UHPFRC from an early age up to the present date is described. The principle, mix compositions, and production methods are discussed. The improved mechanical and durability properties and their dependence on the mix compositions and curing regimes are presented. Some of its applications, from structural to architectural designs around the world are listed. The advantages and limitations of using UHPFRC in highway bridge application are discussed. Finally, a brief introduction to the finite element modelling options for UHPFRC is included.

2.2 Development of UHPFRC

The development of UHPFRC can be linked to the outcome of a quest that began in the 1930's by the French engineer Eugène Freyssinet (Freyssinet 1936). Freyssinet was investigating high strength concrete with low creep for use with the new prestressing technique and demonstrated that compressing concrete during setting could increase its strength (Rossi 2000). Subsequent studies were undertaken to find better ways of increasing the mechanical properties of concrete, particularly, the compressive strength. In the early 1970's, several researchers investigated reducing the porosity of hardened Portland cement paste using vacuum mixing and high pressure at high temperatures (Yudenfreund et al. 1972, Roy et al. 1972, Odler et al. 1972). These studies reported significant strength enhancement of cement paste with compressive strengths up to 680 MPa. Following this, a number of studies in the 1980's were conducted to investigate the particle packing and improve the density of concrete with the use of superplasticisers and pozzolanic admixtures, such as silica fume (Bache H 1981, Birchall et al. 1981, Hjorth et al. 1983, Alford and Birchall 1985, Bache H 1987). The results of these studies led to the development of two kinds of very compacted materials, macro-defect-free cements (MDF) and densified silica fume (DSF). However, such concretes were very brittle and could not be used in construction. Therefore, further investigations were carried out to overcome this problem and the inclusion of fibres was found to be essential to improve the ductility problems of these very high strength concretes. In the

1990's, the development of UHPFRC began after mixing fibres with high strength concrete; in particular, when the new superplasticisers based on polycarboxylate ethers were developed. The new superplasticisers were essential to the performance improvement of the mix and improved the mechanical properties of the concrete significantly. Subsequently, UHPFRC emerged under several commercialised names such as engineered cementitious composites (ECC), multi-scale fibre reinforced concrete (MSFRC), special industrial concrete (BSI), compact reinforced composites (CRC), Ductal, and reactive powder concrete (RPC) (Li and Leung 1992, Richard and Cheyrezy 1994, Andrade et al. 1996, Rossi 1997, Semioli 2001).

The principal differences of all the different types of UHPFRC lie in their mixture compositions, water/cement ratios, aggregate sizes, and fibre volume fractions. Following the commercialisation of many different types of UHPFRC, the first RPC structure (footbridge) in the world was built in Sherbrooke, Quebec, Canada in 1997 (Habel et al. 2008). From the early 2000's, research on UHPFRC began to increase to characterise and improve the mechanical properties of this promising material (Chanvillard and Rigaud 2003, Benson and Karihaloo 2005a, Graybeal 2006, Ulm and Acker 2008, Wille et al. 2012). To date, a large number of studies have investigated various aspects of UHPFRC including its raw materials, rheology, hydration, time dependant behaviour in terms of failure, fatigue, durability, strength, design and construction (Schmidt 2012).

The references listed above are some of the key developments, further studies regarding the development of UHPFRC can be found in the literature (Rossi 2000, Habel et al. 2008, Naaman and Wille 2012, Schmidt 2012).

2.3 Principle of UHPFRC

The basic principle of UHPFRC is creating a material with enhanced strength and durability properties compared to conventional concrete. According to studies (Richard and Cheyrezy 1994, Acker and Behloul 2004) the main principles of UHPFRC design can be summarised as:

- Enhancement of homogeneity
- Enhancement of compaction
- Enhancement of the microstructure
- Enhancement of ductility
- Finally, the use of mixing and casting procedures that are close to existing practise.

The homogeneity of the mix is improved by removing the coarse aggregate and replacing it with fine aggregate in the cementitious paste, a like mortar mix. This minimises the number of defects such as microcracks and voids in the concrete (Acker and Behloul 2004). In addition, the density of the mix is increased by optimisation of the granular mixture. The selection of fine particle sizes of cement, sand and supplementary cementitious materials with particle sizes ranging from approximately 0.03 to 100 μm, results in a very dense mixture with minimised voids.

Furthermore, the microstructure of the mix is improved by applying the post-set heat treatment for a period of time, usually 48 hours at 90 ^{o}C. The heat treatment accelerates and increases the pozzolanic reaction, which leads to an extremely high compressive strength concrete. At the same time, pressure treatment is often applied to the fresh mix of UHPFRC to increase the density by reducing the entrapped air, and removing excess water from the mix. The techniques described above result in a very brittle concrete type, with ductility not better than that of conventional concrete (Cheyrezy 1999). However, the incorporation of steel fibres into the mix improves the ductility and tensile properties of UHPFRC significantly. Finally, the mixing and casting procedures are similar to the existing practise for normal concrete. Therefore, most of the standard industrial batching facilities are able to mix this concrete with only minor adjustments.

2.4 Constituents of UHPFRC

The main constituents of UHPFRC are cement, aggregates, supplementary cementitious materials such as (silica fume, ground granulated blast furnace slag and pulverised fuel ash), superplasticisers, water, and steel fibres. Table 2.1 shows a typical mix design of UHPFRC (Richard and Cheyrezy 1994).

Table 2.1: A typical UHPFRC mix composition (Richard and Cheyrezy 1994).

Material	(kg/m^3)
Portland cement	955
Fine sand	1051
Silica fume	229
Precipitated silica	10
Superplasticisers	13
Steel fibre	191
Water	153

Each of the material constituents and their proportion in the mix are described below.

2.4.1 Cement

UHPFRC contains a high content of cement, approximately (700-1000 kg/m^3) which contributes to its high strength (Richard and Cheyrezy 1994, Graybeal 2005, Le 2008). The cement content is nearly two times higher than for normal strength concrete. This makes the concrete more vulnerable to high shrinkage and environmentally unfriendly. Therefore, it has been recommended that the cement should be low in C_3S and C_3A (Aitcin 2000). A typical Portland cement, even when used in combination with cementitious materials, can be used.

Generally, cement types of CEM I 42.5 or CEM II 52.5 are used for UHPFRC (Collepardi et al. 1997, Le 2008, Ghafari et al. 2012). Other types of cement such as CEM III/B has also being used successfully (Richard and Cheyrezy 1995, Schmidt and Schmidt 2012).

2.4.2 Aggregate

Unlike normal concrete, coarse aggregate has been removed from UHPFRC mix to obtain higher compaction and lower permeability. Fine aggregate such as silica sand is the only aggregate used in the concrete.

Silica sand is a very fine material with a mean particle size of smaller than 1 mm (Habel 2004, Graybeal 2005, Le 2008). This fineness makes it a suitable aggregate for the concrete, although, greater particle sizes up to 8 to 16 mm were used successfully in the

past (Richard and Cheyrezy 1995). Another advantage of silica sand in UHPFRC is its high silica content in the form of quartz. This enables the silica content at high temperatures, i.e. 90 ^{o}C, during mixing and curing to react with $Ca(OH)_2$ from the hydration of cement to form calcium silicate, which contributes to the strength of UHPFRC.

Suitable selection of fine aggregate in UHPFRC mix is very important. The type, size, and shape particles of the fine aggregate affect the workability of the concrete. It has been reported that fine sands with high water absorption should be avoided to minimise the water content in the mix (Rangan 1998). Furthermore, bond strength between the smaller size aggregates was found to be greater than for larger sizes (Shah and Ribakov 2011).

2.4.3 Supplementary cementitious materials

Supplementary cementitious materials may include silica fume (SF), Ground Granulated Blast Furnace Slag (GGBS), and/or Pulverised Fuel Ash (PFA). These materials are used either as cement replacement or as additives in the concrete mixture to improve strength, durability and workability. The use of supplementary cementitious materials in UHPFRC and concrete has the potential to reduce the environmental impact, i.e. CO_2 emissions, caused by the industrial production of cement. A brief description of each material with their advantageous in UHPFRC is presented below.

2.4.3.1 Silica fume (SF)

Silica fume, also called microsilica, is a highly pozzolanic mineral. It contains fine particles of silica condensed from the waste gases exhaled in the silica metal production process. To facilitate handling, silica fume is often blended into slurry with superplasticisers, or supplied as a densified powder.

Silica fume is used in concrete as a partial cement replacement or as an admixture. It is a relatively expensive material, approximately four times the cost of cement (Le 2008). The particles of silica fume have an average diameter of 0.1 μm, which is approximately 100 times smaller than an average cement particle. The particles are small enough to fill

voids between the cement grains to enhance the packing density and form hydration products by pozzolanic activity in the concrete to improve compressive strength and durability properties (Habel 2004, Graybeal 2005, Xing et al. 2005). In addition, the bond strength between the fibres and the matrix of hardened UHPFRC was reported to be increased considerably with a silica fume content of 20 to 30% (Chan and Chu 2004). Despite these advantages, the use of silica fume with high carbon content in concrete could have an adverse effect on workability, unless high range water reducing admixtures are used (Bayasi 1992). Therefore, the type of silica fume used in UHPFRC is considered carefully.

2.4.3.2 Ground granulated blast furnace slag (GGBS)

GGBS is a waste by-product of the iron and steel making industry. It is obtained by quenching molten iron slag from a blast furnace in water or steam, to produce a glassy and granular product. It is then dried and ground into a fine powder with a mean particle size of 3-100 μm.

GGBS is usually used as a cement replacement material in concrete and is very cheap. This makes it a cost effective substitute to cement in UHPFRC. The presence of GGBS in UHPFRC was reported to improve the workability significantly (An and Ludwig 2012). Therefore, UHPFRC contains up to about 250 kg/m^3 of GGBS and significant amounts of other mineral fillers (Schmidt 2012).

Despite its benefits, the high content of GGBS may lower the early age temperature rise of the concrete. Such behaviour tends to delay the setting time and reduce compressive strength of the concrete at early age. However, the literature reports cement replacement in RPC of up to 40% with GGBS had no detrimental effects on its compressive strength and can be used (Yazici 2007).

2.4.3.3 Pulverised fuel ash (PFA)

PFA is ash from the burning of pulverized coal in power stations and a considerably cheap material. It is a pozzolanic material that reacts with lime to form hydrates and is been used widely in normal concrete and UHPFRC as a supplementary cementitious material.The

advantage of PFA in UHPFRC is to reduce bleeding by allowing concrete to be designed to have lower water content for the same workability. It also reduces the overall CO_2 footprint of the cement production when it is used as cement replacement. The availability of vast amounts of PFA at low cost makes it sensible to be incorporated in the relatively expensive UHPFRC.

2.4.4 Superplasticisers

Superplasticisers, also known as high range water reducers, are chemical admixtures composed of powerful organic polymers used in concrete. The main purpose of using a superplasticiser is to produce a flowing concrete and to reduce the water to cement ratio. Prior to the discovery of superplasticisers, a large amount of water had to be added to the concrete mixture. The water/cement (w/c) ratio was normally in the range of 0.6-0.70. The compressive strength of the resulting concrete was, therefore, limited to about 20-40 MPa. However, with the discovery of superplasticisers, the water content in normal concrete mixes was able to be reduced considerably, ranging from 0.25-0.40 and keeping the same strength (Shah and Ribakov 2011).

Superplasticisers are used in UHPFRC to disperse cement and silica fume particles, fibre distribution, and to improve the flowability without sacrificing the workability of the mix (Aitcin et al. 2000, Hirschi and Wombacher 2008). This results in improving the mechanical properties of the hardened concrete significantly. Generally, the w/c ratio of UHPFRC is very low, about 0.20 (Schmidt 2012, Le et al. 2007). Thus, the optimum amount of superplasticiser in the mix is relatively high, with a solid content of approximately 1.6 percent of the cement content (Richard and Cheyrezy 1995). This large amount of superplasticiser tends to delay the initial setting of UHPFRC compared to normal concrete.

There are different types of superplasticisers such as naphthalene sulfonate based, melamine sulfonate based, and polycarboxylate-based polymer in powder and liquid forms. The polycarboxylate liquid type is the most common within UHPFRC mixtures.

2.4.5 Water

Water like any other composition in concrete is an important ingredient in the mix, initiating the chemical reactions among the materials to form the concrete paste. The water content in UHPFRC is generally small, and is determined based on the w/c ratio. Some studies have taken the water into account including the superplasticiser and some have excluded it (Le 2008, Shah and Ribakov 2011). Nevertheless, there is no specific requirement regarding the quality of water in UHPFRC. Generally, clean tap water is used for normal and high strength concrete, including UHPFRC.

2.4.6 Fibres

Since the matrix of UHPFRC shows very brittle rupture, steel fibres are of great importance to provide sufficient ductility to the concrete. The benefits of steel fibres in UHPFRC includes improvement in stiffness, compressive and tensile strength, impact resistance, fatigue, safety, and post-cracking stiffness (Banthia and Mindess 1996, Holschemacher et al. 2010). The improved mechanical properties of UHPFRC depend on the type and amount of fibre added to the mix.

Commercially available fibres are made of different materials such as steel, glass fibre, carbon fibre, aramid fibre, basalt fibre, polypropylene, and polyethylene. Some of these fibre types are very expensive, such as steel and carbon fibres. Generally, steel fibres are used for UHPFRC. The steel fibres differ in size, shape, and mechanical properties, as shown in Figure 2.1.

Figure 2.1: Different types of steel fibres (Holschemacher et al. 2010).

It has been reported (Schmidt 2012) that the inclusion of randomly distributed steel fibres in UHPFRC improves the tensile and flexural strengths up to about 15 and 40 MPa, respectively. This significant improvement in the tensile properties allows UHPFRC members to carry tension forces even without additional reinforcing bars. The behaviour of UHPFRC is similar to that of concrete with reinforcement. The steel fibre in UHPFRC carries all the tension forces across microcracks once the matrix has cracked. Similar to the reinforcing bars in reinforced concrete, carrying the tension forces across cracks in a concrete member. Hence, the load carrying capacity in tension and compression of UHPFRC are much higher than those of normal concrete.

Despite the benefits of steel fibre reinforcement in UHPFRC, fibres significantly affect the workability of the concrete. This depends on the fibre content and dimensions. The workability of UHPFRC in known to decrease inversely with the increase of fibre content and dimensions. The optimum dosage of 13 mm long and 0.15 mm diameter steel fibres in UHPFRC was reported to be up to 2.5% by volume before the concrete becomes unworkable (Rossi 2005). However, in a different study (Nielsen 1998) the maximum content of the same fibre was reported to be 4%. Ideally, 2% is identified to be the most common and economic content of fibre by volume in UHPFRC (Richard and Cheyrezy 1995). Fibres are randomly distributed in UHPFRC as shown in Figure 2.2.

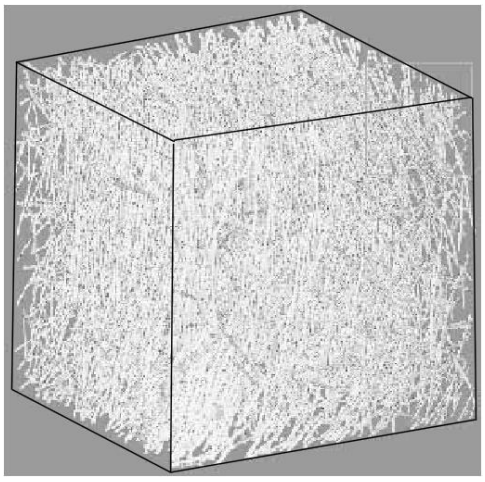

Figure 2.2: Random distribution of fibre (Acker and Behloul 2004).

2.5 Production of UHPFRC

2.5.1 Mixing

The mixing procedure for UHPFRC is not greatly different from mixing normal/high strength concrete. The same mixing equipment as normal concrete is used. The mixing process might require a slightly longer time to ensure a homogenous mix among the high content of smaller particles.

Generally, dry constituents (cement, aggregates, and supplementary cementitious materials) are mixed together firstly for 1-5 minutes. During this process, smaller particles such as (micro silica) progressively fill the voids between the coarser particle (Ma et al. 2004). Then, water and superplasticisers are added to the dry mix to facilitate the transformation of the dry mix to a cement paste. Depending on the type of superplasticiser and water content, this process could take 5-10 minutes. Finally, steel fibres are added to the wet mix and mixing continues for further 1-5 min. In the final stage of mixing, care must be taken to ensure proper fibre dispersion. This can be achieved by adding the steel fibres slowly and evenly in the mix. The total mixing time varies, 12 to 16 minutes were reported by different studies (Schachinger et al. 2004, Le et al. 2007).

2.5.2 Casting

Casting procedure of UHPFRC is similar to normal concrete with the exception of some extra care due to fibre content in the mix. The direction of placing during casting was reported to be crucial. This is because the distribution and alignment of fibres during casting affects its tensile behaviour significantly. The casting procedure of this concrete has been the subject of many studies (Bayard and Plé 2003, Kang and Kim 2011). It was reported that placing UHPFRC parallel to the longitudinal direction of the specimen results in higher flexural strength compared to UHPFRC placed transversely (Kang et al. 2011). Therefore, appropriate casting procedure to ensure adequate fibre distribution throughout UHPFRC members is required.

For laboratory specimens, UHPFRC is generally placed in one end and allowed to flow to the other end. This method helps fibre alignment in the direction of flow (Lappa 2007, Le 2008). The mixture of UHPFRC is very fluid and self-compacting, so vibration is rarely required.

During casting, pressure can be applied to improve the packing density of the concrete. In the past, casting pressure was applied to remove out the entrapped air and improvement in the mechanical properties was reported (Kowald et al. 2008, Le 2008, Dils et al. 2012). However, this method is expensive and not practical in construction industry.

So far, UHPFRC have been cast in the form of precast members and this has proved to be very expensive. However, alternative ways of exploiting this promising material, i.e. cast in-situ applications, are yet to be investigated. The potential use of UHPFRC in cast in-situ applications to minimise its environmental impact and high cost has not been investigated in great details.

2.5.3 Curing

Since the current production of UHPFRC units is generally precast members, the standard manufacturers' recommendations are for members to be cured at ambient temperature for the first 24 hours from initial setting (Graybeal 2005). During this time, members are kept in their moulds and a similar practise, as used for conventional concrete, applies here to prevent moisture loss. This is followed by 48 hours curing at an elevated temperature of 90 ^{o}C.

The post-heat treatment is applied to improve the microstructure of the concrete by enhancing the hydration reaction and reduce porosity. This process was reported to accelerate the early age strength development significantly (Richard and Cheyrezy 1995). Maximum strength within days of casting was reported, usually less than 7 days (Kamen et al. 2007, Richard and Cheyrezy 1994). It is, therefore, believed that the full promises of UHPFRC's benefits are not only gained due to the particle packing, but also because of the method of curing. Despite this, experimental investigation conducted in

this PhD indicates an adverse effect on the tensile flexural strength development of UHPFRC due to the post-heat treatment. Therefore, in this study, a detailed investigation in this area of research was carried out and presented in the following sections of this thesis.

Generally, the standard heat treatment temperature is 90 ^{o}C for 48 hours. However, the temperatures can range from 90 to 400 ^{o}C and last from 2 to 6 days (Voort et al. 2008).

2.6 Mechanical Properties

For normal concrete, tensile strength is neglected and assumed to be equal to zero, while compressive strength is the principal parameter used in structural design. However, UHPFRC exhibits a high tensile strength which can be considered in structural design. The mechanical properties of this concrete are affected by many parameters like the fibres' geometry and content, fibre orientations, bond strength between fibre and binder matrix, strength of the matrix, size and shape of specimen, methods of testing etc. Therefore, detailed knowledge of its mechanical properties and factors affecting them are essential for design.

In this section, values of the mechanical properties of UHPFRC reported in the literature are listed and compared to those of normal concrete. Factors affecting the compressive, tensile and shear behaviours are presented. Furthermore, test methods and guidance that are used and available for testing this material are included.

2.6.1 Compressive behaviour

The compressive behaviour of UHPFRC is characterised by the compressive strength, modulus of elasticity, and Poisson's ratio. These properties have been investigated in detail by many researchers and were reported to be dependent on the mixture compositions (Richard and Cheyrezy 1995, Said 1996, Acker and Behloul 2004, Graybeal 2005, Lafarge March 2009, Shah and Ribakov 2011).

Figure 2.3 shows a typical compressive stress-strain curve for UHPFRC compared to normal concrete (Acker and Behloul 2004). In this figure, the high compressive stress-strain values, modulus of elasticity, the post-cracking and ductile behaviour are very different to that of normal concrete.

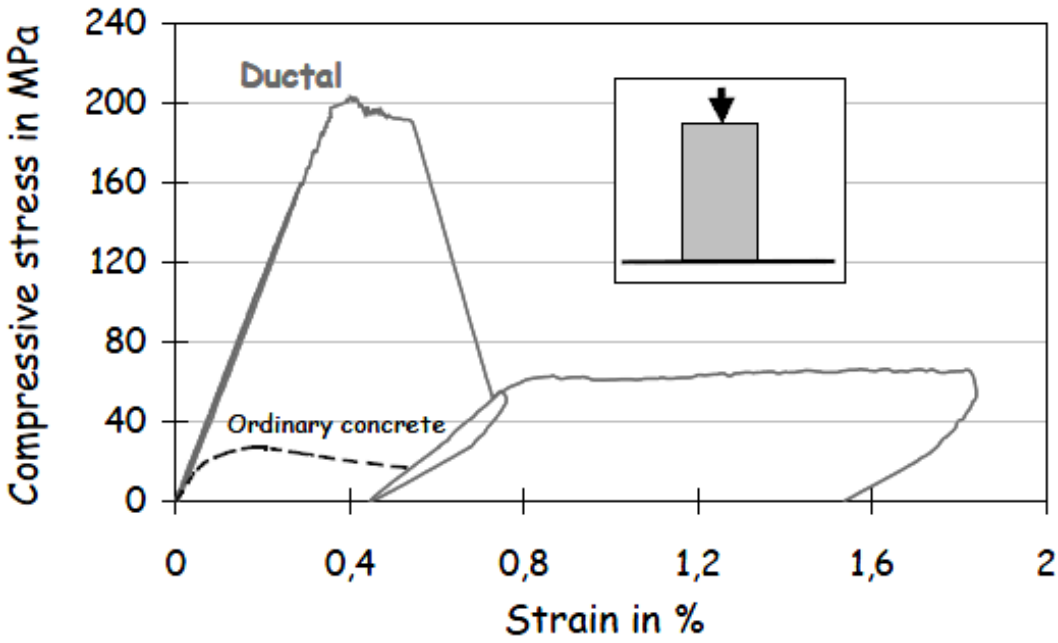

Figure 2.3: Compressive behaviour of UHPFRC compared to normal concrete (Acker and Behloul 2004).

Generally, the same static test methods used for normal concrete have been used to study the compressive behaviour of UHPFRC. However, this study found such test methods are not fully appropriate for this concrete due to the post-cracking behaviour which cannot be measured accurately. Therefore, modification or developing new test methods were found essential to determine its compressive behaviour more precisely.

2.6.1.1 Compressive strength

UHPFRC exhibits very high compressive strength compared to conventional concrete. Generally, cube or cylinder specimens are tested at 7 or 28 days and typical values of greater than 150 MPa have been reported (Richard and Cheyrezy 1994, Acker and Behloul 2004, Graybeal 2005, Yang et al. 2009).

The value of compressive strength, f_c, is reported to be highly dependent on the mix composition, type and duration of the curing regime. Experimental studies (Yang et al. 2009, Voort et al. 2008) indicated that high curing temperatures such as 90 ^{o}C has a profound effect in improving the compressive strength, particularly at an early age. It was reported that UHPFRC with standard heat treatment of 90 ^{o}C for two days, can gain its maximum compressive strength within seven days of casting, approximately 180 MPa. So far, the maximum compressive strength reported for UHPFRC was 810 MPa using a very special mix composition (Richard and Cheyrezy 1995). In this particular UHPFRC mix, steel aggregate was incorporated while temperature curing of 400 ^{o}C with the application of high confining pressure was applied during setting. This type of UHPFRC requires a demanding production process and is very expensive.

Fibre addition was reported to have less influence on the value of this parameter (Schmidt et al. 2003). While the brittleness with low strain capacities of the matrix can be overcome by the addition of steel fibres, little enhancement in the compressive stress and peak axial strain was reported (Song and Hwang 2004, Lu and Hsu 2006). Compressive strength of UHPFRC with fibres was found to be slightly higher than those without fibre content, an increase of 5-10% was reported (Nielsen 1998, Lu and Hsu 2006).

In the UK, compression tests are usually performed on 100 and 150 mm cube specimens. The test is measured using universal testing machines for normal concrete. There are many recognized standards which a study can follow; the most recognized one is BS EN 12390-3. At least three cube specimens are tested to failure at 28 days and the average result is considered as a criterion for quality and strength of the concrete. Although the compression test is straight forward, the uniaxial compression test for determining the stress-strain relationship for UHPFRC is challenging. A number of studies have attempted to obtain the stress-strain relationship of this concrete using uniaxial compressive test (Tue et al. 2004, di Prisco et al. 2008). However, the relationship only up to maximum strength was investigated. The post-peak behaviour, which distinguishes UHPFRC from normal concrete, was neglected. Therefore, in this study, a suitable test

method for capturing the post-peak behaviour of UHPFRC was carried out (Hassan et al. 2012).

2.6.1.2 Modulus of elasticity

Similar to its compressive strength, the modulus of elasticity of UHPFRC is considerably higher compared to ordinary concrete. For normal concrete, the modulus of elasticity, E, ranges from 29 to 36 GPa while UHPFRC exhibits a higher value, approximately 50 to 60 GPa (Richard and Cheyrezy 1994, ACI Committee 363 1997, Gowripalan and Gilbert 2000, Schmidt and Fehling 2002).

For UHPFRC, the value of, E, was reported to be dependent on the curing regime. According to studies (Graybeal 2006, Richard and Cheyrezy 1994) standard heat treatment (90 ^{o}C) can increase the value by 23% and even higher temperature treatment such as (250 ^{o}C) can increase it by an additional 23%. Moreover, using densely graded aggregate, incorporating silica fume and reducing the w/c ratio in UHPFRC was reported to increases this property considerably (Simeonov and Ahmad 1995).

In structural design, the modulus of elasticity is an important parameter for the determination of strain distribution and displacement of concrete members. Modulus of elasticity is usually obtained from the linear stress-strain responses in uniaxial compression tests in accordance to one of these standards or recommendations (BS 1881-121 1983, BFUP AFGC 2002, ASTM C469-02 2002). Alternatively, non-destructive testing techniques and empirical equations, both originally developed for normal/high strength concrete could be used in obtaining the modulus of elasticity of UHPFRC. However, so far, only limited studies have investigated the applicability of non-destructive testing techniques to determine this parameter (Hassan and Jones 2012).

2.6.1.3 Poisson's ratio

Poisson's ratio, ν, is another important parameter in the analysis of concrete structures, particularly for plate, shell and slab structures (Voort et al. 2008). The value of Poisson's ratio for an isotropic and linear elastic material is constant. However, for normal concrete, values ranging from 0.16 to 0.22 were reported (Neville 2012).

According to the French recommendation (BFUP AFGC 2002), a value of 0.2 can be assumed for UHPFRC. However, research studies reported different values ranging from 0.13 to 0.25 (Dugat et al. 1996, Voo et al. 2001). For normal concrete, Poisson's ratio was reported to be influenced by age, strength, stress level, and the mix proportion (Allos and Martin 1981). For UHPFRC, increasing fibre content was reported to increase the value of Poisson's ratio (Shah and Ribakov 2011).

The standard test method used for the determination of the direct compressive and tensile strength, is usually used to obtain the value of the Poisson's ratio of UHPFRC. Alternatively, non-destructive testing techniques can be used. So far, very limited study on the latter method to determine the Poisson's ratio of UHPFRC has been reported in the literature (Washer et al. 2005, Hassan and Jones 2012).

2.6.2 Tensile behaviour

The tensile behaviour of UHPFRC is significantly higher compared to normal concrete. Figure 2.4 presents the tensile behaviour of a UHPFRC beam specimen in flexure. The result is compared to a beam test of normal concrete and significant improvement was reported in terms of strength and ductility (Acker and Behloul 2004). The improvement is due to the dense matrix and fibre content in the mix content of UHPFRC. Unlike conventional concrete, the tensile strength of UHPFRC is not directly related to its compressive strength.

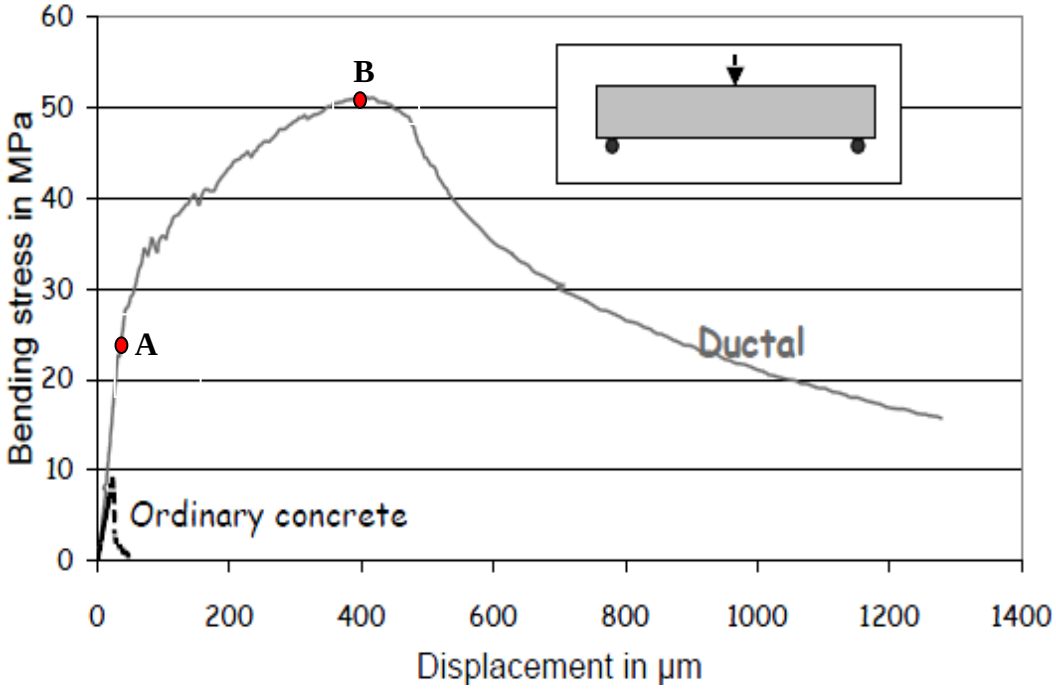

Figure 2.4: Tensile behaviour of UHPFRC compared to normal concrete (Acker and Behloul 2004).

According to the French recommendations (BFUP AFGC 2002), tensile behaviour of UHPFRC is characterised by an elastic stage limited by the tensile strength of the matrix. The major part of the tensile strength is obtained in the elastic stage with little deformation, up to Point A in the figure above. This is followed by a post-cracking stage characterised by the tensile strength of the composite material after the matrix has first cracked. In this stage, a number of microcracks occur while the tensile strength and deformation of the composite keeps increasing. This behaviour is known as strain hardening, Point A to B. Once the maximum tensile strength has attained, one macrocrack develops which results in rapid deformation and loss of strength. This behaviour in the post-cracking stage is known as strain softening, Point B onwards.

To date, many experimental investigations have studied the tensile behaviour of fibre reinforced concrete (Richard and Cheyrezy 1995, Graybeal 2005, Benson and Karihaloo 2005b, Le 2008, Mallat and Alliche 2011). These studies have performed various direct and indirect tension tests to obtain the tensile strength, tensile flexural strength, fracture energy, and flexural toughness. The direct tests were performed using uniaxial tensile test to determine uniaxial tensile strength of the concrete. In the mean time, indirect tests

were performed using cylinder splitting and flexural tests to determine the tensile splitting and tensile flexural strength, respectively. The direct test is rarely performed due to the implications involved, while the indirect ones are most commonly used.

2.6.2.1 Direct tensile strength

The direct tensile strength also known as uniaxial tensile strength, represents the true tensile properties of concrete. Normal concrete has a low tensile strength, typically between 2.1 to 4.8 MPa with low ductility. However, the tensile strength of UHPFRC is reported to be in range 8 to 13.5 MPa with better ductility properties (Chanvillard and Rigaud 2003, Hajar et al. 2004, Benson and Karihaloo 2005b). This improvement was reported to be highly dependent on the type, quantity and orientation of steel fibres in the mix. Moreover, the fibre-matrix bond strength was reported to influence this parameter significantly (Gowripalan and Gilbert 2000). The behaviour and value of the tensile strength of UHPFRC is considerably enhanced compared to normal concrete. Therefore, studying the tensile strength and ductility of this concrete is vital due to its contribution to tensile resistance in structural applications, in particular, for highway bridge applications.

To obtain the direct tensile strength and the tensile stress-strain relationship for UHPFRC, uniaxial tensile tests needs to be performed. However, this test is avoided due to many implications involved during the test, in particular, for fibre reinforced concrete. So far, no standard exists to provide guidance in performing this test. In addition, many research studies have attempted to design suitable test methods for fibre reinforced concrete, each with their own interpretation (Graybeal 2005, Benson and Karihaloo 2005b, Mallat and Alliche 2011). The reliability of the test methods reported in the literature are questionable due to the variation of the results reported. It is, therefore, in this study, a test method was developed to obtain the tensile stress-strain relationship of this specific UHPFRC mix. Results from this test were used to determine the constitutive material model of the concrete and was also used in finite element modelling (Hassan et al. 2012, Mahmud et al. 2012).

2.6.2.2 Splitting tensile strength

The splitting tensile strength, f_{ct}, is another parameter to measure the tensile properties of normal concrete and UHPFRC. Values ranging from approximately 11 to 12.5 MPa have been reported for UHPFRC, which is nearly two times higher than those reported for normal concrete (Graybeal 2005). The value of this parameter was reported to be significantly dependant on curing regimes and fibre content in the concrete (Shaaban and Gesund 1993, Graybeal 2005).

The splitting tensile strength is demined form splitting test which is originally developed for normal concrete. It is an indirect tension test usually performed on cylinder specimens, the BS EN 12390-6:2009 provides full guidance in performing this test for normal concrete. This test is simple to perform and believed to provide results close to the direct tensile strength for normal concrete (Neville 2012). So far, limited study have investigated the accuracy of this testing method for UHPFRC (Graybeal 2005). Therefore, in this study, the applicability of this testing method for the UHPFRC mix was investigated and the results were compared to those obtained from direct tensile tests.

2.6.2.3 Tensile flexural strength

The tensile flexural strength, $f_{ct,flexure}$, is another parameter that has been used to evaluate the tensile properties of normal concrete and UHPFRC. Non-reinforced concrete structures such as highway pavement slabs and airfield runways are designed based on tensile flexural strength (Neville 2012). Therefore, studying this parameter of UHPFRC with corresponding deformations under service conditions and ultimate limit state for structural design is vital. The tensile flexural strength of UHPFRC, also known as the modulus of rupture, is reported to be in the range 15 to 40 MPa (Perry and Seibert 2012). This is significantly greater, nearly four to six times, than those reported for conventional concrete, as shown in Figure 2.4.

So far, numerous studies have attempted to characterise the tensile flexural strength of UHPFRC (Richard and Cheyrezy 1994, Chanvillard and Rigaud 2003, Reineck and

Greiner 2004, Yang et al. 2009, Collepardi et al. 1997, Schmidt and Fehling 2002). From the results reported, it appears that the flexural strength of this concrete is significantly influenced by the mix proportions, sample casting and preparation, and in particular specimen size. However, so far, very little information exists on the influence of curing temperatures that are similar to site conditions. Therefore, in this study, an experimental investigation on the tensile flexural strength development of the concrete due to a range of curing temperatures (i.e. 10, 20 and 30^{o}C) was studied. The results of this study were essential in evaluating the suitability of UHPFRC for cast in-situ applications.

Tensile flexural strength is determined by flexural test. This test is performed on notched and unnotched beam specimens under 3 or 4 point loading arrangements. It is an indirect tensile test which overestimates the true tensile strength of the concrete. Therefore, empirical relationship is proposed to correlate the tensile flexural strength to the tensile strength of UHPFRC (BFUP AFGC 2002). According to the AFGC recommendation, it is possible to obtain the true tensile strength of UHPFRC from the first cracking strength in this test after taking into account a size effect concept. However, the validity of the proposed relationship was found questionable in this study. This is because the relationship was derived on a limited number of tested specimens. Furthermore, the influence of curing regime on the value of first cracking strength was not taken into account which was found here to be significantly influential.

To perform this test, a number of standards and recommendations for normal and fibre reinforced concrete can be found in the literature (BS EN 12390-5 2009, BFUP AFGC 2002, JSCE-SF4 1984, RILEM TC 162-TDF 2002).

2.6.2.4 Flexural toughness

Flexural toughness, T_b, is a similar concept to the fracture energy and is an important material property of concrete to measure ductility. It relates to the ability of concrete to absorb energy after the formation of the first crack. Flexural toughness for a typical UHPFRC mix with and without fibres was reported to be approximately 120 and 0.99 J, respectively (Le 2008). The inclusion of fibres in UHPFRC and bond strength was reported to have significant beneficial effect on this parameter. However, increasing the

fibre content to a very high percentage, i.e. 6%, might have an adverse effect and result in fibre balling which can reduce the workability. This was demonstrated experimentally where the ideal percentage was reported to be in range of 2 to 3.5% (Le et al. 2007). Furthermore, flexural toughness was reported to be influenced by the casting procedure, size of the specimen and method of testing depending on the stiffness of the machine (Ferrara et al. 2012). Higher values of fracture toughness were reported for smaller size beam specimens for the same concrete mix (Le et al. 2008). While closed-loop testing machine was found to be most suitable to perform this test (Majdzadeh 2003).

A number of standards and recommendations (ASTM C1018-97 1997, JSCE-SF4 1984) have provided guidance for the determination of flexural toughness of fibre reinforced concrete. Similar to the tensile flexural strength, investigating the flexural toughness of UHPFRC at various curing temperatures was found to be essential for the future cast in-situ application of this concrete.

2.6.3 Shear strength

In structural design, shear strength of plain concrete is almost zero due to its low tensile strength and brittle behaviour. Therefore, steel reinforcement in the form of stirrups or inclined bars is usually used in concrete members to enhance its shear strength. However, UHPFRC exhibits high tensile strength with improved ductility properties; this is known to enhance its shear strength significantly.

So far, numerous studies have investigated the shear capacity of steel fibre reinforced concrete (SFRC) and UHPFRC (Narayanan and Darwish 1987, Mansur et al. 1986, Theodorakopoulos and Swamy 1993, Tan and Paramasivam 1994, Harris 2004, Cheng et al. 2010, Moreillon et al. 2012). These studies have reported significant improvement in first crack and ultimate shear strength capacity of beams and slab-column connections of the concretes compared to those of normal concrete. The improved shear strength capacity of UHPFRC was reported to be mainly dependent on the tensile behaviour of the concrete. As previously reported, tensile behaviour of UHPFRC is improved substantially due to the inclusion of fibres in the mix. Various studies (Kwak et al. 2002, Harris and Roberts-Wollmann 2008) have reported fibre type, shape and distribution in

the mix influence the shear strength of the concrete considerably. Steel fibre types with elongated hooked or crimped ends were reported to provide better fibre pull-out and resist tension forces more than stocky or smooth fibres. Hence, the former types were reported to improve the shear strength considerably. Furthermore, a random distribution of fibres was reported to influence crack width, development, and propagations in UHPFRC members. As a result, casting procedure is known to affect the shear strength of this concrete significantly.

The shear behaviour of concrete is complex and difficult to analyse theoretically and experimentally. From extensive experimental investigations, reasonably simplified procedures for normal concrete design and analysis have been adopted in Eurocode 2 (BS EN 1992-1-1 2004). To date, a number of studies have developed semi-empirical equations for calculating the shear strength of FRC and UHPFRC (Narayanan and Darwish 1987, Imam et al. 1997, Ashour et al. 1992, Shaaban and Gesund 1994, BFUP AFGC 2002). However, these equations are limited to specific mix designs and found to be not very accurate. Furthermore, setting up experimental procedures to investigate this parameter in particular was also reported to be problematic. Thus, little on the punching shear capacity of UHPFRC is available in the literature. Since in concrete highway bridge design, punching shear strength is an important design criteria, detailed investigation on this parameter of UHPFRC was carried out in this study.

2.7 Durability Properties

Compressive strength has been the standard parameter used to determine the quality of concrete for construction. Increasingly, concrete durability has become an important property in modern concrete designs due to the high maintenance cost of normal concrete structures. Recently, more and more research has been conducted on investigating the durability aspects of concrete.

The durability properties of UHPFRC have been the subject of extensive studies (Cheyrezy et al. 1995, Richard and Cheyrezy 1995, Bonneau 1997, Bonneau et al. 2000, Schmidt and Fehling 2002, Graybeal 2006). The resulting studies reported significant improved durability properties of this concrete due to the excellent granular compactness

of its matrix. This has made the concrete to be an attractive material for structures where resisting the penetration of liquids, gas and other aggressive agents are of importance. Furthermore, total porosity of UHPFRC was reported reduce considerably with heat treatment due to the low and disconnected pore structures of fine powder materials in the mix. Pore sizes were reported to be nearly non-existent or very small, not greater than 0.1 mm (Cheyrezy et al. 1995). Thus, UHPFRC is known to be extremely resistant to chloride permeability, freezing and chloride attacks with reduced reinforcement corrosion risks.

The improved durability properties of UHPFRC may result in reducing maintenance costs compared to normal concrete. However, it has disadvantageous at the same time. The dense structure of the matrix could lead to poor fire performance since there is little extra void space for gaseous expansion. However, using a combination of steel and polypropylene fibres in the concrete was found to be a good solution to overcome this problem (Schmidt et al. 2003).

2.8 Applications

The applications of UHPFRC have increased over the last decade. However, most of its applications have been predominately in the construction of small scale structures, such as footbridges, durability resistance coatings, protective panels, and architectural applications (Rebentrost and Wight 2008b). In this section, some of its worldwide applications are presented.

The first significant structure to be built with this material was the footbridge in Sherbrooke, Quebec, Canada in 1997 (Dowd and Dauriac 1996, Blais and Couture 1999). Following this, several other footbridges were built entirely or partially with UHPFRC such as the Footbridge of Peace in South Korea, Sakata Mirai and Yokemuri Footbridges in Japan, Papatoetoe and Penrose Footbridges in New Zealand, and Gartnerplatz Footbridge in Germany (Schmidt and Fehling 2002, Fehling E et al. 2004, Vergoossen 2008, Rebentrost and Wight 2008b, Lafarge 2012). In addition, UHPFRC has also become popular for highway bridge applications. Recently, a number of short span highway bridges have been constructed, such as the Bourg-lès-Valence bridges in

France, Shepherds Creek bridge in Australia and the Mars Hill-Cat Point Creek with Jackway Park Bridges in the USA (Hajar et al. 2004, Rebentrost and Wight 2008b, Ahlborn and Steinberg 2012). Furthermore, UHPFRC has been used successfully for the rehabilitation, widening and strengthening a number of existing highway bridges in Switzerland and France (Samaris 2005, Thibaux 2008, Brühwiler and Denarié 2008). Some of the footbridges and highway bridges described above are shown in Figure 2.5.

Figure 2.5: Applications of footbridges and highway bridges of UHPFRC: (a) Footbridge of Peace in South Korea, (b) Bourg-lès-Valence highway bridge in France, (c) Gartnerplatz footbridge in Germany, and (d) Shepherds Creek bridge in Australia (Dowd and Dauriac 1996, Hajar et al. 2004, Vergoossen 2008, Rebentrost and Wight 2008b).

UHPFRC has also been an excellent choice for durability applications and have been used widely (Behloul et al. 2008). In the Cattenom Nuclear Power Plant in France, more than 2000 prestressed UHPFRC beams and girders were used for the exchange body of a cooling tower. For this project, UHPFRC was chosen to ensure durability to withstand freeze-thaw cycles in cold weather (Voort et al. 2008). In addition, UHPFRC has been

used to resist aggressive environmental conditions such as in offshore structures. It was reported (Behloul et al. 2008) that more than 6000 plates of UHPFRC were used to stabilize a sea wall on Reunion Island in France. Moreover, this concrete has been reported to exhibit outstanding blast resistance, making it ideal against projectile impacts. In Australia, protection of government and important facilities are protected using UHPFRC panels (Rebentrost and Wight 2008a). In Figure 2.6 some of the applications of UHPFRC for durability and explosive resistance are presented.

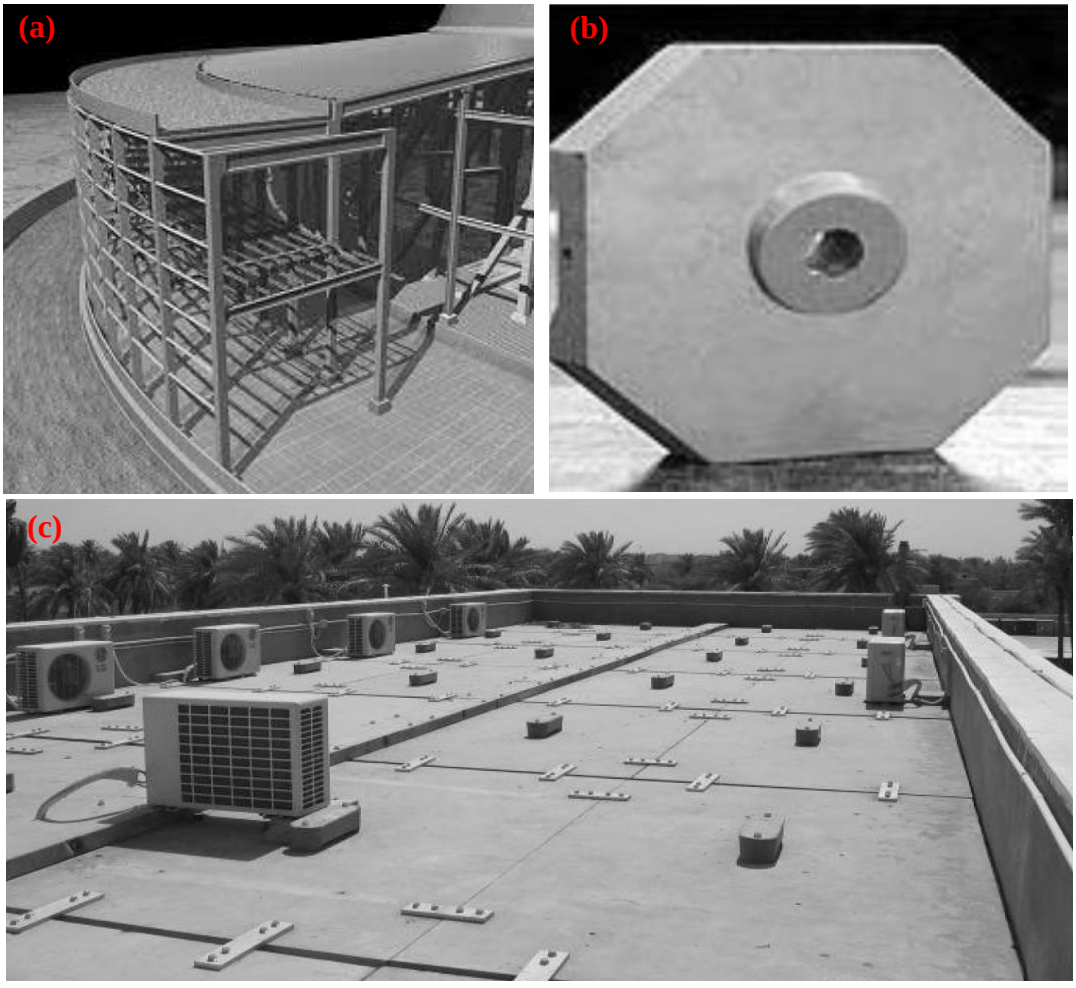

Figure 2.6: UHPFRC durability applications: (a) Cattenom cooling tower in France, (b) Anchor plates for sea walls-Reunion Island in France, and (c) UHPFRC panels for protection of government facility in Australia (Acker and Behloul 2004, Voort et al. 2008, Rebentrost and Wight 2008b).

For architectural design, this concrete provides access to unexpected new shapes and volumes. It is architectural applications range from balcony slabs, staircases, bus stops

to facade panels and canopies. In Figure 2.7 a wide range of architectural applications of UHPFRC are presented.

Figure 2.7:UHPFRC architectural applications: (a) Spiral stair case in Denmark, (b) Shawnessy LRT Station in Canada, (c) Martel Tree sculpture in France, and (d) Toll plaza of the Millau Viaduct in France (Smallsmalls 2007, Aarup 2007, QAGOMA 2010, Lafarge 2012).

2.9 UHPFRC for Highway Bridge Applications

Highway bridges encounter high loads, cyclic loading and harsh environments. For such structures, UHPFRC with high strength and improved durability properties could be a good solution. However, so far, only a few highways bridges have been built using this material. This is due to the implication involved with the use of this concrete. In this

section, the advantages and limitations of UHPFRC for highway bridge applications are discussed.

2.9.1 Advantages

In highway bridge applications, UHPFRC is used for its improved mechanical properties, light self-weight, and superior durability. High compressive, tensile and flexural strengths along with a higher modulus of elasticity are desirable requirements for highway bridge designs. The compressive strength of UHPFRC is about four times that of normal strength concrete. This makes it possible to design slender members in highway bridge structures, particularly in the case of prestressed concrete members. This is illustrated in Figure 2.8, in which a UHPFRC, steel, prestressed concrete, and reinforced concrete beam with equal moment capacities are compared. It was reported (Voort et al. 2008) that the UHPFRC beam requires only half the section depth of the reinforced or prestressed concrete beams and the same section depth as the steel beam. A reduction of 70% or more of the UHPFRC beam weight was reported when compared to the prestressed and reinforced concrete beams. This can lead to a significant saving in dead load and thus essential savings in lower material consumption, lower transport costs, faster fabrication, and considerable environmental benefits.

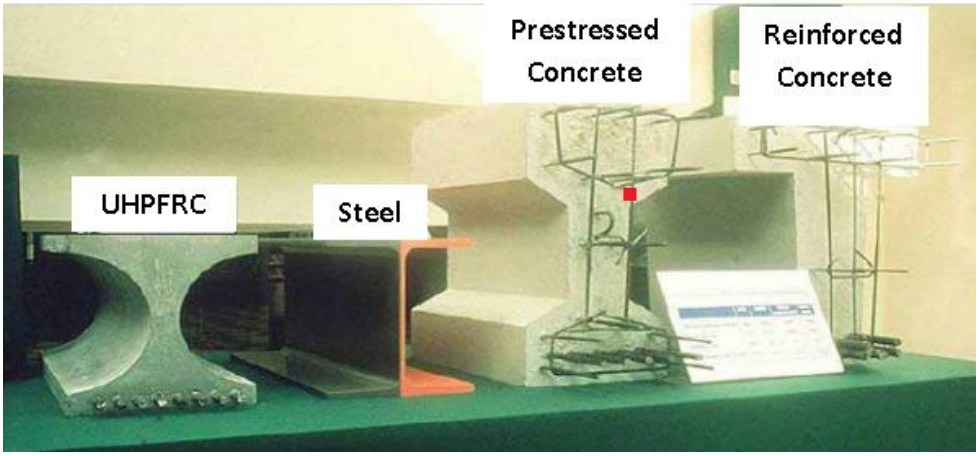

Figure 2.8: A UHPFRC, steel, prestressed, and reinforced concrete beams with equal moment capacities (Voort et al. 2008).

There are still more benefits of UHPFRC for highway bridge applications. For instance, longer span bridges with this material are achievable to construct. This can reduce the number of piers and foundations. Furthermore, the use of fibres in the concrete could be used to reduce or even eliminate the need for steel reinforcement in the members. This can lead to the reduction of high labour costs and construction management.

As noted previously, another potential use of UHPFRC in highway bridge applications is for the rehabilitation and widening existing concrete bridge structures which has been applied successfully in the past. The rehabilitation construction cost of UHPFRC was reported to be about 10% more expensive than conventional solutions (Samaris 2005, Brühwiler and Denarié 2008). However, the improved structural and durability properties ensure lower maintenance costs and a longer design life of the bridge compared to conventional concrete.

Many studies have investigated the potential use of UHPFRC in various ways for bridge applications. This ranges from ribbed deck slabs to box girders and prestressed π and bulb-tee shaped precast beams. Optimised UHPFRC precast bridge decks in a waffle configuration has been investigated by the Iowa Department of Transportation (Iowa DOT) and Wapello County in the US (Bierwagen et al. 2009). It was reported (Bonneau et al. 1996) that a UHPFRC box girder with the same dimensions and load requirement could be constructed with only one third of the amount of material compared to normal concrete. Moreover, various precast prestressed girders such as π and bulb-tee shapes have been used in short span highway bridges in the US. The benefit of using such shapes is reported to minimise the cross section of the beams by taking advantages of the advanced properties of the material.

To date, limited studies on the potential use of UHPFRC for highway bridge applications have been carried out and majority of this work was conducted in the United States by the FHWA (Federal High-Way Administration) (Graybeal 2007a). It is, therefore, evident that more research in this area of study needs to be done.

2.9.2 Limitations

Despite its excellent mechanical and durability properties, the application of UHPFRC in practise is currently hampered, particularly for highway bridge structures. While the few short span highway bridges have served to validate the performance of the material, UHPFRC is still not widespread in large structural applications. The main reasons are due to its high initial cost and lack of design codes for structural applications.

The constituents of UHPFRC are expensive, in particular the steel fibre content. It was reported (Kim et al. 2008) that 1% of steel fibres by volume in the mix cost more than the entire cement matrix. This makes the material extremely expensive compared to other type of concretes. However, a different study (Stengel and Schießl 2008) has recommended the use of less expensive steel fibres, such as larger diameter steel fibres to minimise the cost of UHPFRC, both environmentally and financially. Despite the high material costs, the current precast production of the concrete contributes to its high cost significantly. Storing UHPFRC members for at least 48 hours and applying heat treatment in factories results in increasing the cost considerably. Therefore, investigating potential ways to minimise the cost by utilizing this material for cast in-situ applications is essential. So far, very little has been done in this area of research and further studies are required.

The cost of UHPFRC has been reported to be several times greater than that of conventional strength concrete. According to various studies at different times (Bonneau et al. 1996, Blais and Couture 1999, Semioli 2001) prices quoted range from $750 to $1500/m^3. A more recent study (Cousins et al. 2008) estimates the price to be between $1829 to $2222/m^3. Compared to the price of normal strength concrete (50 MPa) from Easy Mix Concrete with a rate of $150/m^3, this is approximately 10 to 15 times more expensive on a volumetric basis. However, in most cases, the volume of UHPFRC required to meet strength criteria will be less than that of normal strength concrete, thereby, reducing the initial costs significantly.

In addition to its high cost, the lack of design codes/standards to provide guidance to engineers in the design of highway bridges is another significant challenge. In recent

years, there has been progress in different countries to develop interim design guidelines for this material (BFUP AFGC 2002, JSCE-USC 2006) . However, current design specifications are mainly based on conventional concrete standards. This requires members to have certain minimum dimensions, which results in over designed members and, thus, unnecessary increase in overall cost of UHPFRC structures. Therefore, until a recognised standard is specifically developed for UHPFR and finalised, the application of this material in large scale structures will be limited.

2.10 Finite Element Modelling (FE)

The finite element analysis (FEA) originated from the need for solving complex linear and nonlinear problems in engineering applications. Since its development in the late 1940's, various finite element software packages for aerospace, mechanical and civil engineering have been developed. So far, a number of sophisticated software packages like Abaqus, ANSYS, and DIANA have been used to study the linear and nonlinear behaviours of UHPFRC (Grohmann and Zimmermann 2008, Lohaus. L et al. 2012, Schnellenbach-Held. M and Prager. M 2012). These FE software packages can be used for detailed simulations of the structures, identify critical components and helps to estimate the distribution of stress and displacement at very low cost.

From the literature survey, Abaqus is seen to be the most widely used software for UHPFRC. This software has an extensive library of material models that can be used for modelling the structural behaviour of this concrete successfully (Chen and Graybeal 2010, Mahmud et al. 2012).

Since UHPFRC is becoming more popular in structural applications. Detailed studies regarding its material and structural behaviour in every aspect are vital. While experimental work is expensive and time consuming, FE analysis can be used to study more variables. Therefore, the present work aims to contribute to this ongoing research effort. For this purpose, finite element analyses using Abaqus have been carried out in this study. The analysis aims to predict the structural behaviour of beam and slab specimens in flexure and shear. In the meantime, experimental works were conducted to examine the accuracy of the FE models.

2.11 Summary

Over the past two decades, considerable efforts to improve the behaviour of cementitious materials have led to the development of a concrete known as ultra high performance fibre reinforced concrete (UHPFRC). This material is a new type of concrete that offers the unique combinations of improved strength, ductility and durability properties compared to all the other type of concrete. Since becoming commercially available, UHPFRC has the potential to influence many applications in structural designs. It allows for aesthetically pleasing, lighter and longer lasting concrete structures that have not been able to be constructed before. Despite all this, its application has been limited in large scale structures, such as in highway bridge applications. This is mainly down to its high initial cost and lack of design standards. To date, a very limited number of studies have investigated the potential use of UHPFRC for highway bridge designs. Therefore, detailed studies on UHPFRC from its material properties to cost and its structural behaviour for highway bridge applications are required.

Chapter III: Material Characterisation

3.1 Introduction

To date, a number of UHPFRC mixes have been reported in the literature. Each of these varies in their constituents and strength. The UHPFRC mix that was adopted in this PhD study was developed by a previous research study at the School of Engineering, University of Liverpool (Le 2008). Some of the mechanical properties of this mix have been reported in the literature (Le et al. 2007, Le 2008, Yang et al. 2009, Millard et al. 2009, Barnett et al. 2010). However, its material behaviour in tension and compression is still not fully studied. Therefore, this study attempts to define the stress-strain relationship in tension and compression, as both properties are required for the design of any structural elements or FE analysis.

As noted in the literature review, UHPFRC exhibits unique tensile and compressive behaviour. This includes significant strain hardening and softening behaviours compared to conventional concrete. The determination of these properties requires appropriate test methods that are different to those that have been used for normal concrete. Therefore, in this study, suitable test methods to obtain both properties with a high degree of accuracy were investigated. Initially, standard tests used for normal concrete such as the splitting, flexural and compression tests were used for UHPFRC. However, the results obtained showed inconsistency of the test methods, hence, modifications and the development of new test methods were required.

In this study, two direct test methods were developed and used in detailed experimental investigation. The material's initial linear-elastic modulus, stress-strain values and post peak behaviour in both tension and compression were studied. The effect of steel fibres on strength and ductility at different ages were investigated. Furthermore, results obtained from the traditional tests were compared to those from the direct tests and the accuracy of the tests procedures was studied. Finally, from the direct test results, constitutive material model for the UHPFRC mix was determined and used in detailed numerical modelling.

3.2 Tensile Behaviour

The tensile behaviour of plain concrete is of prime importance for the design of structures at serviceability limit state, such as slabs, prestressed members, estimating cracking loads and water retaining structures. However, it is usually ignored or not used directly in designs due to its low value. Therefore, steel reinforcement is used to enhance this property of concrete. In contrast, the tensile behaviour of UHPFRC varies significantly than those of normal concrete. The strain hardening and softening behaviour reported for UHPFRC can be exploited and used in structural designs. The tensile behaviour of UHPFRC could be as important as its compressive behaviour; therefore, understanding this behaviour is vital in structural design.

Generally, the tensile strength of normal concrete is determined using three types of test methods. These are the direct tension test, the splitting tension test and the flexural test. The direct tension test is usually performed by testing concrete specimens in uniaxial tension such as notched cylinder or beam specimens. While the splitting tension and flexural tests are performed on cylinder and beam specimens in indirect tensile tests. The results on the tensile behaviour of UHPFRC found in the literature are mainly derived from indirect tests. However, indirect test methods cannot accurately capture the true tensile behaviour of steel fibre reinforced concrete. Therefore, in this study, both direct and indirect test methods were used to characterise the tensile behaviour of the concrete and the results were compared to each other and the literature. In the following sections, the suitability of a number of direct and indirect testing methods for UHPFRC is described, assessed and conducted.

3.2.1 Uniaxial tensile test

The uniaxial tensile test, also known as the direct test, is the most suitable test method to capture the true tensile strength of concrete accurately. This is because in this test concrete specimens are tested in a direct application of a pure tension force and the true stress-strain values are determined. In the uniaxial tensile test, the entire volume of the specimen is subjected to the maximum stress and the possibility of failure at a weak element occurring is high. However, performing this test free from eccentricity is very difficult, careful consideration and detailed preparations is required (Benson and

Karihaloo 2005b, Mallat and Alliche 2011, Neville 2012). Therefore, due to its complexity it is rarely performed.

For this test, notched and unnotched concrete specimens of cylinder, beams and dog-bone shaped samples are used. So far, a number of studies have attempted to develop suitable and repeatable uniaxial test methods to capture the stress-strain relationship for normal concrete and fibre reinforced concrete (Morris and Garrett 1981, Saito 1983, Wang et al. 1990, Rossi 1997, Li et al. 1998, Graybeal 2005, Benson and Karihaloo 2005b, Mallat and Alliche 2011). However, so far, standardised procedures are not currently available for the design and implementation of this test.

From the literature survey, it is evident that this test is much easier to perform for normal concrete than UHPFRC. This is because normal concrete fails in a brittle manner and failure is governed by the formation of a single crack in tension. However, the strain hardening behaviour of UHPFRC due to the steel fibre content makes this test more challenging, in particular, once multiple cracks have occurred. To obtain acceptable results from a direct tensile test, the testing criteria should satisfy the following:

- Finding a suitable specimen shape and size to ensure a near pure tensile loading condition is achieved.
- Sufficient rigidity in the testing apparatus, so that when crack formation starts, it does so uniformly across the width of the specimen.
- Suitable measuring devices, i.e. scanning rate of the data output, so that post-crack response is measured accurately.
- Avoid notched specimens to minimise stress concentration and ensure the application of load without eccentricity, such that a pure tensile stress condition is achieved.

To achieve the above criteria, a great deal of research and engineering precision is required. However, in this study, a direct test method was developed and used to determine the uniaxial tensile stress-strain relationship for this specific UHPFRC mix design. The test program was an agglomeration of the testing techniques that were found

in the literature. For the test, dog-bone shaped specimen was selected and the shape of the specimen was used so that a uniaxial stress field was created through the central section of the specimen and localisation of cracks and failure occurs in this area.

3.2.2 Splitting tensile test

The tensile splitting test, also known as cylinder splitting test, indirectly measures the tensile strength of concrete. It is an easy test to perform and widely used due to its simplicity and commercially available equipment. For this test, cylinder specimens, the same that are used for compressive strength determination are used.

In this test, a cylinder specimen is placed with its axis horizontal and compressed with a line load along its entire length. The load is increased until maximum tensile stress develops at the centre of the specimen and failure occurs in the form of splitting along its vertical diameter. The British Standard BS EN 12390-6:2009 indicates that the maximum tensile strength for a normal concrete cylinder specimen can be calculated based on Equation 3.1.

$$f_{ct} = \frac{2F}{\pi L d} \qquad \text{Equation 3.1}$$

where f_{ct} = tensile splitting strength (MPa),

F = maximum load (N),

L = length of the line of contact of the specimen (mm), and

d = diameter of the specimen (mm).

Splitting test is preferable for materials with brittle behaviour only such as normal concrete, where complete failure occurs with a single crack. So the peak load attained during the test can be used to determine the tensile strength of the concrete. Results from this test have to be carefully analysed due to the direct punching which may occur during the test and can influence the accuracy of the result.

This test is not recommended for steel fibre reinforced concrete, in particular UHPFRC. This is due to the tensile behaviour of the concrete after the formation of cracks, the strain hardening behaviour. Furthermore, in this test, the specimen is subjected to a complex combination of shear, tension, compression stresses with significant stress gradients which may lead to an inaccurate tensile strength result(Mallat and Alliche 2011, Graybeal 2005). The local zones of high compressive stresses at the extreme fibres of the specimen usually result in higher values than the actual tensile strength of the concrete. Thus, standards such as the ACI committee 544.2R, hardly recommends the use of this test on steel fibre reinforced concrete.

The cylinder splitting test for normal concrete is defined by many standards (ASTM C496-96 1996, BS EN 12390-6 2009). The test can also be conducted using cube specimen. However, the BS EN 12390-6:2009 standard restricts this test to cylindrical specimens only. This is because results of this test were found to be dependent upon the shape and size of the tested specimen. Splitting tensile strength of 150 mm cube specimens were reported to be lower than those of 100 mm sizes. While little variation for different size of cylinder specimens were reported. Furthermore, cube specimens were found to result in higher measured tensile splitting strengths than the cylinders by approximately 10%. Thus, for this test, UHPFRC cylinder specimens were tested according to the BS EN 12390-6:2009 standard for normal concrete. In this research, splitting test was performed for comparison reasons only. The results were compared to those determined from the direct tensile test.

3.2.3 Flexural test

The flexural test is another indirect tensile test which has been used commonly to determine the tensile strength of concrete in the absence of direct tensile tests. This test is performed on beam specimens using two different loading configurations, three and four point bending. In this test, a beam specimen is subjected to flexure until failure occurs.

In this study, the tests were conducted in accordance with the JSCE-SF4 in a four point bending configuration (JSCE-SF4 1984). During the test, load and deflection is usually recorded and the tensile flexural strength is determined using Equation 3.2.

$$\sigma_b = \frac{P_u\, l}{b\, h^2} \qquad \text{Equation 3.2}$$

where σ_b = tensile flexural strength (MPa),

P_u = ultimate load (N),

l = length of the beam specimen (mm),

b = width of the beam specimen (mm), and

h = height of the beam specimen (mm)

It must be noted that Equation 3.2 is based on elastic beam theory in which linear elastic stress-strain behaviour up to failure is assumed. In this theory, the tensile stress in the beam is assumed to be proportional to the distance from its neutral axis and the stress block is triangular. However, concrete is a non-linear material and the assumption of a linear stress distribution and the behaviour at peak load is elastic are not correct. The actual shape of the stress block under loads nearing failure is reported to be parabolic not triangular for a flexural beam test (Neville 2012). Therefore, results obtained using this method overestimates the actual tensile strength of the concrete and is always greater than the direct tensile strength for the same concrete. Furthermore, in this test, the maximum fibre stress reached on the tensile side of the specimen will be higher than in direct tension due to less stressed sections nearer to the neutral axis which blocks the propagation of a crack. Therefore, empirical relationships exist to relate the tensile flexural strength to the direct tensile strength of the same concrete and researchers have different views on these models. It is important to notice that the acceptance of this test for concrete can be related to the difficulties that are encountered with the uniaxial tensile test.

Detailed guidance for performing this test for concrete and UHPFRC is provided in several standards and recommendation (JSCE-SF4 1984, ASTM C293-94 1994, BFUP AFGC 2002, BS EN 12390-5 2009, BS EN 14651:2005+A1:2007 2008). Further

discussion regarding the suitability of this test for estimating the tensile strength for concrete can be found in the literature (Neville 2012). In this study, flexural test was conducted and the results were compared to those reported from the uniaxial tensile tests.

3.3 Compressive Behaviour

As described earlier, the compressive behaviour of concrete is characterised by its compressive strength, modulus of elasticity, and Poisson's ratio. These properties are determined from direct compression test, which is an easy test to perform and widely available for normal concrete. In this study, attempts to determine the uniaxial compressive stress-strain relationship and the modulus of elasticity for the UHPFRC were conducted. The experimental techniques that are available to determine both properties are discussed below.

3.3.1 Uniaxial compression test

The most common test on hardened concrete is the compressive strength test. Many recognised standards have provided detailed guidance for the measurement of the compressive strength and modulus of elasticity for normal concrete using cylinder and cube specimens (BS 1881-121 1983, ASTM C469-02 2002). This study has followed the test configuration described in the BS 1881-121 and ASTM C469-02 for the determination of the compressive stress-strain relationship and modulus of elasticity of this UHPFRC. However, the test methods proposed in both standards were found to be unsuitable, especially in the measurement of post-cracking behaviour of the concrete. Therefore, modifications to the standard tests were applied and a simpler test method was developed and proposed.

3.4 Experimental Procedure

This section describes the materials, mixing, casting and curing procedures for the UHPC and UHPFRC mix designs used in this PhD study. The materials and procedures were the same for all the experimental work conducted in this study, except when reported otherwise.

3.4.1 Materials

The UHPFRC mix design used in this study was developed by a previous research study at the School of Engineering, University of Liverpool (Le 2008). Table 3.1 shows the mix proportions.

Table 3.1: Mix design for UHPFRC.

Material	(kg/m^3)
Cement (CEM1: 52.5N)	657
GGBS	418
Silica fume	119
Silica sand (average size 0.27 mm)	1051
Superplasticisers	40
Water	185
Steel fibre (2% volume)	157

A brief description of each material used in the mix is presented below.

3.4.1.1 Portland cement (PC)

High strength Portland cement type CEM1 with a strength class of 52.5N was used. This type was used to provide rapid strength gain at early age. The cement was manufactured by the Hanson Heidelberg Cement Group.

3.4.1.2 Ground granulated blast-furnace slag (GGBS)

The GGBS used in the mix was supplied by Appleby Group Limited (Civil and Marine). This material was used as a partial cement replacement in the mix. Further studies on acceptable amounts of GGBS in UHPFRC can be found in the literature (Yazici 2007, Le et al. 2007).

3.4.1.3 Silica fume (SF)

The silica fume (SF) used in the mix was the undensified type. It was supplied by Appleby Group Ltd. The material had a bulk density of 250 to 300 kg/m^3. The undensified type was chosen over the densified type for economic reasons only. Similar to the GGBS, this material was used as a partial cement replacement in the mix.

3.4.1.4 Silica sand

The silica sand in this mix had an average particle size of 270 microns. The material was manufactured by WBB Minerals UK. The void content and water absorption was reported to be approximately 38% and 1.1%, respectively.

3.4.1.5 Superplasticisers

The polycarboxylate-based superplasticiser known as Structuro 11180 was used. The material was supplied by FOSROC Ltd and had an active solid content of 25% by weight.

3.4.1.6 Water

Normal tap drinking water was used for mixing.

3.4.1.7 Steel fibres

The steel fibres in the mix were made from carbon steel. This type has a high tensile strength of 2000 MPa. It was a straight type fibre of 13 mm in length and 0.20 mm in diameter, supplied by Bekaert Ltd. The shape of the fibres is shown in Figure 3.1.

Figure 3.1: Straight carbon steel fibres.

The fibres have a thin brass coating, which is applied during the drawing process. However, virgin fibres may be gold-coloured. This coating disappeared during the

mixing process and was no longer clearly visible during the casting of the UHPFRC specimens. For all the studies conducted in this research, fibre dosage was limited to 2.0% by volume.

3.4.2 Mixing

For the mixing process, materials were weighed and placed in a horizontal pan mixer in the following order: silica fume, cement, GGBS and silica sand. The materials were first dry mixed for nearly 5 minutes until the dry mix appeared to be properly mixed, as shown in Figure 3.2 (a). Then, water with superplasticiser, previously mixed together was added to the mix and the mixing process continued for a further 10 minutes until the dry powder mix had transformed into a wet paste concrete. At this stage, the mix is known in this study as ultra high performance concrete (UHPC) since steel fibres are not included. For any parts of this study where the effect of steel fibres on the mechanical and structural behaviour of the material was investigated, UHPC specimens were cast. However, for UHPFRC, the mixing process was continued and steel fibres were slowly added to the UHPC mix. The mixing process was continued for at least 2 minutes to ensure proper dispersion of fibres in the mix. A 100 litre capacity pan mixer (Croker Cumflow RP100) was used for nearly all the mixes. The mixing process is shown in Figure 3.2.

Figure 3.2: Mixing process: (a) dry mix, (b) the wet concrete (UHPC), (c) steel fibres inclusion, and (d) UHPFRC.

3.4.3 Casting

After mixing, flow table measurements and the casting process for both concrete mixes were completed. The casting of UHPC specimens was just like normal concrete, while the UHPFRC specimens were not very different.

The UHPC specimens were cast into their moulds manually using scoops in one layer without any tamping. Similarly, for the UHPFRC cube specimens, the moulds were filled from the top. However, for beam and slab specimens, the concrete was always placed in one end of the mould and allowed to flow to the other end. This was conducted to ensure random fibre distribution in the specimen. After casting, both concretes were compacted on a vibrating table for nearly one minute. It must be noted, this is a self compacting concrete and vibration is not required. However, the vibration process was applied during this study to follow on the research study previously conducted at the

University of Liverpool (Le 2008). Following the vibrations process, curing process commenced. The casting method of UHPFRC has been reported to influence the tensile strength significantly (Moreillon et al. 2012). Therefore, the casting process was kept the same for both concrete mixes for all specimens made throughout this study.

3.4.4 Curing

After casting, specimens for both concretes were covered with damp hessian and polythene sheets, and kept at laboratory temperature (approximately 20 ^{o}C) for the first 24 hours. Demoulding took place at approximately 24 hours, once initial setting had occurred. After demoulding, specimens were placed in a curing tank in an elevated temperature of 90^{o}C for the next 48 hours. In this study, this process is known as normal high temperature curing. After temperature curing, all the specimens were dry kept at laboratory temperature until their testing days.

3.5 Specimen Preparation

For the tensile and compression tests, all the UHPC and UHPFRC specimens were cast and cured as described in Section 3.4. Specimens for both concretes were tested at 7, 14 and 28 days after casting. To eliminate variations in the testing procedures, the same equipment and procedures were used at all times. Detailed discussions regarding the development and complication involved with each test methods used here are provided below.

3.5.1 Tension tests

3.5.1.1 Uniaxial tensile test

For this test, two unnotched dog-bone shaped specimens of slightly different geometries, each with an overall length of 200 mm, were cast. The cross section of the specimens starts with 50 x 50 mm and changes to a prismatic shape of 26 x 50 mm after either 25 or 50 mm away from each ends of the specimens, as shown in Figure 3.3.

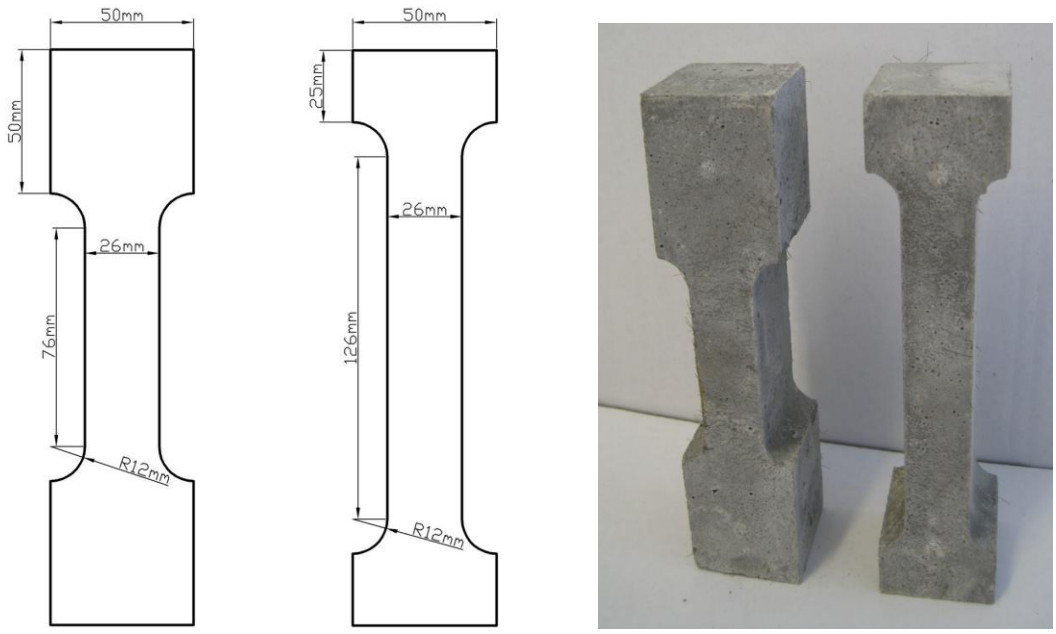

Figure 3.3: Dog-bone shaped specimen geometries.

The width of the tapered cross section was chosen to be equal to at least two fibre lengths (26 mm). This is in order to avoid fibre balling, ensuring random fibre distribution and enabling failure in this part of the specimen. The lengths of the reduced cross section were set as 126 and 76 mm, respectively, in order to examine the effect of different lengths on the test results.

Preparation of the test involved designing a jig and two square steel end plates connected to 12 mm diameter steel rods. The end plates were designed to grip the specimen at both ends, so the tensile load can be applied during testing. The cross-section of the end plates was 52 and 15 mm in width and depth, respectively. The specimens were held using the jig and the end plates were glued at each end of the specimen using epoxy resin, as shown in Figure 3.4. The epoxy was applied at least 24 hours prior to the test to allow maximum bond strength. Various types of epoxy were used until the right type (Epoxy Potting Compound) with sufficient strength was found. The jig setup was designed to minimise misalignment during specimen preparation and ensure a test setup free from eccentricity.

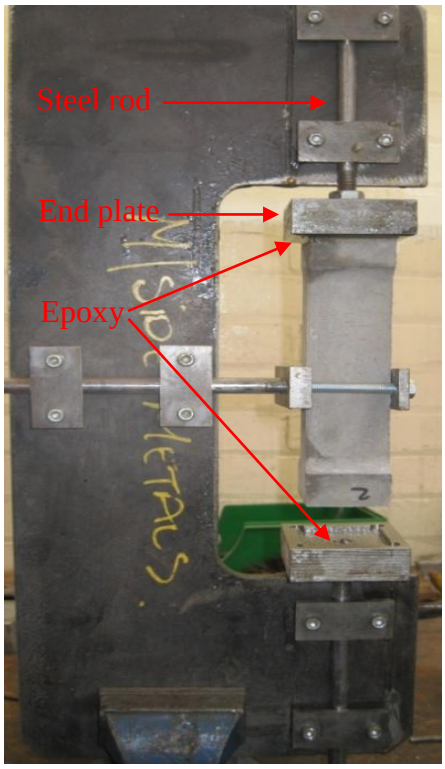

Figure 3.4: Dog-bone specimen held in jig.

This test was conducted using a Denison displacement control testing machine with a capacity of 100 kN. Rigid connections to the loading fixtures were used during testing to ensure the load was applied without eccentricity. Furthermore, two linear variable displacement transducers (LVDT's) were mounted on opposite sides of the specimen to measure displacement along the length of the narrow cross section. In this test, displacement control at a rate of 0.4 mm/minute was applied to the steel rods and the tensile load was transmitted to the specimen. The load-displacement diagram was produced digitally as the test proceeded, and the entire load-displacement curve in both the ascending and descending branches was recorded. Failure of some test occurred along the radius between the square and rectangular cross section of the specimen. This is due to stress concentration at these points. Results of these tests were declared void and not included here. The test setup is shown in Figure 3.5.

Figure 3.5: The uniaxial tensile test setup during testing.

The problem of misalignment could arise during testing. However, this was not evident in this designed uniaxial test. The LVDT readings on both sides of the specimen were analysed and found to be identical for the elastic stage of the test. However, with the formation of cracks on one side and propagating to the opposite side, bending was introduced to the tested specimen as expected. From this point onward, readings from the LVDT on the side of crack formation was taken to represent the true behaviour of the test. In the meantime, cross head movement from the testing machine was also recorded and compared to those obtained from the LVDT's.

Finally, before developing this test, a number of preliminary FE analyses were preformed to investigate the stress state of various geometry dog bone specimens. Elastic analyses using Abaqus were run with the values of modulus of elasticity and Poisson's ratio assumed to be 45 GPa and 0.2, respectively. The FE analysis was conducted using displacement control for the loading conditions and the test setup was assumed to be perfectly aligned. In Figure 3.6, the contour plot of von Mises stress distribution is shown for specimens with various geometries. It is evident that maximum

stress would occur at the reduced cross section of all the specimens. However, stress concentration in the curvatures of each specimen is very high. The third specimen in the figure appears to be performing better than the other two since higher stress concentration occurs in greater area of its reduced cross section. This trial FE analysis was run several times to find the most efficient reduced cross section and curvature line until the selected geometry of both specimens presented above were decided.

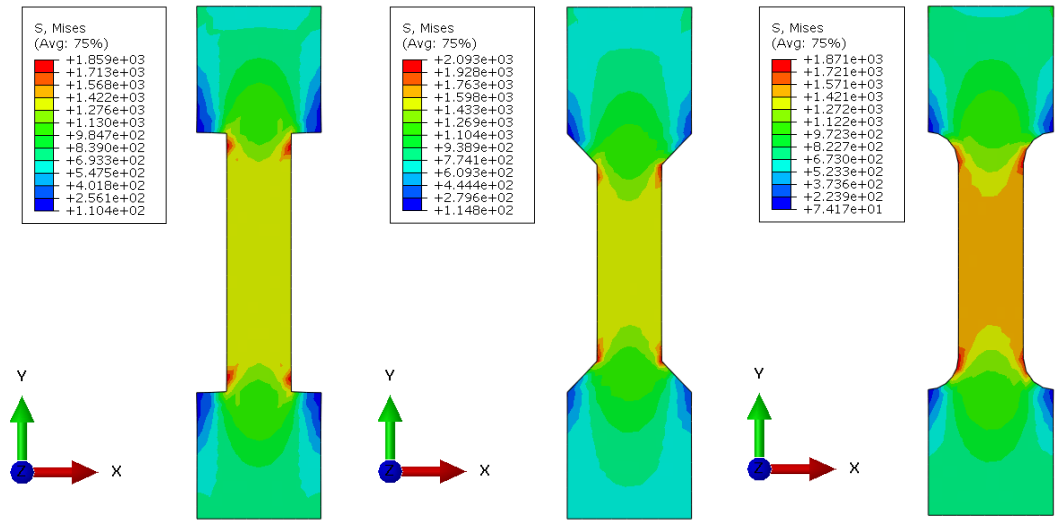

Figure 3.6: Preliminary FE analysis showing von Mises stress distributions for various specimen sizes.

3.5.1.2 Cylinder splitting test

This test was conducted according to the BS EN 12390 (BS EN 12390-6 2009)-6:2009 using cylinder specimens of 300x150 mm diameter. The specimen was held in a jig and hardboard packing strips were placed at the top and bottom as shown in Figure 3.7. The test was conducted using a ToniPACT compression testing machine with a capacity of 3000kN. A loading rate of 2.1 kN/second was applied until failure occurred. The failure of the specimen was defined by the testing machine; this is when an abrupt change in the specimen's lateral stiffness occurred.

Figure 3.7: Tensile cylinder splitting test setup.

In this test, the maximum load at failure was recorded and the tensile strength of both concretes was determined using Equation 3.1. Consideration was given to record the load-deformation relationship during this test. For the UHPC specimens, this appeared to be suitable since failure occurred in a brittle manner. However, direct punching on the failure line of the UHPFRC specimens were observed during the tests. After a few trial tests, results for UHPFRC appeared to be inconsistence and no further development of this test was carried out in this study. The specimen preparation and test setup is described in details in the standard (BS EN 12390-6 2009).

3.5.1.3 Flexural test

The flexural test was performed in a four-point bending test on beam specimen of 100x100x350 mm in width, depth and length, respectively. The test was conducted in accordance to the JSCE-SF4 standard (JSCE-SF4 1984). For this test, not a great deal of specimen preparation was required. The same testing machine and procedures that are followed for normal concrete were used for UHPFRC.

The test was performed under displacement control in a 250 kN Zwick testing machine. The machine was controlled by a constant deflection rate of 0.1 mm/minute over a span of 300 mm length. The midspan net deflection measured by two LVDT's mounted on

the opposite vertical sides of the beam specimen at the centre of the span. The deflection readings were averaged and recorded digitally against corresponding load values every 0.2 seconds. Furthermore, the surface of the specimens was painted white to better highlight the formation of fine cracks and their propagation. The test setup is shown in Figure 3.8.

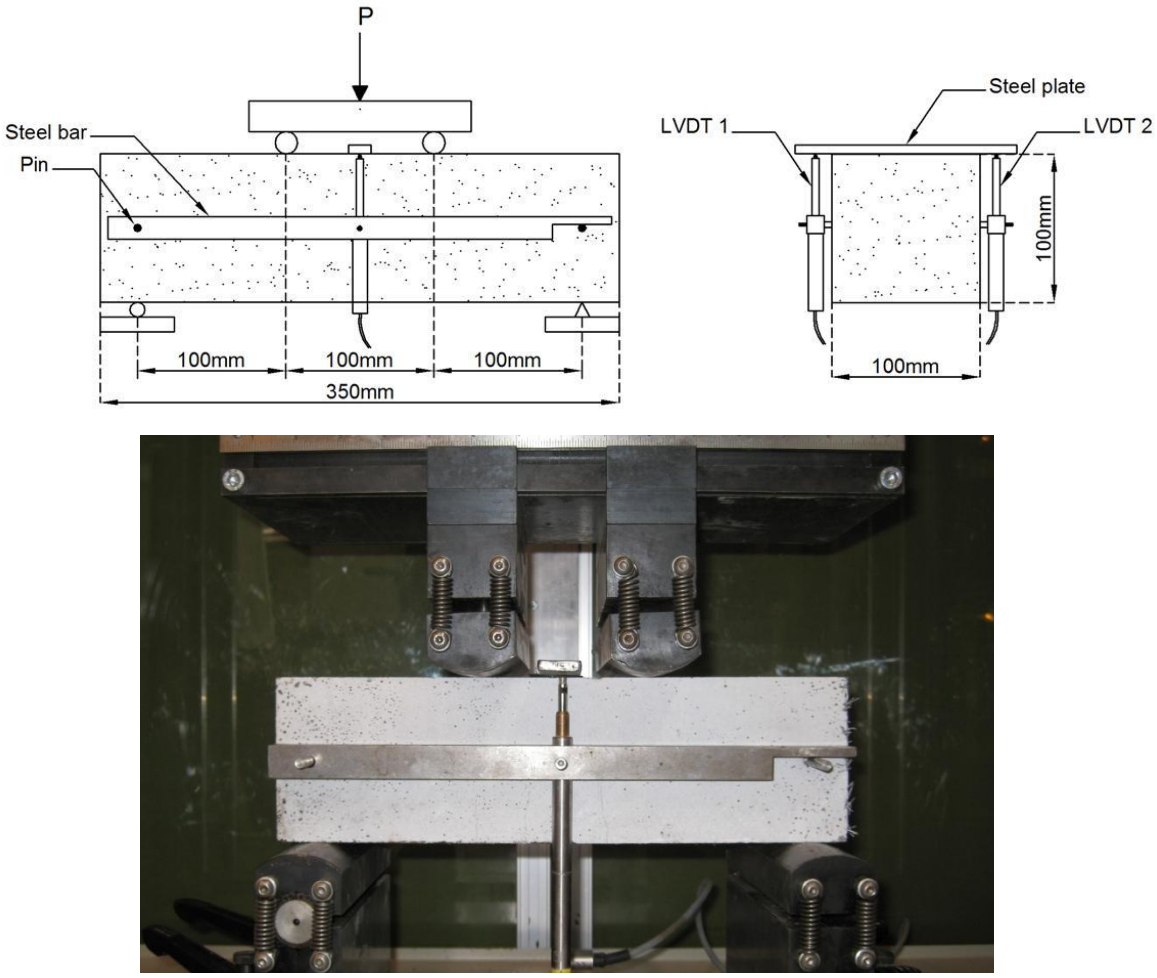

Figure 3.8: Flexural test setup for concrete beam specimen.

3.5.2 Compression test

3.5.2.1 Uniaxial compression test

The uniaxial compression test was performed on cylinder specimen of 100x50 mm in diameter. The test was performed using three different methods.

The first method was performed using the guidance from the BS 1881-121:1983. In this test, cylinder specimen was loaded at a rate of 0.5 MPa/second and deformation measurement was taken using electrical strain gauges. As this method is designed only for the determination of the static modulus of elasticity, it was unable to capture the post-cracking behaviour for the UHPFRC specimen. The strain gauges were detached from the surface of the specimen and came off at approximately peak strength due to concrete spalling and macrocrack formations, see Figure 3.9.

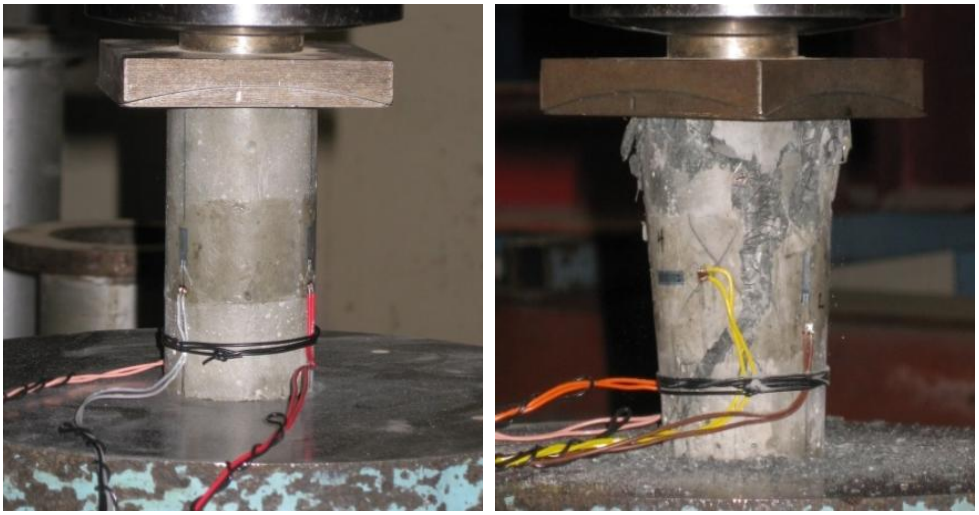

Figure 3.9: Uniaxial compression test in compliance with the BS 1881-121:1983 standard.

The second method was carried out in compliance with ASTM C469 using two rigid circular rings, which were secured at approximately two thirds the height of the specimen using clamping screws. The position of the circular rings on the specimen was chosen to take the platen restraint effect into account. The platen restraint effect occurs during compression test when both ends of the specimen are restricted to freely deform laterally due to the variation of the values of Poisson's ratio of the concrete and steel plates of the testing machine. Therefore, deformation measurement of the sample should be restricted to an area where this effect is not present, usually two thirds the height of the sample. In this test, two LVDT's were introduced between the rings and positioned on opposite sides of the specimen. Tests were conducted using a deflection control testing machine at a rate of 0.04mm/minute and measurements were recorded. This method was able to capture the stress-strain values up to the first crack strength for the

UHPFRC specimens (or ultimate strength for the UHPC samples). However, this method appeared to be unsuitable for capturing the post-cracking behaviour of the UHPFRC specimens. This is due to the movement and rotations of the clamping screws with the occurrence of shear line failure, see Figure 3.10.

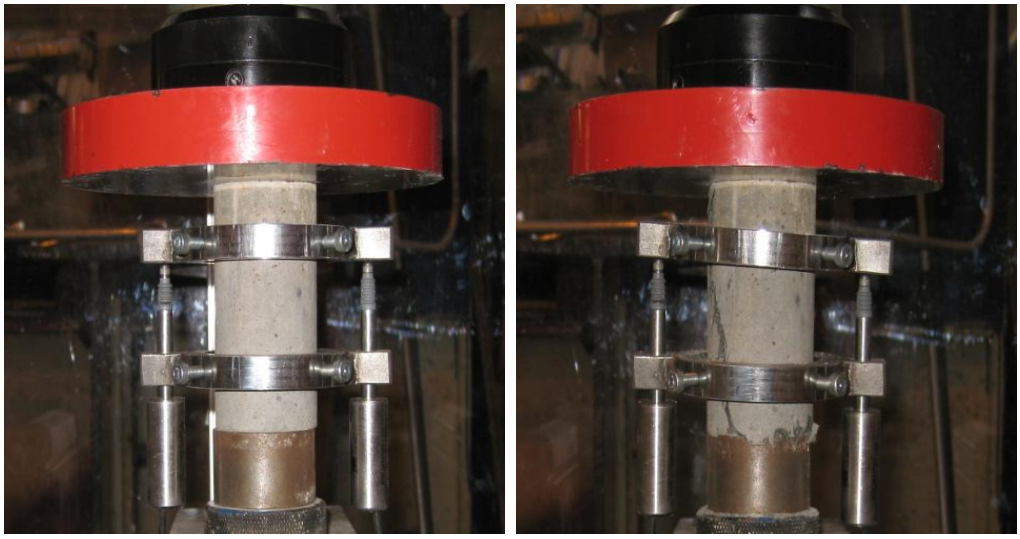

Figure 3.10: Uniaxial compression test in compliance with the ASTM C469 standard.

The results of the two methods described above, were not the true representative of the compressive behaviour of UHPFRC after initial cracking. Therefore, the third method of testing was proposed.

In this method, cross head movement of the testing machine was used to capture the compressive behaviour of the concrete. However, to take the platen restraint effect into account, similar to the ASTM Standard, circular rings with two LVDT's were mounted on the cylinder specimen to measure the elastic stage of the test. In this way, the effect of platen restraints from the testing machine which is very pronounced in the elastic stage of compression tests, were minimised and uniaxial compressive behaviour up till first crack was correctly measured. In addition, two more LVDT's were placed parallel to the specimen to measure the cross-head movement of the testing machine, and to record the post-cracking compressive behaviour of the concrete once the circular rings have started to displace and its measurement became unreliable, as shown in Figure 3.11.

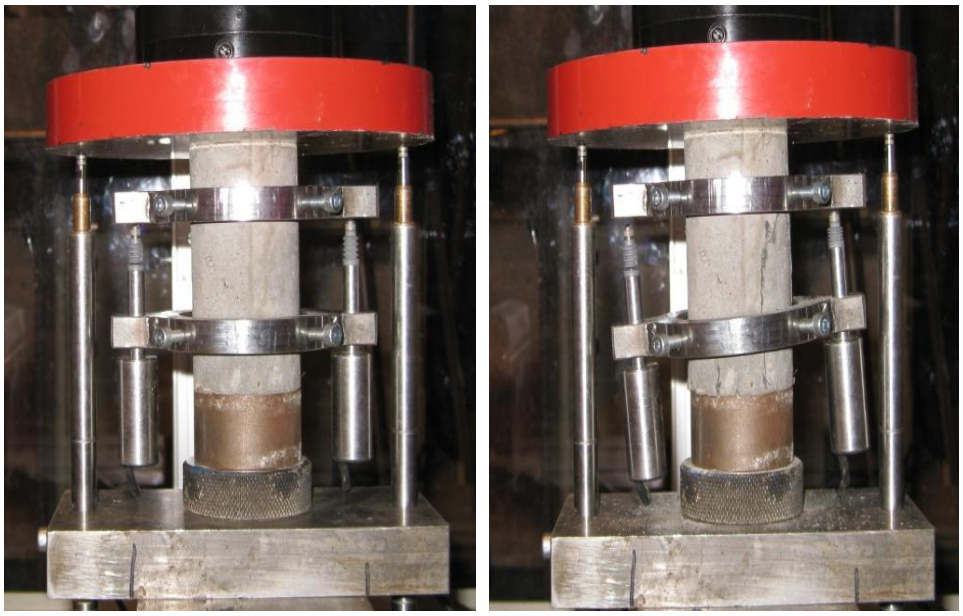

Figure 3.11: Uniaxial compression test setup in the modified test.

It must be noted that often cross-head displacement measurement are used alone for uniaxial compression test. However, this method is not reliable and results obtained usually overestimated the strain measurement and leads to a lower value for the initial elastic modulus due to the platen restraint effect. . Therefore, cross-head displacement measurement should always be used with the conjunction of some testing procedures where the elastic stage of the test is measured independently, i.e. the procedure discussed above.

In the third method, once the test was conducted, results from the cross-head displacement were amended until the initial elastic modulus and strain values in the elastic region were equal to the circular ring measurement. Then, results from both sets of readings were combined together to present the full stress-strain response of the material to plot the pre and post-cracking behaviour of the concrete. For UHPC, the circular ring method can be used only since total failure occurs with the formation of first crack. However, for UHPFRC, both methods have to be used together to maximise the accuracy of the results. The test setup is shown in Figure 3.11.

Furthermore, in this test, a pinned cross-head was employed for all the tests to avoid end constraint induced by friction between the rigid loading platen and the specimen (Lu and

Hsu 2006). Prior to each uniaxial compression test, the cylinder specimens were grinded according to the BS EN 12390-3:2009 to minimise uneven surfaces at both ends.

3.6 Results and Discussion

For each test in tension and compression, at least three specimens from both concrete mixes were tested and an average value is presented here.

3.6.1 Tensile behaviour

3.6.1.1 Uniaxial tensile strength

The uniaxial tensile stress-strain curves for UHPC and UHPFRC at various ages are shown in Figure 3.12. In this test, strain was obtained by dividing the average of the LVDT extension with the LDVT gauge length. Stress was obtained by dividing the machine load by the cross-sectional area of the narrow section of the specimen. From Figure 3.12, it is evident that both concrete have gained maximum tensile strength within 7 days. This maximum early age strength can be attributed to the curing regime. Failure of the UHPC specimens was very brittle and the presence of fibres in UHPFRC shown to be very important to obtain ductility and improve the tensile strength of the concrete. The first cracking and maximum tensile strengths of UHPFRC were approximately 170 to 200% of those of UHPC. Maximum tensile strain attained at peak strength was reported in range of 1.5-2.8‰ compared to the values of 0.15-0.20‰ for the UHPC. For the full test results see Table 3.2.

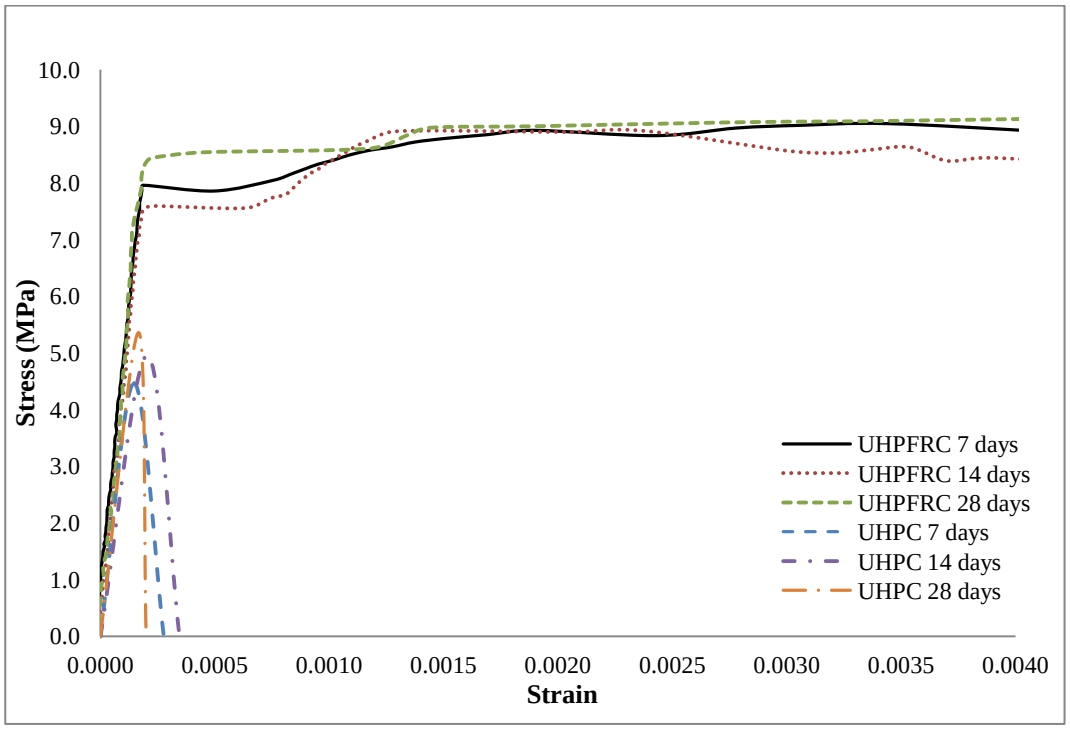

Figure 3.12: Uniaxial tensile stress-strain curve with respect to age for UHPFRC and UHPC.

The characteristic material behaviour for both concretes can be summarised below:

(1) Linear elastic phase: the initial modulus of elasticity with no permanent deformation takes place during this stage. The fibre content in this phase appears to have influenced the overall material behaviour, in particular, peak strength of the UHPFRC. At this stage, the major part of the tensile strength is achieved with a corresponding small deformation as shown in Figure 3.12. Both concretes behave very similarly in this phase and the values of the moduli of elasticity were identical.

(2) Crack developing phase: this phase follows the elastic phase, in which the first microcrack develops. At the start of this phase, the UHPC specimens fail rapidly at the weakest point due to the localisation of the maximum strain in a single crack which is greater than the strain limit of the matrix, see Figure 3.13(a). In contrast, stress is maintained in the UHPFRC specimens by the composite action of the steel fibres and the matrix. With the crack formation, the fibres transmit

the total tensile force across the crack and transfer it into the surrounding concrete along its interface. This process is known as the fibre bridging effect. The process takes place mainly in a relatively small volume of the concrete matrix surrounding the fibre. The fibres crossing the crack will resist further crack opening. In this stage, the tensile strength increases at a very small rate compared to the elastic phase and high deformation takes place with reduced modulus of elasticity. This phase is known as "pseudo strain hardening" or the "pseudo plastic" phase, meaning that no true plastic microstructural changes take place compared to those in a real plastic material (Spasojević 2008). From the beginning of this phase, the first cracking strength for the UHPFRC was determined and found to be in range 7.5 to 8.5 MPa. It is evident that steel fibres in the mix do not improve the modulus of elasticity significantly; however, the first cracking strength improves by a factor of 2.

The strain hardening behaviour distinguishes UHPFRC from all the other types of concrete. In this phase, a large number of microcracks developed along the entire length of the prismatic section of the specimen, see Figure 3.13(b). In this phase, crack width and opening are influenced by the presence of steel fibres in the mix. The crack propagation here is highly dependent on the effectiveness of the fibres in providing crack bridging. Stress is transferred by the fibres bridging across the faces of each crack. Sufficient bond between the matrix and the fibres is important in this phase as well as an even distribution of fibres. This phase ends when the fibres holding both sides of the microcracks are no longer capable of sustaining the maximum stress causing deformation or fibre pull-out to occur.

(3) Failure phase: this phase starts when the ultimate tensile strength of UHPFRC is reached at the end of the strain hardening regime. Deformation localises at the weakest point of the section when several microcracks combine to form a macrocrack, perpendicular to the direction of the extension as shown in Figure 3.13(b). The material behaviour at this stage is governed by the bridging mechanism of the discontinuous fibres in the mix. Generally, failure occurs due to debonding of the interface between the steel fibres and the matrix, and

subsequently causes the fibre pullout. However, in some cases, failure may occur due to fibre rupture if sufficient bond strength between the fibre and matrix exist. The latter one was rarely observed in this study.

From this point onwards the stress-strain curve can no longer be expressed as a function of average deformation, but of localised deformation. The measurement taken in this phase is known as crack mouth opening in which strain is no longer evenly distributed along the specimen. The crack mouth opening measurements was taken directly from the LDVT recording, as shown in Figure 3.14. The stress-crack opening response obtained in this phase is an important property of the concrete and it is an essential parameter for nonlinear FE simulation of UHPFRC beam and slab specimens. In this phase, quantities and properties of the steel fibres govern the shape and length of the stress-crack mouth opening curve and the ductility behaviour. The progressive fibre pull-out behaviour is heavily dependent on the length of the fibres. The limiting value of the crack mouth opening is typically related to half the length of the longest fibre in the mix, for this study 6.5 mm (13 mm steel fibre). Finally, the variation in the length of the prismatic sections (76 or 126 mm) of both specimens appeared to have no influence on the tensile strength of both concretes.

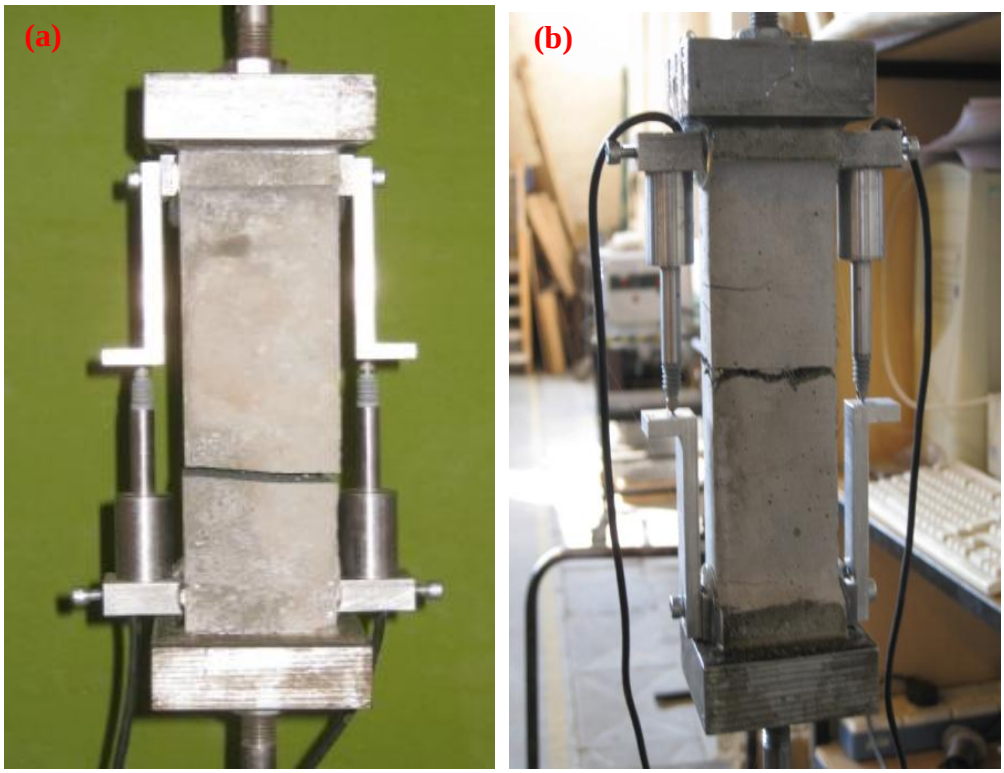

Figure 3.13: Uniaxial tensile tests: (a) UHPC failure. (b) Formation of macrocrack and post peak UHPFRC failure.

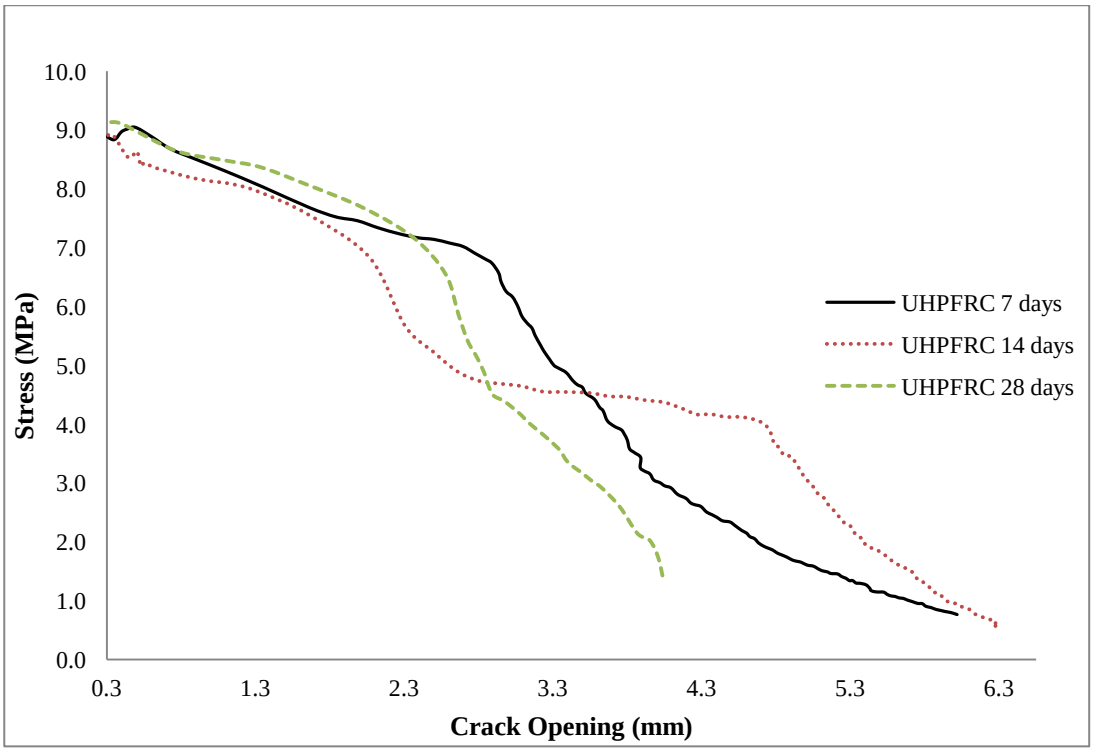

Figure 3.14: Stress-crack opening relationship for UHPFRC at different ages.

It must be noted that some of the UHPC uniaxial tensile tests exhibited very low tensile strength compared to the results reported in Table 3.2 (page 72) for the concrete. These test results were declared void and was not included in here.

3.6.1.2 Cylinder splitting strength

The cylinder splitting strength for the concrete was determined using Equation 3.1 and presented in Table 3.2 (page 72). Similar to the uniaxial test results, both concretes appeared to have gained maximum strength within 7 days. The effect of steel fibres on strength and ductility were apparent and significant. The UHPC strength results were approximately 53 to 70% of those of UHPFRC. Failure of the UHPC specimens occurred in a very brittle manner, similar to its uniaxial tensile tests. Most UHPC tests exhibited strength as expected, while some exhibited very low tensile strength. These latter results were assumed to be void and discarded.

In addition, a very unfamiliar phenomenon was observed on the failure surface of the UHPC specimens which was striking, see Figure 3.15. This phenomenon was noted for almost all the UHPC cylinder specimens and was believed to have been caused due to the curing regime of 90 ^{o}C. The lower tensile splitting strength of the concrete was attributed to this behaviour. A detailed discussion on this behaviour can be found in Section 5.6.2.2 of this thesis.

Figure 3.15: Failed UHPC cylinder specimens.

For both concretes, results reported in this test were greater than those in uniaxial tests by approximately 120% to 180%. The difference between both test results were significant and similar results have been reported in the literature (Graybeal 2005). The major overestimation occurred for the UHPFRC test results. This overestimation is believed to be due to the loading configuration in which vertical compressive stress and lateral tensile stress in the specimen causes a biaxial stress state. The vertical compressive stress parallel to the failure line results in the fibres bridging between the cracks carrying higher load prior to pulling out. Furthermore, considerable compressive crushing on the specimens occurred before failure due to the platens of the testing machine, see Figure 3.16. It is evident that this test is not suitable for concrete with fibre reinforcement and ductile behaviour, in particular UHPFRC. For the UHPC, the test results cannot be taken as accurate since the results were subjective within almost every test. Results from this test were only used for comparison purposes.

Figure 3.16: Failed UHPFRC cylinder specimens.

3.6.1.3 Flexural strength

The flexural tensile strength of the concrete was determined using Equation 3.2 and presented in Table3.2. Flexural strength-deflection responses for both concretes at various ages are presented in Figure 3.17 and 3.18. The trends of the curves for both concretes were very similar to that of the uniaxial tensile test. For both concretes, the maximum strength was achieved within 7 days. The effect of fibre on ductility and strength in this test was also similar to both tensile test results reported earlier.

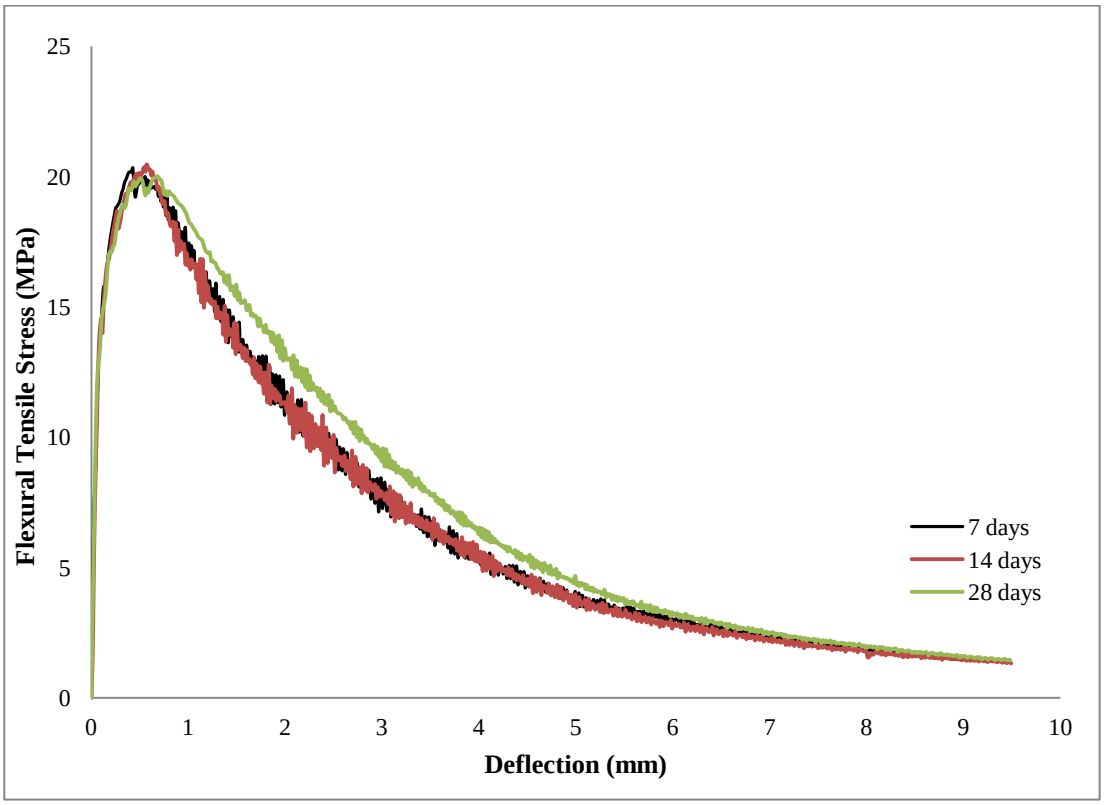

Figure 3.17: Flexural tensile behaviour of UHPFRC beams at various ages.

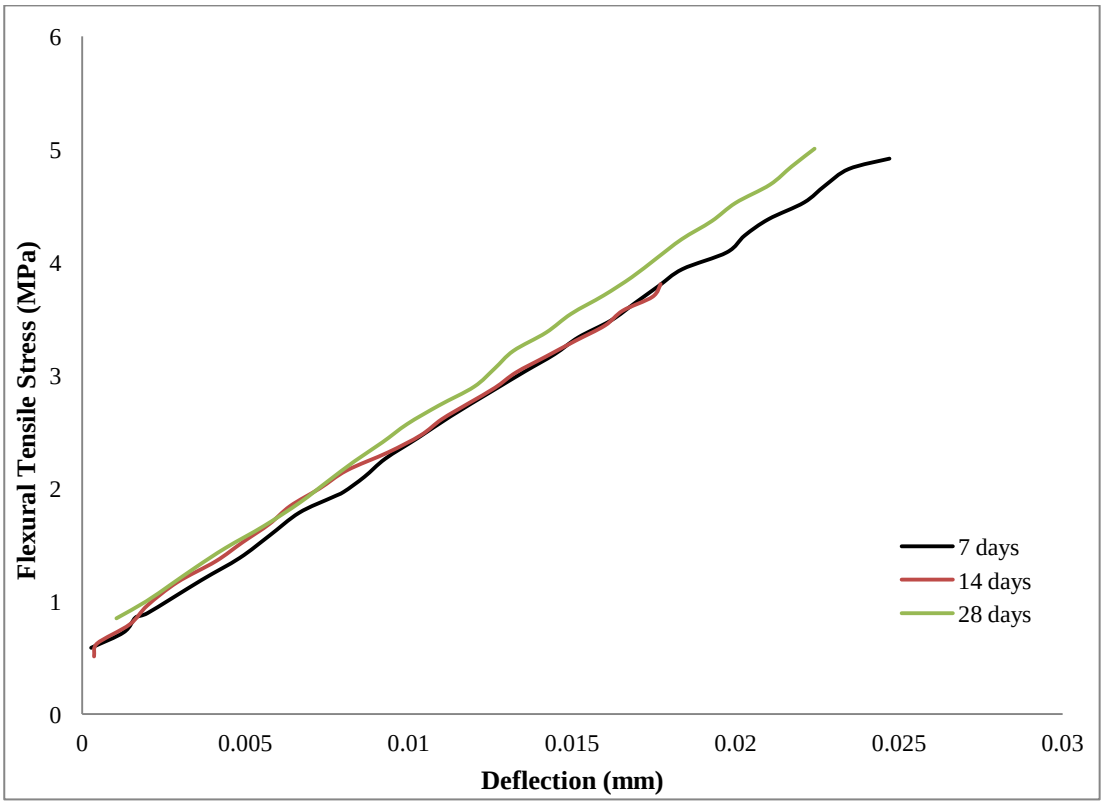

Figure 3.18: Flexural tensile behaviour of UHPC beams at various ages.

The UHPC test results were approximately 16 to 24 % of those of UHPFRC. These results were very low compared to the results of the other two tensile tests for the same concrete. Therefore, results in this test for UHPC concrete were regarded as void. To further investigate the possibility of this lower tensile flexural strength, compressive strength of the concrete was examined by testing sections of the failed beam specimens. The results appeared to be satisfactory and matched those reported for the cube tests for the same concrete. However, the same defect phenomenon reported for the failed UHPC cylinder specimens were noted on the failure surface of the beam specimens, see Figure 3.19. This behaviour was believed to have caused the low tensile flexural strength of the concrete. To further investigate this behaviour, a number of beam specimens were cast and cured at different curing temperatures and were tested at various ages. The results of this study are presented in Section 5.6.2.2 of this thesis.

Figure 3.19: Failed UHPC beam specimens from flexural test.

On the other hand, UHPFRC flexural test results were approximately 229 and 247% of those reported for the direct tensile test. This is a big difference and significantly high. The possible reasons for these overestimations were discussed previously.

Furthermore, tensile flexural strength was related to the direct tensile strength based on the relationship presented in Section 5.6.2.2 of this thesis. However, discrepancies in a

range of 15 to 20% were reported. From these results, it is evident that flexural test results are an approximate and overestimate the true tensile strength of the concrete. This test might be a good method to provide an indication of the tensile behaviour of UHPFRC. However, direct results from this test are not accurate indications of the true tensile strength of the concrete.

3.6.2 Compressive behaviour

3.6.2.1 Uniaxial compressive strength

For the uniaxial compressive tests, results only from the modified method (the third method) are presented here. Strain for the elastic stage was attained by dividing the average of the LVDT deformations by the LVDT's gauge length held by the circular rings. After the occurrence of the first crack, strain was obtained by dividing the average of the LVDT deformation measuring the cross-head movement by the total specimen height. The stress was obtained by dividing the machine load by the initial cross-sectional area of the cylinder specimen. The compressive stress-strain curves for the UHPFRC and UHPC concretes at different ages are illustrated in Figure 3.20.

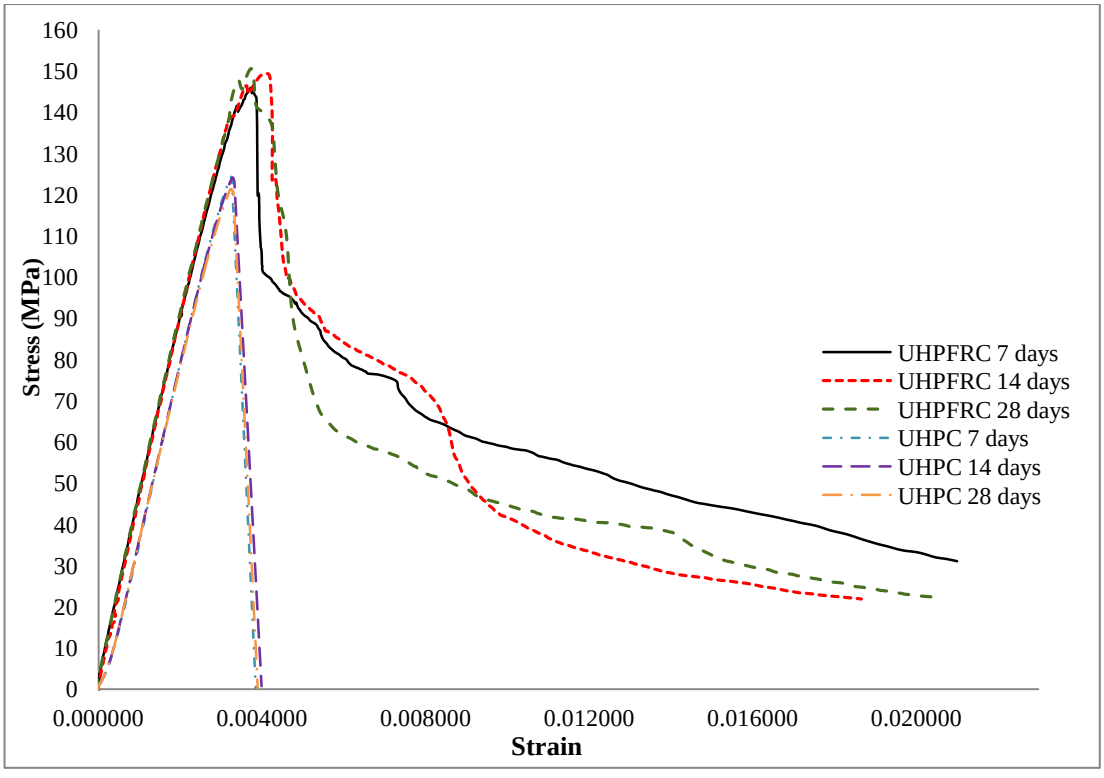

Figure 3.20: Compressive stress-strain curves with respect to age.

In Figure 3.20, only small differences in strength developments were found for both UHPFRC and UHPC between the ages of 7 to 28 days. The concretes appear to have reached their ultimate strength within 7 days, similar to their tensile strength. This is due to the curing regime of the elevated temperature of 90^{o}C. Furthermore, the elastic behaviour for both concretes at different ages follows a similar trend up to the first crack strength. The steel fibre content in UHPFRC appears to have a relatively small effect on the pre-cracking compressive strength and elastic modulus. The presence of steel fibres in UHPFRC increases the modulus of elasticity and peak strength over that for UHPC by (6 to 9%) and (15 to19%) respectively. This is not a significant increase compared to the results reported for the tensile tests. However, steel fibre content was influential on the post-cracking behaviour of UHPFRC compression tests, see Figure 3.20 and 3.21.

For the UHPC concrete, the elastic behaviour was followed until the peak strength. Failure occurred with a sudden strain softening, similar to its tensile strength. Failure of the UHPC specimen occurred with the formation of first crack, when lateral deformation exceeded its tensile capacity. The UHPC specimens lost all their strength and failed in an abrupt explosive manner, see Figure 3.21(a). In contrast, the UHPFRC specimens behaved elastically up to approximately 90-95% of their compressive strength. At the end of the elastic stage, the formation of hairline cracks occurred which was then followed by strain hardening behaviour (compression hardening) up to the peak strength. Although in some tests strain hardening behaviour did not occur but failure after initial cracking. Following the peak strength, a progressive strain softening occurred in which the presence of steel fibres governs this stage, similar to its tensile behaviour. The interaction between the fibres and the matrix contributed to the ductile compressive failure, where the concrete surface remained intact even after a total strength loss, see Figure 3.21 (b). Furthermore, results obtained from this method for the modulus of elasticity of the UHPFRC at different ages were compared to conventional test methods using strain gauges; these are reported in Table 4.3. Both sets of results were found to be in close agreement.

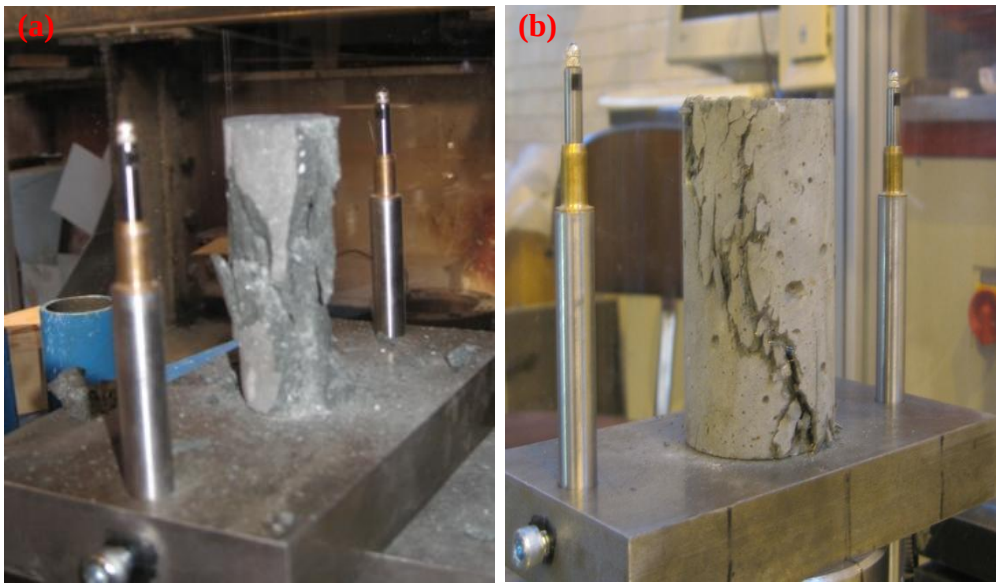

Figure 3.21: Compression tests: (a) UHPC at failure, and (b) Formation of cracks and UHPFRC at failure.

At the same time as the cylinder tests, UHPFRC cube specimens of 100 mm were also tested for maximum compressive strength. Generally, the cylinder compressive strength is lower than its cube strength for the same concrete due to the confining effect of the testing machine platens and the aspect ratio of the specimen. A strength reduction factor is usually used to convert the cube strength to cylinder strength and the factor is in the vicinity of 0.82 for normal concrete and increases toward 1.0 as the concrete strength increases (De Larrard et al. 1994). It is reported that the differences for UHPFRC are not greater than 10% (Graybeal 2005). However, results reported here are different and in a range of 11-13%. This could be due to the variations of the testing methods and specimen sizes applied here and those in the literature.

From the test results presented here, it is clear that the shape of the softening behaviour for the UHPFRC specimens in both tension and compression is hard to predict. This is due to the fact that the fibres in the concrete were distributed and orientated unevenly. To get to more consistent material properties of this material, further studies on fibre distribution and orientation in the concrete are needed.

Table 3.2: Tensile strength development for UHPFRC and UHPC at different ages.

Age (days)	UHPFRC					UHPC				
	Uniaxial tensile strength (MPa)	Corresponding strain (microstrain)	Cylinder splitting strength (MPa)	Flexural tensile strength (MPa)	Deflection (mm)	Uniaxial tensile strength (MPa)	Corresponding strain (microstrain)	Cylinder splitting strength (MPa)	Flexural tensile strength (MPa)	Deflection (mm)
7	8.97	2781	11.45	20.65	0.572	4.47	156	8.01	4.91	0.020
14	8.92	1499	11.79	20.52	0.515	4.96	204	6.22	3.82	0.021
28	9.07	2749	11.17	20.73	0.617	5.36	166	6.47	3.33	0.018

Table 3.3: Compressive strength development for UHPFRC and UHPC and different ages.

Age (days)	UHPFRC			UHPC		
	Uniaxial compressive strength (MPa)	Corresponding strain (microstrain)	Modulus of elasticity (GPa)	Uniaxial compressive strength (MPa)	Corresponding strain (microstrain)	Modulus of elasticity (GPa)
7	145.96	3751	45.37	124.34	3260	41.14
14	149.05	4168	44.83	124.13	3284	42.09
28	150.56	3730	45.55	121.32	3238	42.08

3.6.3 Stress-strain relationship

From the test results obtained here, this PhD proposes a simplified stress-strain relationship for the UHPFRC in both compression and tension, see Figure 3.22. The relationship was developed based on numerous uniaxial tensile and compressive tests and was adopted for FE modelling later in this study. Figure 3.22 represents the generalised mean stress-strain relationship for this particular concrete mix. In the view of various test results obtained, the relationship represents the approximate stress-strain behaviour of the concrete with a relative accuracy of 90%.

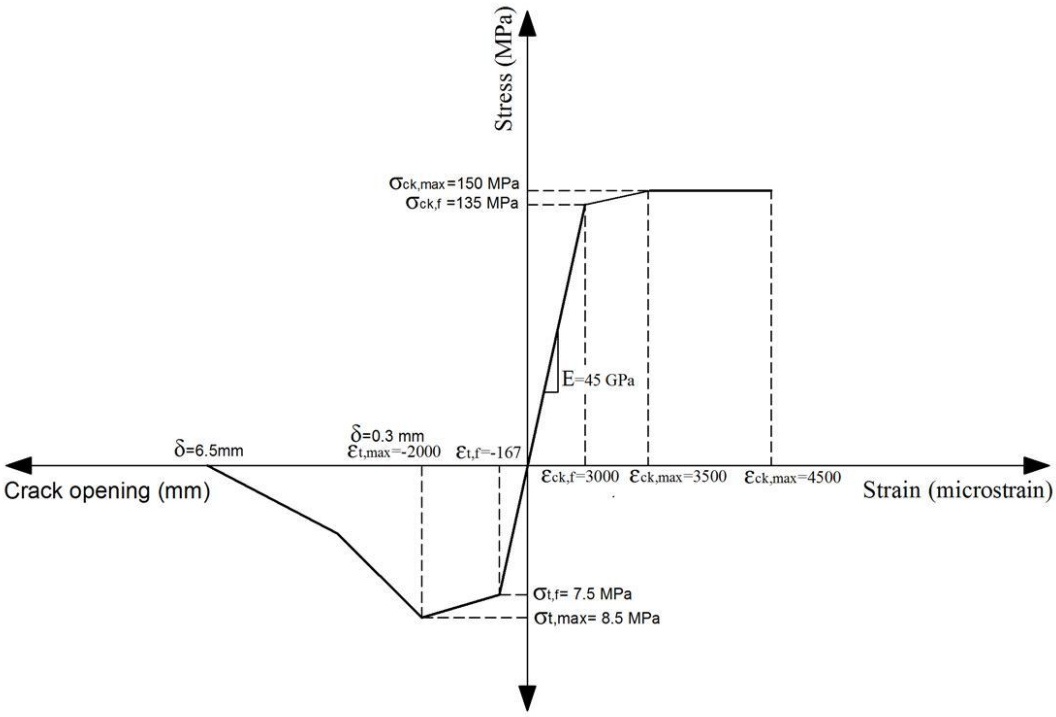

Figure 3.22: Stress-strain relationship for the UHPFRC mix used in this study (not to scale).

In Figure 3.22, the compressive stress-strain behaviour was represented by a tri-linear relationship which is very similar to the relationship proposed in the AFGC recommendation (BFUP AFGC 2002). The initial ascending segment of the model has a slope equal to the value of the elastic modulus of the material, 45 GPa, and extends to first crack compressive stress, $\sigma_{ck,f}$, equal to 135 MPa . As discussed previously, most of the uniaxial compressive tests exhibited strain hardening after the initial crack

formation. Therefore, at compressive stress of 135 MPa, approximately 90% of the maximum cylinder compressive strength, the stiffness of the material is modelled with a slope equal to 30 GPa. This to represent crack formations in compression hardening and the behaviour of the material is modelled with the reduced stiffness value until maximum compressive stress, $\sigma_{ck,\max}$, equal to 150 MPa. This relationship assumes if the load was removed at anywhere after crack formation, the stiffness of the concrete is damaged and the value is smaller than the initial value. After maximum compressive stress is reached, the compressive behaviour of the material changes to a straight horizontal line with stiffness equal to zero, representing the stiffness degradation of the material. This behaviour extends to a compressive strain of 4500 x 10^{-6}. The softening behaviour in compression is not included in Figure 3.22 as this property is not significant in structural design or FE analysis. Note, the maximum cylinder compressive strength was assumed to be 150 MPa.

Similarly, the tensile stress-strain behaviour of the material was characterised by an initial linear segment with a slope equal to 45 GPa up to first crack tensile stress, $\sigma_{t,f}$, equal to 7.5 MPa. From this point onwards, the slope of the segment reduces to 0.5 GPa, this to represent crack formations and strain hardening behaviour of the material. This part of the segment extends to a maximum tensile stress, $\sigma_{t,\max}$, equal to 8.5 MPa. Similar to the compressive behaviour, this relationship assumes if the load was removed at anywhere after tensile crack formations, the stiffness of the concrete is damaged and the value is smaller than the initial value. The behaviour thereafter is modelled with two linear lines in terms of crack mouth opening, assuming maximum tensile strength occurs at a crack opening of 0.3 mm and extends to 6.5 mm. The slope of the lines was modelled to be very close to results obtained from the uniaxial tests, see Figure 3.14. The total tensile failure is modelled to occur at 6.5 mm crack opening, which is equal to half the length of steel fibres.

The stress-strain behaviour presented in Figure 3.22 is drawn to be very close to results obtained from the uniaxial tests and is very similar to the one proposed in the AFGC recommendation, see Figure 3.23. Furthermore, Figure 3.22 represents the constitutive

material model for the UHPFRC mix used in this study that is when the concrete is cured at 90 ^{o}C and is of at least 7 days of age or above.

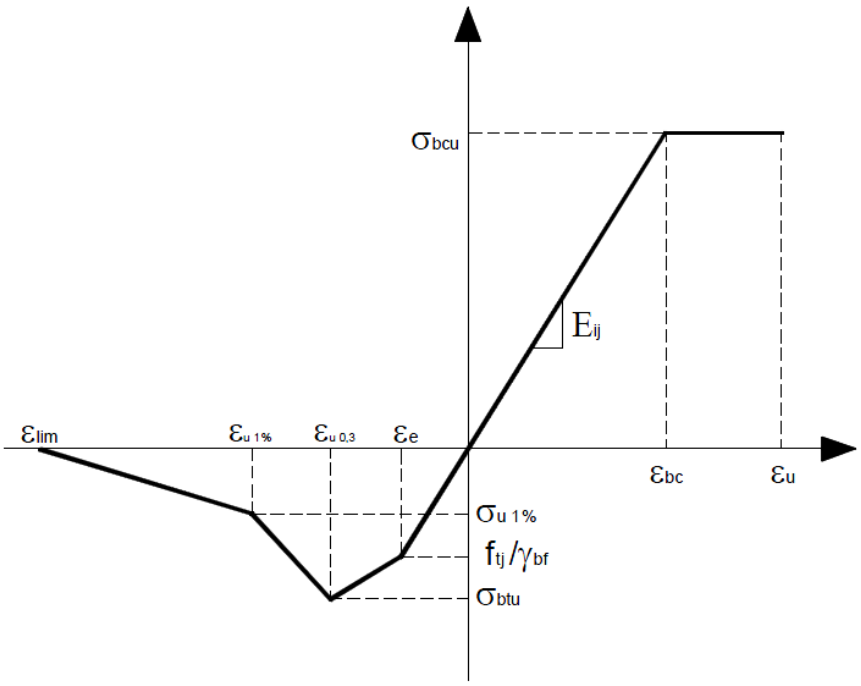

Figure 3.23: Proposed stress-strain relationship from the AFGC recommendation for UHPFRC (BFUP AFGC 2002).

3.7 Summary

In this study, conventional test methods developed for normal concrete such as tensile splitting, flexural and compression tests were tried to define the stress-strain relationship of UHPFRC in both tension and compression. However, these tests were found to be unreliable, in particular, for capturing the post-cracking behaviour of the concrete. In order to overcome these limitations, simple uniaxial test methods in tension and compression were developed and used successfully to determine the stress-strain relationship of the concrete both with and without fibres. Numerous tests at different ages were conducted and the consistency of the results justifies the simplicity and credibility of the test methods developed. The results strongly indicate that such testing methods for UHPFRC are promising options for material characterisations.

In addition, the significance of steel fibres on ductility and strength were investigated. Substantial improvements in the ductile behaviour of UHPFRC specimens were reported. The concrete exhibited strain hardening and strain softening behaviour in both tension and compression. In contrast, the UHPC concrete exhibited brittle behaviour and its failure mechanism was very sudden. In terms of strength, the fibre content in UHPFRC was found to be very important in improving the tensile strength by almost double compared to that of UHPC. This is significant for concrete structures where punching shear failure is an important consideration such as in bridge deck designs. However, the steel fibres' influence on the compressive strength and modulus of elasticity was found to be relatively small.

Furthermore, only small differences in strength development in tension and compression were found for both UHPFRC and UHPC between the ages of 7 to 28 days. The concretes appeared to have reached their ultimate strength within 7 days. This is due to the curing regime of the elevated temperature of 90^{o}C. However, a defect phenomenon on the surface of the failed UHPC tensile test specimens was observed, in particular, for the cylinder and beam specimens. This phenomenon was believed to have occurred due to the curing temperature of 90 ^{o}C and resulted in considerable loss of strength to the concrete. Further studies regarding this behaviour are presented in Chapter 5. In addition, significant difference in the results of the UHPFRC flexural and uniaxial tensile tests was reported. From the results obtained, it is evident that the former test method overestimates the true tensile strength of the concrete. Therefore, attempts were made to relate the tensile flexural strength of the concrete to its direct tensile strength based on the relationship presented in Section 5.4.2. However, discrepancies in a range of 15 to 20% were still reported. From these results, it is evident that flexural test results are an approximate and overestimate the true tensile strength of the concrete.

From the tests results reported here, a stress-strain relationship for this specific mix of UHPFRC was determined. This relationship is important and required for formulating and calibrating any potential constitutive material model for design purposes or FE modelling for the concrete.

Chapter IV: Non-destructive Testing Methods for UHPFRC

4.1 Introduction

For UHPFRC to be utilised more in construction industry, easy and reliable testing methods to assess its mechanical properties needs to be developed or identified such as non-destructive testing techniques. The ultrasonic pulse velocity (UPV) and resonant frequency are two non-destructive testing (NDT) techniques which have been used to measure the elastic properties of hardened normal concrete for decades. The UPV testing technique is the more common of the two. This method of testing is used to study laboratory specimens and existing structures, whilst resonant frequency testing is more often used in laboratory testing only. The applicability of both methods for normal concrete have been well demonstrated in the literature (Bungey et al. 2006, Malhotra and Carino 2004) and their accuracy is within acceptable limits. However, to date, only a very few studies (Washer et al. 2004, Washer et al. 2005) have considered the use of non-destructive testing techniques for the investigation of the elastic properties of UHPFRC. These studies have conducted some important but preliminary analyses on the suitability of both testing procedures for UHPFRC.

In the current study, the ultrasonic pulse velocity and resonant frequency testing methods were chosen to determine the elastic properties of the UHPFRC. The accuracy and validity of both testing methods and the effect of steel fibres in the mix on the test results were investigated. To validate the results, conventional destructive (static) testing methods were carried out on specially prepared samples to determine the elastic properties of the concrete and used as a datum. From this study, the relative merits of the two non-destructive testing methods for UHPFRC were investigated.

In addition, from the literature, a number of empirical equations to predict the elastic properties of normal and high strength concrete from their compressive strength were found and used for this concrete. The accuracy of these equations was also investigated and compared to the results obtained from the static tests.

4.2 Elastic Properties of Concrete

The elastic properties of concrete can be described by its modulus of elasticity and Poisson's ratio. In particular, the modulus of elasticity is an important parameter in the design of concrete structures. The modulus of elasticity is used in design calculations to predict the deflection of structures and cracking of concrete members without stress relaxation. It is also essential in sizing structural members, especially in the design of prestressed members. The Poisson's ratio is a variable required in design of many types of concrete structures such as arches, tunnels, flat slabs and pavements. These properties of UHPFRC are required for any structural analysis and numerical modelling. Therefore, in this study, detailed investigation to find reliable test methods to determine both properties with high degree of accuracy were carried out.

So far, various test methods exist to determine both properties of UHPFRC. These tests are either destructive (static) and non-destructive (dynamic) testing methods. While the destructive testing method, similar to those presented in Chapter 2, has been used widely for UHPFRC, little investigation on the applicability of the non-destructive testing methods has been carried out (Washer et al. 2005, Hassan and Jones 2012). Therefore, in this study, the ultrasonic pulse velocity and resonant frequency non–destructive testing techniques for the determination of the modulus of elasticity and Poisson's ratio of the UHPFRC were investigated. In the following sections, the backgrounds, theory and apparatus involved with each testing techniques and those of the static test are discussed. From the results, the most suitable non-destructive test method for the concrete was identified and compared to the results obtained from the conventional destructive test method.

4.3 Non-destructive Testing

The non-destructive testing techniques are usually carried out on hardened concrete to investigate various mechanical properties of existing structures. It can also be used in the laboratory on fresh and hardened concrete specimens. The main advantage of these testing methods is that they are portable, allow repeated testing on the same specimen, can be used at any time, and result in no significant damage to the structural member.

There are a wide range of non-destructive tests for concrete; the ultrasonic pulse velocity and resonant frequency testing methods are two of the most widely used. Both testing methods were developed for normal strength concrete with compressive strengths in the range 30 to 60 MPa. However, their potential use for UHPFRC is investigated here.

4.3.1 Ultrasonic pulse velocity (UPV)

4.3.1.1 Background

The ultrasonic pulse velocity is a preferred non-destructive testing method that has been used successfully to assess the mechanical properties of concrete such as strength development, crack detection, and environmental deterioration due to frost or fire. The UPV measurement on concrete was first reported in the USA in the mid-1940s (Bungey et al. 2006). The velocity of ultrasonic waves was found to be primarily dependent upon the elastic properties of the concrete and not influenced by the geometry. However, measurement problems due to the mechanical pulse equipment were reported to be considerable and this lead to the subsequent development of the technique in countries like France, Canada and the UK. A detailed historical background on the development of this testing method is well presented in the literature (Malhotra and Carino 2004, Bungey et al. 2006).

In the past, this technique has been used successfully to obtain the modulus of elasticity and Poisson's ratio of normal concrete (Qixian and Bungey 1996, Jin and Li 2001, Mesbah et al. 2002, Malhotra and Carino 2004). The principle of UPV is to measure the velocity of an ultrasonic wave passing through concrete. Form the velocity of the wave, the elastic properties of the material can be assessed. It must be noted, there are three types of waves that are associated with the UPV testing method. These are surface, shear and compression waves. The surface waves are the slowest, while shear (also known as transverse waves) are slightly faster than surface waves and compression (also known as longitudinal waves) are the fastest. Depending on the measurement procedures, there are three types of wave transmissions during testing. These are direct, semi direct and indirect transmissions as shown in Figure 4.1.

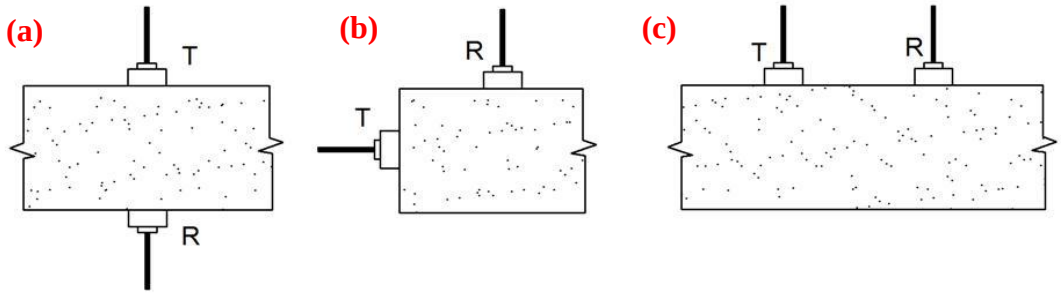

Figure 4.1: Types of wave transmissions: (a) direct, (b) semi-direct, and (c) indirect.

This test is very flexible and can be used with existing structures and laboratory specimens. The easiest and most accurate method is the direct transmission, see Figure 4.1 (a). This is recommended to be used in most applications since the path length and velocity of the transmitted pulse can be determined accurately (BS EN 12504-4 2004). However, if the direct measurement is not possible due to the restraints and the shape of the structure, the semi direct method can be used, as shown in Figure 4.1 (b). The accuracy of this method is in between of the other two methods. While the indirect method is recommended to be used only when one side of the concrete is accessible, see Figure 4.1 (c). It is the least satisfactory method due to the difficulty in determining the exact path length between the transducers and detecting a clear pulse. However, when this method is used, it is preferable to make a series of measurement points along the specimen to increase the accuracy of the test results. Furthermore, this arrangement gives pulse velocity measurements which are usually predominantly influenced by the concrete near the surface. This region is often of different composition to that of concrete within the body of the specimen and the test results may be misleading. The indirect velocity is invariably lower than the direct velocity on the same concrete element. This difference in detecting the pulse between the indirect and the direct measurement may vary from 5% to 20% depending largely on the quality of the concrete under test (BS 1881-203 1986). Despite this, the indirect compression UPV measurement has been popular in assessing the elastic properties of conventional concrete (Qixian and Bungey 1996, Bungey et al. 2006).

Previously, compression and shear waves have been used to study the elastic properties of UHPFRC (Washer et al. 2004). In their study, UPV was used for crack detection and

determination of the modulus of elasticity of the concrete. However, surface waves for UHPFRC has not yet being tested. A previous study by (Qixian and Bungey 1996) used the UPV surface transmission successfully to determine the modulus of elasticity and Poisson's ratio of normal concrete. The results reported in their study appeared to be promising. Therefore, in this study, the same procedure was applied on UHPFRC specimens to assess the accuracy and validity of the UPV surface transmission method for the concrete.

The use of the UPV testing method in concrete is relatively straightforward. There are many international standards that provide detail guidance on its use in conventional concrete such as (BS EN 12504-4 2004, ASTM C597-09 2009). The results obtained from this test method for normal concrete are satisfactory and influenced by many factors such as moisture content, reinforcement in the concrete, shape and size of the specimen. The practical issues/limitations associated with using this method are described in detail in the literature (BS 1881-203 1986, Malhotra and Carino 2004, Bungey et al. 2006).

4.3.1.2 Theory

The basic theory of ultrasonic wave propagation in concrete has been described in detail in the literature (Jones 1962). The velocity of ultrasonic waves in concrete are influenced by the same properties that determines its elastic stiffness and mechanical properties (BS 1881-203 1986). It is primarily dependent on the elastic properties and the density of the concrete (Bungey et al. 2006). Therefore, if the density and velocity of the wave propagation are known, then the elastic properties can be determined.

The relationship between the elastic modulus and the velocity of an ultrasonic pulse travelling in a homogeneous isotropic elastic medium is described in Equation 4.1 (Bungey et al. 2006).

$$V_{p,s} = \sqrt{\frac{E_{d,u}\ K}{\rho}} \qquad \text{Equation 4.1}$$

where $V_{p,s}$ = compression wave velocity (m/s)

$E_{d,u}$ = dynamic modulus of elasticity (GPa)

$K = \frac{(1-\nu_u)}{(1+\nu_u)(1-2\nu_u)}$, and

ρ = the density of the concrete (kg/m^3)

Now Equation 4.1 can be re-written as:

$$V_{p,s} = \sqrt{\frac{E_{d,u}}{\rho}\frac{(1-\nu_u)}{(1+\nu_u)(1-2\nu_u)}} \qquad \text{Equation 4.2}$$

Meanwhile, the velocity of shear and surface wave velocities are described in Equations 4.3 and 4.4, respectively (Qixian and Bungey 1996).

$$V_s = \sqrt{\frac{E_{d,u}}{\rho}\frac{1}{2(1+\nu_u)}} \qquad \text{Equation 4.3}$$

$$V_r = \frac{0.87+1.12\nu_u}{1+\nu}\sqrt{\frac{E_{d,u}}{\rho}\frac{1}{2(1+\nu_u)}} \qquad \text{Equation 4.4}$$

Concrete usually does not fulfil the physical requirement for the validity of the homogeneous isotropic elastic medium (Neville 2012). However, a previous study by (Washer et al. 2004) on the propagation of ultrasonic waves using the direct transmission method in UHPFRC has determined that the material exhibits isotropic elastic properties within normal operating stress limits. Therefore, by assuming UHPFRC as a homogeneous isotropic elastic medium and using Equations 4.2 to 4.4, the elastic properties of the concrete can be determined. Furthermore, using the longitudinal and surface wave velocities in Equations 4.2 and 4.4 to derive Equation 4.5, the Poisson's ratio can also be determined.

$$\frac{V_{p,s}}{V_r} = \frac{(1+\nu)}{(0.87+1.12\nu_u)}\sqrt{\frac{2(1-\nu_u)}{(1-2\nu_u)}} \qquad \text{Equation 4.5}$$

Substituting the value of, ν_u, into Equations 4.2 or 4.4, the value of, $E_{d,u}$,can also be determined. The subscripts, u, for the modulus of elasticity with Poisson's ratio and, s, for the compression wave velocity denote that the values are determined using UPV testing techniques.

4.3.1.3 Apparatus

In accordance with BS EN 12504-4:2004, the apparatus should consist of an electrical pulse generator, a pair of transducers, an amplifier and an electronic timing device for measuring the time interval lapsing between the onset of a pulse generated at the transmitting transducer and the arrival of the pulse at the receiving transducer (BS EN 12504-4 2004). An oscilloscope is usually connected to the test equipment as the timing device and it can also be used to study the nature of the received pulse. A calibration bar is usually used to provide a datum for the velocity measurement. The basic circuitry requirements for the UPV testing technique is shown in Figure 4.2.

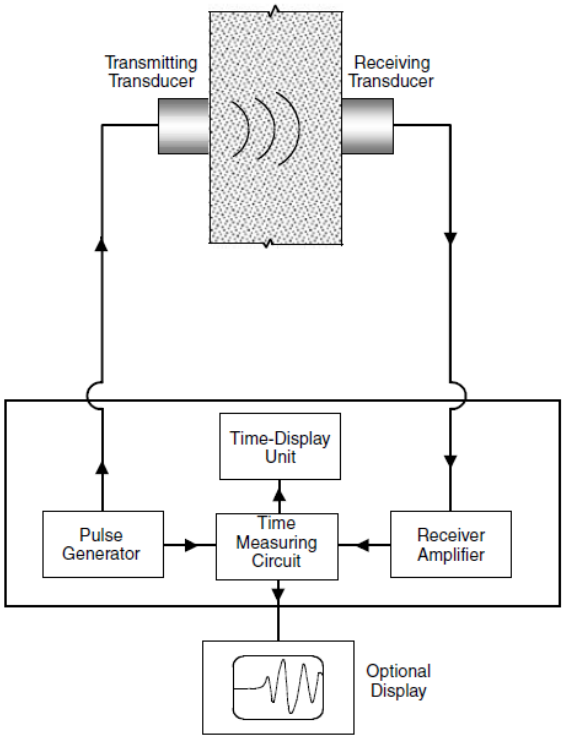

Figure 4.2: Typical UPV testing equipment arrangement (Malhotra and Carino 2004).

Various test equipments are available for this test. However, in the current study, two pairs of conventional compression transducers with different frequencies of (0.082 and 2 MHz) were used. An additional piece of apparatus known by its acronym "PUNDIT", derives its name from "Portable Ultrasonic Non-destructive Digital Indicating Tester" was also used. This device generates low frequency ultrasonic pulses when connected to the twin compression transducers (C. N. C ELECTRONICS LTD 1989). It is a simple device to operate and is fully portable.

In addition to the pundit unit, another device known as C.R.O. Add-On Unit was also used. The C.R.O. unit was plugged into the pundit and the transducers. This is to display and analyse specific signal waveforms received since the wave undergoes multiple reflection at the boundaries of the different material phases of the concrete. This unit also provides the attenuation measurement and transit time when connected to an oscilloscope. A digital storage oscilloscope was used and connected to the C.R.O. Add-On Unit to display the waveforms and to measure transit times of each different wave. The test specimen was a UHPFRC slab and the test setup is shown in Figure 4.3 below.

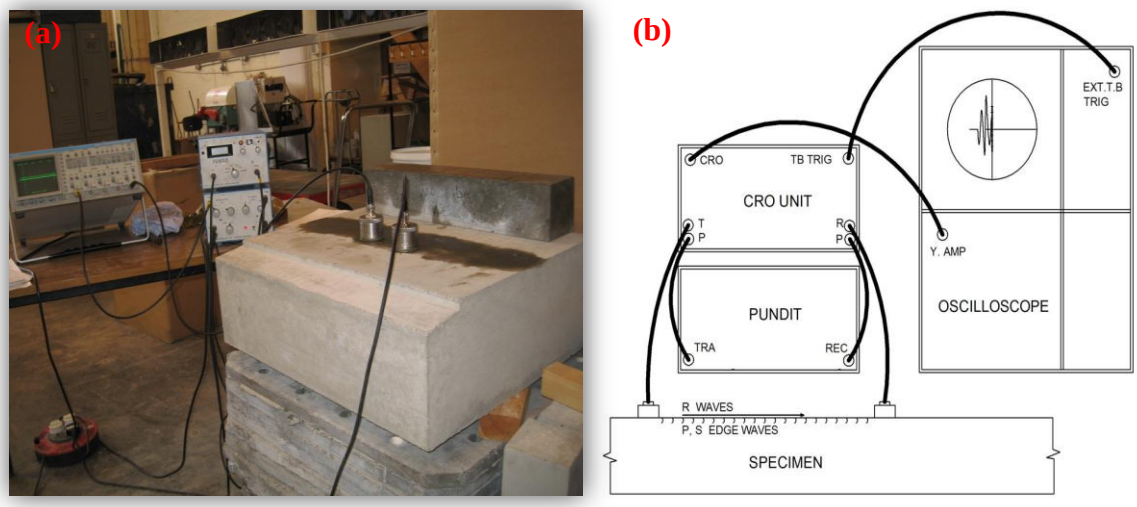

Figure 4.3. Ultrasonic pulse velocity test setup: (a) Apparatus setup in the laboratory, and (b) A schematic sketch of the equipment setup.

Multipurpose grease was used between the concrete surface and the faces of the transducers for the coupling to eliminate air pockets in-between both faces. This is essential for a good acoustic coupling and to obtain accurate results.

4.3.2 Resonant frequency

4.3.2.1 Background

Resonant frequency method is an alternative to UPV for the determination of dynamic elastic modulus and Poisson's ratio of concrete. It was first developed by Powers in the United States in 1938 (Malhotra and Carino 2004). The resonant frequency of a 51x51x241mm beam was determined by matching the musical tone created by the concrete specimen when tapped by a hammer with the tone created by the orchestra bells calibrated according to frequency. Subsequent development of this method was carried out by many researchers such as Horrinbrook 1939, Thomson 1940, Obert and Duvall 1941 and Stanton 1944 (Malhotra and Carino 2004).

This method of testing, unlike the UPV, is only suitable to laboratory specimens rather than structural members on site. The size and shape of specimens in this test are limited to only cylinder and beam specimens. In this study, only beam specimens were used.

A number of international standards available to provide detail guidance on its use for conventional concrete such as (BS 1881-209 1990, ASTM C215-08 2008). Similar to the UPV testing, results obtained by this testing method are influenced by many factors such mix proportion, specimens size, age and curing condition. More detailed studies on the practical issues/limitations associated with using this method can be found in literature (de Graft-Johnson and Bawa 1969, Swamy and Rigby 1971, Malhotra and Carino 2004, Neville 2012).

4.3.2.2 Theory

From the literature, for a vibrating beam of known dimensions, the natural frequency of vibration in the longitudinal mode is mainly related to the dynamic modulus of elasticity and the density of the material (Malhotra and Carino 2004). Therefore, the dynamic modulus of elasticity of a solid medium of known density can be determined from its natural of frequency of vibration.

Similarly, the resonant frequency theory was derived for materials of homogenous, isotropic with perfectly elastic behaviour. However, it has also been applied for heterogeneous materials such as concrete.

The vibration in this method can be applied in longitudinal, transverse (flexural) or torsional mode (Neville 2012). From the theory of sound, the flexural vibration of a long-thin rod under a free-free boundary condition, can be described by Equation 4.6 (Malhotra and Carino 2004).

$$N = \frac{m^2 k}{2\pi L^2}\sqrt{\frac{E_d}{d}} \qquad \text{Equation 4.6}$$

and re-arranging for E_d

$$E_d = \frac{4\pi^2 L^4 N^2 d}{m^4 k^2} \qquad \text{Equation 4.7}$$

where E_d = dynamic modulus of elasticity (GPa)

d =density of the material (kg/m^3)

L = length of the specimen (mm)

N =fundamental flexural frequency (Hz)

k = radius of gyration of the section about an axis perpendicular to the plane of bending, and for rectangular cross sections $k = t/12$ where;

t =thickness

m = a constant of 4.73 for the fundamental mode of vibration.

The dynamic modulus of elasticity of plain concrete can also be determined using resonance of vibration in the longitudinal mode under a free-free boundary condition (specimen clamped in the middle), using Equation 4.8.

$$E_{d,r} = 4n^2 L^2 \rho 10^{-15} \qquad \text{Equation 4.8}$$

where n = fundamental frequency in the longitudinal mode of vibration (Hz), and

ρ = density of the material (kg/m^3)

In this study, the modulus of elasticity was determined in accordance with the BS 1881-209:1990 using the resonance natural frequency in the longitudinal mode of vibration only. The subscript, r, denotes that the values are determined using the resonant frequency testing techniques.

It is known that non-destructive testing techniques of concrete always overestimates the values of the modulus of elasticity compared to those reported for static testing (Qixian and Bungey 1996, Washer et al. 2004, Bungey et al. 2006, Mosley et al. 2007). The difference was found to be dependent on the degree of accuracy of the chosen non-destructive test, age and strength of the specimen (Malhotra and Carino 2004). Therefore, so far, a number of empirical relationships have been derived for relating the static and dynamic moduli of concrete (Neville 2012). One commonly adopted relationship in UK practice for normal concrete (Mosley et al. 2007) is presented in Equation 4.9, in which the secant modulus of elasticity, E_{cm}, is related to the dynamic modulus of elasticity, $E_{d,r}$, determined from the resonant frequency testing method.

$$E_{cm} = 1.25E_{d,r} - 19 \qquad \text{Equation 4.9}$$

Furthermore, the BS 1881-203:1986 allows for the determination of the value of the Poisson's ratio, ν_r, using a relationship between the direct compression wave velocity and longitudinal resonant frequency of a concrete specimen in Equations 4.2 and 4.8, respectively. Re-arranging both equations will result in Equation 4.10 below:

$$\frac{4n^2L^2\rho 10^{-15}}{V_{p,d}{}^2} = \frac{(1+\nu_r)(1-2\nu_r)}{(1-\nu_r)} \qquad \text{Equation 4.10}$$

where $V_{p,d}$ = the direct compression wave velocity of the concrete determined using the UPV testing technique.

4.3.2.3 Apparatus

The testing apparatus for this method consists primarily of two separate functions, one generates mechanical vibrations and the other senses the resulting vibrations (Malhotra and Carino 2004). In this test, electrical oscillations are supplied to a vibration generator from a variable frequency vibrator. The resonance conditions are achieved by varying the frequency of the oscillator until resonance is obtained and the frequency is noted. More details on the test equipment for this test method and their operation can be found in the literature (Malhotra and Carino 2004, Neville 2012).

The equipment for measuring the resonance frequency of vibration in the longitudinal mode for a beam specimen according to BS 1881:209-1990 is shown in Figure 4.4. In the test setup, a concrete beam is clamped at its midpoint and is vibrated by an oscillator. A pick-up point is made by mechanical contact at one end of the specimen whilst the vibrating oscillator contact is made at the other end. It must be noted that the vibrating oscillator and pick-up points must not restrain either end of the specimen, which should remain free to vibrate in the axial direction. This is the recommended arrangement for unrestrained longitudinal vibration to occur. A pulse is sent through the specimen and the response of the beam is measured. The pulse frequency is varied until the resonant frequency is found.

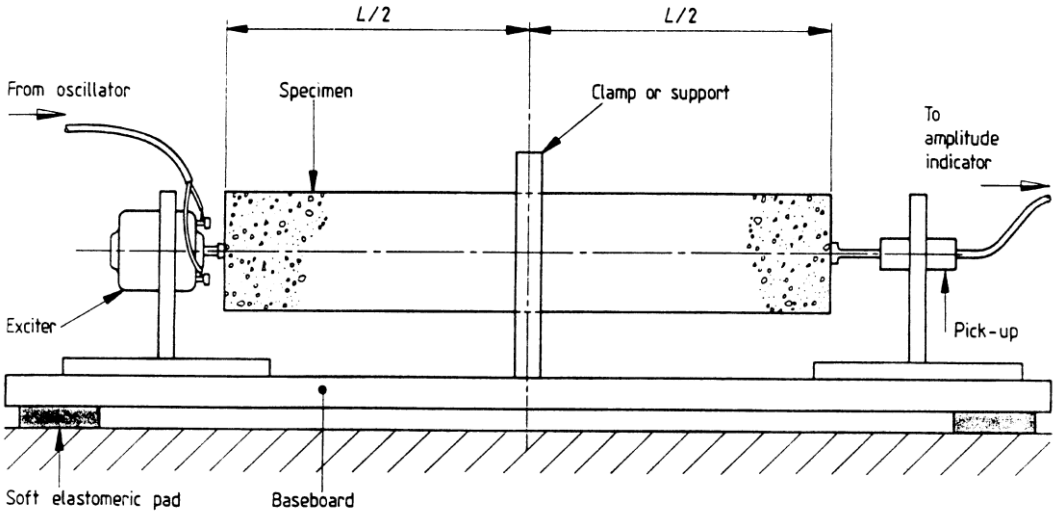

Figure 4.4: Test configuration for measuring the resonance frequency of vibration in the longitudinal mode (BS 1881-209 1990).

In this study, a variable frequency oscillator complying with the BS 1881-209:1990 was used. For this test, a commercial instrument known as an Erudite was used for measuring the resonant frequency of the UHPFRC beam specimens. The test was carried out three times for each beam specimen and a mean value for the resonance frequency was calculated in Hz. The test setup is shown in Figure 4.5 below.

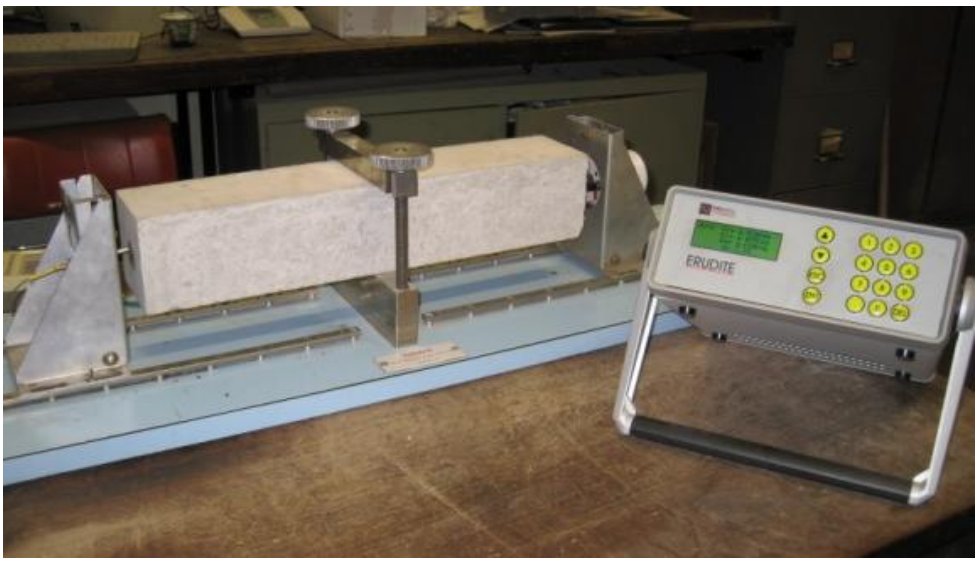

Figure 4.5. Resonant frequency test setup using an Erudite.

4.4 Destructive Testing

The destructive (also known as static or direct) tests are usually carried out on small scale laboratory specimens and tested to failure such as the direct compression and tension tests presented in Chapter 2. The advantages of these testing methods are easy to carry out, cheap and well established.

In this study, direct compression tests were carried out to determine the compressive strength, modulus of elasticity and Poisson's ratio of UHPFRC. The compressive strength results were used in empirical equations to predict the value of the secant modulus of the concrete. The results of the modulus of elasticity and Poisson's ratio obtained from the direct compression tests were used as a reference for the results obtained from the UPV, resonant frequency and empirical equations.

4.4.1 Compression test

4.4.1.1 Background

The most common of all tests on hardened concrete is the compression test. This test has been used for many decades and performed frequently on hardened concrete. Different test methods and techniques are used in different countries based on many available standards. Regardless of the standards used, this test provides measured properties of importance in concrete designs such as strength evaluation. It can also be used for the determination of the modulus of elasticity and Poisson's ratio. There are many standards and recommendation that provides detailed guidance for the determination of these two properties of concrete (BS 1881-121 1983, ASTM C469-02 2002, BFUP AFGC 2002). Amongst these, the BS 1881-121:1983 was used in this study for the determination of the modulus of elasticity of the UHPFRC. The tests were carried out in accordance with the standard with some modifications to improve the reliability of the test. The Poisson's ratio was also determined from this test.

4.4.1.2 Theory

For concrete, the modulus of elasticity is determined from the stress-strain relationship in either direct compression or tension tests. In compression test, a concrete specimen is loaded and unloaded up to a stress well below its ultimate strength, while the stress-strain relationship is measured. The secant modulus of elasticity of the concrete is then calculated using Equation 4.11(BS 1881-121 1983).

$$E_{cm} = \frac{\sigma_a - \sigma_b}{\varepsilon_a - \varepsilon_b} \qquad \text{Equation 4.11}$$

where σ_a = the upper loading stress (in MPa), $\sigma_a = f_c / 3$

σ_b = the basic stress (i.e. 0.5 MPa)

ε_a = the mean strain under upper loading stress, and

ε_b = the mean strain under the basic stress.

In accordance with the standard, three specimens (cube or cylinder) must be tested first in compression to determine the mean compressive strength of the concrete. Then, a fourth sample is used for the determination of the secant modulus of elasticity. At the beginning of the fourth test, a basic stress, σ_b, of 0.5 MPa needs to be applied and then stress is increased steadily at a constant rate of 0.6 MPa/second until the stress is approximately equal to one-third, σ_a, of the compressive strength of the concrete. The corresponding longitudinal strains were measured at the start and end of the test using strain gauges that were mounted on the specimen in the direction of the load. After obtaining these results, Equation 4.11 can be used for the determination of the modulus of elasticity of the concrete.

The standard test method used for the determination of the modulus of elasticity can also be used at the same time to obtain the value of the Poisson's ratio of the concrete. This is done by obtaining lateral strain measurements perpendicular to the direction of the load on the specimen. Then the value of the Poisson's ratio, ν, is calculated from the longitudinal and transversal strain recorded using Equation 4.12.

$$\nu = \frac{\varepsilon_c - \varepsilon_d}{\varepsilon_a - \varepsilon_b} \qquad \text{Equation 4.12}$$

where ε_c = the mean lateral strain under upper loading stress, and

ε_d =the mean lateral strain under the basic stress.

In this study, UHPFRC cylinder specimens were used to measure both properties as described above according to the BS 1881-121:1983. The direct compression tests were conducted at the Queen's University Belfast, UK. For convenience, cylinder specimens were used instead of cubes since cylinders were easy to handle. In addition to this, cube specimens were also tested for the determination of the cube compressive strength of the concrete at the University of Liverpool.

4.4.1.3 Apparatus

There are many commercial testing machines that are used for compression tests. The testing machines are widely available and performing this test is straight forward. For the determination of the modulus of elasticity and Poisson's ratio, strain gauges are required for strain measurements. However, other instruments such as dial gauge extensometers, inductance gauges and compressmeters can also be used for strain measurements. The position and length of the strain gauges proposed for this test is well described in the BS 1881-121:1983.

The direct compression tests were undertaken using hydraulic compression testing machines; a 600 kN Dartec at Queen's University Belfast, and a 3000 kN ToniPACT at the University of Liverpool. The Dartec testing machine was used for the determination of the cylinder compressive strength, modulus of elasticity and Poisson's ratio using the cylinder specimens. While the ToniPACT testing machine was used for cube compressive strength measurements only, using cube specimens. The test setup for both testing machine is shown in Figure 4.6. For strain measurement, six electrical aluminium strain gauges, 12 mm in length, were attached on the surface of each cylinder specimen to measure the longitudinal and transverse strain during the test.

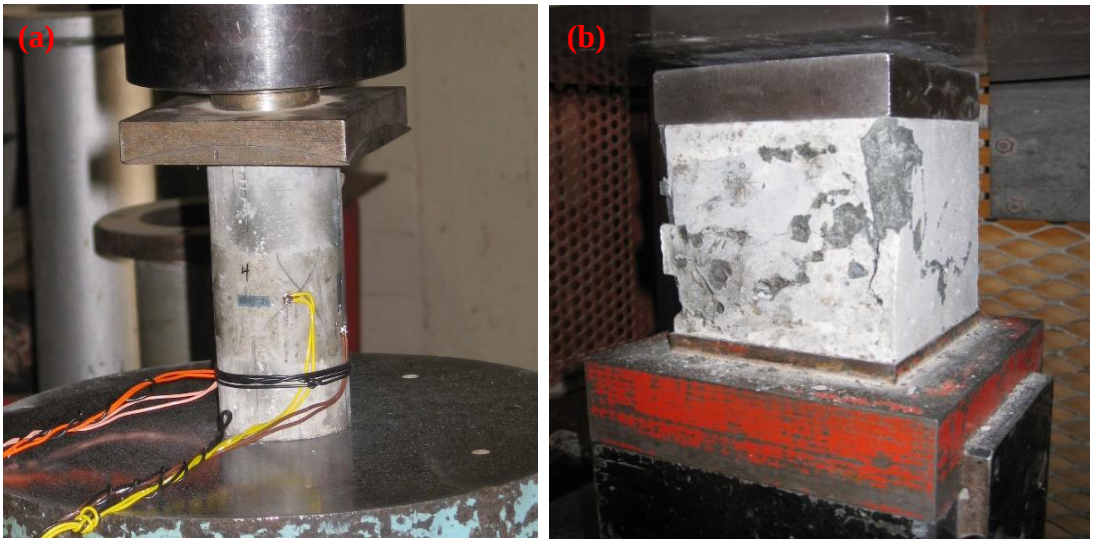

Figure 4.6: Static test setup for the: (a) cylinder specimens, and (b) cube specimens.

4.4.2 Empirical equations

Another method for determining the modulus of elasticity of concrete is from its compressive strength as both properties are dependent on each other. The modulus of elasticity of concrete is reported to increase with increasing compressive strength (Neville 2012). However, the precise form of this relationship is still unknown. So far, numerous attempts have been undertaken to develop a relationship between both properties for normal and high strength concrete. Recently, some studies have also attempted to find empirical relationship between both properties for UHPFRC (BFUP AFGC 2002, Ma et al. 2004, Graybeal 2007b). However, the accuracy and validity of these relationships are still questionable. Therefore, in this study, some of the proposed relationship for high strength and UHPFRC were used to predict the modulus of elasticity of the concrete mix. Among these is the well-known relationship proposed in the ACI 363R for high strength concrete up to compressive strengths of 83 MPa (ACI Committee 363 1997). The relationship is described in Equation 4.13. For UHPFRC, Equation 4.14 was derived from experimental results for a concrete mix very similar to the concrete used in this study (Ma et al. 2004). Furthermore, the AFGC recommendation has proposed a relationship, presented in Equations 4.15, from the work conducted at the Cattenom nuclear power plant (BFUP AFGC 2002).

$$E_{cm} = 3320\sqrt{f_c^{'}} + 6900 \qquad \text{Equation 4.13}$$

$$E_{cm} = 19000\sqrt[3]{\frac{f_c^{'}}{10}} \qquad \text{Equation 4.14}$$

$$E_{cm} = k_0 . \sqrt[3]{f_{cj}} \qquad \text{Equation 4.15}$$

where $f_c^{'}$ & f_{cj} = 28 days cylinder compressive strength (MPa), and

k_0 = a constant of 9500.

The reliability of Equations 4.13 to 4.15 were assessed by predicting the value of the modulus of elasticity in (GPa) for this particular UHPFRC mix.

4.5 Specimen Preparation

The mixing, casting and curing procedures were the same as described in Chapter 3, Section 3.4. A single mix of 100 litres was produced to cast 9 cubes of 100 mm, 9 cylinders of 100 x 50 mm diameter, a slab specimen with dimensions of 200 x 600 x 600 and 3 beams specimens of 100 x 100 x 500 in depth, width and length, respectively. For the UPV testing, the slab and beam specimens were used together. In the mean time, the beam specimens were also used for the resonant frequency testing. Cube specimens were used to measure the density and cube compressive strength of the concrete, while cylinders specimens were used for the determination of the cylinder compressive strength, modulus of elasticity and Poisson's ratio.

4.6 Experimental Test Methods

In this section, the experimental procedures are discussed for each test.

4.6.1 Ultrasonic testing method

For this test, two pairs of compression transducers with capacities of 0.082 and 2 MHz were used. The transducers were placed on the middle of a smooth area on the surface of the UHPFRC slab specimen, see Figure 4.3 (a). According to the literature (Qixian and Bungey 1996), when ultrasonic waves are transmitted through the transmitting transducer, several types of waves starts propagating through the sample as shown in Figure 4.7.

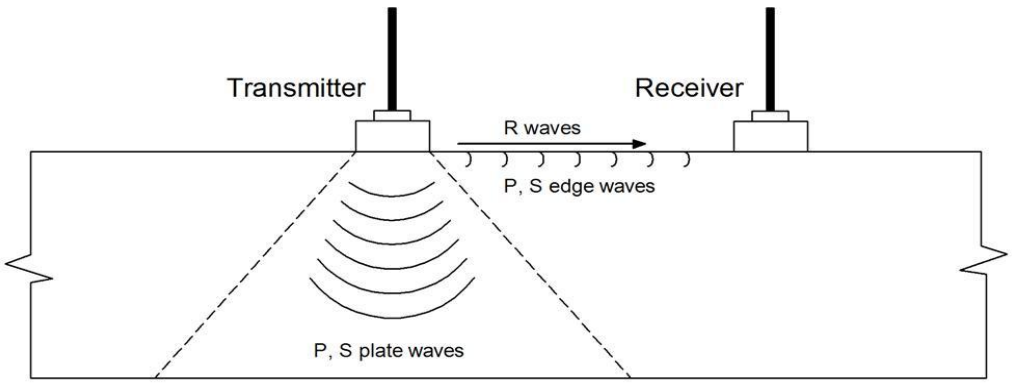

Figure 4.7. Wave propagation in indirect transmission using compression wave transducers.

The transmitting transducer issues propagating plate waves, P & S, in the axial direction as well as surface waves P, S and R in the radial direction. The compression waves, P, in the radial direction were characterised with high velocity and low amplitude, while the surface waves, R, have lower velocity and higher amplitude. Therefore, the arrival amplitudes of the, P & R, indirect waves were picked up by the receiving transducer, and using a digital storage oscilloscope, the waveforms were captured and displayed, as shown in Figure 4.8.

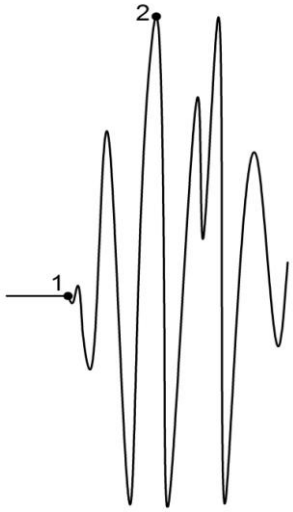

Figure 4.8. Received waveform from oscilloscope.

In Figure 4.8, point 1 indicates the arrival of the, P, waves due to its great velocity. The sudden increase in the amplitude of the following waveform at point 2 indicates the arrival of the, R, waves due to its high amplitude (Qixian and Bungey 1996). The UPV tests were carried out in accordance to the guidelines of BS EN 12504-4:2004. The indirect compression and surface wave velocity, $V_{p,s}$ & V_r, respectively, were measured on the slab specimen. For the measurement of the direct compression wave velocity, $V_{p,d}$, the beam specimens were used by placing the transmitting and receiving transducers on both ends of the specimen.

It must be noted, the size of the slab was chosen to avoid interference from reflecting P waves from the boundaries of the specimen. Furthermore, in order to avoid the influence of heterogeneity of the concrete, a line located in the centre of the specimen was drawn and several readings were taken to minimise any possible errors. First, the transmitting

transducer was fixed at a point and the location of the receiving transducer was moved in increments of 50 mm along the drawn line as shown in Figure 4.9. Transit times of the pulses were recorded for a complete series of distances between the transducers from 50 mm to 400 mm. Then, the results were plotted for all the readings and the mean values of wave velocities were given by the slope of the best straight lines, see Figure 4.10.

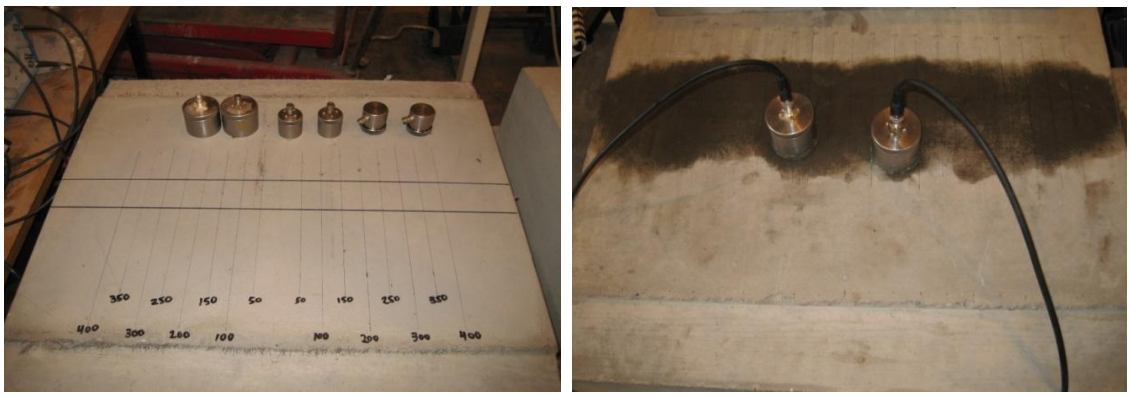

Figure 4.9: UPV reading at various points using different frequency transducers.

4.6.2 Resonant frequency testing method

This test was conducted according to the B. S. 1881-209:1990. In the current study, three beam specimens were excited to resonance in the fundamental longitudinal vibration mode using an Erudite and their resonance frequencies, n, were recorded in Hz. The lowest frequency at which longitudinal resonance occurs is the fundamental resonant frequency. For each specimen, three readings were taken and a mean value was obtained. After the tests were carried out at 58 days, the beam specimens were tested in flexure to examine the strength and quality of the concrete. The test was carried out in a four-point bending configuration, similar to the test setup description presented in Section 3.5.1.3. The point loads were applied at a distance of 150 mm to each other and the supports, and the clear span between the two supports was 450 mm. The tensile flexural strength of the concrete was 24.50 MPa.

4.6.3 Compression testing method

The compression tests of the cylinder specimens to determine the secant modulus of elasticity and the Poisson's ratio were carried out in accordance with BS 1881-121:1983.

It is important to note that the standard provides guidance for the determination of the modulus of elasticity only. However, Poisson's ratio was also determined during the direct compression tests.

In this test, three cylinder specimens were initially tested to determine the cylinder compressive strength of the concrete. Then, six more cylinder specimens were tested for the determination of the modulus of elasticity and Poisson's ratio. Each of these specimens was first positioned in the middle of the testing machine with an initial stress of 0.5 MPa applied. Then, the stress was increased up to one-third of the sample's compressive strength, approximately 50 MPa. The applied stress was maintained for 60 seconds and strain readings recorded electronically were taken at one second intervals during the succeeding 30 seconds. Then, the applied stress was reduced at the same loading rate as used during loading. This preloading cycle was carried out for two further cycles and the results were recorded. The individual strain readings at each strain gauge were within a range of less than ± 10% of their mean value. When all the strain measurements in the elastic range were completed, the specimen was loaded at the same loading rate until failure occurred.

In addition, in Section 3.6.2.1, compression tests were conducted to determine the uniaxial compressive stress-strain relationship for the UHPFRC mix. From these tests, the modulus of elasticity of the concrete were determined at various ages and compared to the results reported here. Finally, the cube compressive strength of the concrete was determined using the cube specimens according to the BS EN 12390-3:2009.

4.7 Results

4.7.1 Ultrasonic pulse velocity

Measurements on the slab and beam specimens were taken at ages of 7, 14, 28 and 56 days. For the slab specimen, the measured surface transmission times are plotted on the X axis against the corresponding distance apart of the transducers on the Y axis in Figure 4.10. The slopes of the lines were calculated using the least squares method and the velocity of each wave was determined. The slope of Line 1 represents the velocity of the indirect compression wave and Line 2 represents the velocity of the surface wave.

From Figure 4.10, the velocity of the compression wave, $V_{p,s}$, and the surface wave, $V_{p,r}$, at 28 days were 4655 and 2499 m/s, respectively. Once $V_{p,s}/V_{p,r}$ was determined, the values of the Poisson's ratio, ν_u, were calculated using Equation 4.5. The density of the concrete was determined using the 100 mm cube specimens. By substituting the results of density, ρ, and direct compression wave velocity, $V_{p,d}$, back into Equation 4.2, the value of the modulus of elasticity, $E_{d,u}$, was determined at each testing age. The full set of test results for this method is presented in Table 4.1.

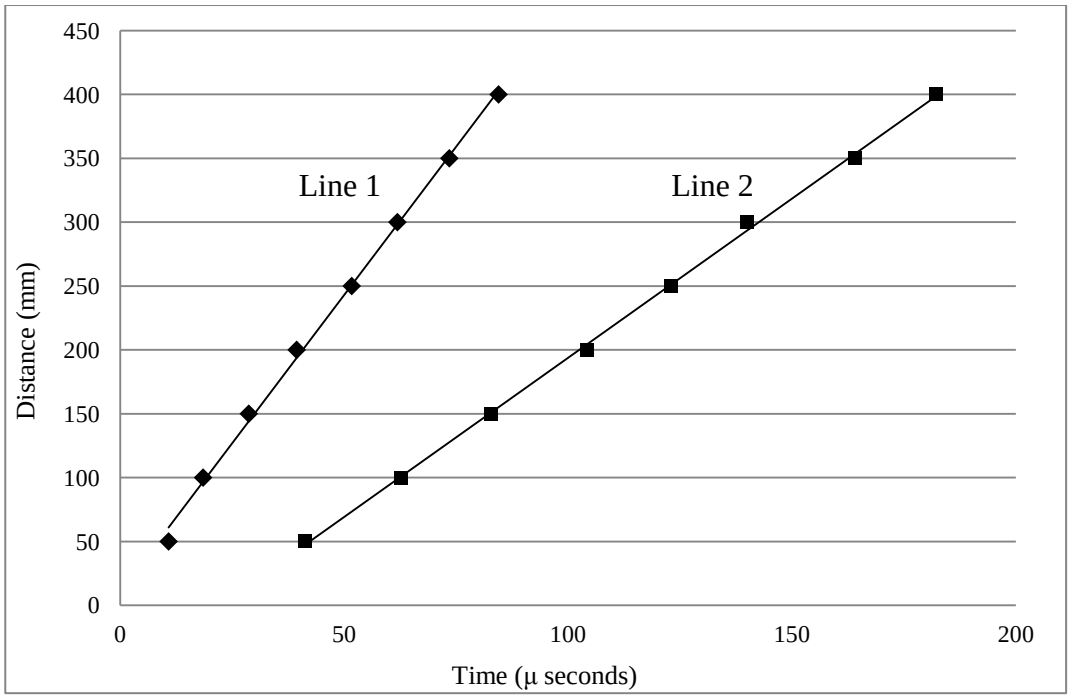

Figure 4.10: Relationship between distance and propagation time at 28 days using the slab specimen.

Table 4.1: Ultrasonic test results.

Age (days)	$V_{p,d}$ [1] (m/s)	$V_{p,s}$ [2] (m/s)	V_r (m/s)	$V_{p,s}/V_r$	$E_{d,u}$ (GPa)	ν_u
7	4751	4544	2492	1.823	48.44	0.220
14	4765	4697	2507	1.874	46.70	0.246
28	4822	4655	2499	1.863	48.25	0.241
56	4835	4701	2523	1.863	48.51	0.241

[1] =compression wave velocity using direct transmission for the beam specimens.
[2] =compression wave velocity using surface (indirect) transmission for the slab specimen.

At the same time, the beam specimens were used to measure direct compression wave velocities and the readings were used in Equation 4.10 in conjunction with resonant frequency testing measurements for the determination of the value of the Poisson's ratio, ν_r. During testing of the slab and beam specimens, various waveforms for both surface and direct transmissions from the two different frequency transducers were obtained and analysed, see Figure 4.11.

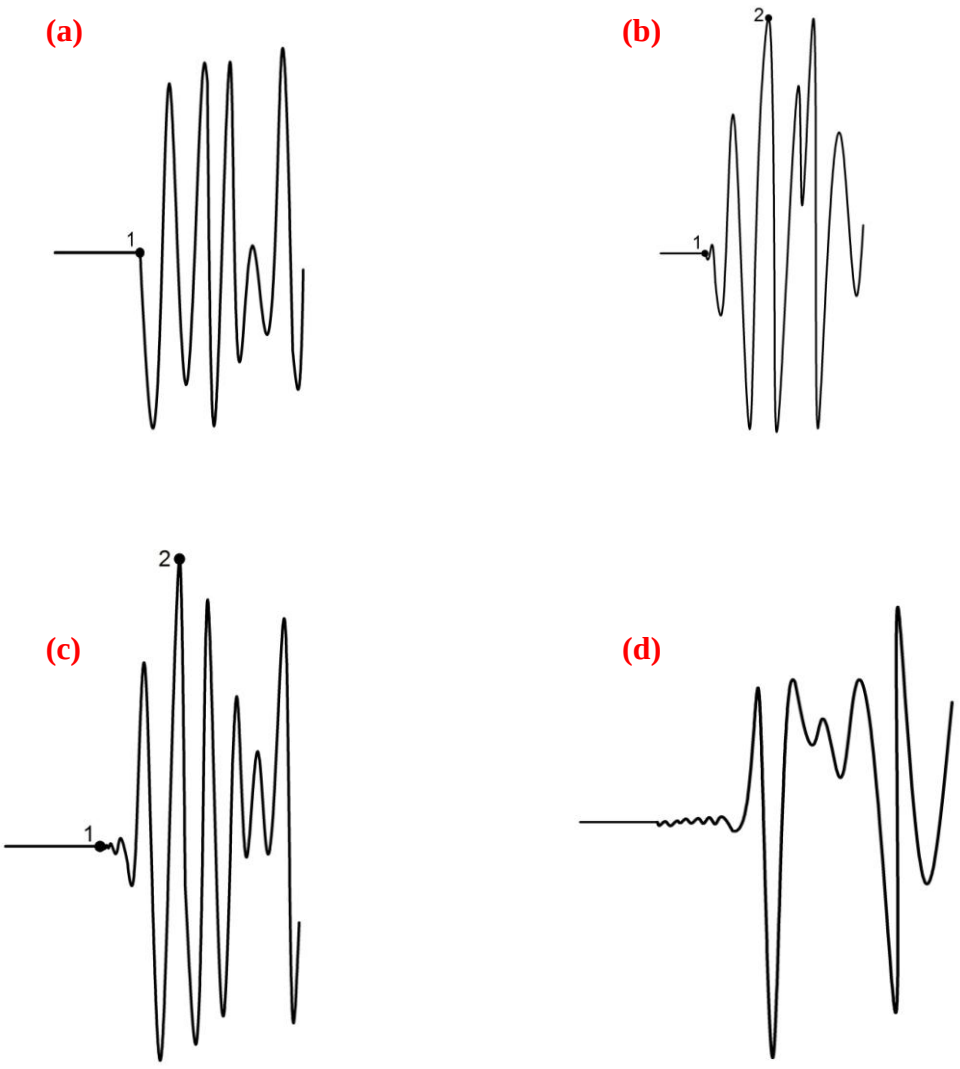

Figure 4.11: Waveform from direct and indirect (surface) transmission over different lengths using different frequency transducers: (a) direct transmission (100 mm) 2 MHz, (b) surface transmission (100 mm) 2 MHz, (c) Surface transmission (200 mm) 2 MHz, and (d) Surface transmission (100 mm) 0.082 MHz.

4.7.2 Resonant frequency

At the same time as the UPV testing, resonant frequencies of the beam specimens were taken. Three beams were tested and three readings for each specimen were recorded at each curing age. The average resonant frequencies were obtained. The dynamic modulus of elasticity, $E_{d,r}$, and Poisson's ratio, ν_r, were calculated using Equations 4.8 and 4.10, respectively. Furthermore, Equation 4.9 was used to predict the static modulus of elasticity, $E_{cm,r}$, of the concrete form the results obtained using Equation 4.8. The results for this method are given in Table 4.2.

Table 4.2: Resonant frequency test results (beams).

Age (days)	η (kHz)	$E_{d,r}$ (GPa)	$E_{cm,r}$ (GPa)	ν_r
7	4530	50.28	43.85	0.192
14	4570	51.13	44.91	0.182
28	4580	51.30	45.13	0.200
58	4610	51.99	45.99	0.193

4.7.3 Compression

Direct measurements using compression tests were carried out to determine, E_{cm}, at 7, 14 and 28 days using the cylinder specimens, while the value of , ν, was determined at 28 days only. For compressive strength measurements, both cylinder and cube specimens were tested at each age. Generally, it is accepted for normal strength concrete that cylinder test will result in a lower compressive strength by approximately 0.8 of the cube strength. This is due to the confining effect of the testing machine platens and the aspect ratio of the specimen. In this study, the ratios of cylinder to cube strength were found to be in a range of approximately 0.87 to 0.91, similar to those reported in Section 3.6.2.1. The direct test results are presented in Table 4.3.

Table 4.3: Direct test results for cylinder and cube specimens.

Age (days)	$f_{c,k}$ (MPa)	$f_{c,u}$ (MPa)	$f_{c,k} / f_{c,u}$	E_{cm} [3] (GPa)	ε_{peak} [4]	ν
7	140.9	160.8	0.876	44.17	3236	-
14	141.6	163.1	0.868	45.79	3864	-
28	149.4	164.3	0.909	46.16	3455	0.213

Furthermore, the test results for the values of modulus of elasticity presented in Section 3.6.2.1 were compared to those presented in Table 4.3. The results of both set of tests were in close agreement, with discrepancies less than 3%.

4.7.4 Empirical equations

As discussed earlier in Section 4.4.2, there are several different models to correlate the value of the modulus of elasticity to the compressive strength of the concrete. However, only three of these appeared to be relevant to the UHPFRC mix used in this study. Therefore, Equations 4.13 to 4.15 with the results of cylinder compression tests were used to predict the modulus of elasticity of the concrete. The results are presented in Table 4.4.

Table 4.4: Empirical equations test results.

Age (days)	$E_{eq\,4.13}$ (GPa)	$E_{eq\,4.14}$ (GPa)	$E_{eq\,4.15}$ (GPa)
7	46.31	45.89	49.43
14	46.41	45.97	49.52
28	47.44	46.76	50.38

4.8 Discussion

In Table 4.5, results from the static and dynamic test methods are presented and compared. The static test values were taken for the purposes of validating the dynamic test results. From Table 4.5, the values of the modulus of elasticity and Poisson's ratio of the concrete appear to increase with age for both the destructive and non-destructive testing techniques. However, the increase is very small. Similar results have also been reported in the literature (Graybeal 2005).

[3] =from cylinder tests.
[4] =peak microstrain.

Table 4.5: Static and dynamic test results.

Age (days)	E_{cm}	$E_{d,u}$	Error %	$E_{d,r}$	Error %	ν	ν_u	Error %	ν_r	Error %
7	44.17	48.44	9.66	50.28	13.84	-	0.220	-	0.192	-
14	45.79	46.70	1.98	51.13	11.66	-	0.246	-	0.182	-
28	46.16	48.25	4.52	51.30	11.13	0.213	0.241	13.15	0.200	6.10
58	-	48.51	-	51.99	-	-	0.241	-	0.193	-

For the values of the modulus of elasticity, the correlation between the static and those determined from the UPV and resonant frequency testing were relatively good. In particular, for the UPV test results with errors less than 10%. On the other hand, resonant frequency test results exhibited a greater value than the static ones with errors up to approximately 14%. This was expected as this method is known to overestimate the static modulus of elasticity of normal concrete in the range of 20-25% (Mosley et al. 2007). This is because specimens in the dynamic tests are under low levels of stress and so effectively the initial tangent modulus is measured rather than the secant modulus. However, accuracy of the resonance frequency test results improves with errors up to approximately 2% when Equation 4.9 was used to correlate the dynamic to the static modulus of elasticity. Although, this equation provides a good result at this instance for UHPFRC, it is used for normal concrete only.

Furthermore, results obtained from the empirical relationships were found to be in close agreement with the static test results, with errors up to approximately 12%. Equation 4.14 predicted the static test results with high accuracy, while Equation 4.15 was the opposite. It must be noted, many general relationships exist between the compressive strength and modulus of elasticity of concrete. However, the limited static test data reported here cannot be used to validate the accuracy of these equations. Therefore, a higher number of static test results are required. Nonetheless, from the results obtained here, it is safe to conclude that these equations can possibly be used as an indication to predict the value of the modulus of elasticity of UHPFRC.

In the meantime, BS 1881-203 1986 provides an empirical relationship between static and dynamic moduli of elasticity to pulse velocity, see Table 4.6. It states that values for the static and dynamic modulus of elasticity can be estimated from pulse velocity

measurements (BS 1881-203 1986). The relationship between these properties for this study was found to be very close to Table 4.6, with errors of approximately 5%.

Table 4.6: Empirical relationship between static and dynamic moduli of elasticity and pulse velocity (BS 1881-203 1986).

Pulse velocity	Modulus of elasticity	
	Dynamic	Static
km/s	MN/m^2	MN/m^2
3.6	24 000	13 000
3.8	26 000	15 000
4.0	29 000	18 000
4.2	32 000	22 000
4.4	36 000	27 000
4.6	42 000	34 000
4.8	49 000	43 000
5.0	58 000	52 000

Results of the dynamic Poisson's ratios of both methods are also in close agreement with the static ones. The UPV results appear to overestimate the static value, while the resonant frequency results tend to underestimate it. This is because Poisson's ratio is directly proportional to the ultrasonic pulse velocity and inversely proportional to the velocity of the resonant frequency waves. However, not knowing the value of Poisson's ratio of the concrete correctly would not make a large difference in determining the value of the modulus of elasticity in Equations 4.2 to 4.10. A change in the value over a full range of 0.16 to 0.22, reduces the computed values of the modulus of elasticity by only about 11% (Neville 2012). The value of Poisson's ratio for an isotropic and linear elastic material is constant but for conventional concrete, the value is reported to be in a ranges from 0.16 to 0.22 (Neville 2012). This is in close agreement with the test results reported in this study.

Finally, from the results and comparisons made above it is evident that both non-destructive testing techniques could predict the values of the modulus of elasticity and Poisson's ratio of the UHPFRC mix used in this study with relatively high degrees of accuracy. With similar or even better accuracies that has been reported for normal

concrete in the literature (Malhotra and Carino 2004, Bungey et al. 2006, Neville 2012). The UPV testing technique was found to be the most reliable and easy testing technique to operate in comparison to the resonant frequency and direct tests.

As noted previously, two different types of compression wave frequency transducers (0.082 and 2 MHz) were used for the UPV testing technique. The effect of the concrete mix on the velocity and shape of the waveforms were also investigated from using both set of transducers. The velocities of the compression waves from the 2 MHz transducers for the direct transmission were found to be higher than those for the indirect transmission measurement. This is believed to be due to the variation of stiffness of the concrete in the longitudinal and transverse direction, in which higher stiffness results in faster pulse velocity. Furthermore, the difference in moisture content between the concrete on the surface and the internal core of the specimen affects the velocity of the pulse, in which drier concrete results in lower wave velocities. This is in agreement with what has also been reported in the literature (Bungey et al. 2006).

Generally, the high frequency 2 MHz transducers resulted in clear signal waveforms as shown in Figure 4.11(a, b and c). The arrival of the, P & R , waves (Points 1 and 2) were easily identified. However, the lower frequency 0.082 MHz transducers were found to be unsuitable for the UHPFRC tests. This is believed to be due to the dense and fine grained nature of the matrix and high content of steel fibres in the mix (Glaubitt and Middendorf 2008) as only weak or unreliable signals were obtained. Furthermore, the arrival of the, P & R , waves from the 0.082 MHz transducers were found to be hard to identify, see Figure 4.11 (d). Therefore, this study believes that high frequency transducers that are usually used for metal are essential for UPV measurements for UHPFRC. Lower frequency transducers that are usually used for normal strength concrete containing large particles of aggregate and no steel fibres might need to be avoided for UHPFRC.

Furthermore, various waveforms from direct and indirect transmissions using both frequency transducers are shown in Figure 4.11. The direct transmission wave on the beam specimen using the 2MHz transducers is shown in Figure 4.11 (a). In this figure,

the compression wave, P, is very strong in the axial direction and its arrival can be seen clearly. However, the surface wave, R, is confined on the surface of the specimen and their arrival cannot be detected. In contrast, Figure 4.11 (b) and (c) show the surface transmission of the, P & R, waves on the slab specimen at various distances. The front of the waveform consists of high velocity with low amplitude compression waves. The subsequent increase in the amplitude of the waves was due to the arrival of the surface waves as can be seen clearly in both cases. The shape of the waveforms, shown in Figure 4.11, are all in close agreement to the theory explained in Section 4.6.1 and the literature (Qixian and Bungey 1996).

Finally, the velocity of the compression and surface waves obtained here were compared to those reported for normal concrete. It was evident that faster pulse velocities were recorded for UHPFRC compared to conventional concrete (Qixian and Bungey 1996). This is believed to be influenced beneficially by the steel fibre content and high density of the matrix.

4.9 Summary

In this study, the potential use of two non-destructive testing methods (ultrasonic pulse velocity and resonate frequency) to determine the values of the modulus of elasticity and Poisson's ratio for UHPFRC have been investigated. Furthermore, the reliability of a number of empirical relationships to predict the modulus of elasticity from the compressive strength of the concrete was also studied. The results of the non-destructive testing methods and empirical relationships were validated against results from static compression tests.

For the modulus of elasticity results, the conventional compression transducers with a frequency of 2MHz in the UPV approach were found to produce comparable results to the static test values, with errors of less than 10%. While the resonant frequency testing technique produced results with an acceptable degree of accuracy, with errors less than 14%. However, empirical relationships that exist for the resonant frequency method improves the results to errors of just 2%. Furthermore, results obtained from the empirical relationships were also found to be in good agreement to those of the static

tests, with errors less than 11%. For the values of the Poisson's ratio, both non-destructive testing techniques were also in good agreement to the static test, with errors less than 14%.

From this study, it is evident that the dynamic test results were satisfactory and comparable to the static tests results. The reliability of both non-destructive testing methods for the concrete was found to be acceptable, in particular, the UPV testing method. This method is easy to use, portable and a reliable non-destructive testing method which can provide results with good accuracy for this concrete. The findings reported here are vital for the widespread of UHPFRC in construction industry. It indicates that the UPV testing method can now be used with certainty for the determination of the elastic properties of existing UHPFRC structures. One good application can possibly be the periodic maintenance check of UHPFRC highway bridge structures which can be very cost effective compared to static testing methods. This method can equally be used in laboratory testing (Hassan and Jones 2012). Furthermore, suitability of the resonant frequency testing method was also found to be good for UHPFRC. The only drawback involved with this method is that limited to laboratory testing only.

Results presented in Figure 4.11 demonstrate the necessity of high frequency transducers in the UPV testing technique for UHPFRC. This is contrary to the literature stating the requirement of lower frequency transducers for normal concrete. From the same figure, faster pulse velocities were also recorded for the concrete when compared to normal concrete test results reported in the literature (Qixian and Bungey 1996). The requirements for high frequency transducers and measurements of higher pulse velocities for UHPFRC are linked to the steel fibre content and high density of the matrix. This indicates minor modifications and care might be required for the UPV testing technique for UHPFRC. Finally, further studies are also recommended for a range of UHPFRC mixes containing different volumes of steel fibres, possibly higher volume than 2%, to confirm the reliability of the non-destructive test methods described here.

Chapter V: UHPFRC Cast in-situ Application

5.1 Introduction

To date, UHPFRC has been used in the form of precast units with few examples of cast in-situ applications. The industrial production of UHPFRC units has proved to be very expensive. Current production involves long storage times (at least 48 hours) at elevated curing temperatures, such as 90 ^{o}C to improve the microstructure of the mixture and to encourage rapid strength gain. In recent years, special environmental and financial concerns such as reducing energy consumption have increased worldwide. Therefore, alternative ways of exploiting this promising material, i.e. cast in-situ applications, needs to be investigated.

So far, UHPFRC in cast in-situ applications have been limited to a few highway bridge girders and decks in the United States, Australia and Japan (Matsubara et al. 2008, Rebentrost and Wight 2008b). The potential use of this material in cast in-situ applications and long term strength gain in varying environmental conditions to minimise its environmental impact and high cost has not been investigated in detail. Therefore, detailed studies in this area of research are required; in particular, the suitability of this material for cast in-situ bridge applications.

In this study, the influence of four different curing temperatures of 10, 20, 30 and 90 ^{o}C on the compressive and tensile flexural strength development of UHPFRC for periods of up to a year was investigated. The three lower curing temperatures were chosen to represent conditions that are likely to be encountered for cast in-situ applications, while the 90 ^{o}C curing temperature has been used for precast production of UHPFRC components. Moreover, the effect of the curing temperatures on the compressive and tensile flexural strength development of the matrix alone (UHPC) for 28 days was studied. This is to further investigate the defect phenomenon reported in Sections 3.6.1.2 and 3.6.1.3 of this thesis. The results obtained here are based on extensive experimental work and are significant to the construction industry for exploiting this material for cast in-situ applications at the range of environmental conditions typically encountered on construction sites.

5.2 UHPFRC Curing Regimes

Curing is the procedure used in concrete for promoting the hydration of cement. This process consists of a control of temperature and of the moisture movement from and into the concrete (Neville 2012). The curing process of UHPFRC is slightly different compared to normal concrete. The current productions of UHPFRC units are mainly precast members. The standard manufacturer recommended members to be cured under room temperature for the first 24 hours for initial setting (Graybeal 2005). During this time, members are kept in their moulds and similar practise used for conventional concrete applies here to prevent moisture loss. This is followed by 48 hours at an elevated temperature at 90 ^{o}C. Moreover, elevated heat treatment curing can range from 90 to 400 ^{o}C and last from 2 to 6 days (Voort et al. 2008).

The post-set heat treatment is applied to accelerate the hydration reactions of cement and the pozzolanic reaction of silica fume and calcium hydroxide produced from the hydration of cement. This area of research has been investigated in detail by a number of studies (Cheyrezy et al. 1995, Zanni et al. 1996). The influence of various curing temperatures on the pozzolanic reaction ratio for UHPFRC members is shown in Figure 5.1. The increase in reaction due to high curing temperatures result in a rapid improvement in strength and other mechanical properties in a shorter time compared to normal curing temperature at 20 ^{o}C.

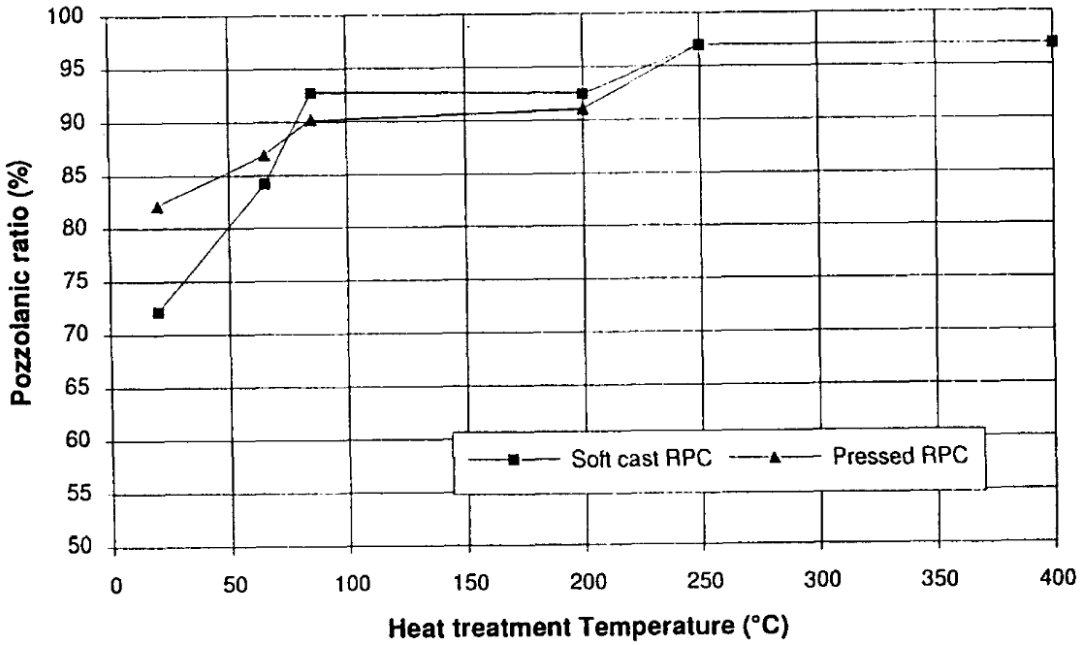

Figure 5.1: Pozzolanic ratio versus heat treatment temperature (Cheyrezy et al. 1995).

Despite the standard 48 hours of 90 ^{o}C curing, other types of curing regimes have been used for UHPFRC production. Improved performance has been observed after using a combination of heat, steam, and pressure treatments (Richard and Cheyrezy 1995, Graybeal 2006, Le 2008). The combined method is usually used in research studies only and is very expensive.

5.3 Research Significance

There are many factors contributing to the cost of UHPFRC being so expensive. The curing process used in precast production is one of them. As well as this, precast production may limit the dimensions and weight of UHPFRC segments due to transport practicalities. Therefore, identifying possible ways to reduce the energy consumption in UHPFRC production is desirable and using this concrete in cast in-situ structures is imperative for its application to become widespread. However, so far, the literature survey indicates studies investigating the suitability of this material for cast in-situ applications have been rather limited (Graybeal 2005, Le 2008, Yang et al. 2009, Hong et al. 2010). Most of these studies have investigated the influence of 20 ^{o}C curing temperature on the mechanical properties of UHPFRC for a short period of time, i.e. 28 days. However, investigating a wider range of possible different curing temperatures i.e.

10, 20, and 30 ^{o}C over a longer period such as one year has not been studied yet. The influence of temperatures that are similar to site conditions in hot and cold climates on compressive and tensile flexural strength development, particularly in the longer term, are essential to be investigated in detail. Therefore, in this study, an extensive experimental investigation was conducted to study the potential use of UHPFRC for cast in-situ applications at different curing temperatures of 10, 20, and 30 ^{o}C. The results obtained from these curing temperatures were compared to specimens cured at 90 ^{o}C temperature.

Furthermore, the defect phenomenon observed and reported in Sections 3.6.1.2 and 3.6.1.3 was further investigated. UHPC cube and beam specimens were cast and cured at the same curing temperatures as the UHPFRC specimens. A detailed study was conducted to further examine the influence of various curing temperatures and the steel fibre absence on the reported phenomenon and mechanical properties of UHPC up to 28 days of age. In particular, the maximum flexural load of UHPC beam specimen (equivalent to first cracking load for UHPFRC specimens). The results obtained here were compared to those reported for the UHPFRC specimens.

5.4 Specimen Preparation

In this study, a large number of cube and beam specimens were cast and cured at four different curing temperatures of 10, 20, 30 and 90 ^{o}C. The mixing and casting of the specimens followed the same procedures presented in Sections 3.4.2 and 3.4.3, respectively. However, the curing procedure was different. After casting, specimens for the 10, 20 and 30 ^{o}C curing temperatures were wrapped in their moulds using polythene 'cling film' and tape. Then, they were submerged in water curing tanks of matching temperatures, as shown in Figure 5.2. Water curing was used to minimise moisture loss during setting and ensure good quality concrete for the investigation. For each curing temperature at least 60 cubes of 100 mm and 40 beams of 100x100x350 mm in width, depth and length, respectively, were cast. De-moulding took place once the specimens had gained sufficient hardening, 1 day for the 20 and 30 ^{o}C temperatures and 2 days for the 10 ^{o}C temperature. After de-moulding, all the specimens were submerged back into their curing tanks till the age of testing. The temperatures of all the tanks were monitored

throughout the experimental programme; a maximum variation of ±3 ^{o}C was recorded. However, specimens for the 90 ^{o}C curing temperature were covered with damp hessian and polythene sheets after casting, and kept at laboratory temperature (~20 ^{o}C) for 1 day. The following day, de-moulding took place and the specimens were immersed in a water curing tank for 2 days at a temperature of 90 ^{o}C. Following the curing programme, the 90 ^{o}C specimens were removed from the water tank and dry kept at laboratory temperature until the testing days. The procedures described above were followed to replicate the cast in-situ and precast applications of UHPFRC.

Figure 5.2: Specimen preparation and curing for 10, 20 and 30 ^{o}C curing.

In addition, 9 cube and 9 beam UHPC specimens were cast for each curing temperature. The same casting, curing and testing procedures were followed as described for the UHPFRC specimens in this study.

5.5 Test Procedures and Measurement

In this study, the test procedures followed standard testing methods in compliance with recognised standards and recommendations for conventional concrete and steel fibre reinforced concrete such as (JSCE-SF4 1984, BFUP AFGC 2002, BS EN 12390-3 2009). Each result reported here was taken from the average of three or more test results.

The testing procedures and various mechanical property measurements obtained here are summarised below.

5.5.1 Compression test

Compressive strength development was measured in compliance with the BS EN 12390-3:2009, by testing standard 100 mm cube specimens for both concretes. Compression tests for UHPFRC cube specimens were conducted at ages 0.25, 0.5, 1, 2, 3, 5, 7, 14, 28, 60, 90, 120, 150, 180, 270 and 360 days, while the UHPC specimens were tested at 7, 14 and 28 days only. The tests were performed under a loading rate of 3 kN/second in a 3000 kN ToniPACT compression testing machine. The specimens of the three lower age curing regimes were removed from the curing tank an hour before testing. The density was measured and then the specimens were tested. The compressive strength was reported to the nearest one decimal place.

5.5.2 Flexural test

The development of first cracking strength, flexural strength, and flexural toughness were measured using beam specimens in a four-point loading flexural test. The flexural test followed the same procedure described in Section 3.5.1.3 of this thesis. The test was conducted in compliance with the JSCE-SF4 recommendation (JSCE-SF4 1984).The flexural tests for UHPFRC specimens were conducted at ages of 7, 14, 28, 60, 90, 120, 150, 180 and 360 days, while the UHPC specimens were tested at 7, 14 and 28 days only. For each flexural test, following properties were recorded:

- Density of the concretes using Archimedes principle
- Cross sectional area of the specimen using Electronic Vernier Calliper (EVC)
- Load at first crack, P_y
- Ultimate load, P_u
- Deflection at first crack, δ_y
- Deflection at ultimate load, δ_u
- Macrocrack width, and
- Flexural toughness, T_b .

The first cracking strength was determined in this study as it is an essential parameter which has been suggested to be used for studying the tensile performance of UHPFRC in the absence of a direct tensile test (BFUP AFGC 2002). The ASTM C1018-97:1997 in connection with ASTM C78-10:2010 proposes a relationship to calculate this parameter from flexural test using Equation 5.1 (ASTM C1018-97 1997, ASTM C78-10 2010).

$$f_{ct,flexure} = \eta \frac{P_y \, l}{b \, d^2} \qquad \text{Equation 5.1}$$

where $f_{ct,flexure}$ = flexural tensile cracking strength (MPa),

P_y = load at first crack (N),

l = span length (mm),

$b \& d$ = width and depth of the specimen in (mm), respectively, and

η = variable for the loading configuration, for the current setup is equal to 1.

In this study, the first cracking load for UHPFRC was identified from the load deflection curve at which the form of the curve first becomes nonlinear. It must be noted that Equation 5.1 is widely used and is based on the elastic beam theory as discussed in Section 3.2.3. However, other studies(Carpinteri and Chiaia 2002, Chanvillard and Rigaud 2003) have indicated the incompatibility of this equation for UHPFRC since it does not take the specimen's size and fibre reinforcement effects into account. Therefore, the AFGC recommendations (BFUP AFGC 2002) have proposed a different relationship based on experimental data. This relationship is shown in Equation 5.2, which allows to determine the first cracking strength of UHPFRC using a correction factor depending on the cross section of the tested specimen. In this study, Equation 5.2 was used to calculate the first cracking strength of the 90 ^{o}C cured UHPFRC specimens and was related to its direct tensile strength reported in Section 3.6.1.1.

$$f_{ct,1} = f_{ct,flexure} \frac{2.0\left(\frac{d}{d_0}\right)^{0.7}}{1 + 2.0\left(\frac{d}{d_0}\right)^{0.7}} \qquad \text{Equation 5.2}$$

where $f_{ct,1}$ = corrected first crack flexural tensile cracking strength in (MPa), and

d_0 = reference depth of 100 mm.

For tensile flexural strength determination, many studies prefer using the first cracking load in Equations 5.1 and/or 5.2 on the basis of ordinary elastic theory, pure bending on a uniform elastic cross-section (Graybeal 2005, Ahlborn et al. 2008). However, in this study, the tensile flexural strength for both concretes was calculated using the maximum flexural load that the beam could attain during testing. This is because first cracking load appeared to be misleading and influenced by the high curing temperature significantly. The factors affecting the first cracking load will be discussed in details in this chapter. The tensile flexural strength development were determined here in accordance with the JSCE-SF4 using Equation 5.3 (JSCE-SF4 1984).

$$\sigma_b = \frac{P_u\, l}{b\, h^2} \qquad \text{Equation 5.3}$$

where σ_b = tensile flexural strength (MPa), and

P_u = ultimate load (N).

Equations 5.1 to 5.3 are presented here to discuss various approaches taken by different studies in investigating the tensile flexural strength of UHPFRC. However, since this study is only concerned with the effect of various curing temperatures on the strength development of the concrete, the validity of these equations are irrelevant and is not further discussed. The parameters investigated here were mainly based on the first cracking and maximum tensile flexural loads versus deflection rather than tensile flexural strength. The values of tensile flexural strength were determined for comparison reasons only.

Flexural toughness is another parameter which has been investigated here to indicate the ductility behaviour of both concretes. Flexural toughness is an important material property of concrete and a similar one to the concept of fracture energy, as described in the literature review. The property of flexural toughness relates to the ability of concrete

to absorb energy after crack formation. The JSCE-SF4 along with other standards and researchers (ASTM C1018-97 1997, ASTM C1550-03 2003, Graybeal 2006, El-Ashkar and Kurtis 2006) have used this property to indicate the ductility behaviour of fibre reinforced concrete. The JSCE-SF4 standard describes the flexural toughness as the work done when the load is applied onto the beam to deflect the beam by a defined distance (midspan deflection). It is characterised by the post-peak portion of the area under the load-deflection curve obtained during a flexural test on 100x100x350 mm beam specimens in four-point loading test. The standard recommends that flexural toughness shall be determined from the area of the load-deflection curve until a deflection of 1/150 times the span is achieved, as shown in Figure 5.3.

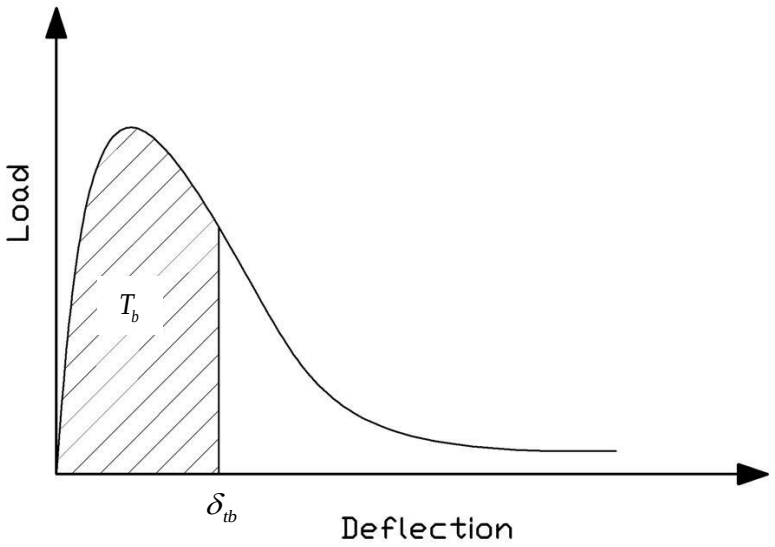

Figure 5.3: Flexural toughness as described in (JSCE-SF4 1984).

In this study, the influence of the curing temperatures, steel fibres and concrete age on this parameter was studied. Flexural toughness was determined in compliance with the JSCE-SF4 standard using Equation 5.4. The area of the load-deflection curve up to a deflection of 2 mm was integrated. Then flexural toughness was expressed by flexural toughness factor using Equation 5.4 below.

$$\overline{\sigma_b} = \frac{T_b}{\delta_{tb}} \frac{l}{bh^2} \qquad \text{Equation 5.4}$$

where $\overline{\sigma_b}$ = flexural toughness factor (MPa),

T_b = flexural toughness (J), and

δ_{tb} = deflection of l/150 (mm).

5.6 Results and Discussion

As is often the case of concrete experiments, the variation in the test results reported here was rather high, especially for the flexural test results. It is apparent that the inconsistency of the results may have occurred from the casting and testing procedures. However, during the entire time of the experimental programme, this study tried to stay consistent and the experimental procedures were kept the same. Significant conclusions can be drawn from the results reported below.

5.6.1 Fresh concrete

For every mix, workability of the concretes were measured using the flow table in accordance with the BS EN 1015-3:1999. The flow diameters for UHPC were in range of 234-241 mm. However, the addition of steel fibres in UHPFRC had a negative influence on the workability and influenced the slowing effect of the concrete. Flow diameters in a range of 223-228 mm were reported. Figure 5.4 shows the measurement of fresh concrete using flow diameters.

Figure 5.4: Measuring the fresh concrete using flow diameters.

5.6.2 Hardened concrete

The hardening process for all the concrete mixes did not initiate until approximately 24 hours after casting, with the exception of the 30 ^{o}C curing specimens which started to harden after 12 hours. The hardening for all the curing temperatures at 3, 6 and 12 hours after casting were checked by de-moulding cube specimens, checking their integrity and testing them in compression. Figure 5.5 shows the hardening process of UHPFRC cube specimens at 12 hours for the 10, 20 and 30 ^{o}C curing temperatures. It is evident that the concrete has not started to harden for the 10 and 20 ^{o}C curing temperatures at this age. However, within 24 hours, all the concrete mixes had gained sufficient compressive strength regardless of their curing temperatures. Similar times for hardening UHPFRC have been reported in the literature by others (Habel et al. 2006, Graybeal 2007b).

Figure 5.5: Hardening process at 12 hours for UHPFRC specimens cured at: (a) 10 ^{o}C, (b) 20 ^{o}C, and (c) 30 ^{o}C.

It must be noted, the dormant period of approximately 24 hours for UHPFRC is significantly longer than that of conventional concrete, despite the high content of Portland cement in the mix. This delay was found to be highly dependent on the high range water-reducing admixtures and the amount of specific cement replacement material such as GGBS in the mix. The polycarboxylate-based superplasticiser Structuro 11180 supplied by FOSROC Ltd, UK was used in the mix and this type of superplasticiser is known to delay the hardening process by at least 6 hours after mixing. Furthermore, the presence of GGBS in concrete was reported to slow the hardening process considerably at an early age (Xiangming et al. 2012). The combination of all the

factors described above is believed to have caused the delay in the hardening process of the concrete considerably.

Before each test, the density for all the cube and beam specimens for both concretes at all the different curing temperatures were measured. Regardless of the curing regimes, the density of the UHPFR and UHPC was in a range of 2430-2480 and 2300-2340 kg/m^3, respectively. The full range of density measurements for all the cube specimens are shown in Table 5.1. The high values of density for both concretes are governed by the minimal amount of water and high content of fillers such as silica fume in the mix. The UHPFRC exhibited higher density values compared to those of UHPC due to the steel fibre content in the mix.

Table 5.1: Density measurement for the UHPFRC and UHPC cube specimens.

	UHPFRC (kg/m^3)				UHPC (kg/m^3)			
Age (days)	10 ^{o}C	20 ^{o}C	30 ^{o}C	90 ^{o}C	10 ^{o}C	20 ^{o}C	30 ^{o}C	90 ^{o}C
0.25	-	-	-	-	-	-	-	-
0.5	-	-	2441	-	-	-	-	-
1	2453	2449	2445	2441	-	-	-	-
2	2461	2453	2430	2458	-	-	-	-
3	2443	2448	2439	2462	-	-	-	-
5	2468	2448	2440	2451	-	-	-	-
7	2463	2461	2435	2457	2341	2341	2300	2325
14	2475	2454	2449	2441	2339	2343	2306	2329
28	2452	2453	2439	2448	2340	2338	2303	2316
58	2472	2457	2420	2455	-	-	-	-
90	2476	2455	2438	2463	-	-	-	-
120	2476	2465	2337	2446	-	-	-	-
150	2477	2473	2442	2464	-	-	-	-
180	2455	2458	2434	2450	-	-	-	-
270	2477	2454	2445	2447	-	-	-	-
360	2477	2469	2337	2443	-	-	-	-

Following the density check, compressive strength, flexural tensile behaviour and durability checks of the concretes were investigated and the results are reported below.

5.6.2.1 Compressive strength

Compressive strength development for UHPFRC specimens with time at various curing temperatures is shown in Figure 5.6. The compressive strength development for all the four concrete mixes was found to be highly dependent on the curing temperatures, particularly at early ages. Compressive strength development increased rapidly from an age of 1 day for all the curing temperatures, particularly in the 30 and 90 ^{o}C curing regimes. Specimens cured at 30 and 90 ^{o}C showed rapid early age strength gain due to the high curing temperatures which accelerates binder hydration in the concrete.

The 90 ^{o}C cured specimens reached their ultimate compressive strength within 5 days and significant strength gain ceased beyond this age. This is believed to be due to the formation of dense hydrated phases around the unreacted cement particles which prevents further hydration, as has been reported for normal concrete (Barnett et al. 2006). The phenomenon known as the crossover effect (Alexander and Taplin 1962) in which high curing temperature above 35 ^{o}C at later ages results in a decrease in the compressive strength of normal concrete was not observed for UHPFRC. Furthermore, compressive strength development between 5 and 360 days for the 90 ^{o}C curing temperature was found to be very small and insignificant, approximately 4% increase.

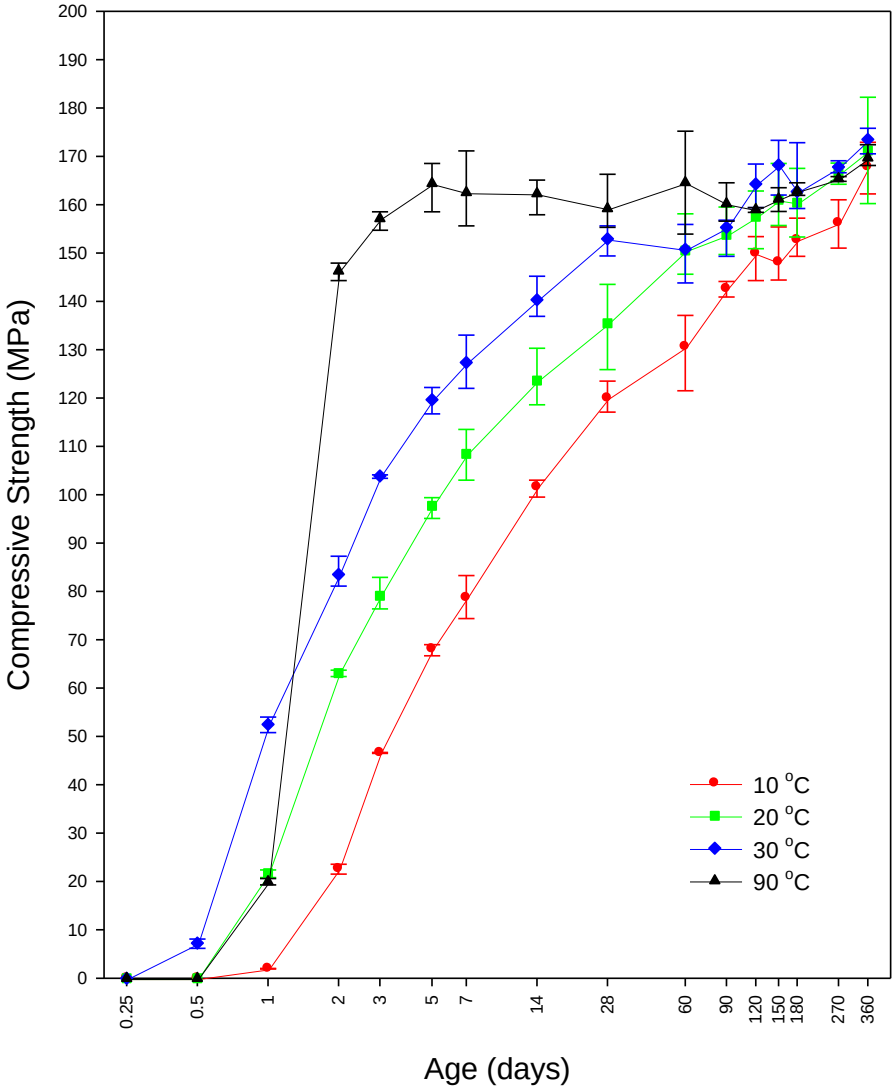

Figure 5.6: Compressive strength development with time.

For the 10 and 20 °C cured specimens, the rate of strength development at early age was lower in comparison to the 90 °C cured specimens. This was expected, since low temperature curing causes a lower rate of cement hydration and requires longer time till full hydration takes place. After 7 days, the compressive strength gain for the 10, 20 and 30 °C cured specimens in comparison with the 90 °C specimens, were approximately 48, 67 and 78%, respectively. In contrast, strength gain for the same concrete mixes at 28 and 90 days, respectively, was reported to be in a range of 75, 85 and 96 %, and 89, 96 and 97 %. At 360 days, all the lower temperature cured specimens have reached the same or even greater strengths that the 90 °C cured specimens and their strength development appeared not to have ceased. This continuous increase in the compressive

strength for the lower temperature cured specimens is promising and can be attributed to the continuous hydration of the unhydrated cement components with time and possibly pozzolanic reaction from the GGBS and microsilica in the matrix (Schachinger et al. 2008, Fall et al. 2010).

The low compressive strength development at early ages (up to 3 days) for the lower temperature curing of 10 and 20 ^{o}C may be outweighed by the extended usability and reduced cost of the concrete compared to precast production. Nevertheless the results obtained for all lower curing temperatures were much greater than that of conventional concrete. The compressive strength development for the three lower temperature cured specimens during the first week after casting is significant. It indicates that with time, cast in-situ UHPFRC can gain sufficient compressive strength, for instance, the 20 and 30 ^{o}C cured specimens at an age of 2 days have reached compressive strengths of 63.1 and 83.5 MPa, respectively. This early age strength gain of UHPFRC with ambient temperatures is considered to be of special importance for the cast in-situ applications of the concrete, particularly in highway bridge designs for stripping formwork and opening the structure to traffic or allowing follow-on construction. The findings reported here on the compressive strength development of UHPFRC can play a significant role in reducing the high initial cost and the energy required in the precast production of the concrete.

For the UHPC specimens, compressive strength development for all the curing temperatures was very similar to those reported for the UHPFRC. Higher compressive strength was observed for specimens cured at high curing temperatures, i.e. 30 and 90 ^{o}C. The compressive strength gain for the 10, 20 and 30 ^{o}C cured specimens in comparison with the 90 ^{o}C specimens at 7 and 28 days, were approximately 55, 70 and 89%, and 75, 90 and 99%, respectively. This is very similar to those reported earlier for the UHPFRC specimens. The defect phenomenon reported in Sections 3.6.1.2 and 3.6.1.3 appeared to have not influenced the compressive strength development of the concrete. The experimental investigation for the UHPC was limited to 28 days only to minimise unnecessary experimental work.

In addition, the effect of the absence of steel fibres on the compressive strength development on the UHPC specimens for all the curing temperatures was very little. The ratio of compressive strength development for UHPC to the UHPFRC specimens at 28 days for the 10, 20, 30 and 90 ^{o}C curing temperatures were 96, 100, 99, 96%, respectively. This shows the importance of curing temperatures compared to steel fibres on the compressive strength development of this concrete. However, the modes of failure for both concretes were considerably different due to the steel fibre content. The failure behaviours for UHPC specimens that cured at 10 and 20 ^{o}C were similar to a typical normal concrete failure, brittle but not very explosive. However, for specimens cured at 30 and 90 ^{o}C, failure was very brittle and explosive. In contrast, failure of the UHPFRC specimens for all the different curing temperatures was all ductile and the cube specimens were intact after failure due to the presence of fibres in the mix. Figure 5.7, shows the failure mode of UHPFRC and UHPC cube specimens cured at 90 ^{0}C. Furthermore, the compressive strength test results for all the curing temperatures for the UHPFRC and UHPC are listed in Table 5.2.

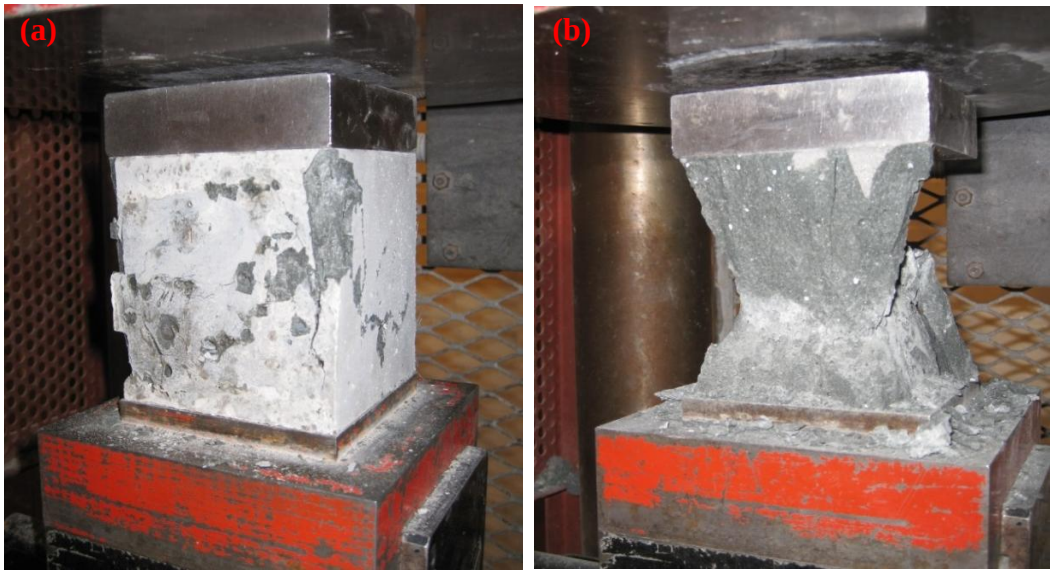

Figure 5.7: Compressive failure mode for cube specimens cured at 90 ^{o}C for: (a) UHPFRC, and (b) UHPC.

Table 5.2: Compressive strength development for UHPFRC and UHPC cube specimens at various curing ages.

	UHPFRC (MPa)				UHPC (MPa)			
Age (days)	10 ^{o}C	20 ^{o}C	30 ^{o}C	90 ^{o}C	10 ^{o}C	20 ^{o}C	30 ^{o}C	90 ^{o}C
0.25	-	-	-	-	-	-	-	-
0.5	-	-	7.3	-	-	-	-	-
1	2.0	21.7	52.5	20.0	-	-	-	-
2	22.6	63.1	83.5	146.3	-	-	-	-
3	46.6	79.1	103.9	157.1	-	-	-	-
5	68.1	97.7	119.7	164.4	-	-	-	-
7	78.7	108.5	127.4	162.5	79.0	100.6	127.9	143.3
14	101.6	123.6	140.4	162.3	89.1	123.2	142.0	145.5
28	120.0	135.5	153.0	159.2	115.6	138.9	152.0	153.6
58	130.6	150.5	150.8	164.6	-	-	-	-
90	142.6	153.8	155.3	160.2	-	-	-	-
120	149.9	157.5	164.3	159.0	-	-	-	-
150	148.1	161.0	168.2	161.2	-	-	-	-
180	152.7	160.4	162.7	162.8	-	-	-	-
270	156.2	166.4	167.8	165.4	-	-	-	-
360	167.8	171.2	173.5	169.7	-	-	-	-

5.6.2.2 Flexural behaviour

In this study, extensive investigation on the effect of curing temperatures and steel fibre content on the flexural tensile behaviour of UHPFRC and UHPC using four point bending tests were conducted. The flexural tensile behaviour of the concretes was investigated by studying the first cracking load, flexural load, and flexural toughness. Figure 5.8 shows the typical flexural load-deflection curves at different curing temperatures obtained at 28 days of age for UHPFRC beam specimens.

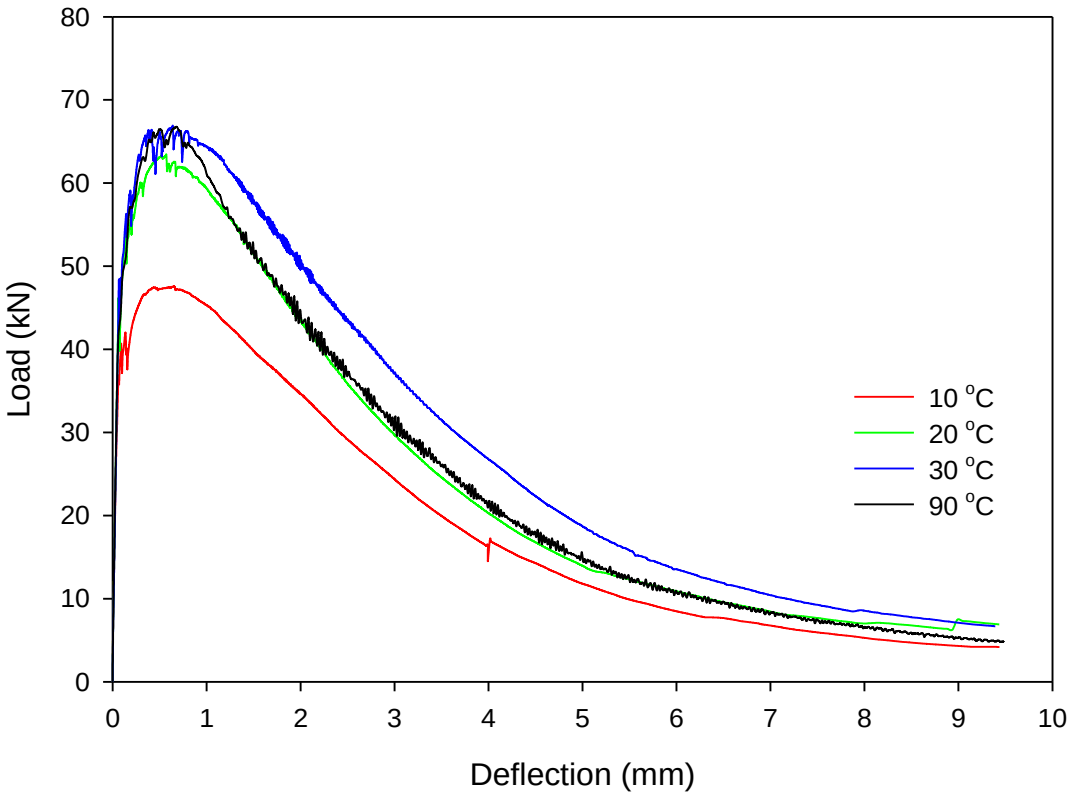

Figure 5.8: Flexural load versus deflection for UHPFRC beam specimens cured at various curing temperatures at 28 days.

The results show that all the tests responded linearly until the development of the first crack regardless of the curing temperatures. Prior to the point of first crack formation (microcrack), the cementitious matrix and the steel fibres are strained, however, without damage. This has resulted in the initial linear response which was observed for all the tests. However, with the formation of first crack, a sudden decrease in the load carrying capacity occurred over a very short time. This load is known as the first cracking load. Soon after this, the load started to increase again in which a number of cracks in both sides of the specimen occurred as the test continued, see Figure 5.9. Initially, the cracks were spaced approximately 20 to 40 mm apart throughout the area of the maximum load, however, this spacing decreased as the test continued. The flexural load carrying capacity at this stage is held due to the steel fibre content in the mix and highly dependent on the steel fibre distribution along the fracture plane. The fibres control the opening and propagation of the microcracks. Similarly, this behaviour was reported for the uniaxial tensile tests using the dog bone specimens, see Section 3.6.1.1 (Hassan et al.

2012). This part of the curve is known as deflection hardening or pseudo-strain hardening stage. At the end of the hardening stage, the microcracks' spacing decreased as more cracks appeared until a few microcracks merged to form a macrocrack. With the formation of a large macrocrack, the specimens' resistance to the flexural load rapidly diminished and finally resulted in failure, this part of the curve is known as deflection or pseudo-strain softening stage. Regardless of the curing temperatures, all the tests exhibited deflection hardening and softening behaviour. In Figure 5.8, the 30 ^{o}C cured specimens exhibited greater ductility compared to the 90 ^{o}C concrete, this will be discussed in details in latter part of this section. Figure 5.9 shows the resistance and failure mode of a UHPFRC beam specimen under the bending test, including the formation of micro/macrocracks.

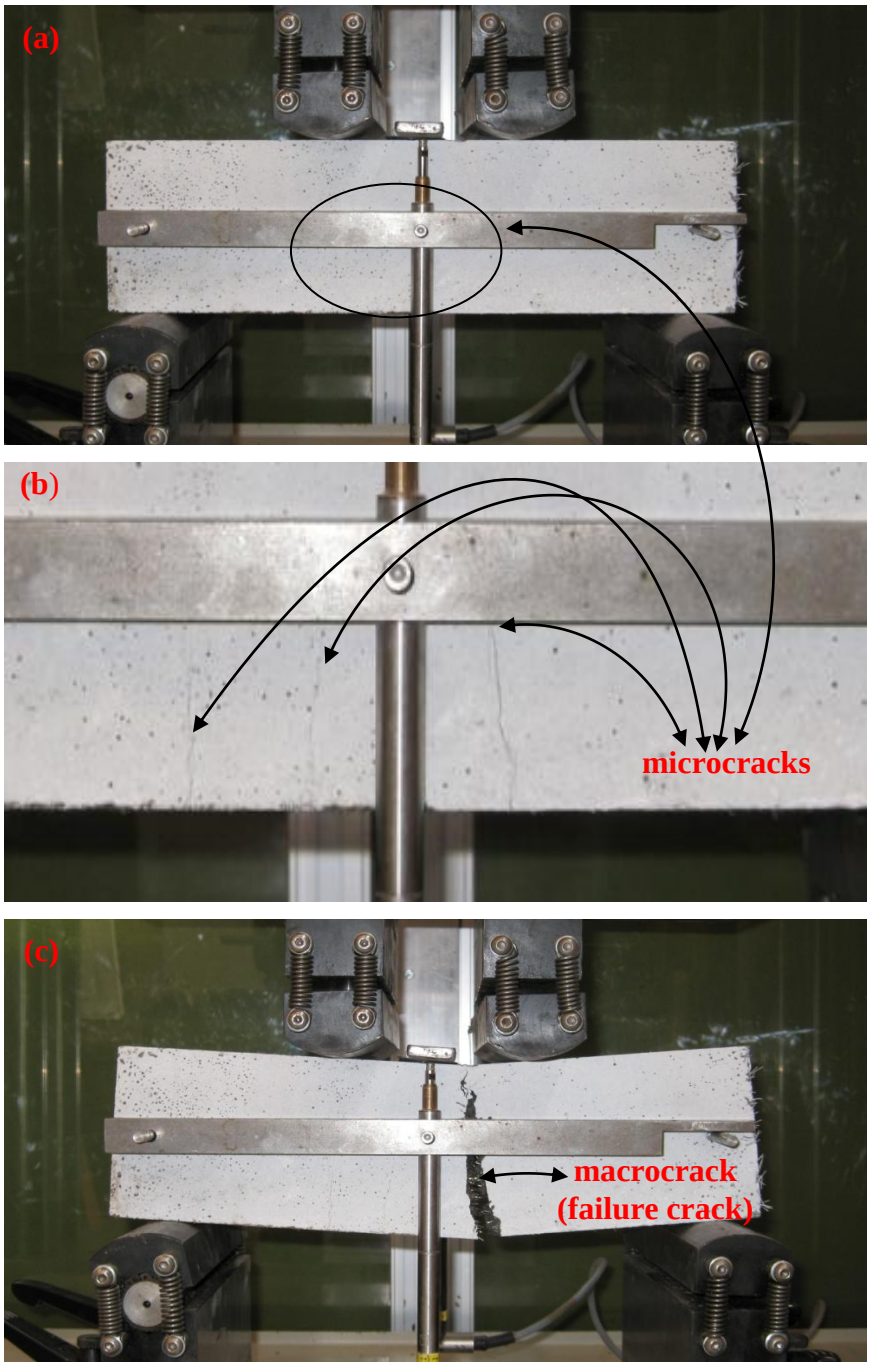

Figure 5.9: Flexural beam test for 90 ^{o}C cured UHPFRC specimen at 28 days, showing: (a) linear stage, (b) formation of microcracks, and (c) formation of macrocrack at failure.

Examination of the fracture planes after completion of the tests showed fibre pull-out had caused failure in almost all the tests. Fibre pull-out began as the width of the macrocrack kept increasing due to the applied load. At approximately 12 mm vertical deflection, the tensile capacity of the specimen was close to zero load. The crack width

at failure was in a range of 10 to 15 mm at the base, see Figure 5.10. The width of the macrocrack was approximately as big as the length of a fibre, 13 mm.

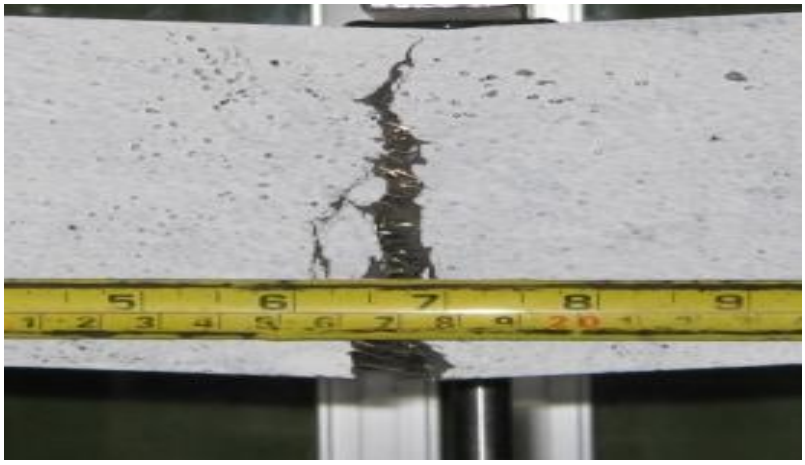

Figure 5.10: Crack width of UHPFRC at failure.

For the UHPC specimens, brittle failure was observed and total failure occurred with the formation of the first crack regardless of the curing temperatures. This is very similar to a typical normal concrete flexural failure and such failure was expected. Figure 5.11 shows the flexural load-deflection curve of the concrete at different curing temperatures at an age of 28 days.

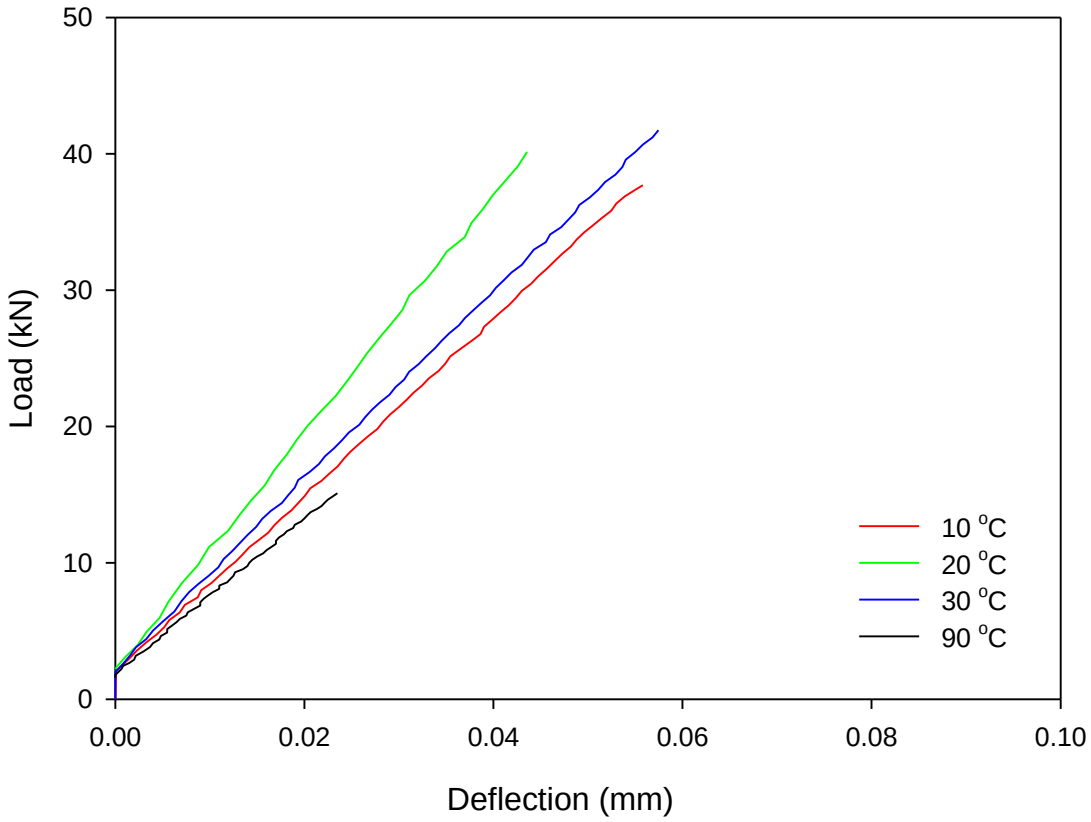

Figure 5.11: Flexural load versus deflection for UHPC beam specimens at 28 days.

First cracking and tensile flexural strength

The first cracking load, P_y, maximum tensile flexural load, P_u, and their corresponding deflections, δ_y & δ_u, for the UHPFRC and UHPC specimens are shown in Table 5.3 and 5.4, respectively. In a similar manner to their compressive strength development, the first cracking load for the UHPFRC specimens cured at 10, 20 and 30 °C appeared to increase with time and temperature between the ages of 7 to 28 days, while the 90 °C cured specimens reached the maximum first cracking load within 7 days. However, from 28 days onwards, this parameter was seen to be independent on the curing temperature and age. In fact, from 28 to 360 days, the 90 °C cured specimens exhibited the lowest first cracking load values while the 20 °C cured specimens were the highest. In contrast, the 90 °C cured UHPC specimens at 7, 14 and 28 days exhibited the lowest maximum flexural loads (equivalent to the first cracking load of the UHPFRC specimens) compared to the 10, 20 and 30 °C cured specimens of the same concrete. From the

results obtained here, the 90 ^{o}C curing temperature appeared to have an adverse effect on the tensile flexural strength development of the UHPFRC's matrix and UHPC. This seems unusual, since the literature states that high curing temperature is usually applied in the production of UHPFRC to improve its microstructure. However, this was not observed for the flexural test conducted here.

The values of the first cracking load for the UHPFRC specimens obtained for curing temperatures of 10, 20 and 30 ^{o}C are similar to the maximum flexural load reported for the UHPC specimens under the same curing temperatures and age conditions. However, a big variation was seen for specimens cured at 90 ^{o}C for both concrete mixes. It is evident that the 90 ^{o}C curing temperature has adversely influenced the first cracking strength of both concretes and this effect has not been reported in the literature. This study believes that high curing temperature such as 90°C results in shrinkage shock within the concrete during early age strength development. This shock occurs when specimens are suddenly exposed from an ambient temperature during hardening to high curing temperatures in which the temperature is at least 4 to 5 times greater. Such sudden change in temperature may result in the free water content in the concrete being driven out and resulting in crack formation in the weakest points of the concrete. Further studies to investigate this effect are extremely important.

For both concretes cured at various temperatures, the corresponding deflection for the first cracking load ranges from 0.05 to 0.09 mm, except for the 90°C cured UHPC specimens. The 90°C cured UHPC specimens exhibit smaller deflection, approximately 0.02 mm due to their lower tensile flexural strength development. Furthermore, the deflection attained at the maximum load for the UHPFRC specimens at all the different curing temperatures differs significantly. Generally, deflection at both first cracking and ultimate flexural loads for the lower temperature cured UHPFRC specimens were greater than those cured at 90 ^{o}C. This finding is significant for UHPFRC cast in-situ application. As it indicates that precast members of UHPFRC may result in greater ultimate flexural load, but cast in-situ members could result in greater deformation at first crack and maximum flexural loads, hence, better ductility.

Table 5.3: Influence of the curing temperatures on the development of the first cracking and ultimate flexural load with their corresponding deflection at various ages for UHPFRC.

Age (days)	**10 °C**				**20 °C**				**30 °C**				**90 °C**			
	P_y (kN)	δ_y (mm)	P_u (kN)	δ_u (mm)	P_y (kN)	δ_y (mm)	P_u (kN)	δ_u (mm)	P_y (kN)	δ_y (mm)	P_u (kN)	δ_u (mm)	P_y (kN)	δ_y (mm)	P_u (kN)	δ_u (mm)
7	19.39	0.045	32.53	0.692	30.86	0.060	42.96	0.828	35.74	0.062	44.55	0.348	41.14	0.061	68.83	0.572
14	26.45	0.066	36.67	0.801	34.96	0.051	48.20	0.698	36.11	0.060	52.37	0.287	39.41	0.049	68.41	0.515
28	42.09	0.086	48.13	0.489	49.51	0.068	64.21	0.589	53.13	0.076	68.06	0.525	42.85	0.060	69.09	0.617
60	44.06	0.063	54.88	0.587	52.56	0.070	62.04	0.469	58.95	0.079	72.82	0.599	40.26	0.056	71.74	0.627
90	44.97	0.066	55.67	0.788	53.87	0.072	67.88	0.561	56.86	0.077	75.10	0.596	37.07	0.055	68.59	0.623
120	46.07	0.074	57.46	0.535	54.94	0.075	62.12	0.422	42.43	0.080	70.45	1.033	43.52	0.063	73.16	0.582
150	51.77	0.065	64.32	0.467	57.63	0.071	62.27	0.371	38.90	0.077	70.49	1.106	44.83	0.063	69.49	0.700
180	47.37	0.072	58.88	1.070	62.07	0.082	65.20	0.230	41.76	0.085	73.11	1.090	46.03	0.066	71.38	0.724
360	59.91	0.087	63.87	0.249	67.61	0.088	69.52	0.463	43.21	0.086	74.23	1.072	44.46	0.064	81.20	0.618

Table 5.4: Influence of the curing temperatures on the development of the ultimate flexural load and corresponding deflection at various ages for UHPC.

Age (days)	**10 °C**		**20 °C**		**30 °C**		**90 °C**	
	P_u (kN)	δ_u (mm)	P_u (kN)	δ_u (mm)	P_u (kN)	δ_u (mm)	P_u (kN)	δ_u (mm)
7	34.51	0.060	40.23	0.064	38.72	0.063	16.38	0.020
14	30.17	0.056	37.32	0.056	43.53	0.069	12.73	0.021
28	37.70	0.058	40.15	0.044	41.74	0.058	15.10	0.024

The corrected first cracking strength was calculated using Equation 5.2 for the 90 ^{o}C cured UHPFRC specimens at 7, 14 and 28 days. The results were compared to the uniaxial tensile strength of the concrete at the same curing conditions and age as reported in Section 3.6.1.1, see Table 5.5. The results illustrate that Equation 5.2 underestimates the actual tensile strength of the concrete by approximately 15 to 20%.

Table 5.5: Correlation between the corrected first cracking tensile flexural strength and uniaxial tensile strength for UHPFRC.

Age (days)	$f_{ct,1}$ (MPa)	σ_t (MPa)	Error (%)
7	7.41	8.97	17
14	7.09	8.92	20
28	7.71	9.07	15

The error may not seem significant. However, the results reported in Table 5.3 to 5.5 raises a question on the validity of the first cracking load for the determination of the direct tensile strength of UHPFRC using Equation 5.2. It is evident that the first cracking load for specimens cured at 90 ^{o}C were lower than those cured at normal curing temperatures, i.e. 20 and 30 ^{o}C,. This adverse effect on the first cracking load has not been considered in Equation 5.2. Therefore, further studies to investigate the validity of this equation are also essential.

As proposed in the JSCE-SF4, Equation 5.3 was used to determine the tensile flexural strength development of the UHPFRC and UHPC beam specimens. Figures 5.12 and 5.13 show the tensile flexural strength development for both concretes.

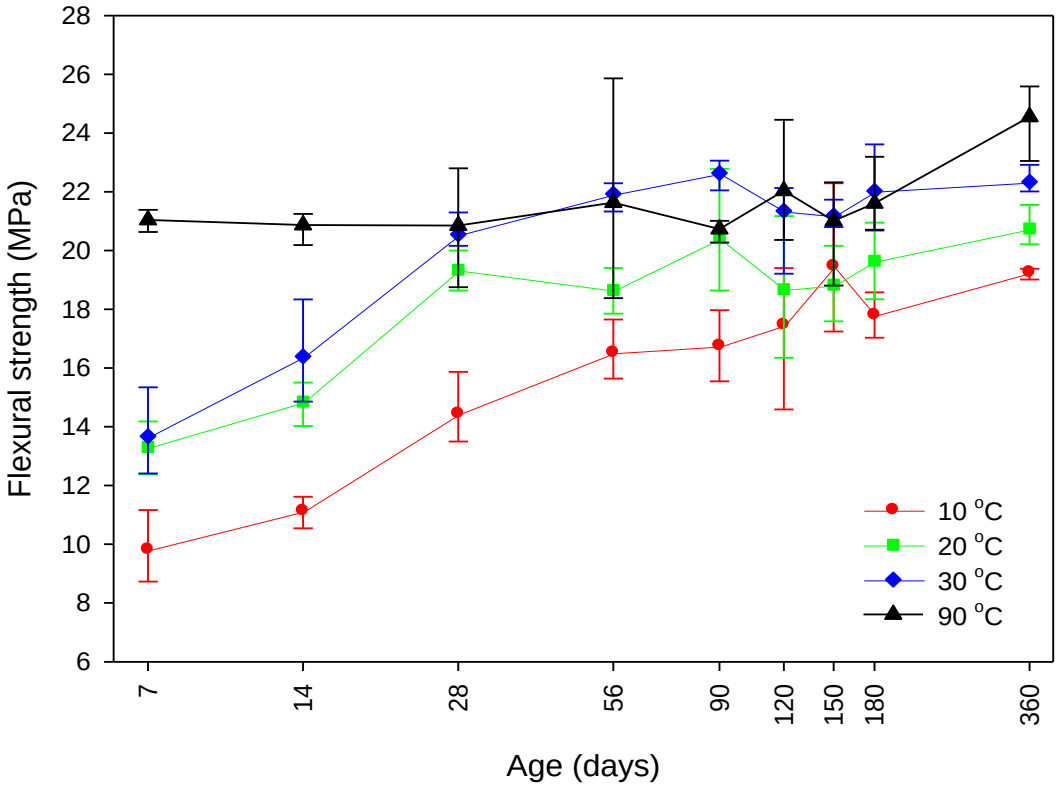

Figure 5.12: Tensile flexural strength development for UHPFRC.

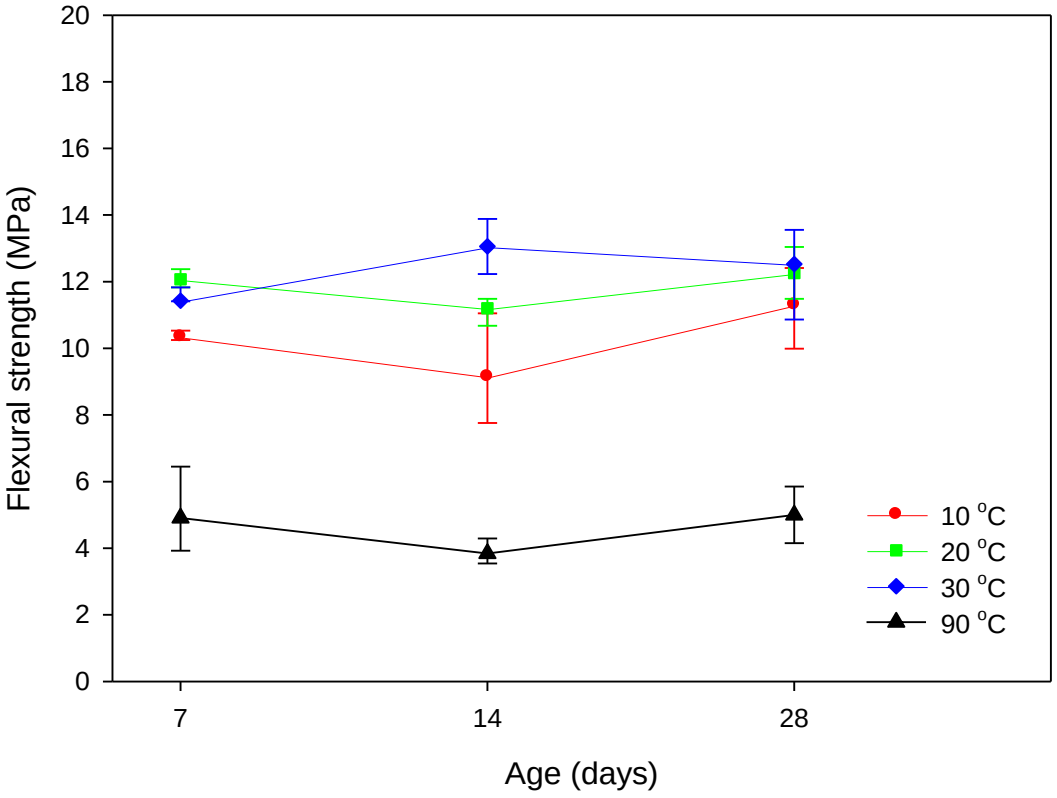

Figure 5.13: Tensile flexural strength development for UHPC.

In a similar manner to the compressive strength trend, the tensile flexural strength development for UHPFRC specimens increased with time and temperature, particularly at early ages. However, the rate of increase was not as pronounced as the compressive strength at later ages. The maximum increase in tensile flexural strength from 28 to 360 days was limited to 4.81 MPa for 10 ^{o}C and the minimum increase was 1.4 MPa for 20 ^{o}C curing. In contrast to their compressive strength development, it is unlikely that the tensile flexural strength of both curing temperatures (10 and 20 ^{o}C) would ever reach that of those cured at 90 ^{o}C. Although, rate of increase was low after 28 days, the tensile flexural strength for the three lower curing temperature regimes are still considered high when compared to normal concrete. For example, tensile flexural strength for the 10 and 20 ^{o}C cured specimens at 28 days have reached 14.45 and 19.35 MPa, respectively. The reported values are approximately two times greater than values are usually attained for normal concrete, 5 to10 MPa.

In Figure 5.13, the 90 ^{o}C cured UHPC test results are extremely low and tensile flexural strength development does not match its compressive strength development. The postulated reasons for this are discussed next in this chapter. Furthermore, tensile flexural strength development for the three lower cured UHPC specimens with time and temperature appeared to be small and insignificant. Form the results obtained here; it is evident that the tensile flexural strength of UHPFRC is highly dependent on the steel fibre content in the mix rather than the curing temperature.

High temperature curing effect

To further investigate the low tensile strength development of the 90 ^{o}C cured UHPC specimens and the phenomenon reported in Sections 3.6.1.2 and 3.6.1.3 of this thesis, the surface of the failed UHPC specimens were checked for any defects or abnormal appearances after testing, see Figures 3.15, 3.19 and 5.14. In these figures, a defect phenomenon of roughly circular shapes within the body of the sample can be seen for all the cylinder and beam specimens. To ensure the quality of the concrete is acceptable, the failed UHPC beam specimens cured at 30 ^{o}C were also presented with the 90 ^{o}C cured specimens in Figure 5.14. From this figure; it appears that the core of the 90 ^{o}C cured specimens was subjected to a type of defect of circular shape, while this was not

apparent for the 30 ^{o}C cured specimens of the same concrete mix. This behaviour was believed to have damaged the integrity of the concrete and have caused the lower tensile strength test results that are reported in Tables 3.2 and 5.4.

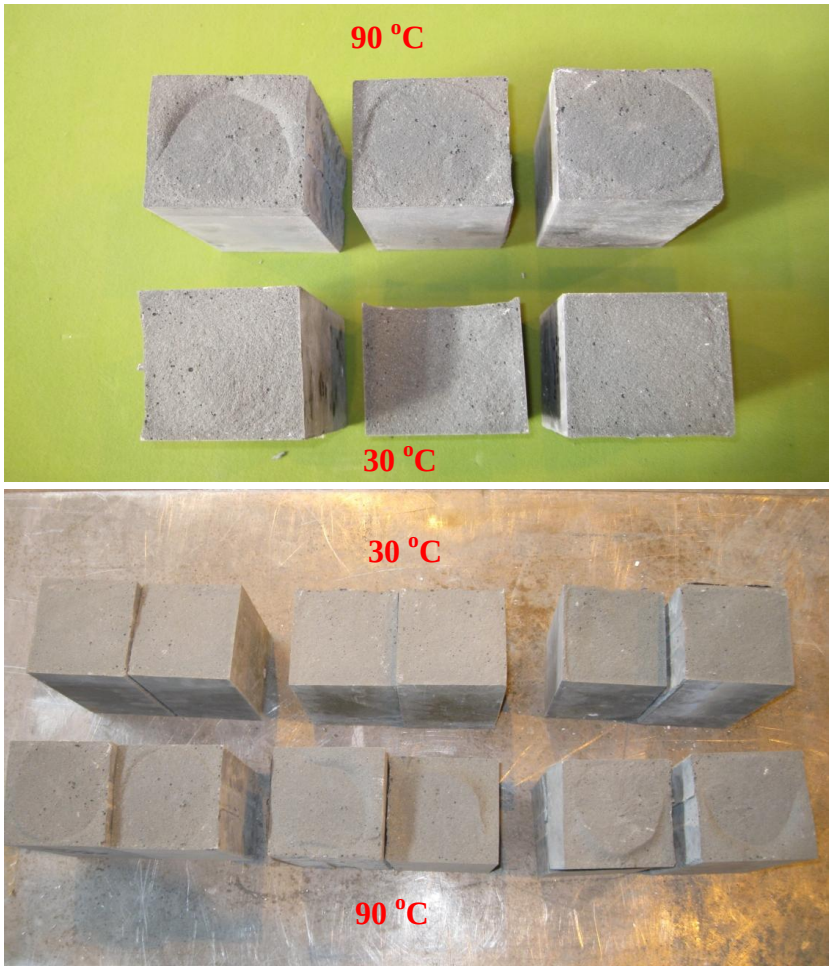

Figure 5.14: Failed UHPC specimens cured at 30 and 90 ^{o}C.

As discussed earlier, one plausible explanation to this defect is attributed to the thermal expansion of incorporated water in the core of the specimen due to the high temperature curing. This thermal expansion would result in an internal pressure build up in the pores of the specimen and causing microscopic areas of fracture as a result of hydraulic loading. Similar encounters with normal concrete and mortar have been noted and discussed in the literature (Alexanderson 1973, Leung and Pheeraphan 1995, Neville 2012). The study conducted by (Alexanderson 1973) reported that long term strength development of steam cured normal concrete were adversely affected by the curing

process. The high temperatures of the steam curing applied to the concrete in the early stages of hardening (before 6 hours) was reported to have caused very fine cracks in the concrete due to the expansion of air bubbles in the cement paste. The thermal expansion of the air in the concrete was reported to be at least two orders of magnitude greater than that of the surrounding solid materials. Therefore, the expansion of the air bubbles in the concrete is normally restrained and this causes tensile stress inducement in the surrounding cement paste. Such behaviour was reported to cause permanent cracks and loss of strength at all ages. Furthermore, the study conducted by (Leung and Pheeraphan 1995) on the microwave curing of concrete and mortar found similar behaviour. The high temperature generated by the microwave curing was found to cause expansion of the mortar phase and bubble formation and this lead to generate more pores and microcracks in the mortar specimens, hence, loss of strength. However, this was not more pronounced for the concrete specimens since the presence of aggregate restrained the expansion of the mortar more effectively. For normal concrete, the literature suggests that high curing temperature's adverse effect may cease if the curing process is applied after 6 hours. However, the results reported in this study suggest otherwise for UHPFRC.

All the factors discussed above are believed to have caused the low tensile flexural strength development for the UHPFRC and UHPC concretes cured at 90 ^{o}C. Although, this behaviour is more pronounced for the UHPC test results, this study believes it has affected the UHPFRC equally. However, the loss of strength for the UHPFRC test results may have been reduced due to the steel fibre content in the concrete, similar to the results reported by (Leung and Pheeraphan 1995). This is because the steel fibres are used to reinforce the concrete and strengthen all the fine cracks that may occur due to either the curing regime or external loadings. Furthermore, the excellent tensile flexural strength development with the three lower curing temperatures at 28 days is a clear evident of the suitability of UHPFRC for cast in-situ applications.

The hypothesis presented here is based on numerous test results and the phenomenon observed for the 90 ^{o}C UHPC cured cylinder and prism specimens. Therefore, it is safe to conclude that high curing temperature such as 90 ^{o}C might not be as beneficial as

thought for the tensile strength development of UHPFRC's matrix. This contradicts the accepted view that high temperature curing improves all the mechanical properties of this concrete. It must be noted that this behaviour had not affected the compressive strength development of the concretes. This was found by testing the already broken beam specimens in compression, see Figure 5.15. The results of these tests were in good agreements with the results of their corresponding cube compressive tests.

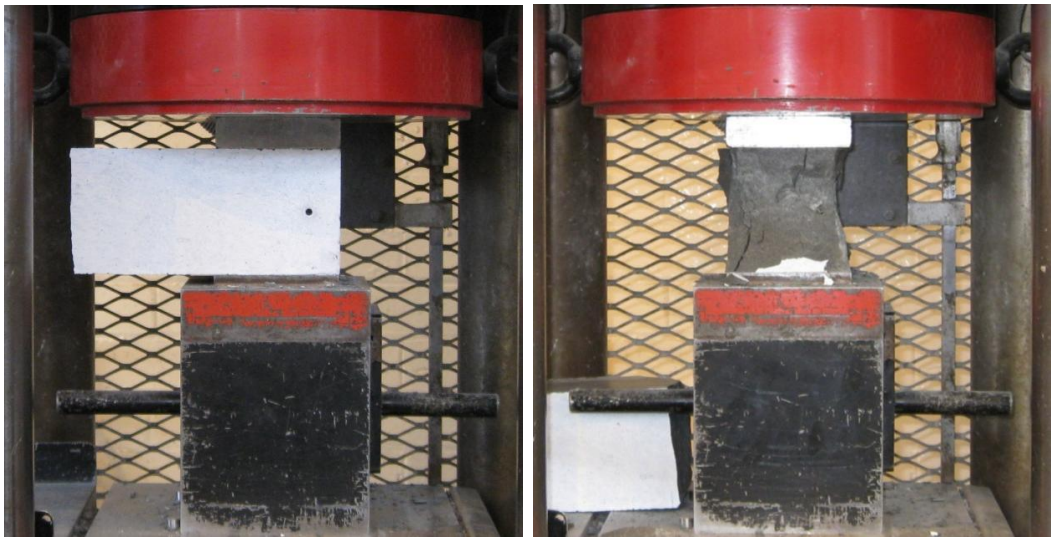

Figure 5.15: Compressive test of a half UHPC beam specimen.

In the literature, acceptable limits on the variations between the temperatures of curing regimes and concrete during hardening have been proposed. However, the variation is only limited to curing temperatures that are lower than the temperature of the concrete during hardening. For example, the ACI 308-01 standards recommends that the difference should not exceed 11 ^{o}C between both (ACI Committee 308 2001).While nothing on the curing temperature being significantly higher than the temperature of the concrete, i.e. 4 to 5 times, has been reported. Therefore, this is an area of research that is important and strongly related to the curing process of UHPFRC which can be exploited to further improve the tensile behaviour of the concrete. So far, no study in the literature in this area of research is available.

The short coming in the tensile flexural strength development due to the 90 ^{o}C curing temperature for this concrete can possibly be controlled by applying more effective

curing methods, i.e. applying the temperature rise slowly over a longer time. For example, applying the application of high temperature curing from 20 to 90 ^{o}C over 3 phases and in each phase by 23 ^{o}C. For instance, increasing the curing temperature from 22 to 44 ^{o}C in a period of 2 to 5 hours and again to final 90 ^{o}C as it has being recommended by others for steam curing (Neville 2012). During which process the tensile strength of the concrete could possibly be improved even better and the risk of early cracking with sudden thermal expansion in the core of the specimen could be minimised. Due to the limitation of this research, more detailed investigation was not possible in this area. However, further studies to investigate the effect of high curing temperature when applied suddenly to UHPFRC are of great interest.

Flexural toughness

Toughness for both concrete mixes was determined by integrating the load-deflection curve up to deflection of 2 mm as described earlier in the chapter. The flexural toughness versus age for UHPFRC at various curing temperatures is shown in Figure 5.16. In a similar manner to their compressive and tensile flexural strength development, toughness of the UHPFRC specimens cured at lower temperature increased with time and temperature. While flexural toughness development for the 90 ^{o}C cured specimens appeared to be very slow from 7 days onwards. Despite the increase of toughness for the lower curing temperature specimens, the rate of development at early ages (7 to 28 days) is slower than their compressive strength.

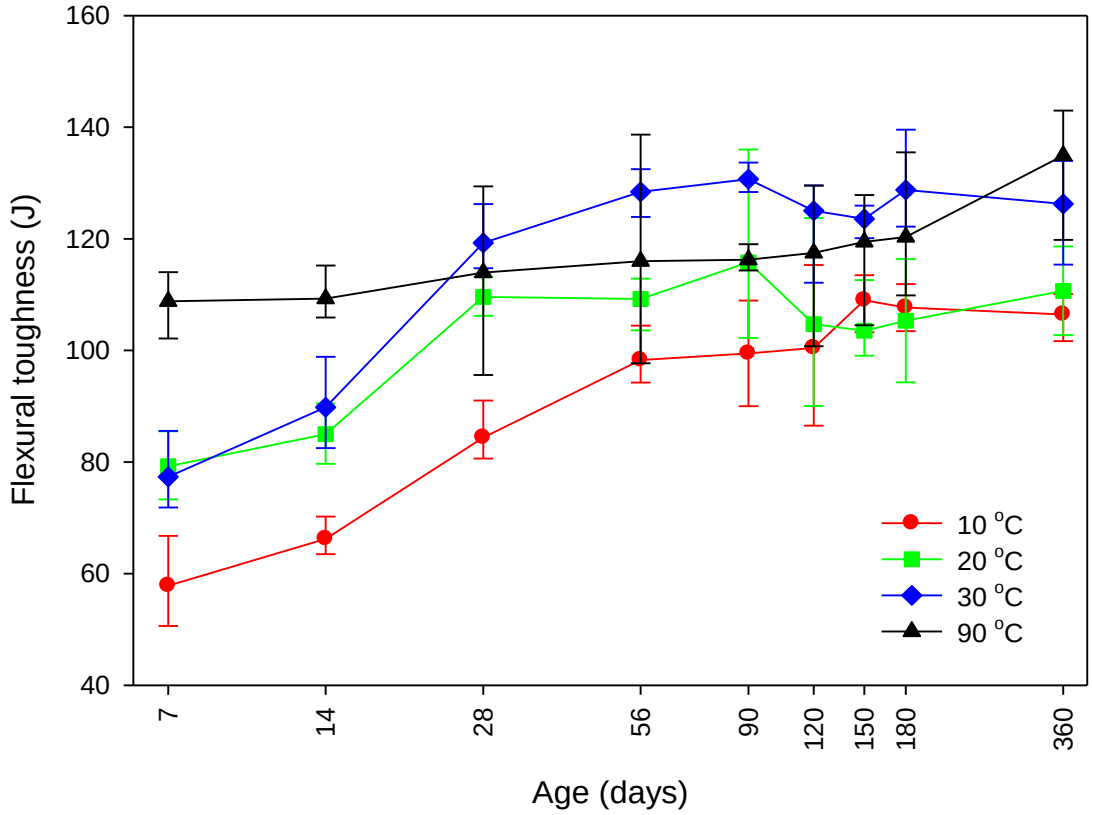

Figure 5.16: Flexural toughness development for UHPFRC up to a deflection of 2 mm.

The development of flexural toughness is largely dependent on fibre distribution and fibre bond strength in the concrete. The efficiency of the fibre bond strength in the fibre-bridging effect is dominant in carrying further loads after the occurrence of the first crack. A number of studies (Şahin and Köksal 2011, Yang and Diao 2009) have reported that the higher compressive strength of the matrix results in the improvement of such bonds and consequently the tensile behaviour of UHPFRC. However, this relationship was not observed here. For example, the compressive strength development for the 10, 20 and 30 ^{o}C cured specimens from ages of 28 to 120 days continuously increased. Therefore, flexural toughness development was expected to improve similarly. However, little or no improvement was seen for this period, in particular, for the 20 and 30 ^{o}C cured specimens.

To quantify the ductility of UHPFRC at various curing temperatures, the full area of the load deflection curve up to a deflection of 9.5 mm, near failure, were used to determine the flexural toughness development of the concretes at different curing ages, see Figure

5.17. As expected, the largest value was reported at 360 days for all the different curing temperatures.

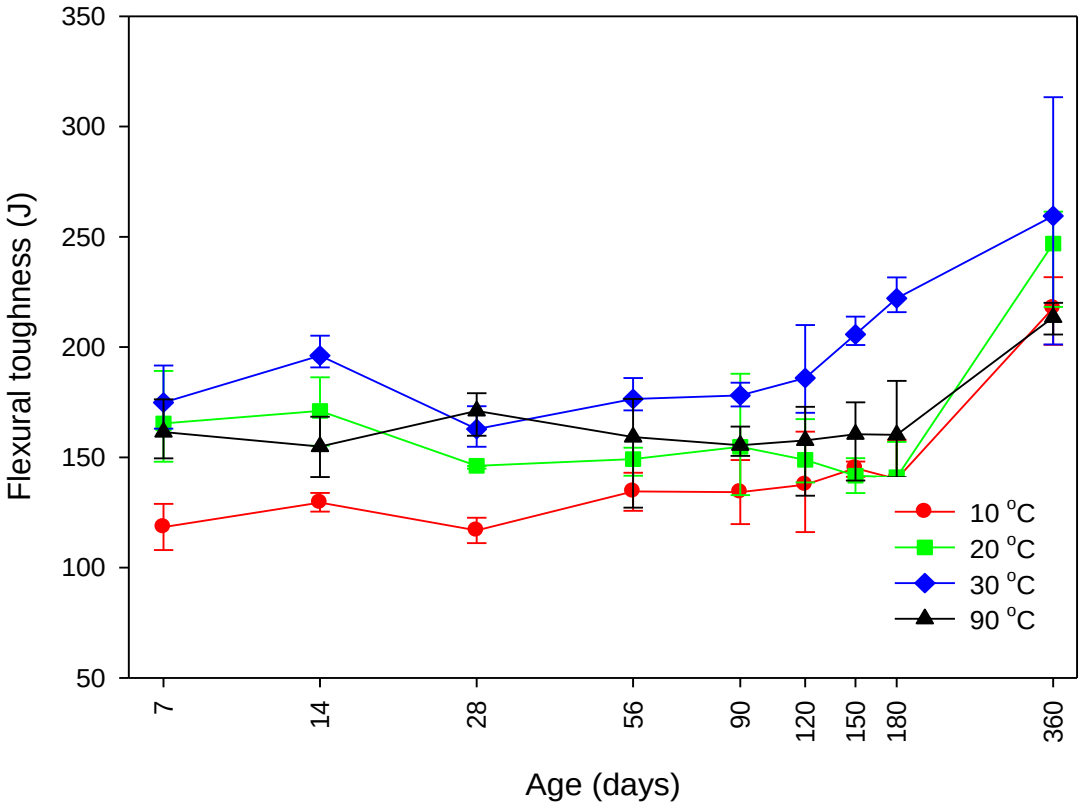

Figure 5.17: Flexural toughness development for UHPFRC up to a deflection of 9.5 mm.

In general, the flexural toughness values for the 30 °C cured specimens in Figures 5.16 and 5.17 were greater than those obtained for 90 °C. The toughness values for the 20 °C cured specimens were also very close to those cured at 90 °C. The high toughness values for the 20 and 30 °C cured specimens can be explained from Figure 5.8, since toughness is determined from the load-deflection curve. From this figure, it is evident that the 90 °C cured specimens exhibited a greater decreasing rate in the softening part of the load-deflection curve than those cured at 20 and 30 °C. This behaviour was reported for almost all the test results obtained for the 90 °C cured specimens. These results indicate again that the high curing temperature must have had some adverse effects on the matrix of the concrete, consequently, the fibre bond strength. As a result, the fibre bond strength becomes weaker for the 90 °C cured specimens and has resulted lower toughness values compared to those cured at 30 °C.

Figure 5.18, shows the flexural toughness versus age for UHPC at various curing temperatures. In this figure, flexural toughness values are very small regardless of the curing temperatures. Similar to its tensile flexural strength development, the highest and lowest toughness values were reported for the 30 and 90 ^{o}C cured specimens, respectively. Despite the differences in the toughness values for all the curing regimes, the results obtained were very small compared to those reported for UHPFRC. The toughness values reported for the UHPFRC specimens were in a range of approximately 100 to 875 times greater than those reported for UHPC. The largest difference occurred between the 90 ^{o}C cured specimens of both concretes due to the reasons presented previously. The values of flexural toughness in Figures 5.17 and 5.18 shows the significant influence of steel fibre content on the ductility behaviour of UHPFRC. Despite the variation of flexural toughness development due to the curing temperatures and possibly errors in the test setup, the values reported for the UHPFRC were quite impressive compared to those reported for UHPC. This indicates the full advantage of using UHPFRC in construction industry. The results reported here are also in close agreement to the literature (Habel 2004, Voort et al. 2008).

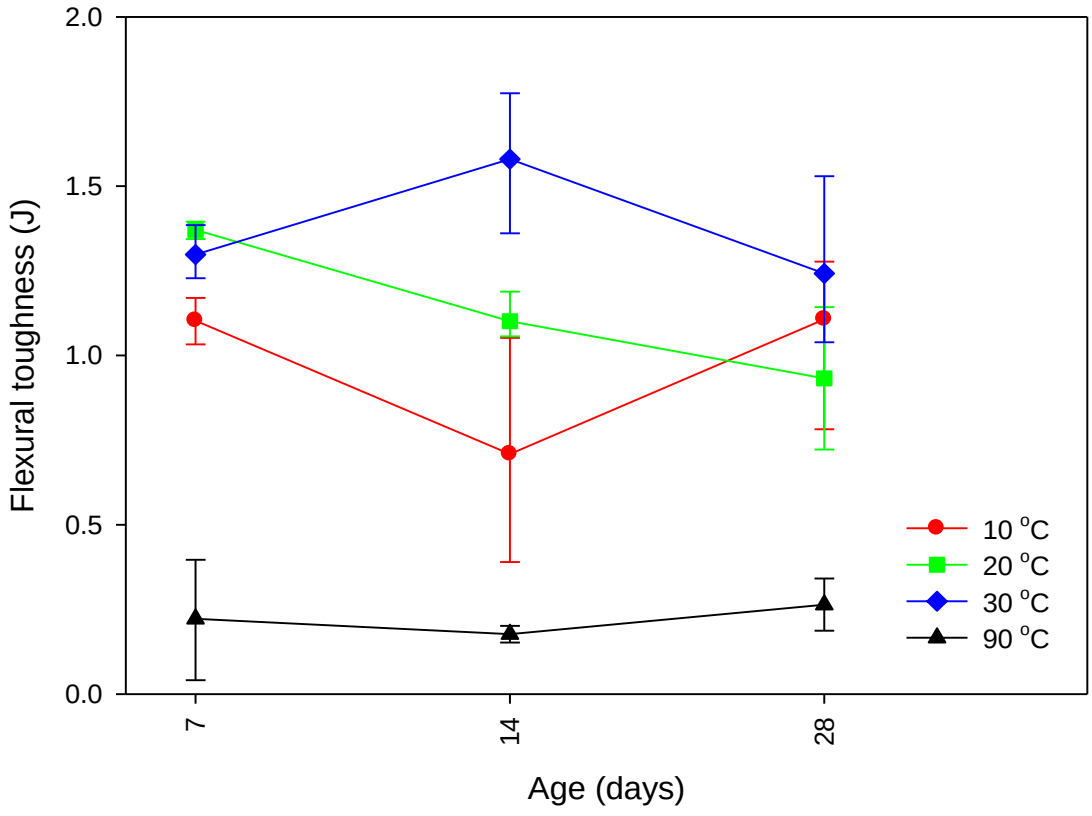

Figure 5.18: Flexural toughness development for UHPC.

As noted previously, the 10, 20 and 30 ^{o}C cured specimens were kept in water until testing, while the 90 ^{o}C cured specimens were dry cured from 3 days of age. This study is aware that the wet and dry curing could have influenced the compressive and tensile flexural strengths development of the concretes. However, the hydration of the 90 ^{o}C cured specimens appears to have reached their peak at early ages, since the 3 days compressive strength development is of 99 and 93% of those at 28 and 360 days, respectively.

Furthermore, the literature indicates that the maximum possible hydration of the Portland cement in UHPFRC is reached within 5 days, which is 35 to 40 % due to the low w/c ratio (Schachinger et al. 2008). Therefore, this study believes that the dry curing of the 90 ^{o}C specimens beyond 3 days of age could not have had significant influence on the strength development of the concrete. In practise, the period of curing cannot be prescribed in a simple manner and it depends on many factors. However, this is outside the scope of this study.

Finally, the results reported here were all made in the laboratory under known conditions with small specimen sizes. However, the behaviour on site in hot and cold climates will not be the same. Additional factors such as ambient humidity, direct radiation of the sun, wind velocity, method of curing, size of structural members and many more factors could influence the strength development of the concretes reported here. In particular, the increased rate of evaporation from the fresh mix of concrete in hot climates ≥ 30 ^{o}C during mixing, placing and curing. Furthermore, on site cast in-situ concrete will usually results in a lower quality concrete due to difficult condition that cannot be controlled compared to laboratory testing. It must be noted that none of these factors were considered here.

5.6.3 Durability

The 10, 20 and 30 ^{o}C cured UHPFRC specimens were submerged in their water curing tanks at all times while the 90 ^{o}C specimens were dry cured, except for the 48 hours during curing. With time, the exposed steel fibres on the outer surface of all the different specimens showed the initiation of corrosion, particularly those kept in water at all

times. To investigate the condition of the steel fibre content in the concrete, at ages of 180 and 360 days, several beam specimens from all the different curing temperatures were sawn in half for visual inspection, as shown in Figure 5.19.

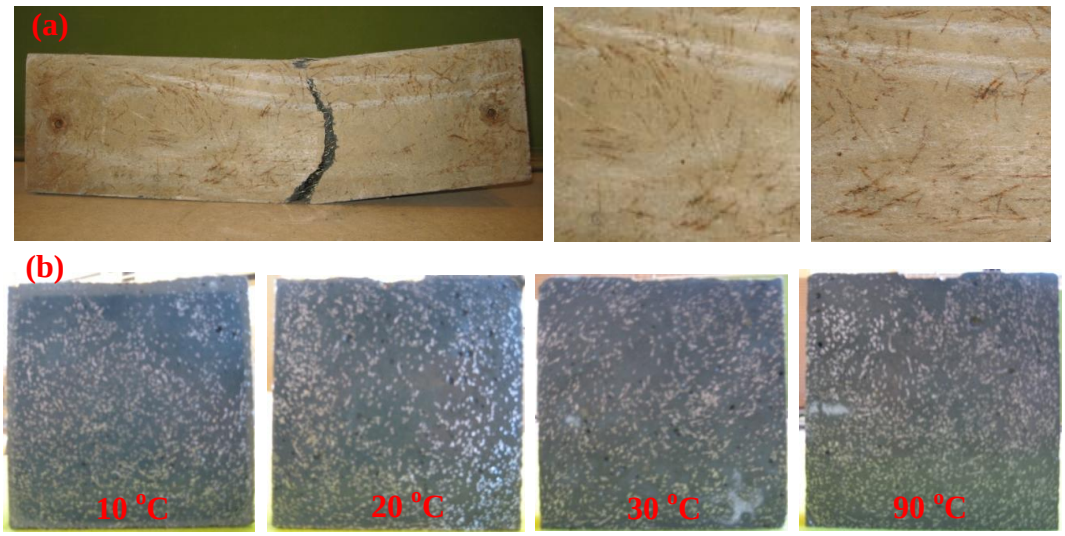

Figure 5.19. Steele fibre condition for beam specimens: (a) surface zone (b) sections of various temperatures cured specimens.

In Figure 5.19, the excellent ability of UHPFRC regardless of curing temperatures and environment to resist corrosion can be seen. The brown lines on the surface of the specimens in Figure 5.19 (a) are indication of corroded steel fibres exposed to air. In contrast, Figure 5.19 (b) shows the unaffected randomly distributed fibres inside the concrete. This protection is due to the high packing density of the concrete which leads to significantly lower permeability as no signs of corrosion could be detected below the surface, even for the fibres close to the edge of the samples. Furthermore, it is important to note that this is not an extensive durability check. However, it is an attempt to simply check the fibre distribution in the concrete and examine the condition of fibres that are exposed to air and those inside the concrete.

5.7 Summary

To reduce the high initial cost of UHPFRC in construction industry due to its current precast production, different options such as cast in-situ application of the concrete requires detailed investigations. Therefore, in this study, extensive experimental work

was carried out to investigate the suitability of UHPFRC for cast in-situ applications. This was conducted by studying the influence of various curing temperatures (10, 20, 30 and 90 ^{o}C) on the development of the compressive strength, first and maximum flexural loads and flexural toughness of UHPFRC and UHPC from an early age up to 360 days. The three lower curing temperatures were chosen to represent conditions that are likely to be encountered for cast in-situ applications, while the 90 ^{o}C curing temperature is currently used in the precast production of UHPFRC components. The UHPC concrete was included to further investigate the effect of 90 ^{o}C curing temperature on the defect phenomenon reported for the tensile tests in Chapter 3. Furthermore, a simple durability check for UHPFRC specimens cured at the different temperatures was also conducted. From this study, the following conclusions were found.

The curing temperature was found to have a significant effect on the early rate of compressive strength development of UHPFRC. However, the effect varied depending on the curing time and temperature. The 90 ^{o}C curing temperature resulted in high early age strength development and ultimate strength within 5 days after casting. While the 10, 20 and 30 ^{o}C curing temperatures provided sufficient compressive strength within 5 days and the strength development continued up until 360 days, matching the same or even higher strengths than those for the 90 ^{o}C cured specimens. Similarly, compressive strength development for the UHPC specimens appeared to be highly dependent on the curing temperature, while little influence due to the absence of steel fibres was observed. However, the presence of fibres in the concrete was crucial to modify the failure mode from an explosive and abrupt manner to a ductile mode which is preferable in structural design.

The flexural tensile behaviour for UHPFRC at early age was found to be dependent on the curing temperature. Generally, higher curing temperatures resulted in higher tensile flexural strength and higher flexural toughness development with age. However, from 28 days onwards, better flexural behaviours were reported for the 30 ^{o}C cured specimens than those cured at 90 ^{o}C. Furthermore, the 90 ^{o}C curing temperature appeared to have an adverse effect on the flexural behaviours of both concretes, more specifically the UHPFRC first cracking flexural load and UHPC maximum flexural load. The tensile

flexural strength and toughness development of the three lower curing temperatures for the UHPC specimens were found to be higher than those cured at 90 ^{o}C. Such findings were striking and had not been reported in the literature previously.

To further investigate the poor flexural behaviour for the 90 ^{o}C cured specimens of both concretes, the failure surfaces of the UHPC specimens at all the different curing temperatures were checked and a phenomenon with the 90 ^{o}C cured specimens was reported. This phenomenon appeared to be a defect in the concrete and have occurred due to thermal expansion of incorporated water in the core of the specimen due to the high temperature curing. As a result, hydraulic loading has formed microscopic areas of fracture and have caused loss of tensile flexural strength. This behaviour was limited to the 90 ^{o}C cured concretes only and was more pronounced with the UHPC test results than those of UHPFRC. This finding is in contrast to the views reported in the literature stating that 90 ^{o}C curing temperature improves all the mechanical properties of the concrete. Therefore, further studies to investigate this defect phenomenon and the hypothesis proposed here are recommended.

The flexural toughness of UHPFRC appeared to be highly dependent on the fibre content in the mix. The toughness values for this concrete were 100 to 875 times greater than those of UHPC. This is a clear indication of improved ductility behaviour of UHPFRC due to steel fibre content in the composition. Furthermore, deflection values at first cracking and maximum flexural loads for UHPFRC specimens cured at lower curing temperatures (20 and 30 ^{o}C) were normally greater than those cured at 90 ^{o}C. In general, the 30 ^{o}C cured UHPFRC specimens exhibited greater flexural toughness and ductility compared to the 90 ^{o}C cured specimens, see Figures 5.16 and 5.17. Such behaviour is important in structural design and can be exploited in UHPFRC cast in-situ applications.

Furthermore, the reliability of the relationship proposed in the AFGC recommendation for predicting the tensile strength of UHPFRC from its first cracking load in flexural test was investigated. Results reported for the uniaxial tensile strength in Section 3.6.1.1 were compared to the values obtained from this relationship and errors in a range of 15

to 20 % were observed. The accuracy might not seem poor, however, since the first cracking load was found to be influenced significantly by the 90 ^{o}C curing regime and this has not being considered in the relationship, the validity of the equation is questionable.

The findings reported here indicate that cast in-situ applications of UHPFRC in warm climates, i.e. 30 ^{o}C exhibits approximately 70% of the compressive and tensile flexural strengths of precast components of the concrete within 7 days and a similar strength within 28 days. This shows the suitability of UHPFRC for cast in-situ applications if the construction programme allows the component to wait a little longer before being subject to design loading. Since the high cost of UHPFRC precast members are mainly determined due to energy consumption, storage and time during production, the findings reported here could have significant beneficial cost and the environmental impact consequences. It also shows the suitability of the concrete for cast in-situ highway bridge applications at a lower material cost. Finally, from visual inspection, the durability of UHPFRC appeared to be significantly improved due to high packing density of the composite and the steel fibre content was well protected in the concrete.

Chapter VI: Punching Shear Strength

6.1 Introduction

From the results reported in this PhD so far, it is evident that UHPFRC exhibits significantly higher tensile and compressive properties compared to conventional concrete. These improved properties allow UHPFRC structural members be built with complex shape, lower volume of conventional steel reinforcement (and maybe none) and lower maintenance costs. The improved tensile behaviour of UHPFRC can be exploited to enhance shear resistance of its structural members, particularly in highway bridge applications. In the United States alone, approximately 603,000 bridges have been reported to be either structurally deficient or functionally obsolete (Gunes et al. 2012). In 2009, the projected cost of repairing the Unites State's infrastructure was reported to be about $2.2 trillion over the next five years (Hansen 2009). Therefore, utilising new materials such as UHPFRC to build highway bridges with improved qualities that can last longer seems to be a good solution.

In the last few years, a number of optimised UHPFRC sections have been proposed to be used in highway bridge applications. The structural behaviour and, in particular, the shear strength of these members without steel reinforcement are necessary to be studied for design purposes. However, so far, limited information on the shear capacity of UHPFRC slabs without conventional reinforcement is available. This is due to the complexity of punching shear behaviour of the concrete and also not having a suitable test available. Therefore, this study aims to conduct detailed experimental investigation on the punching shear capacity of the concrete in isolation from the effects of flexural damage. However, to do this, a suitable test method that can accurately measure this property of the concrete was required. Therefore, a number of punching shear trial tests were conducted here and the implications associated with determining this property was investigated in detail.

In this study, experimental investigation by testing UHPFRC slab specimens subject to a concentrated load was carried out. A test method was designed, in which the relationship between the shear strength and the angle of the shear plane of the slab specimens was

studied. Finally, the results were evaluated and recommendations for future investigation are presented.

6.2 Shear in Bridge Design

In bridge structures, beam and slab failure occurs in two common forms, direct flexural and/or punching shear. The direct flexural failure usually occurs in beam or slab members associated with overall bending. This type of failure arises from the formation of diagonal tension cracks extending across the entire width of the member. However, punching shear failure is a more localised effect associated with thin slabs or two-way slab-column members when subjected to a highly concentrated load.

A concentrated load on a concrete member such as a slab causes shearing stress on the section around its perimeter and this effect is known as punching shear. Punching shear failure occurs when the principal stress across the critical surface of the section exceeds the tensile strength of the concrete due to applied loading. As a result, failure occurs with the potential diagonal crack following the surface of a truncated cone around the load, see Figures 6.22 and 6.23. The failure surface extends from the bottom of the member diagonally upward to the top surface. For normal concrete slab, the angle of inclination of the failure surface in the maximum shear surface area is approximately ranging from 20 to 45 degrees depending on the amount of shear reinforcement (Nilson et al. 2003). However, very little information on this parameter for UHPFRC is available.

The actual behaviour of concrete members in shear is complex and difficult to analyse theoretically. Shear failure usually results from a combination of shearing forces and bending moments. The current codes of practise such as Eurocodes and ACI have proposed reasonably simplified procedures for the analyses and design of conventional concrete members for punching shear using results from many experimental investigations. However, there are limitations with these design equations as improvements in punching shear capacity as a result of improved compressive and/or tensile strength of new types of concrete is not fully taken to account. The BS EN1992-1-1 indicates the critical surface of punching shear for a concrete slab in Figure 6.1.

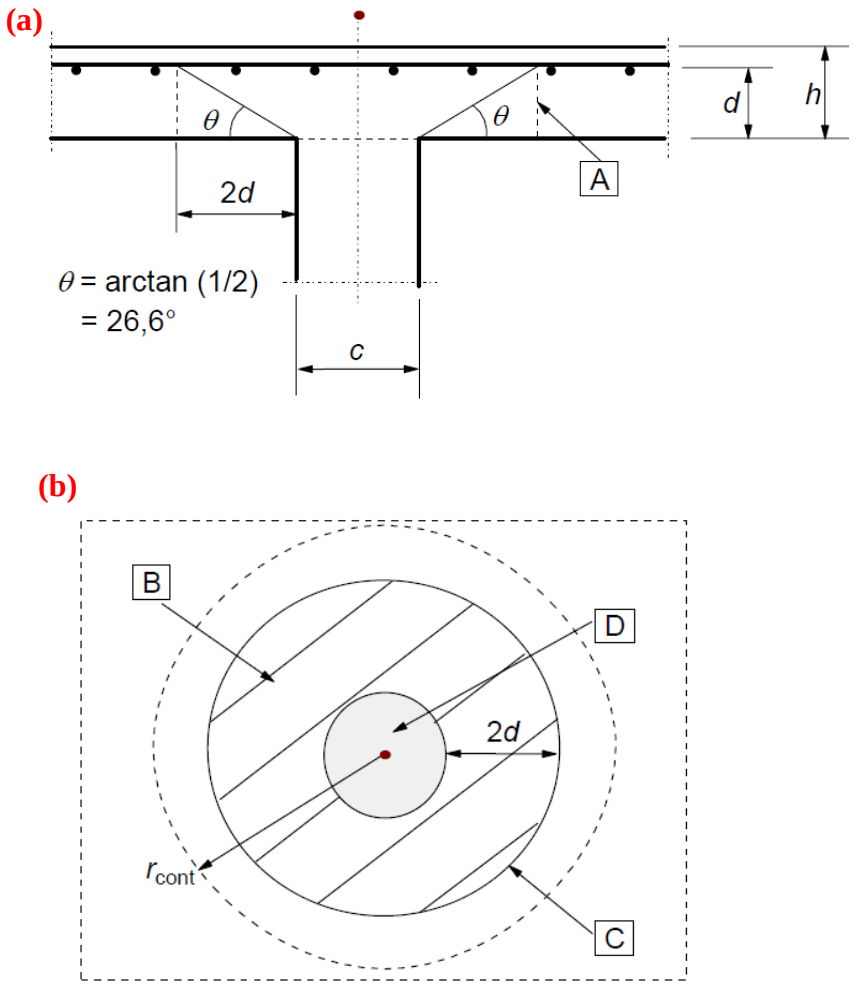

Figure 6.1: Verification model for punching shear at ultimate limit state: (a) Cross - section view, and (b) Plan view (BS EN 1992-1-1 2004).

where d = effective depth of a section,

h = height of a section,

θ = punching shear angle,

c = column diameter,

A = basic control section,

B = basic control area, A_{cont} ,

C = basic control perimeter, u_1 ,

D = loaded area, A_{load} , and

r_{cont} = further control perimeter.

According to the BS EN 1992-1-1:2004, shear resistance check at the face of the loaded area and at the basic control perimeter of the slab is required. The basic control perimeter is usually taken to be at least at a distance of 2d from the loaded area, where d is the effective depth of the section. However, when a section requires shear reinforcement due to high shear stress concentration in the basic control perimeter, a further control perimeter should be determined where shear reinforcement is no longer required.

In conventional highway concrete bridge structures, beams or girders supported by piers are usually used to support bridge decks. The brittle nature of concrete is known to cause loss of strength shortly after the formation of the first crack. For this reason, additional reinforcement is required in the members to support tensile loads. For shear design, reinforcement is usually adopted in column and beam connections. However, in some particular circumstances shear reinforcement may not be enough, nor practical. The punching shear failure of Struve Slough Bridge, California, USA, in 1989 is a good example, see Figure 6.2. The failure of this structure occurred as a result of powerful seismic loads, in which the columns punched through the deck slab despite having shear reinforcement. This is a clear indication of reinforced concrete structures' vulnerability to shear failure.

Figure 6.2: Failure of the Struve Slough Bridge, USA (U.S. Geological Survey 1989).

Punching shear failure is known to occur suddenly and can cause catastrophic results. Currently, various methods such as stirrups and headed-studs have been used to increase the punching shear capacity of concrete highway bridge decks. However, the former

method is not applicable to slabs with shallow depths less than 150 mm (ACI Committee 318 2011), while the later one is expensive and time consuming. From Figure 6.2, it is clear that in highway bridge designs, attention should be given to both strength and ductility of concrete members when punching shear strength is being considered. While the current methods are not effective, UHPFRC might be a good solution. This concrete is known to exhibit high tensile strength with improve ductility compared to conventional concrete. The steel fibre content in the mix improves tensile strength, energy absorption and resistance to the formation and growth of cracks, as shown in Chapters 3 and 5. Exploiting these improved properties of the concrete to enhance the punching shear capacity of bridge decks is an important opportunity.

6.3 UHPFRC Highway Bridge Girders

Recently, the implementation of UHPFRC in construction around the world has led to new research investigating the positional utilization of this material in bridge designs, particularly in the Unites States. From the early 2000s, the Federal Highway Administration (FHWA) in the USA has conducted extensive research into innovative bridge designs and UHPFRC has played a significant role. So far, a number of short span highway bridges have been built with UHPFRC (Vergoossen 2008, Rebentrost and Wight 2008b). However, the popularity of this material in highway bridge applications is not widespread due to its initial high cost.

To date, a number of optimised UHPFRC girder types have been proposed, see Figure 6.3. These types of girder are designed so that the thin top flange of the section would serve as the bridge deck and contains no conventional steel reinforcement to resist shear. The thicknesses of the flanges are designed to be not greater than 100 mm. These girder designs are usually optimised even further when used in conjunction with prestressing to maximise the use of the inherent tensile properties of the concrete.

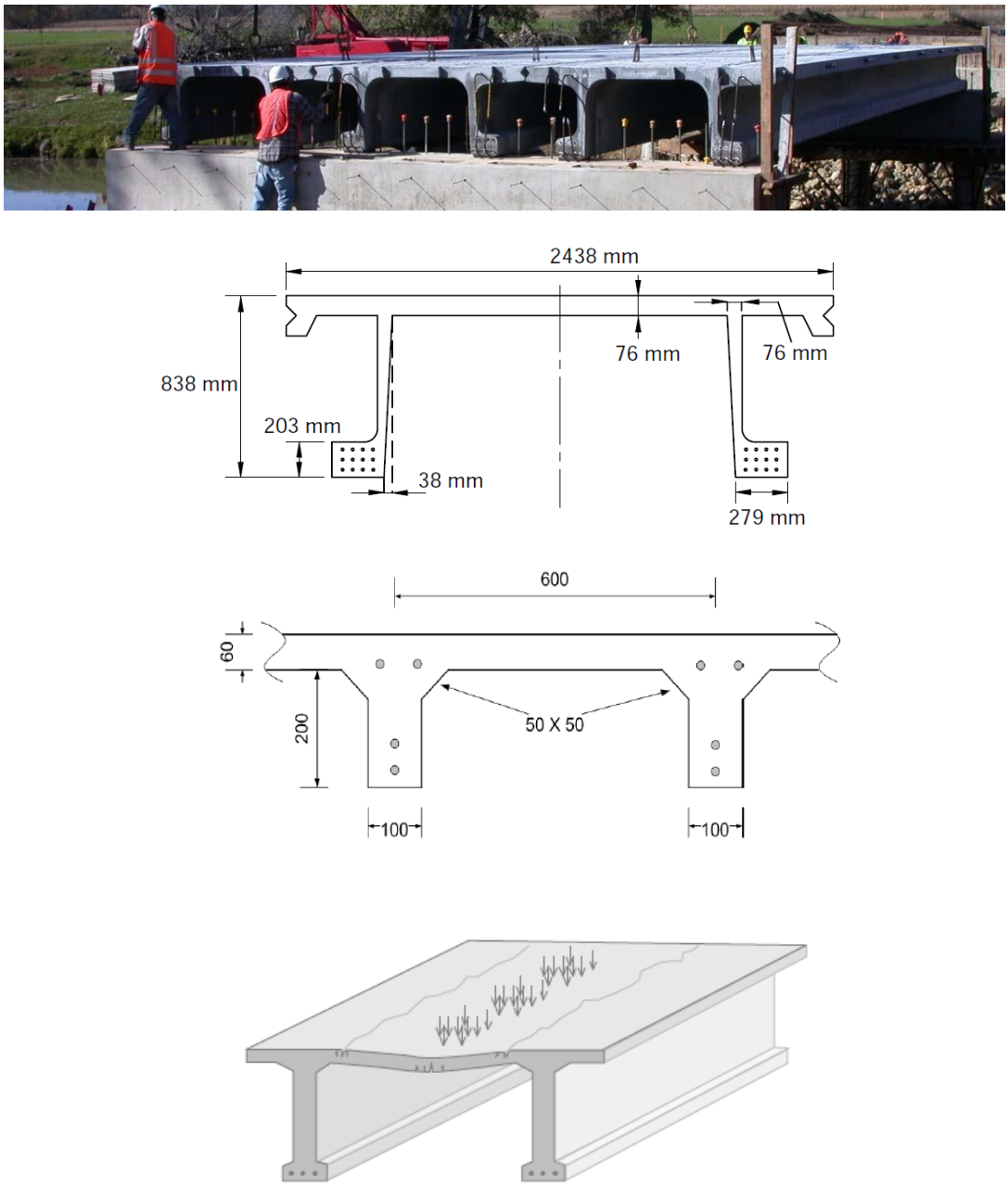

Figure 6.3: Optimised bridge girder designs (Portland cement association, Park H et al. 2003, Park et al. 2012, Spasojevic et al. 2009).

Such designs may offer economic and durability advantages by eliminating reinforcement and reducing the weight of the superstructure. However, the risk of punching shear failure is imminent in the section under a high concentrated load such as wheel patch load. Therefore, in this study, detailed experimental investigations were conducted to study the punching shear strength of thin UHPFRC slabs containing no

conventional reinforcement. The main objective of the study can be summarised as follows:

- Develop a suitable test method for the prediction of punching shear strength of UHPFRC with minimum flexural failure influence.
- Study the relationship between the punching shear strength and its failure angle.
- Study the ductility behaviour relative to the basic control perimeter.
- Evaluate the applicability of the existing equations in predicting the punching shear strength of UHPFRC, and
- Provide structural behaviour of UHPFRC slab specimens applicable for use in finite element modelling.

6.4 Previous Studies

So far, numerous studies have attempted to determine the punching shear capacity of SFRC and UHPFRC. However, results reported indicate the influence of flexural damage due to the method of testing. In this PhD, the results of these studies were used to provide the basis to determine a suitable test regime with minimal flexural failure influence. The following is a highlight of some of the related research studies:

6.4.1 Effect of fibers on the punching shear strength of slab-column connections (Harajli et al. 1995)

This research was one of the early and important studies on the punching shear strength of steel fibre concrete. In this study, an extensive experimental program was conducted to study the ability of steel fibres to increase shear strength in otherwise normal, conventionally reinforced concrete slab-column connections. In addition, it looked at the ability of fibres to alter the failure mode from pure punching shear to pure flexural or combined shear and flexural failure.

The results reported here indicated that the presence of hooked steel fibres in concrete slabs decreased the angle of shear failure plane and increased the perimeter of the failure surface. As a result, the punching shear resistance of the concrete increased significantly.

The presence of steel fibres also modified the failure mode of the slabs from pure punching to flexural failure. Finally, a design equation based on the results and previous studies to predict the ultimate punching shear strength of steel fibre concrete was proposed, see Equation 6.1.

$$V_{rd} = (0.096\, V_f) b_0 d \sqrt{f_c'} \qquad \text{Equation 6.1}$$

where V_{rd} = measured ultimate punching load (N),

V_f = volume fraction of fibers (%),

b_0 = perimeter of critical shear surface (mm),

d = depth to centre of reinforcing steel (mm), and

f_c' = cylindrical concrete compressive strength (MPa).

6.4.2 Bending and punching shear strength of fiber-reinforced glass concrete (Mu and Meyer 2003)

In this study, a series of tests were conducted on circular shape concrete specimens with various types of reinforcement (glass fibre & glass fibre mesh) and aggregate (sand & crushed glass). Specimens with a diameter of 127 mm and a thickness of 19 mm were cast. The specimens were supported on a simple ring with a diameter of 101.6 mm and tested by applying load to their centres. The deflection was obtained from a LVDT placed under the specimen in line with the centre of the load indenter. Figure 6.4 shows some of the specimens after testing. In this study, the circular shape of the specimens and the choice of boundary condition using steel ring were used in order to eliminate warping and this method seemed to be effective for punching shear test.

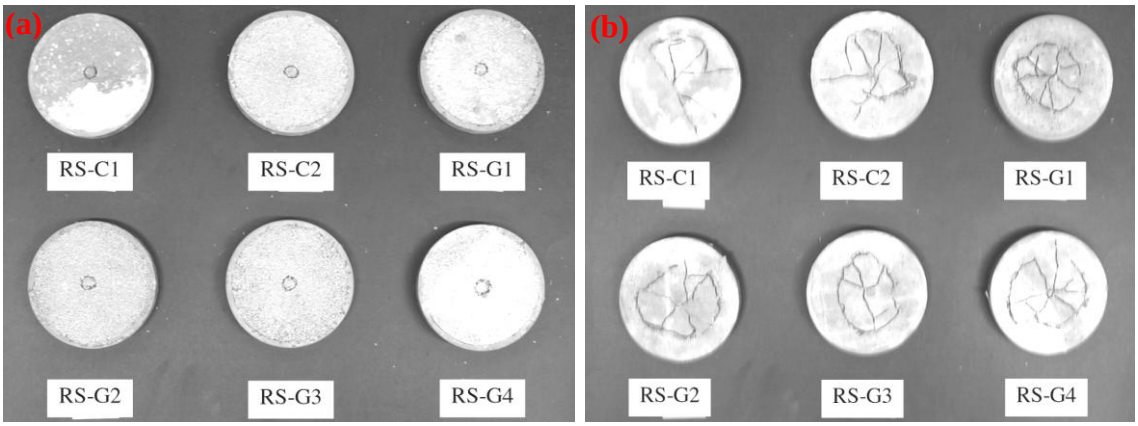

Figure 6.4: Typical cracking patterns of slabs after punching shear failure: (a) Top face and, (b) Bottom face.

6.4.3 Characterization of punching shear capacity of thin ultra-high performance concrete slabs (Harris and Roberts-Wollmann 2008)

In this study, twelve UHPFRC slabs were tested to failure to investigate the punching shear strength depending on the slab thickness and loading plate dimensions. Specimens of 1143 mm in width and length and various thicknesses of 51, 64 and 76 mm were tested. The specimens were fully restrained on all the edges to ensure punching shear failure prior to flexural failure. In addition, the validity of a number of existing equations to predict the punching shear strength of the concrete was studied.

From the results obtained, it was concluded that punching shear failure due to tyre loadings is unlikely for UHPFRC slabs with a thickness of 50 mm and greater. Furthermore, the test method (fixed boundary condition) appeared to be not effective and effects of flexural failure were still present during testing. The modified ACI 318 equation (ACI Committee 318 2011), see Equation 6.2, was reported to be the best model to predict the punching shear strength of this material. This equation is very similar to the one shown in Equation 6.1.

$$V_{rd} = 0.33\, b_0 d \sqrt{f_c'} \qquad \text{Equation 6.2}$$

6.4.4 Punching shear strength estimation of UHPC slabs (Joh et al. 2008)

This research was conducted at the Korea Institute of Construction Technology (KICT). This study is very similar to the one presented previously, Section 6.4.3 (Harris and Roberts-Wollmann 2008). This study reported the result of punching shear tests of 6 square UHPFRC slabs of 1200 mm in length and width with thicknesses of 40 and 70 mm. The specimens were fixed along their edges to simulate fixed boundary conditions and ensure punching shear failure prior to flexure. In addition, a number of existing equations for predicting the punching shear capacity of normal concrete and UHPFRC were used to predict the test results.

The results reported here, indicated that punching shear strength of UHPFRC depends not only on the tensile strength but also on the local composition and fabrication methods. Similarly, the results of some of the tested specimens appeared to be affected by flexural failure and the fixed boundary condition appeared to be not effective.

6.4.5 Punching shear strength of steel fibre reinforced concrete slabs (Maya et al. 2012)

This study presented a mechanical model based on the critical shear crack theory for predicting the punching shear strength of concrete slabs reinforced with steel fibre as well as conventional reinforcement, very similar to Equations 6.3 and 6.4. The accuracy of the model and a number of existing equations were checked in predicting 140 slab-columns steel fibre reinforced concrete test results reported in the literature. It was reported that the current design formulae show significant scatter predictions and are not safe to be used in design. However, the proposed mechanical model presented in their study was reported to provide a good estimate of the punching shear strength of fibre reinforced concrete slabs.

6.4.6 Shear and flexural strength of thin UHPC slabs (Moreillon et al. 2012)

Researchers at the University of Applied Sciences (HES-SO), Fribourg in Germany, have recently completed several tests investigating the shear and flexural capacity of UHPFRC slabs. In this study, forty thin UHPFRC slabs reinforced with and without

conventional steel reinforcement were tested and the advantages of using conventional steel reinforcement on the flexural and shear capacity of the concrete were studied.

For the punching shear test, experimental investigation was carried out using a punching shear test setup that was specifically designed in this study. In their test, square slabs of 960 mm with various thicknesses were supported by eight steel rods and anchored to a steel frame. The support system described a circle with a diameter of 878 mm, as shown in Figure 6.5. The load is applied to the centre of the slab through an 80 mm diameter punch.

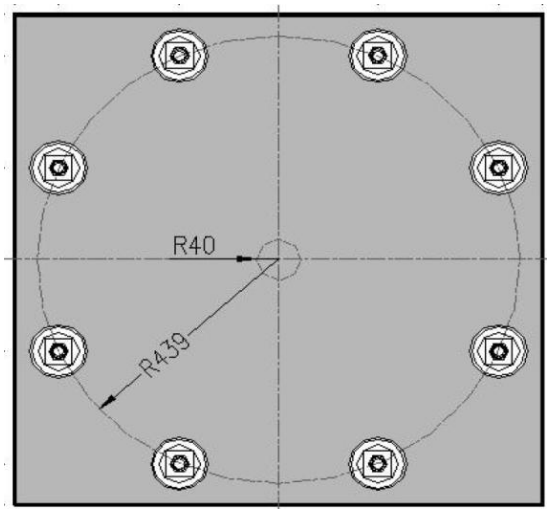

Figure 6.5: Punching shear test-setup.

In this study, a well know model for predicting the punching shear strength of UHPFRC slabs using critical shear crack theory was assessed. The punching shear model, see Equations 6.3 and 6.4, involves the contributions of the matrix, $V_{R,c}$, and the fibres, $V_{R,f}$. This model was proposed by others (Muttoni 2008) for failure criterion for the punching shear strength of reinforced concrete slabs without transverse reinforcement.

$$\frac{V_{R,c}}{b_o d \sqrt{f_c}} = \frac{3/4}{1+15\frac{\psi\, d}{16+d_g}} \qquad \text{Equation 6.3}$$

$$V_{R,f} = \frac{1}{K}\int_{A_p} \sigma_f\ (w)\, dA_p \qquad \text{Equation 6.4}$$

where $V_{R,c}$ = design concrete contribution to punching shear strength (N),

b_o = perimeter of the critical section (mm), distance of d/2 from the face of the column,

d = effective depth of the slab (mm),

f_c = cylinder compressive strength (MPa),

ψ = maximal rotation of the slab,

d_g = maximum diameter of the aggregate (mm), for UHPFRC is zero,

$V_{R,f}$ = fibre contribution to punching shear strength (N),

K = fibre orientation,

A_p = horizontally projected area of the punching shear failure surface (mm^2),

σ_f = fibre bridging stress (MPa), and

w = critical shear crack opening (mm).

This study reported the failure of UHPFRC slabs without steel reinforcement were predominately flexural in the form of yield lines and no punching shear cones could be seen from the failed specimens. However, for specimens reinforced with conventional steel, punching shear failures were reported depending on the thickness and reinforcement ratio. Finally, the authors indicated that the proposed model for UHPFRC based on critical shear crack theory must be validated and simplified before being used by designers.

The studies listed above, are just a selection that were relevant to this study. Despite all the findings reported, the body of research on UHPFRC punching shear strength is limited and incomplete. This is because there is not a punching shear test method available so far to determine the punching shear capacity of the material specifically. Hence, in this study, more detailed experimental work was conducted and is believed to have contributed in studying the punching shear capacity of this concrete significantly.

6.5 Experimental Investigations

In this section, the development of the test method and problems encountered during testing are discussed. Furthermore, specimen preparation and test setup are presented.

6.5.1 Test development

There are no known standards for the proposed punching shear test setup described here. In this study, a number of trial tests were conducted to characterise the punching shear capacity of UHPFRC with minimum influence of bending stress. The trial tests were conducted and modified throughout the test until the final setup was found. The experimental investigation was divided into three phases, and each of them is discussed below.

In the first phase, preliminary tests were carried out on rectangular slabs of 300x300x30 mm in length, width and depth, respectively. The size of the specimens was kept small due to the high cost of the material. However, they were large enough so that punching shear failure could be forced during the test. The initial research was restricted to a slab thickness of 30 mm. The specimens were supported on two different boundary conditions, simply supported on four edges and circular hollow steel rings with various diameters. Load was applied to the centre of the specimen using a 50 mm diameter steel indenter. The small loaded area was used to enhance the punching shear failure possibilities during testing. From the results obtained in this phase, the influence of flexural failure was present and significant. For the simply supported test results, the flexural failure was more pronounced than those obtained for the circular support. A combination of flexural and shear failure was observed from the results of this phase.

From the literature, fixed boundary conditions was reported to improve the possibility of punching shear failure of thin UHPFRC slabs (Harris and Roberts-Wollmann 2008, Joh et al. 2008). However, from the results reported in both studies, the influence of flexural stress appeared to be present. Therefore, this study took a different approach to develop a test setup that can minimise the effect of flexural failure on punching shear failure.

The second phase was to increase the thickness of the slab specimens to 60 mm and incorporate an initial notch, similar to notched beams in bending tests. Circular notches of 30 mm depth of different diameters were introduced to the centre of the specimens, as shown in Figures 6.6 and 6.7 (b). The purpose of the notch was to initiate a shear plane along a predefined path and cause punching failure. These notches were indented to

simulate the effect of macrocracks and plastic hinges formed during flexural cracking in slab specimens. Various notch diameters ranging from 55.5 to 194.4 mm were introduced and provided a wide range of punching shear angles relative to the applied load. In this phase, both boundary conditions as in the first phase were used.

It must be noted, this method forced failure of the slabs at the notches. However, the results may not have determined the weakest section of the specimen due to global tensile stresses. Therefore, multiple tests for each notch size were carried out to determine the mean behaviour for punching shear strength to the punching shear angle. Results obtained in this phase appeared to be promising, but inconsistent. The influence of flexural and hoop stresses were still present, hence, improvement in the test setup was required. Figure 6.6, provides a schematic indicating the test setup in this stage.

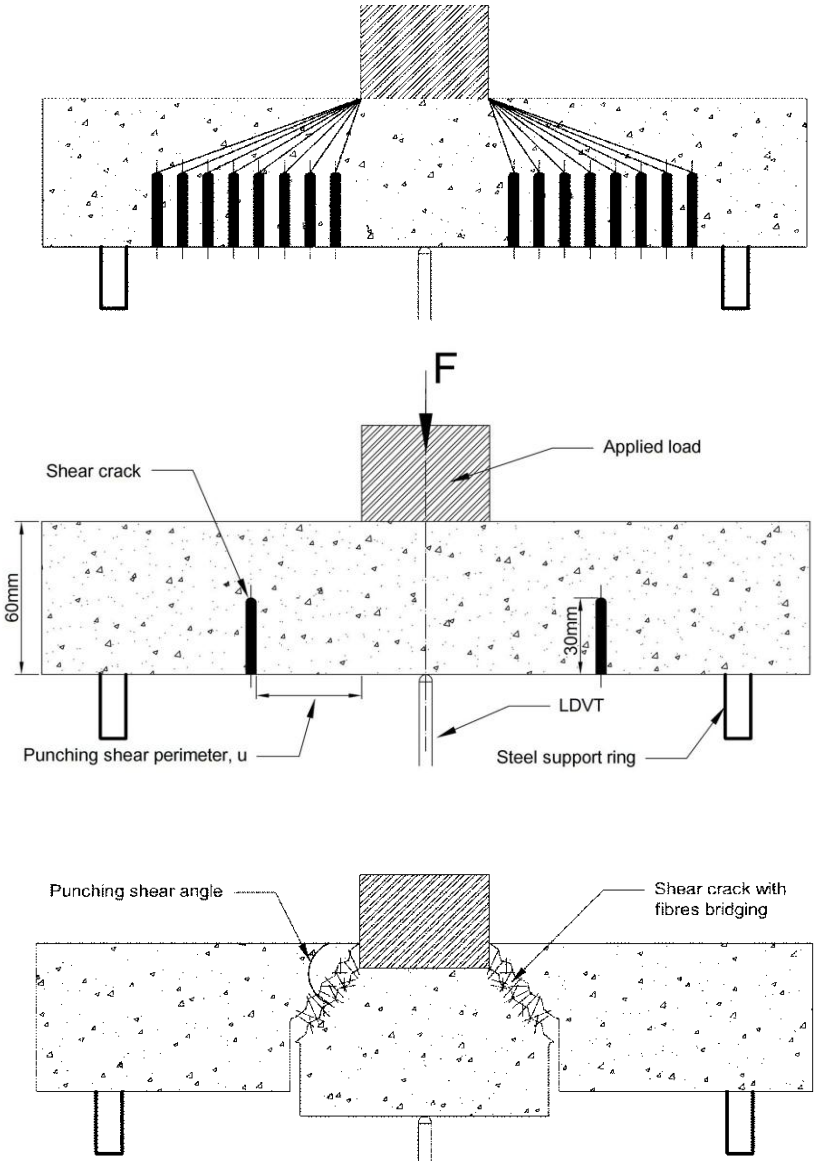

Figure 6.6: Indicative diagram of test setup.

In the third and final phase, the flexural and hoop stress effects were reduced significantly. This was achieved by increasing the depth of the shear notches and using an improved supporting arrangement. The specimen's total thickness was increased from 60 mm to 90 mm. The initial crack depth was increased from 30 to 60 mm and the effective slab thickens was kept at 30 mm. The depth of the notches was increased to minimise flexural stress before the occurrence of punching shear failure. In addition, the specimens were supported around the perimeter of their notches using steel tubes of

various diameters. The inside diameter of each support was equal or smaller than 1.30 the diameter of the notches. The various sizes of circular boundary condition was used to minimise warping and hoop stress as it was encountered in the preliminary stages of the tests. The results obtained from this phase were predominately punching shear failures and the objective of the investigations was achieved. The final test set setup is shown in Figure 6.7.

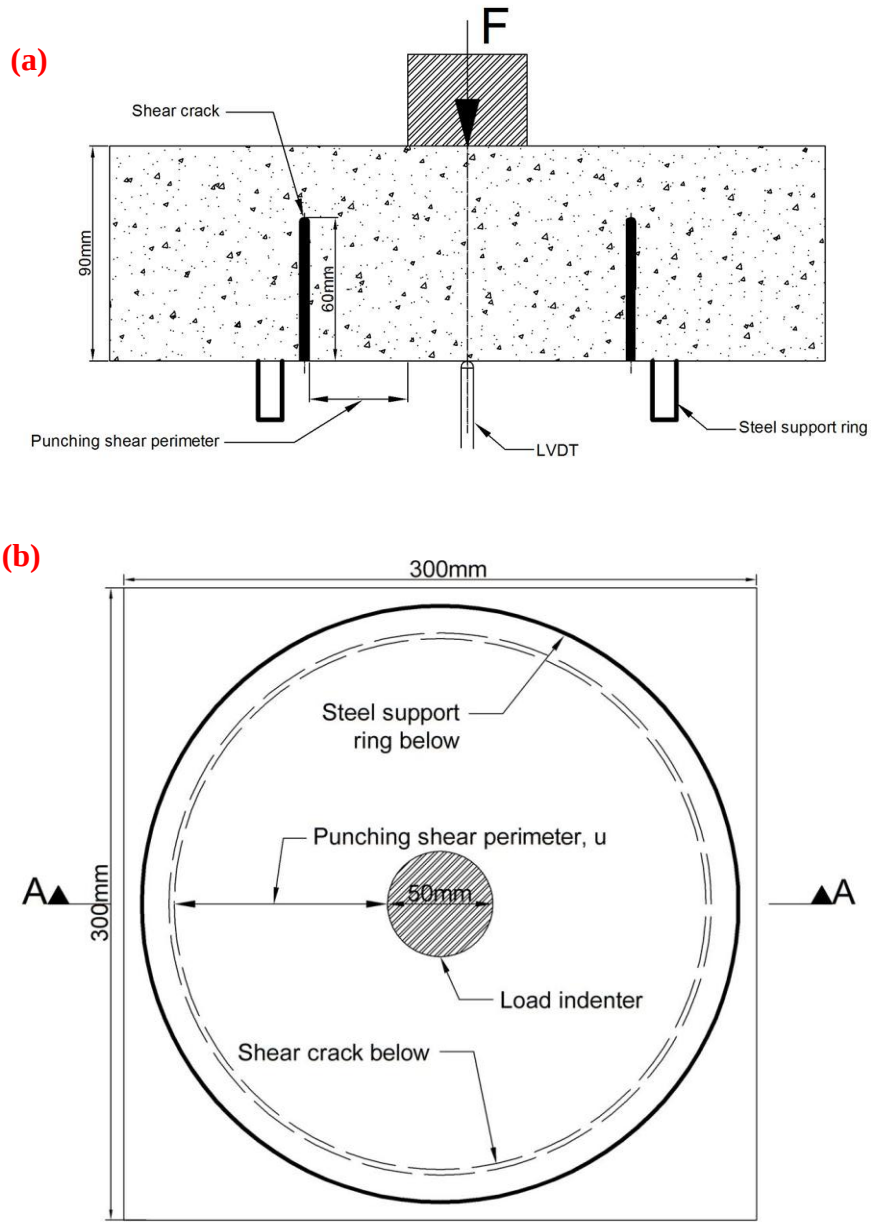

Figure 6.7: The final test setup: (a) Section view, and (b) Plan view.

6.5.2 Specimen preparation

The materials, mixing, casting and curing procedure were the same as described in Section 3.4 of this thesis. For the first and second phases, several specimens were cast. However, since the results of both phases were unsatisfactory, only sample preparation for the third phase is discussed here.

In the third phase, 30 rectangular slabs were cast in total. The dimensions of the specimens were 300x300x90 mm in length, width and depth, respectively. Table 6.1 summarises the notch and support diameters with the punching shear angles of the specimens. For each notch diameter, at least 3 slabs with 6 cubes of 100 mm were cast. The cubes were tested for density and compressive strength measurements at 7 and 28 days.

Table 6.1: Summary of the test specimens and supports in the third phase.

Notch diameter (mm)	Support, inside-diameter (mm)	Support thickness (mm)	Basic control perimeter	Punching shear angle (degree)
55.5	60	8	0.09d	84.8
81.5	98	8	0.53d	62.3
111	143	12.5	1.02d	44.5
133	150	8	1.38d	35.9
147	173	10	1.62d	31.7
162	194	12.5	1.87d	28.2
179	210	12.5	2.15d	24.9
194	210	12.5	2.40d	22.6

After 28 days, the rough surfaces of the slab specimens were ground to provide an even surface for introducing the shear notches, as shown in Figure 6.8. Soon after grounding, a mechanically secured pillar drill with diamond core bits of various diameters were used to introduce the shear notches to the underside of each specimen in the centre, see Figure 6.9. The width of the notches was approximately 4 to 4.5 mm.

Figure 6.8: Specimen before and after grinding.

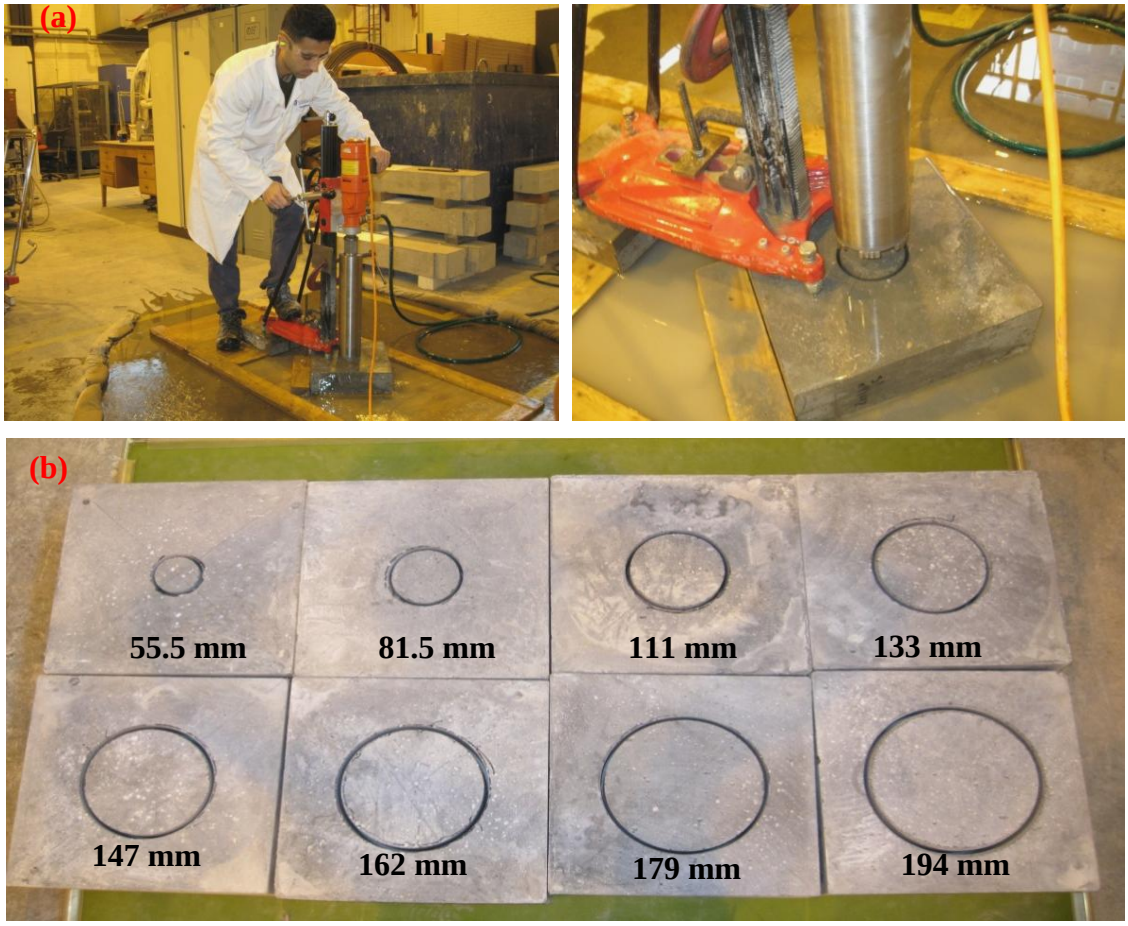

Figure 6.9: Specimen preparation: (a) Shear notch inducers using diamond drills, and (b) Various shear notch diameters.

6.5.3 Test setup

The specimens were tested using a 300 kN Zwick testing machine. The load was applied at the centre and opposite side to the notches using a 50 mm diameter steel indenter. The

test was conducted under displacement control at a rate of 0.1mm/minute up until a vertical deflection of 9.5 mm was recorded. For deflection measurements, an LVDT was positioned under the specimen in line with the centre of the load indenter. For each notch size, three or more specimens were tested and punching shear load against deflection was acquired digitally. Figure 6.10 shows the test setup in the testing rig.

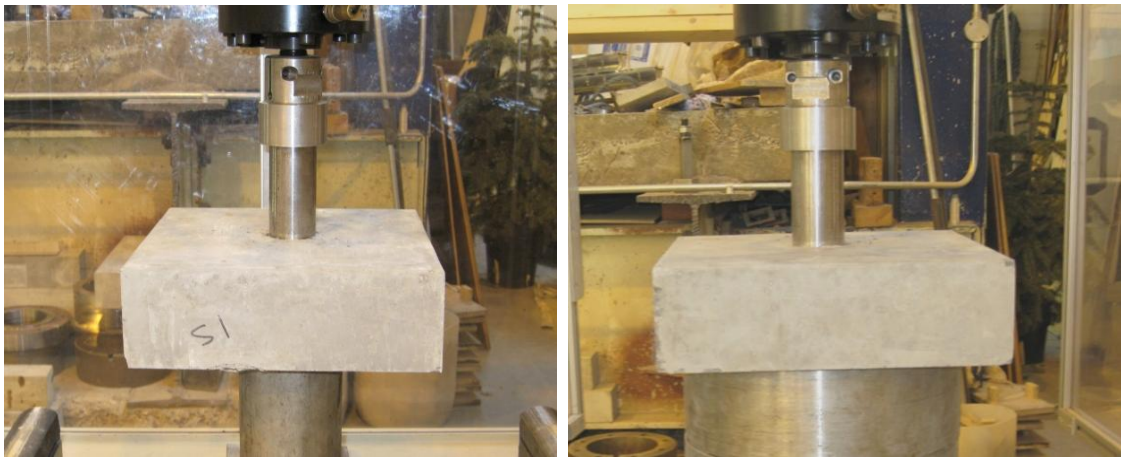

Figure 6.10: Test setup in the testing rig.

After each test, the failed specimen was removed from the testing rig and checked visually to investigate any signs of flexural failure. Finally, the specimen was placed back into the loading rig and reloaded again to cause total failure. In this way, the punching shear cone of the specimen was forced all the way through and investigation on the modes of failure and fibre distribution in the concrete was carried out.

6.6 Results and Discussion

In this section, only limited results of the first and second phases are presented. Since these were preliminary tests and the results were significantly influenced due to flexural failure. Furthermore, the implications encountered during testing in both phases are discussed briefly. However, results of the final phase are discussed and evaluated in detail.

6.6.1 Phase one

The specimens of this series were unnotched with a constant thickness of 30 mm. The slab specimens here were first tested due to the limited knowledge of the behaviour of thin UHPFRC slabs in punching shear. The tests were conducted to determine the natural punching shear strength and failure plane angle of the concrete.

Results from this phase were highly influenced by the types of boundary conditions. Flexural failure was observed for all the tested specimens that were supported on steel ring diameters equal or greater than 174 mm. This was predicted, since a diameter of 174 mm was just outside the basic control perimeter distance of 2d (170 mm for the tested specimens) as specified in Eurocode 2 (BS EN 1992-1-1 2004). In contrast, for specimens on steel support diameters of less than 174 mm (such as 160, 151, 137 mm), punching shear failure was observed. However, the failure occurred around the inside perimeter of the steel supports. It was noted that such support arrangements were restricting the natural punching shear failure of the concrete to occur. The results obtained in here were inconsistence. For specimens that were supported only on the four edges, predominate flexural failure was observed. Figure 6.11, shows the failure modes of some of the specimens in this phase using various steel support diameters.

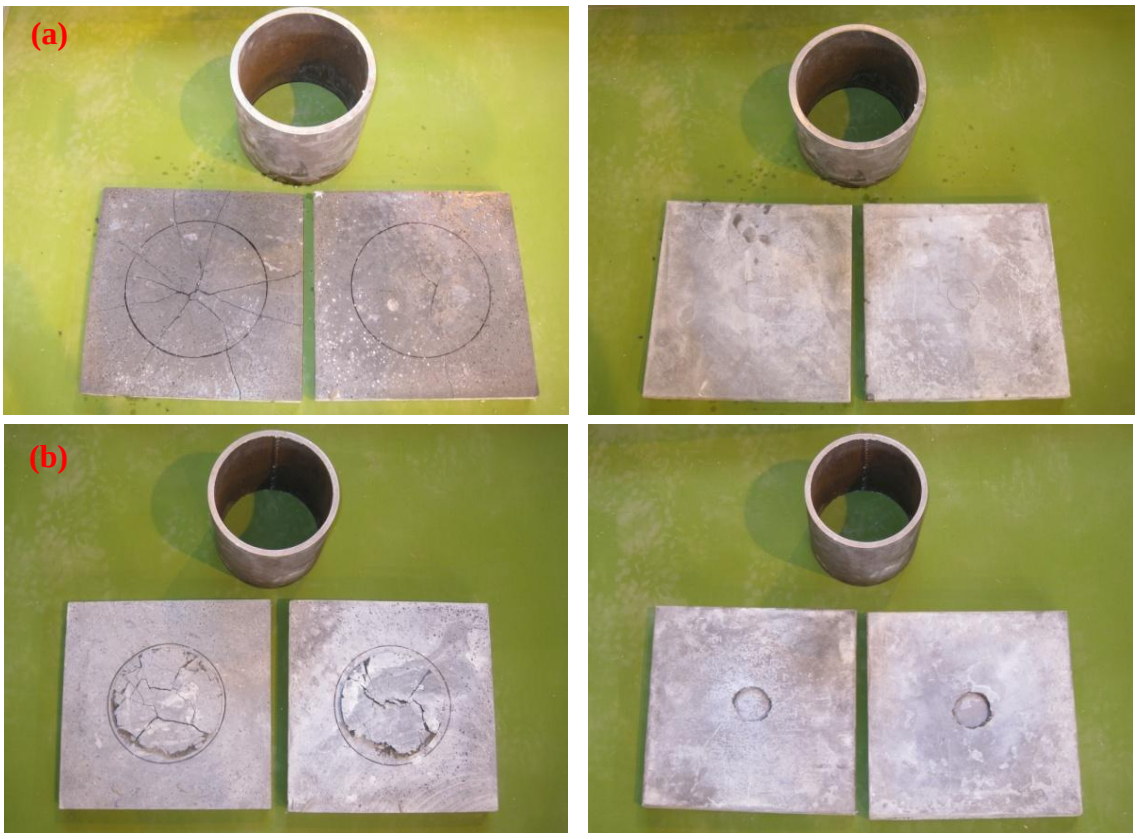

Figure 6.11: Various failure modes for 30 mm slab specimens: (a) Flexural failure for specimens supported on steel ring diameters greater than 2d (174 mm), and (b) Punching failure for specimens supported on steel ring diameters smaller than 2d (151 mm).

At the end of this phase, it was evident that the failure mode of simply supported UHPFRC slab specimen was predominately flexural and a different approach had to be taken. Since the fully fixed approach had been used in previous studies (Harris and Roberts-Wollmann 2008, Joh et al. 2008) and provided results with no high degree of certainty. This study decided to look for a different method with simply supported boundary conditions that can assess this essential property of UHPFRC more precisely. However, the results obtained here were a good starting point to improve the test method. Therefore, investigation on using notched specimens in the next phases commenced.

6.6.2 Phase two

In this phase, notched slab specimens as described earlier in Section 6.5.1 were tested. The boundary condition was provided using a circular steel ring diameter of 210 mm for

all the tests. The results obtained in this phase were predominately flexural failure regardless of the notch diameters. The most successful tests with nearly punching shear failure behaviour were specimens with a notch diameter of 147 mm (punching shear perimeter of 1.62d). Only two of the three samples were tested and both results are presented in Figure 6.12. This is due to the rest of the tests being declared void.

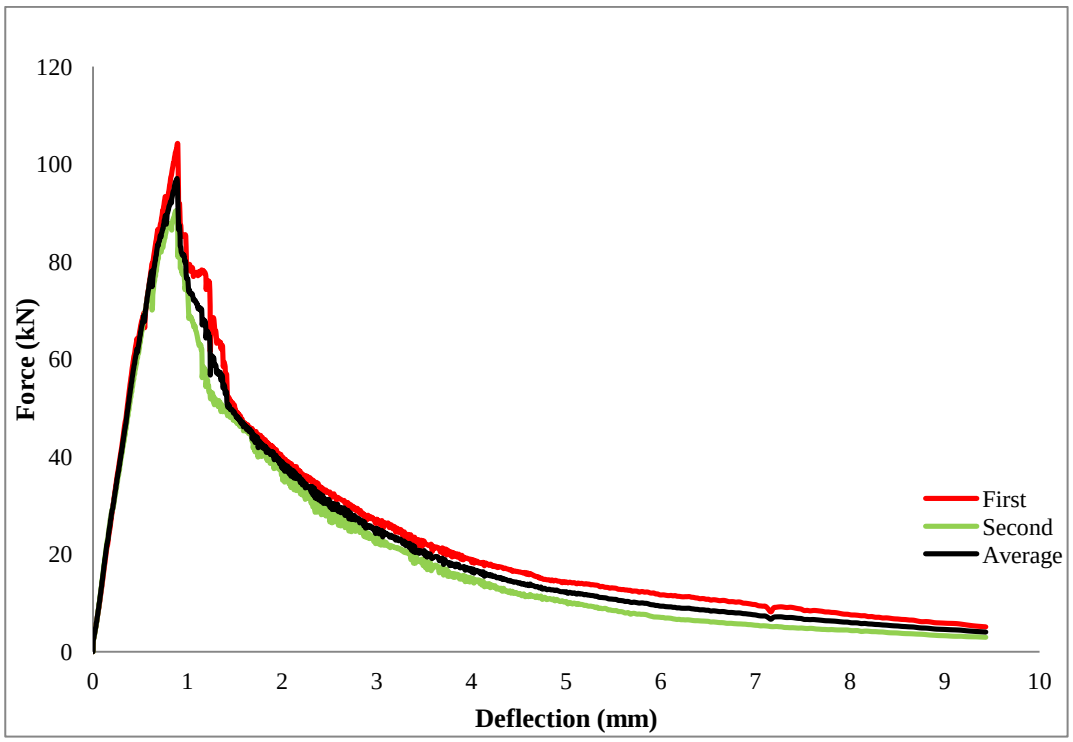

Figure 6.12: Load versus vertical deflection for specimens with a punching shear perimeter distance equal to 1.62d.

In Figure 6.12, the pre-failure load-deflection curves are almost linear for both tests and the failure mode is ductile. From visual inspections on the tested specimens, it was evident that there were flexural and hoop-stress damage prior to the initiation of punching shear failure and improvements in the test method was required. The full objectives of the original outcomes were not delivered at this phase. The inconsistency of the results occurred from a number of factors, including the support option and depth of the shear notches. The results reported in this stage provided crucial and additional data prior to the final stage.

6.6.3 Phase three

In this final phase, the depth of the shear notches was increased to 60 mm. The results reported here were predominantly punching shear failure, which were characterised by the stub punching of the load indenter through the slab and the shape of the failure area, a truncated cone failure shape, see Figures 6.15 and 6.22. The tests results obtained in this phase is summarised in Table 6.2.

Table 6.2: Phase three test results.

Notch diameter (mm)	u_1	V_{rd} (kN)	δ_{rd} (mm)	Failure mode
55.5	0.09d	294.86	0.762	Brittle
81.5	0.53d	183.26	0.561	Brittle[5]
111	1.02d	115.79	0.379	Ductile
133	1.38d	104.18	0.479	Ductile
147	1.62d	92.58	0.453	Ductile
162	1.87d	88.27	0.405	Ductile
179	2.15d	147.11	0.562	Ductile
194	2.40d	154.38	0.658	Ductile

In this phase, concrete crushing at the beginning of each test was observed, in particular, for the slabs with smallest notch diameters as they were exhibiting higher punching shear loads. Specimens with punching shear perimeters of 0.09d and 0.53d failed in a brittle and abrupt manner. The loads versus vertical deflections for both test results are presented in Figure 6.13 and 6.14, respectively. Form the load-deflection curves in both figures, the concrete crushing is apparent. In Figure 6.13, the load increased in a linear rate until the maximum punching shear load, V_{rd}, was attained at first crack and failure occurred with limited warning, as expected in a typical punching shear failure. However, results for specimens with a basic control perimeter of 0.53d experienced crack formation before maximum load was reached and one ductile failure was also reported. The load-deflection response shown in Figure 6.14 indicates failure of the matrix before peak strength was reached. However, since five out of the six tested specimens have failed in a brittle manner, the failure mode for 0.53d specimens was also considered brittle. The deflection at maximum load, δ_{rd}, for specimens with punching shear perimeters of 0.09d and 0.53d were less than 0.8 mm.

[5] Out of six specimens, five brittle and one ductile failure was reported.

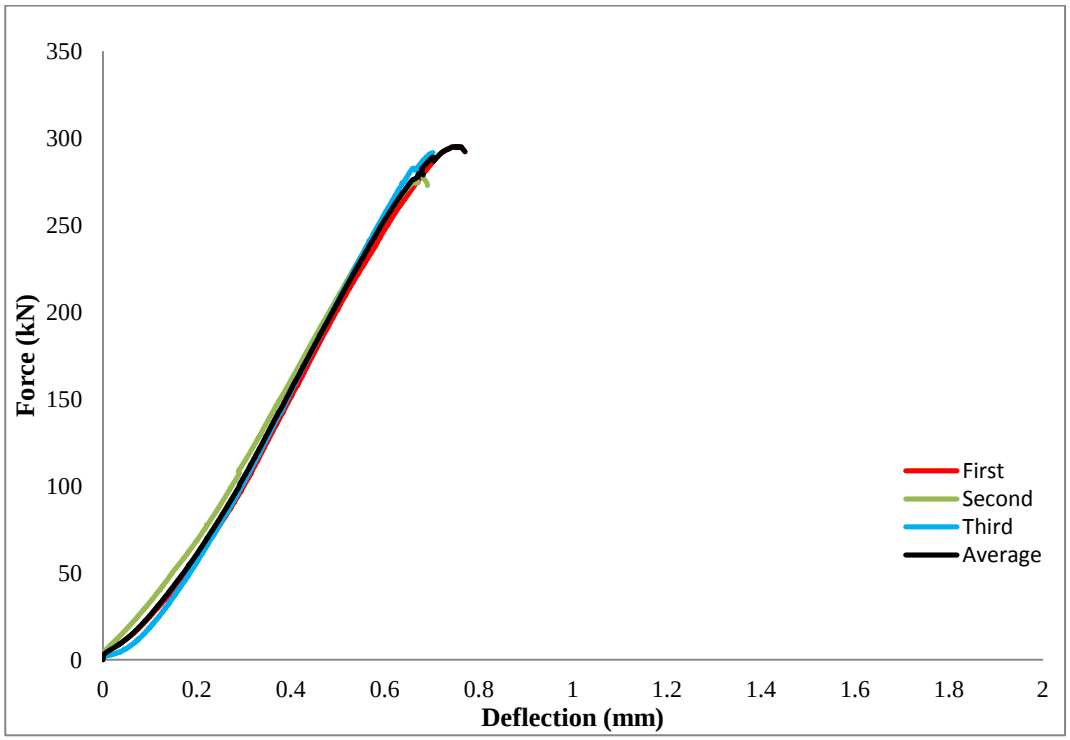

Figure 6.13: Punching shear load versus vertical deflection for specimens with a punching shear perimeter distance equal to 0.09d (55.5 mm notch perimeter).

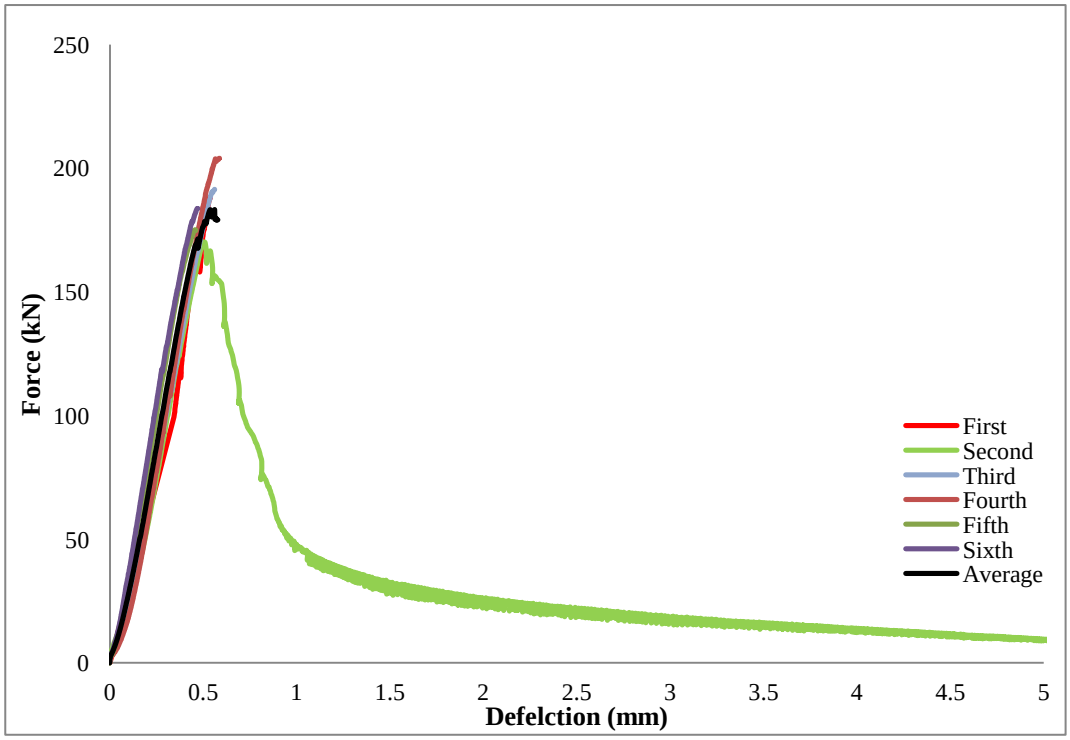

Figure 6.14: Punching shear load versus vertical deflection for specimens with a punching shear perimeter distance equal to 0.53d (81.5 mm notch perimeter).

The failure behaviour for specimens in Figure 6.13 and 6.14 were similar to the description of conventional concrete punching shear failure, as described earlier in this chapter. However, for UHPFRC, the improvement in ductility was expected due to the presence of steel fibres in the concrete. This was not seen for the 55.5 mm shear notch specimens, while little was reported for the 81.5 mm shear notch specimens. The abrupt and brittle failures of these tests resulted from a number of factors, and these can be summarised as:

- The steep punching shear angles,
- Confined shear crack patterns,
- The lack of random fibre distribution along the shear line failure, hence lack of fibre bridging effect, and
- The high intensity of shear stress close to the loading plate.

The punching shear angles in both tests were 84.8° and 62.3°, respectively. With such steep angles, random fibre orientation along the shear line plane was not likely to be achieved. Fibre orientation for UHPFRC is likely to be perpendicular to the formed surface of the specimens as has been reported by others (Harris 2004, Kang et al. 2011). In addition, the number of fibres resisting the shear load for both sets of specimens are small, since the punching shear area is relatively small. As a result, the concrete alone could end up resisting most of the shear load up till the point of failure. Failure occurred when diagonal tension or combined action of shear and direct stress exceeds the tensile strength of the concrete and resulting in the occurrence of confined diagonal shear cracks and the brittle failure behaviour. It is also possible that most of the steel fibres along the shear plane experienced direct shear failure with minimal fibre bridging effect. As a result, tensile load transferred from the fibres to the concrete prior to the immediate failure of the specimen was very small. Another factor could be due to the high intensity of the shear stress in the region close to the loading plate (smaller basic control perimeters). The combination of all the factors described above resulted in the brittle failure for almost all the tests of these specimens.

The conical punching shear failure shapes of both set of specimens are shown in Figure 6.15. It is evident that failure has occurred when shear cracks have initiated and radiated outwards from the point of the applied load to the shear notches on the tension side of the specimen forming a radiated failure cone. From these cones, a mixture of failed fibres and fibre pull-out behaviour were observed, in particular, for the 0.09d specimens. Furthermore, signs of flexural failure were not observed on either side of the tested specimens.

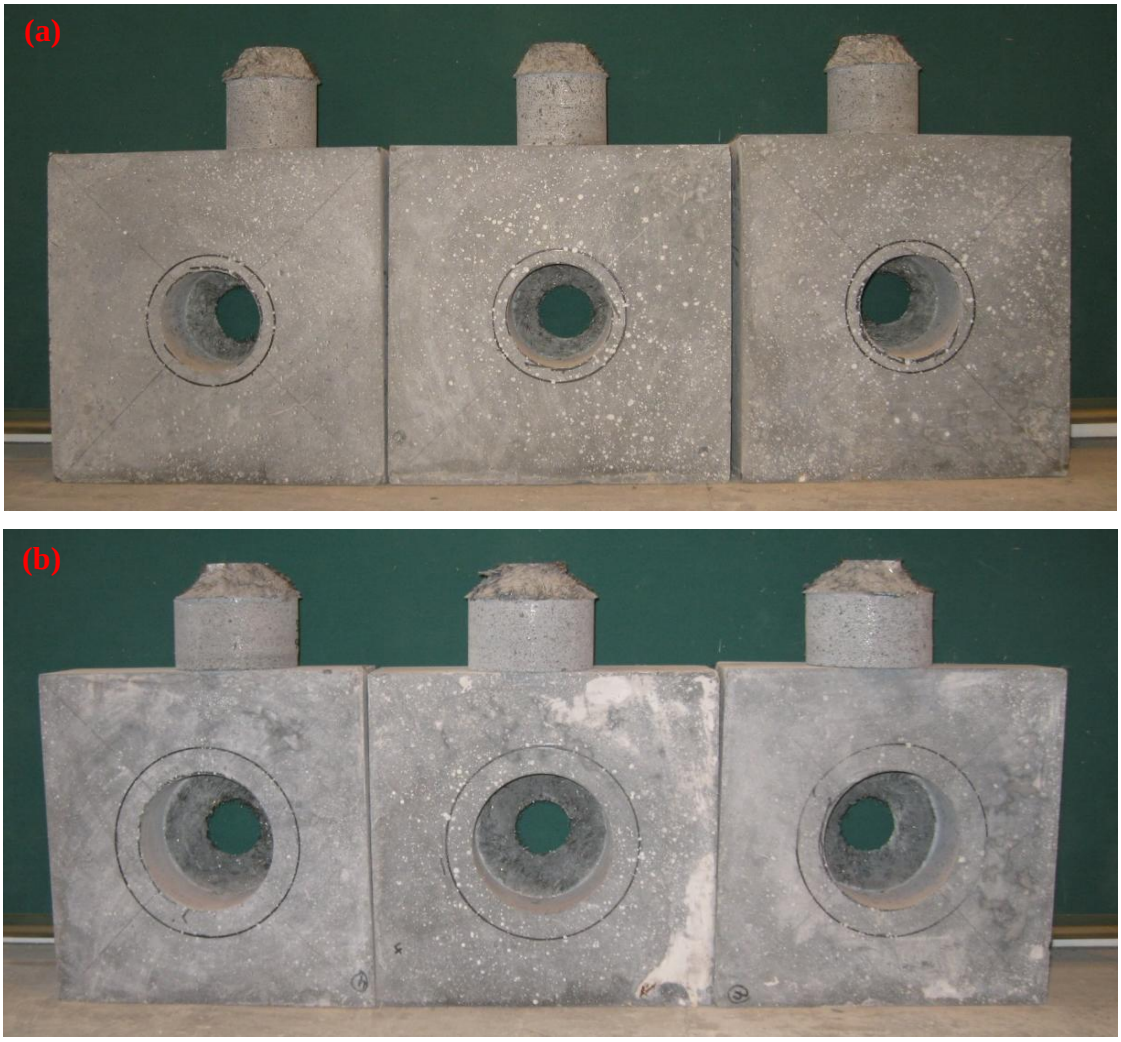

Figure 6.15: The punching shear failure modes for: (a) The 0.09d specimens, and (b) The 0.53d specimens.

The loads versus vertical deflections for the remaining specimens with basic control perimeters of 1.02, 1.38, 1.62, 1.87, 2.15 and 2.40d are presented in Figures 6.16 to 6.21,

respectively. In all these figures, the load increases in a linear manner until approximately 90% of the maximum punching shear loads have attained. Subsequently, strain hardening has occurred for a short period of time till maximum load was reached. The specimens were able to sustain reduced load after peak strength and continued to deform in a ductile manner, similar to a typical flexural failure.

It is evident that the failure behaviour for the tests in Figure 6.16 to 6.21 differs completely to those reported in Figure 6.13 and 6.14. The variation in both sets of results are down to the significance of punching shear angles, punching shear areas, fibre content, and the fibre bridging effect in each tests. With smaller punching shear angles and greater punching shear areas for specimens in Figures 6.16 to 6.21, the number of steel fibres bridging the shear crack surfaces increase. As a result, greater fibre pull-out forces are transferred across the cracks once the maximum load is reached. Hence, the fibre bridging effect after formation of microcracks becomes more effective and results in ductile failure. The failure behaviour of these tests is very similar to the flexural failure tests reported in Section 5.6.2.2. The improved ductility behaviour reported for these punching shear tests are significant. This is because such behaviour can be exploited for structures where punching shear failure is imminent and the option of heavy shear reinforcement is limited in the member, i.e. thin UHPFRC highway bridge decks. Furthermore, this ductility behaviour can be exploited and used in design to reduce the basic control perimeter of the concrete by half (1.02d) compared to what has been specified in EC2 for conventional concrete (2d).

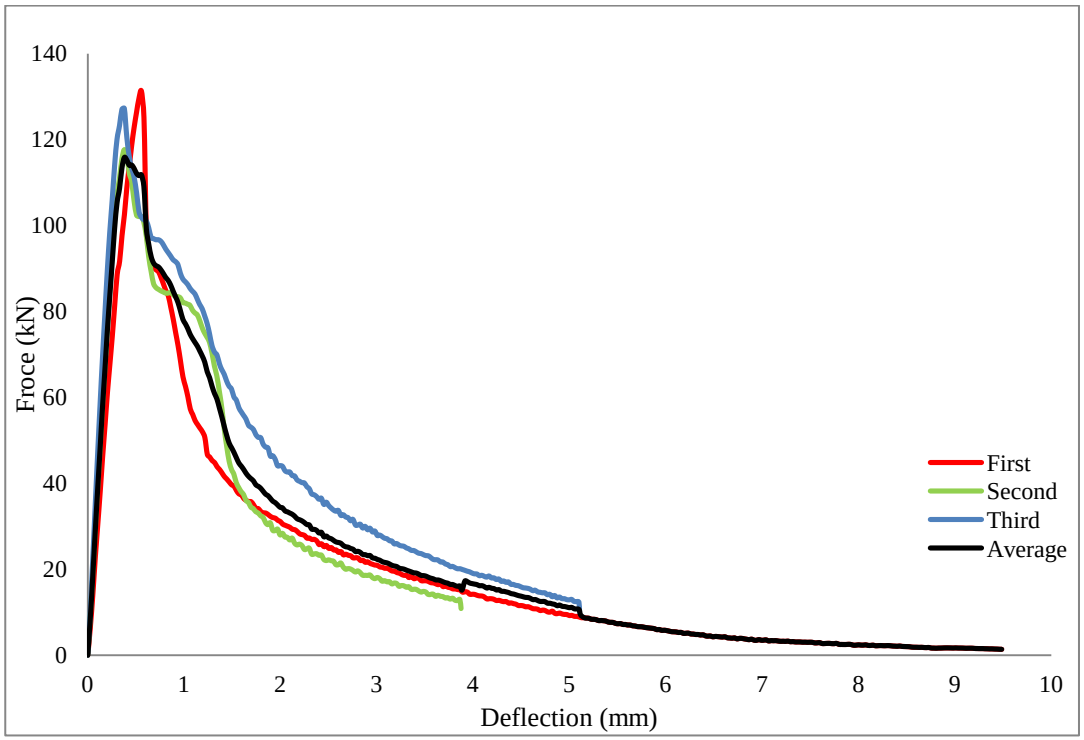

Figure 6.16: Punching shear load versus vertical deflection for specimens with a punching shear perimeter distance equal to 1.02d (111 mm notch perimeter).

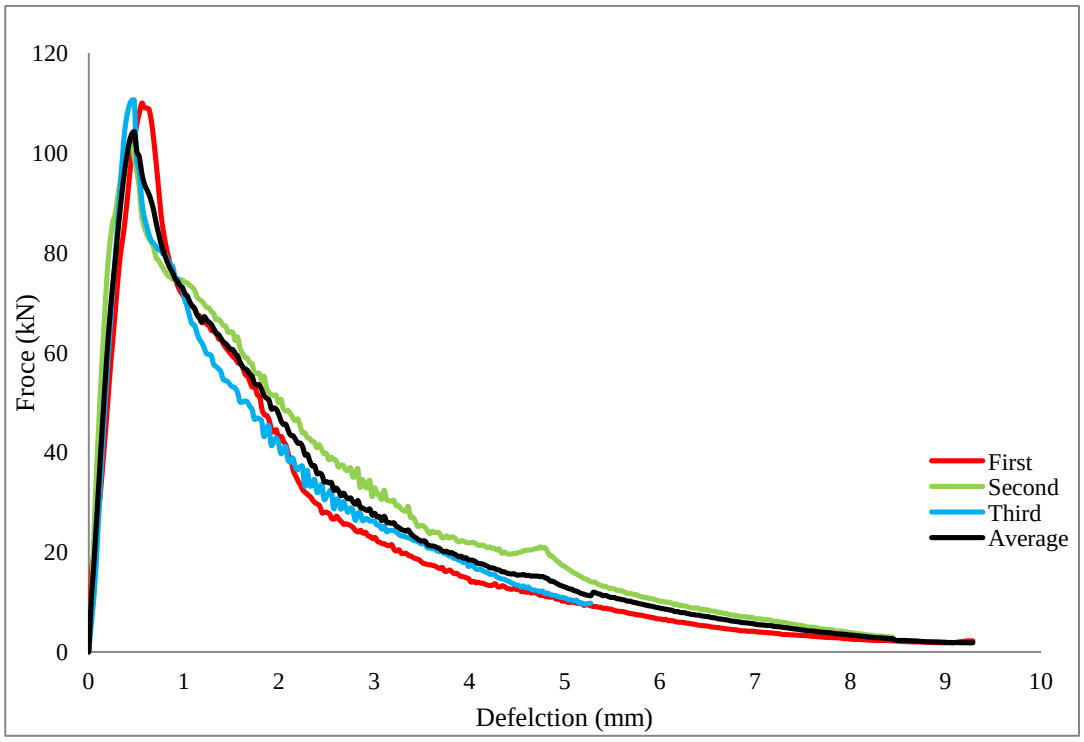

Figure 6.17: Punching shear load versus vertical deflection for specimens with a punching shear perimeter distance equal to 1.38d (133 mm notch perimeter).

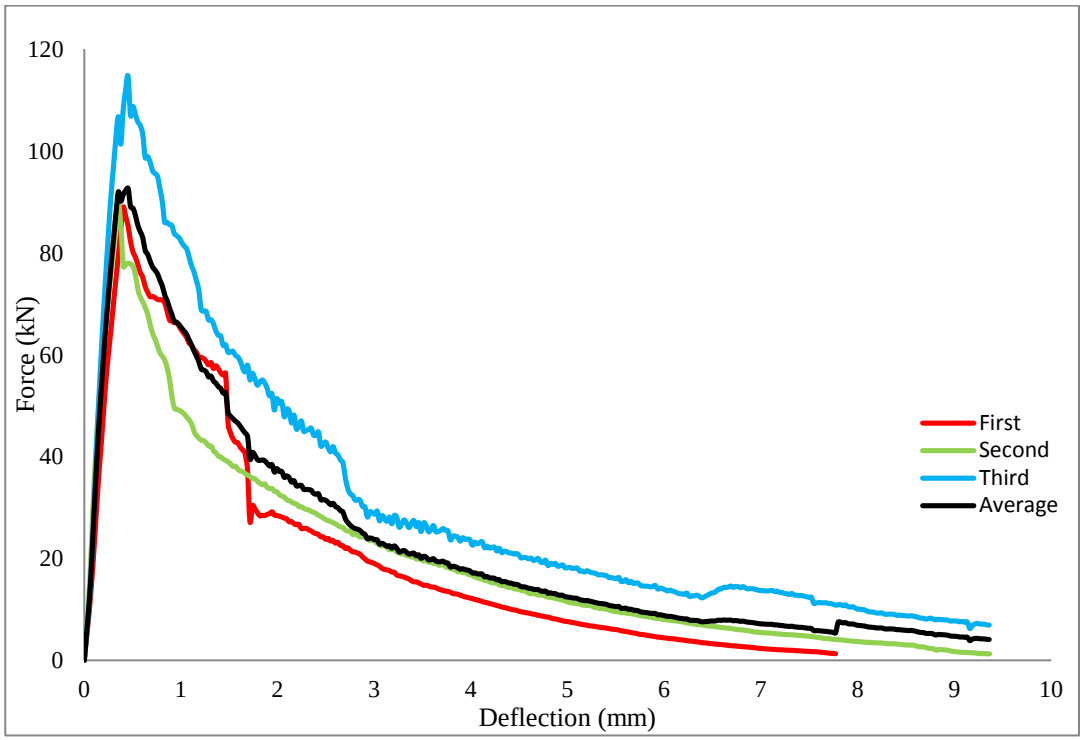

Figure 6.18: Punching shear load versus vertical deflection for specimens with a punching shear perimeter distance equal to 1.62d (147 mm notch perimeter).

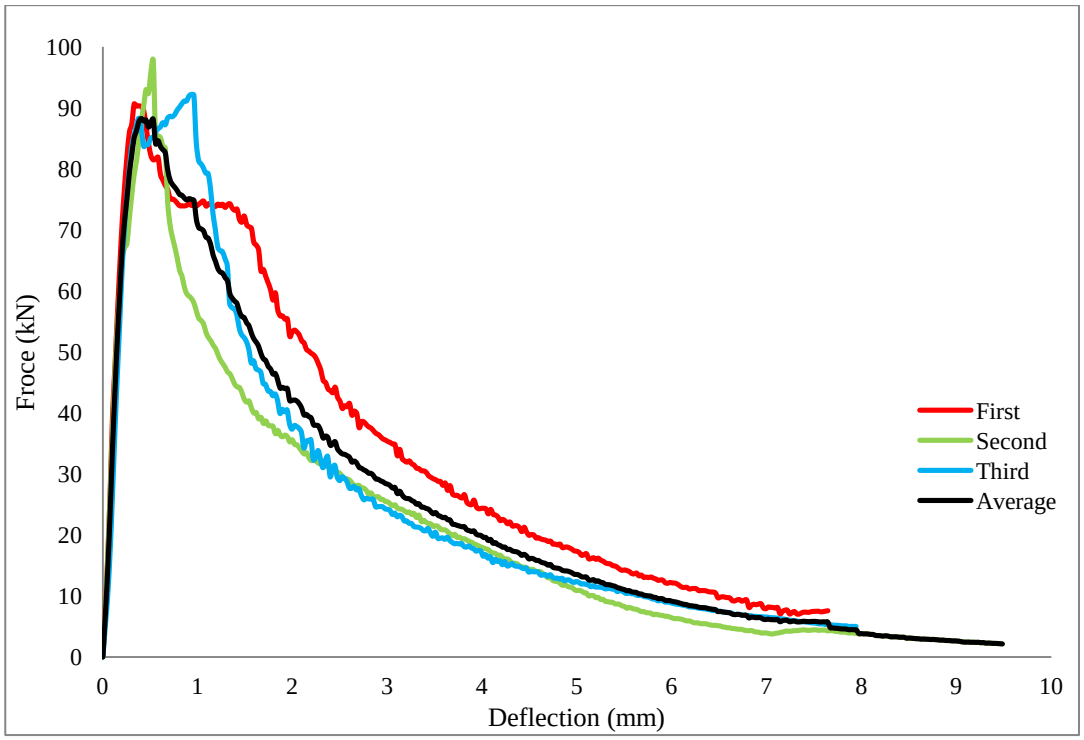

Figure 6.19: Punching shear load versus vertical deflection for specimens with a punching shear perimeter distance equal to 1.87d (162 mm notch perimeter).

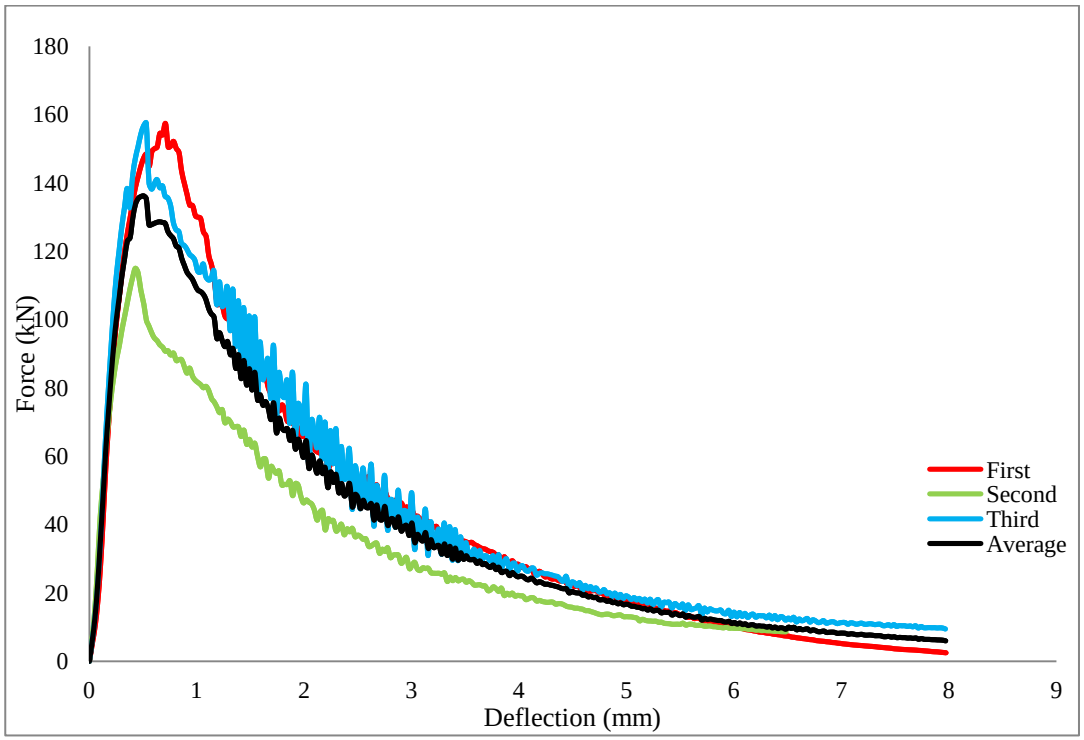

Figure 6.20: Punching shear load versus vertical deflection for specimens with a punching shear perimeter distance equal to 2.15d (179 mm notch perimeter).

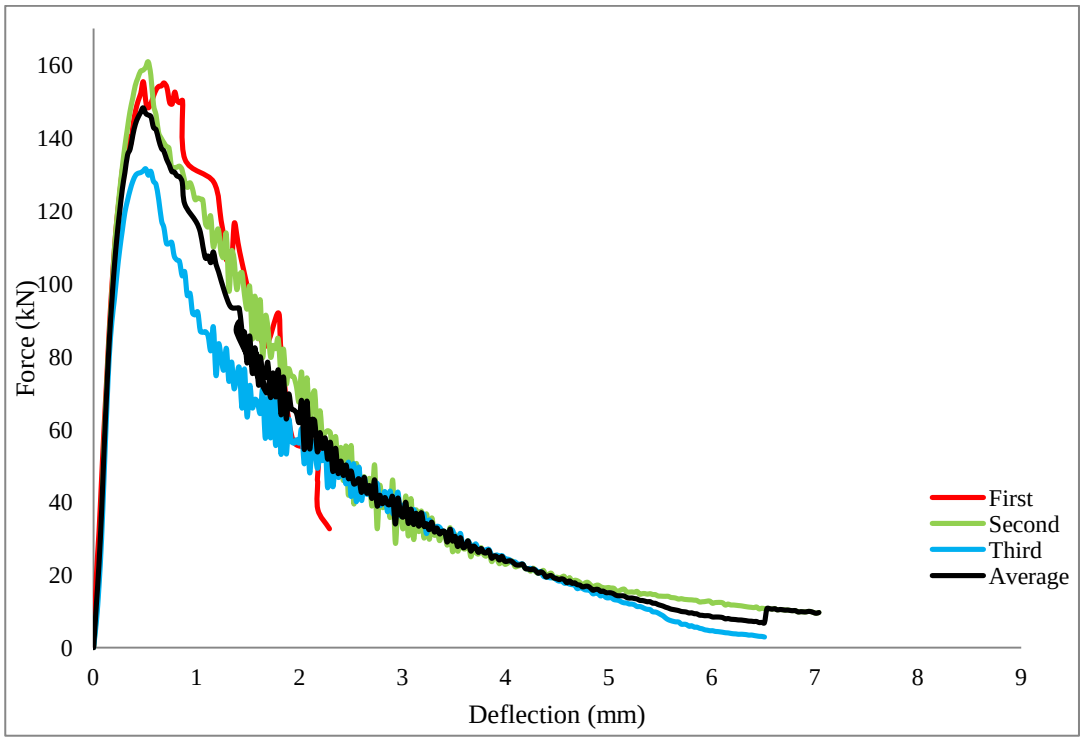

Figure 6.21: Punching shear load versus vertical deflection for specimens with a punching shear perimeter distance equal to 2.40d (194 mm notch perimeter).

The load-deflection curves presented in Figure 6.16 to 6.21 shows ductile failure for all the tested specimens and total failure did not happen suddenly. This is in contrast to typical punching shear failure reported for normal concrete (Neville 2012). However, to ensure the results obtained here were actually punching shear failure, the failed specimens were examined individually. In Figures 6.22 and 6.23, the failure mechanism of some of the tested specimens is shown. In both figures, the truncated cone failure shaped for all the different specimens is very similar to a typical punching shear failure that has been demonstrated in the literature for concrete (BS EN 1992-1-1 2004). Furthermore, the stub punching of the load indenter for all the tests and the crack pattern at the loaded face over a small area with a diameter almost the same of the loading indenter are a clear indication of typical punching shear failure. From both figures, it is evident that punching shear failure had occurred with no signs of flexural failure.

Figure 6.22: Typical failure on the loading side.

Figure 6.23: Typical punching shear failure mode for: (a) 1.62d, and (b) 1.87d.

Figure 6.24 illustrates the relationship between the punching shear angle and punching shear load of the concrete. This figure demonstrates that the ultimate punching shear load generally increases with greater punching shear angle with the exception of two test results. This is understandable because the greater the angle of shearing, the greater the proportion of the force that is resisted by shear strength as opposed to tensile strength. This behaviour is known as shear support enhancement, in which the punching shear capacity of the concrete increases proportionally with the increase of the punching shear angle due to extra enhancement form the compression struts of the concrete. However,

punching shear loads for specimens with punching shear angles of 24.9^{o} and 22.6^{o} increased adversely. There were no reasonable explanation for these test results, except, it was believed to be due to the shear notches being outside the basic control perimeters (26.6^{o} is specified in Eurocode 2 for normal concrete). Results from both tests are outsiders and do not comply with the explanation that has been provided for punching shear analyses in recognised standards, i.e. EC2. As expected, the punching shear load is the smallest at a basic control perimeter of approximately 2d.

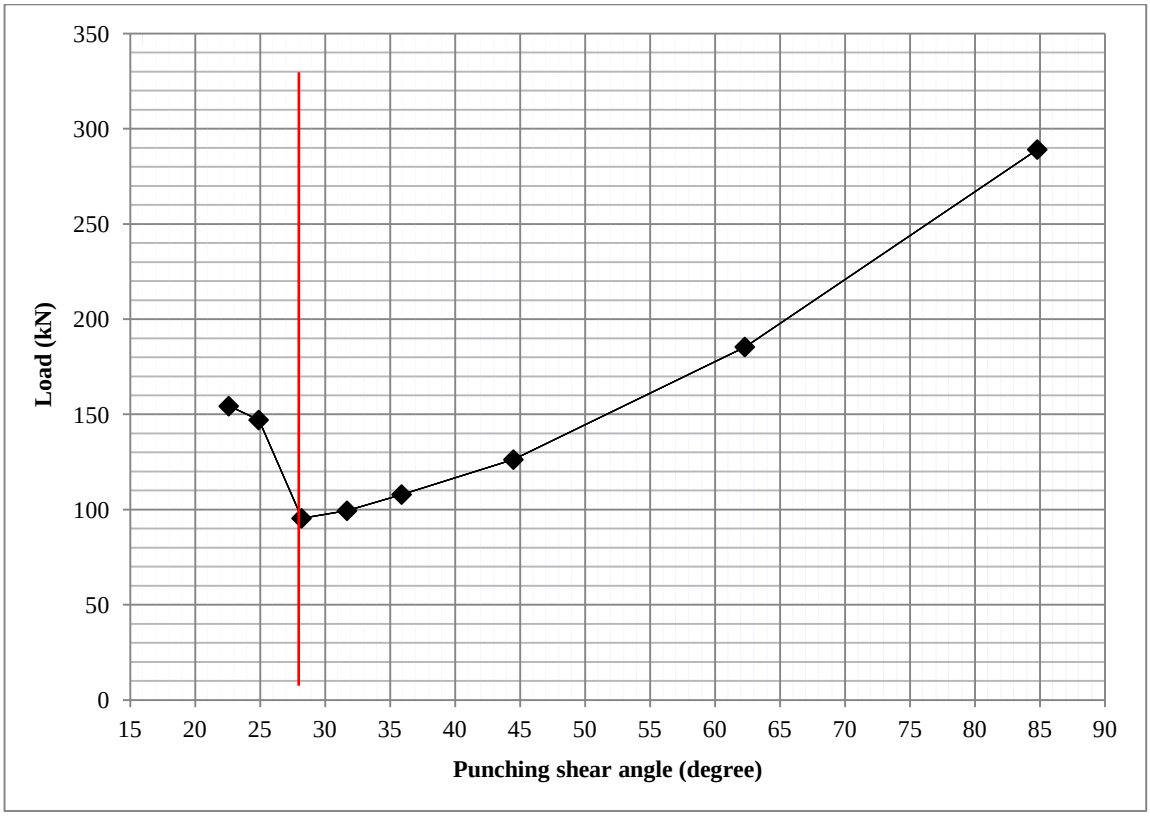

Figure 6.24: Punching shear angle versus punching shear load.

A number of empirical equations to predict the punching shear capacity for SFRC and UHPFRC members were found in the literature, see Equations 6.1 to 6.4 (Narayanan and Darwish 1987, Shaaban and Gesund 1994, Harajli et al. 1995, ACI Committee 318 2011, Higashiyama et al. 2011). The validity of these equations has been investigated by different studies (Harris 2004, Joh et al. 2008, Maya et al. 2012, Nguyen-Minh et al. 2011). So far, none of these equations were capable of predicting experimental slab test results for UHPFRC with sufficient precision. Each of these equations requires different

parameters for the determination of punching shear strength of the concrete ranging from the compressive strength, tensile strength, load-rotation curve, type and volume of fibre in the concrete to shear span to depth ratio of the slab. However, the main parameters studied here were the relationship between the punching shear loads against various punching shear angles and mode of failure. So far, none of the models have considered these parameters specifically for UHPFRC. Therefore, validity of the equations could not be verified against the test results obtained here.

6.7 Summary

Studying the punching shear capacity of UHPFRC has been the subject of a number of studies in the literature. However, difficulties in determining this parameter were reported due to the occurrence of flexural failure prior to punching shear during testing. Therefore, in this study, an extensive experimental programme was carried out to develop a suitable test method to study the punching shear strength of UHPFRC slab specimens with minimal flexural influence. After a detailed study, a test method was designed and used successfully to study the punching shear strength of the concrete using notched slab specimens. The proposed test method incorporated a predefined shear notch in the slab specimens and used circular steel rings for boundary conditions. The shear notches and supporting arrangement resulted in punching shear failure of the specimens during testing with little or no flexural influence.

Results obtained in this study were used to investigate the relationship between punching shear load and angle, failure mode, failure behaviour and the value of the basic control perimeter of UIHPFRC slab specimens under a high concentrated load. From the results, the ultimate punching shear load was found to increase with greater punching shear angle. This behaviour is known as shear support enhancement, in which the punching shear capacity of the concrete increases proportionally with the increase of the punching shear angle due to extra enhancement form the compression struts of the concrete. .. Furthermore, the punching shear load was found to be the smallest at a punching shear angle of 28.2^{o} (basic control perimeter of approximately 2d). This is in close agreement to what has been reported for normal concrete (BS EN 1992-1-1 2004). Furthermore, form the examination of the failure modes of the tests, all the slabs had failed with a

truncated cone shaped in the tensile side and a stub punching in the loaded side due to the load indenter. This failure mode is similar to the typical punching shear failure reported for normal concrete (Mosley et al. 2007), and validates the accuracy of the test method developed in here.

The failure behaviour for UHPFRC slab specimens with punching shear angles equal and greater than 62^o (basic control perimeter of 0.53d and smaller) were reported brittle, similar to a typical punching shear failure behaviour for normal concrete. However, the failure behaviour changed to a ductile mode for specimens with punching shear angles equal and smaller than 45^o (basic control perimeter of 1.02 and greater), similar to the flexural beam failure tests reported in Section 5.6.2.2. The improved ductility of these tests resulted from the fibre bridging effect along the shear planes in the concrete. As a result, the slab specimens could undergo greater deflection after the maximum load was attained. Such behaviour is a preferred failure mechanism for slabs in concrete designs. The results, so far, indicates that all the specimens failed in punching shear.

The findings reported here on the ductile behaviour of punching shear failure of UHPFRC slabs with no shear reinforcement are significant. The results illustrate a reduction of the basic control perimeter for UHPFRC slabs by half compared to what has been specified in EC2 for conventional concrete. This improved ductility of the concrete in punching shear with its high tensile strength can be exploited to limit shear reinforcement in UHPFRC slab members to 1d when required. This behaviour is beneficial in the design of structures where punching shear failure is imminent and the option of heavy shear reinforcement is limited in the member such as thin UHPFRC highway bridge decks.

In the literature, a number of empirical questions have been proposed to predict the punching shear capacity of UHPFRC. However, these equations could not be verified here since the parameters investigated in this study were not considered in the equations. This study has shown that for any models to be used in structural design for predicting the punching shear capacity of UHPFRC slabs, the crack fibre bridging effect and the

basic control perimeter (the angle of punching shear) are vital parameters that have to be considered.

The experimental investigation undertaken in this research programme provides significant insight into the punching shear capacity of UHPFRC slabs. The results illustrate some of the advantages of using UHPFRC compared to normal concrete in highway bridge designs such as improvement in ductility, the ability of undergo significant deflection after peak strength and reduction of the basic control perimeter by half.

Chapter VII: Finite Element Modelling for UHPFRC

7.1 Introduction

The structural behaviour of concrete members and structures has been the subject of intensive investigations for many years. A large number of experimental investigations have been carried out and used to develop many conventional design methods. However, challenges in designing structures using non-conventional concrete, such as UHPFRC, still exist. This has prompted structural analysts to seek alternative methods for fast and cost effective structural analysis methods such as the Finite Element Analysis (FEA). The FEA is a powerful and generic versatile tool that can be applied to analyse structures with arbitrary shape, supports and applied loads. Such generality does not exist in classical analytical methods, even when the structural geometry is simple. The FEA for concrete allows analyses to be run and optimised before the final structure is build or even designed. It can also be used to facilitate parametric studies and minimise physical testing. Therefore, in this study, FE modelling was adopted to investigate the structural response of UHPFRC members in flexure and shear.

This chapter presents the FE theory and methods used to numerically model the linear and nonlinear response of UHPFRC beams and slabs under static loading condition. Two different models (concrete smeared cracking (CSC) and concrete damaged plasticity (CDP)) have been developed based on plasticity and damaged theories for normal concrete (Abaqus theory manual 2010). The applicability of both models was investigated in this study for the application of UHPFRC by simulating various structural behaviour of the concrete. The predictions obtained from both models were verified against experimental investigations reported in Chapters 4, 5 and 6. This allowed the examination of the accuracy and limitations of both numerical models for the concrete. The FE analyses were carried out using the well known commercial FE software, Abaqus (Abaqus theory manual 2010). It is noted that there are a number of FE packages that could be used to carry out the FE modelling. However, in this study, Abaqus was found to be the most suitable one.

7.2 Abaqus

The Abaqus finite element program was originally released in 1978 by Hibbitt, Karlsson & Sorenson Inc. of Rhode Island. The program is popular with academic and research institutions due to the extensive material modelling capability and its ability to solve nonlinear problems. The Abaqus finite element system is available in a few versions: these are Abaqus/Standard, Abaqus/Explicit, Abaqus/CFD and Abaqus/CAE.

Abaqus/Standard is a general-purpose finite element program for static analysis. This solver uses a traditional implicit integration method to solve finite element analysis. It is mainly used to model linear and nonlinear engineering problems. Abaqus/CAE is mainly used for interactive pre-processing and post-processing environment. The other versions of Abaqus are irrelevant to this study; hence, their applications are not discussed.

In this study, Abaqus/Standard & CAE (implicit) were used together to create, run, solve and post-process a number of UHPFRC models. Simplified 3D, 2D and axisymmetric simulations were carried out to predict linear and nonlinear structural responses of UHPFRC members in flexure and shear. The structural response of the concrete was modelled using the constitutive material model presented in Section 3.6.3 of this thesis. The limitations of both models and implications of the material behaviour of the concrete are discussed. The following section presents the theory and constitutive models used for the FE analysis.

7.2.1 Elasticity

Generally, most materials with engineering interest, including concrete, initially respond elastically. In engineering, the elastic behaviour refers to the full recovery process of a deformed member when loads are removed.

In Abaqus, the linear elastic material model is defined to be valid for isotropic, orthotropic, or fully anisotropic materials with small elastic strains (normally less that 5%) and can have properties that depend on temperature and/or other field variables

(Abaqus theory manual 2010). The total stress with linear elastic behaviour is determined from its total strain using Equation 7.1.

$$\sigma = E^{el}\varepsilon^{el} \qquad \text{Equation 7.1}$$

where σ =total stress,

E^{el} =the initial modulus of elasticity, and

ε^{el} =total elastic strain.

Form elasticity theory, the linear elasticity for an isotropic case and the stress-strain relationship is given by Equation 7.2.

$$\begin{Bmatrix} \varepsilon_{11} \\ \varepsilon_{22} \\ \varepsilon_{33} \\ \gamma_{12} \\ \gamma_{13} \\ \gamma_{23} \end{Bmatrix} = \begin{bmatrix} 1/E & -\upsilon/E & -\upsilon/E & 0 & 0 & 0 \\ -\nu/E & 1/E & -\upsilon/E & 0 & 0 & 0 \\ -\nu/E & -\nu/E & 1/E & 0 & 0 & 0 \\ 0 & 0 & 0 & 1/G & 0 & 0 \\ 0 & 0 & 0 & 0 & 1/G & 0 \\ 0 & 0 & 0 & 0 & 0 & 1/G \end{bmatrix} \begin{Bmatrix} \sigma_{11} \\ \sigma_{22} \\ \sigma_{33} \\ \sigma_{12} \\ \sigma_{13} \\ \sigma_{23} \end{Bmatrix} \qquad \text{Equation 7.2}$$

The shear modulus, G , is also expressed in Equation 7.3.

$$G = E/2(1+\nu) \qquad \text{Equation 7.3}$$

where E =modulus of elasticity, and

ν = Poisson's ratio

In this study, the elastic behaviour of the concrete was modelled as an isotropic and temperature independent material. The elastic properties of the concrete were defined from the values of, E & ν , determined experimentally in Chapter 4. The values of the elastic material properties used in the modelling are listed in Table 7.1.

7.2.2 Plasticity

Plasticity refers to permanent deformation of a member after loads are removed. This is due to the load exceeding the yield point and causing permanent deformation. The plasticity behaviour of any solid can be explained either from translation of its physical reality or mathematical models to approximate the behaviour of the medium under certain circumstances. In FE analysis, plasticity is a good tool for describing ductile material behaviour such as UHPFRC; it can also be used for brittle material behaviour such as concrete. It has been generally acknowledged that plasticity theory can be used as an approximation to predict the structural behaviour of normal concrete (Abaqus theory manual 2010).

In Abaqus, three material models are available for describing the plasticity (nonlinear) behaviour of normal concrete. The models are concrete smeared cracking, concrete damaged plasticity, and brittle cracking. These models are designed for plain and reinforced concrete in all types of structures such as beams, trusses, shells, and solids. They provide a general capability for modelling concrete members in tensile cracking and compressive crushing. The theory of each model and their applicability for UHPFRC are presented and discussed in the following sections.

7.1.1.1 Concrete smeared cracking model (CSC)

The concrete smeared cracking model is used in Abaqus/Standard. This model is intended for concrete applications subjected to essentially monotonic (non cyclic) straining at confined pressure. It provides a general capability for modelling concrete in all types of structures, including beams, trusses, shells, and solids. It is primarily designed for the analysis of reinforced concrete structures in which reinforcement is easily modelled. It can also be used for plain concrete.

The CSC model consists of an isotropically hardening yield surface that actives when stress is dominantly compressive and an independent “crack detection surface” detects if a point fails by cracking in the model (Abaqus theory manual 2010). Cracking and post-cracking anisotropic behaviour dominates this model and is assumed to be important. This model uses oriented damaged elasticity concepts (smeared cracking) to describe the

reversible part of the material's response after cracking failure. This means that the model does not track individual “macro” cracks. However, constitutive calculations are performed independently at each integration point of the finite element model. The presence of cracks enters into the calculations, which affect the stress and material stiffness associated with the integration point.

In this model, the linear elastic material behaviour is required to define the elastic properties of the concrete. This includes the values of modulus of elasticity and Poisson’s ratio. For post-failure behaviour, tension stiffening (softening) and compression hardening are required to predict tensile cracking and compressive crushing, respectively.

For tension stiffening, Abaqus proposes two different relationships to allow the cracked concrete behaviour to be modelled. These are stress-strain and fracture energy cracking criteria, as shown in Figures 7.1 and 7.2, respectively.

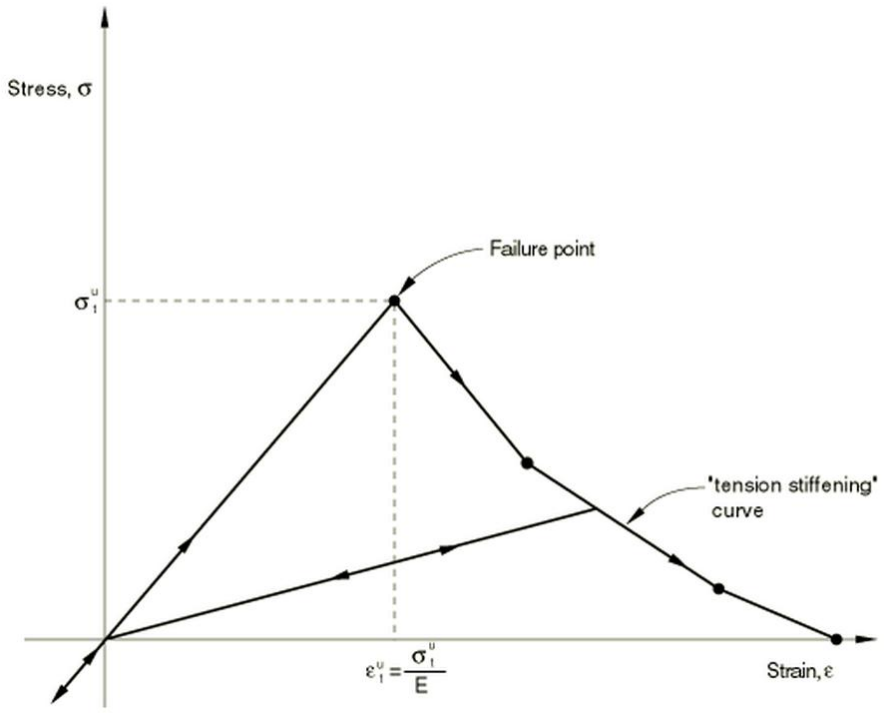

Figure 7.1: Tension stiffening model, stress-strain approach (Abaqus theory manual 2010).

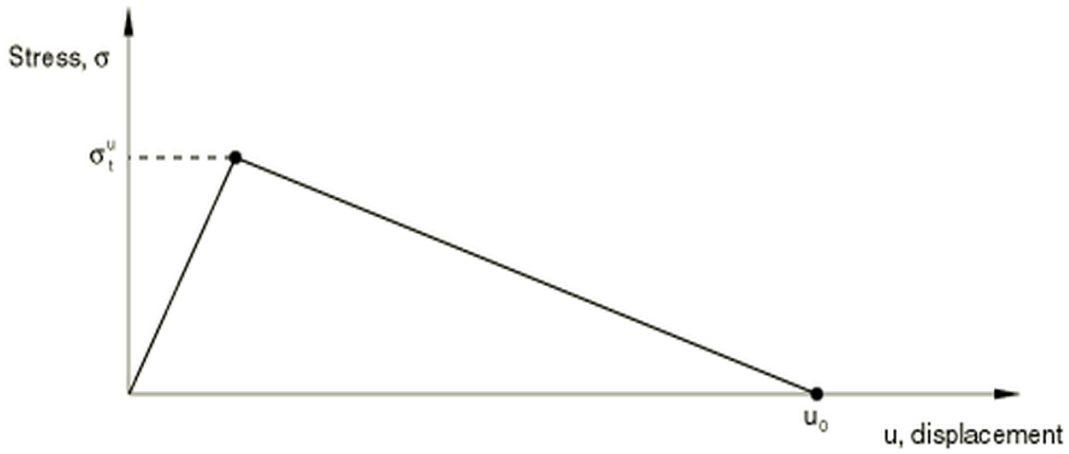

Figure 7.2: Tension stiffening model, stress-displacement approach (Abaqus theory manual 2010).

The stress-strain relationship in Figure 7.1, is assumed to be linear elastic up to the ultimate tensile strength, σ_t^u, and changes to strain softening after the peak strength of the concrete is reached. The post-failure stress is specified as a function of strain across the cracked area of the concrete. In this model, the cracking strain, ε_t^u, and the post-failure stress are both required to simulate the post-peak behaviour of the concrete. The strain softening approach is reported to be efficient for concrete structures with heavy reinforcement when cracks are evenly distributed. However, with little or no reinforcement in the concrete, this approach could result in mesh dependency and convergence problems (Abaqus theory manual 2010). This requires mesh refinement and lead to narrow crack bands which can cause instability in the analysis. Therefore, Abaqus manual recommends the behaviour presented in Figure 7.2, in which tension stiffening is defined in a stress-displacement relationship (fracture energy cracking criterion). This approach assumes that under tension, the concrete specimen will crack across some sections and after the cracks is pulled apart; the stress is totally removed at a length which is dependent on the opening of the crack. In another words, it assumes that the tensile stress is linearly removed as any crack opens up and disappears at a characteristic length, u_0, of crack opening. The latter approach to define tension stiffening seems to be more suitable for UHPFRC since the concrete is modelled as plain concrete, i.e. the fibres were not modelled separately.

The relationship for the compression hardening response in this model is presented in Figure 7.3. Similar to the tension stiffening, the compressive behaviour is modelled with an elastic response equal to the initial elastic modulus. At some point along the curve, an increase in stress associated with some non-recoverable straining (inelastic straining) occurs and the material softens with a reduced stiffness. This relationship assumes if the load was removed any time after inelastic straining has occurred, the stiffness of the concrete is damaged and the value is smaller than the initial value.

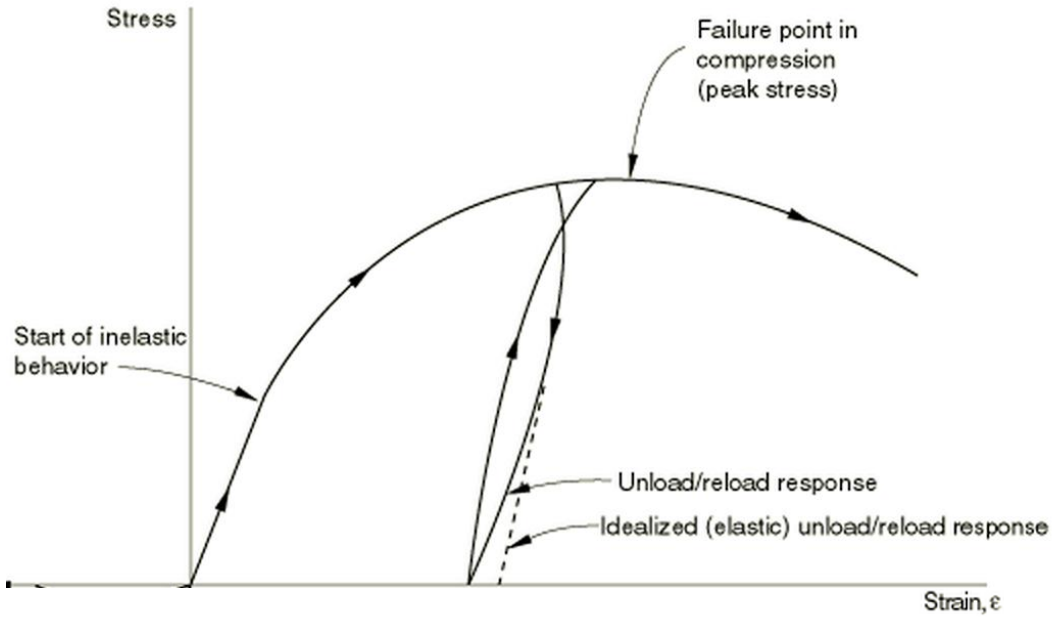

Figure 7.3: Compression hardening model (Abaqus theory manual 2010).

Furthermore, from the existing relationship between uniaxial and multiaxial stress state, this model proposes a failure surface which governs the plastic response of the concrete, see Figure 7.4. The failure surface determines the material behaviour of every integration point in the model depending on the calculated stress value. For any integration point with stress values lying inside the surface perimeter and depending on the position, the material behaviour of the point is calculated. However, when the value lies on or outside the perimeter, failure of the material has occurred and the ultimate strength of the material is reached.

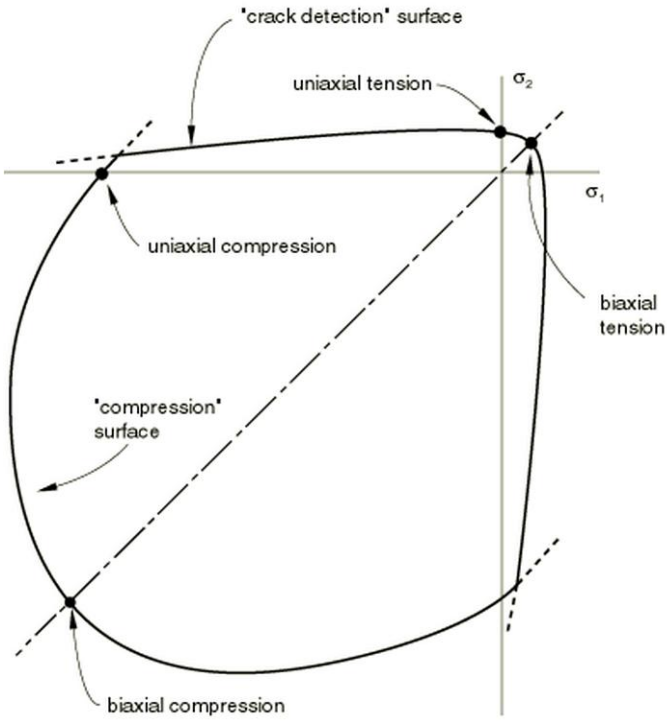

Figure 7.4: Yield and failure surfaces in plane stress (Abaqus theory manual 2010).

From the theory presented above, it is evident that a number of parameters are required for this model; these are the density, modulus of elasticity, Poisson's ratio, compression hardening, and tension stiffening. All these parameters were determined from the direct tests presented in Chapters 3 and 4, see Section 3.6.3.

In addition, the CSC model requires some other parameters: the failure ratio and shear retention values. According to the model, the failure ratio defines the shape of the failure surface of the model and consists of four different parameters, these are:

- The ratio of the ultimate biaxial compressive stress to the ultimate uniaxial compressive stress, the default value is set as 1.16.
- The absolute value of the ratio of the uniaxial tensile stress at failure to the ultimate uniaxial compressive stress, the default value is set as 0.09.
- The ratio of the magnitude of a principal component of plastic strain at ultimate stress in biaxial compression to the plastic strain at ultimate stress in uniaxial compression, the default value is set as 1.28, and

- The ratio of the tensile principal stress at cracking in plane stress, when the other principal stress is at the ultimate compressive value to the tensile cracking stress under uniaxial tension, the default value is set as 0.33.

In this model, only the ratio of the uniaxial tensile stress to the ultimate uniaxial compressive stress at failure was modified to 0.056, based on available test results conducted previously. The other three ratios were kept as recommended for normal concrete.

For shear retention, the model assumes shear stiffness diminishes as the concrete cracks. In the model, the shear modulus reduction is specified as a function of the opening strain across the crack or even for closed cracks. The elastic shear modulus, G, is determined from Equation 7.3. The CSC defines shear modulus of cracks as ρG, where ρ is a multiplying factor. The shear retention model assumes that the shear stiffness of open cracks reduces linearly to zero as the crack opening increases. The relationship is described in Figure 7.5 and Equations 7.4 and 7.5.

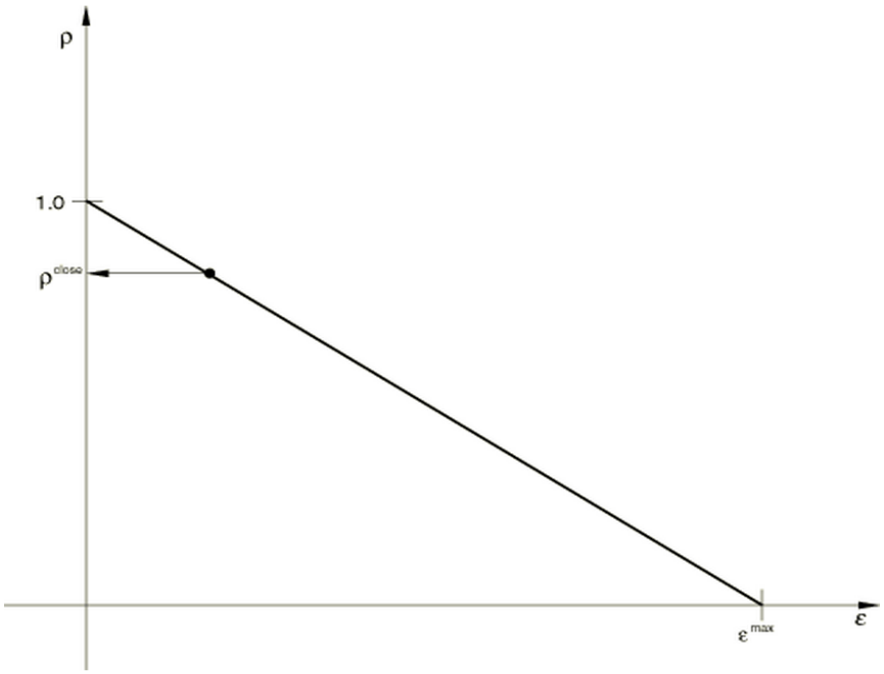

Figure 7.5: Shear retention relationship.

$$\rho = (1 - \varepsilon^{max} / \varepsilon) \quad \text{when } \varepsilon < \varepsilon^{max} \qquad \text{Equation 7.4}$$

$$\rho = 0 \quad \text{when } \varepsilon \geq \varepsilon^{max} \qquad \text{Equation 7.5}$$

where ε =direct strain across the crack, and

ε^{max} =user-specified value.

In addition, the model assumes that cracks which subsequently closes, have a reduced shear modulus and these are described in Equation 7.6.

$$\rho = \rho^{close} \quad \text{when } \varepsilon < 0 \qquad \text{Equation 7.6}$$

where ρ^{close} & ε^{max} can be defined with an optional dependency on temperature and/or predefined field variables.

Despite the theory presented for shear retention parameters, the model assumes that the shear response is unaffected by cracking and default values are automatically activated. This assumption is often used and reported to be reasonable by Abaqus. This is because the overall response of the model is not significantly dependent on the amount of shear retention.

Based on the theory provided on this model, the CSC appears to be suitable for UHPFRC since the strain hardening and softening behaviour is taken into account in both compression and tension. Therefore, this model was used to simulate the structural behaviour of UHPFRC in this study. The material properties used in the model are presented in Tables 7.1 and 7.2. Furthermore, a detailed description of the theoretical background of this model can be found in the following references (Kupfer and Gerstle 1973, Hillerborg et al. 1976, Crisfield 1986, Abaqus theory manual 2010).

7.1.1.2 Concrete damaged plasticity model (CDP)

The concrete damaged plasticity model is used in both Abaqus/Standard and Abaqus/Explicit. This model provides a general capability for modelling concrete and other quasi-brittle materials in all types of structures such as beams, trusses, shells, and

solids. The CDP model is designed for applications in which concrete is subjected to monotonic, cyclic, and/or dynamic loading under low confining pressures. This model uses the concepts of isotropic damaged elasticity in combination with isotropic tensile and compressive plasticity to represent the inelastic behaviour of concrete. The degradation of the elastic stiffness induced by plastic straining in both tension and compression is taken into consideration and accounts for stiffness recovery effects under cyclic loading.

The material properties to define the elastic and post-elastic behaviour are very similar to those reported for the CSC model. The linear elastic material behaviour is defined from the values of elastic modulus and Poisson's ratio. For post-failure behaviour, tension stiffening (softening) and compression hardening are defined to predict tensile cracking and compressive crushing of the concrete, respectively.

For tension stiffening, three different methods are proposed to model the behaviour of the cracked concrete. These are post-failure stress-strain, post-failure stress-displacement and post-failure stress-fracture energy relationships, as shown in Figures 7.6, 7.7 and 7.8, respectively.

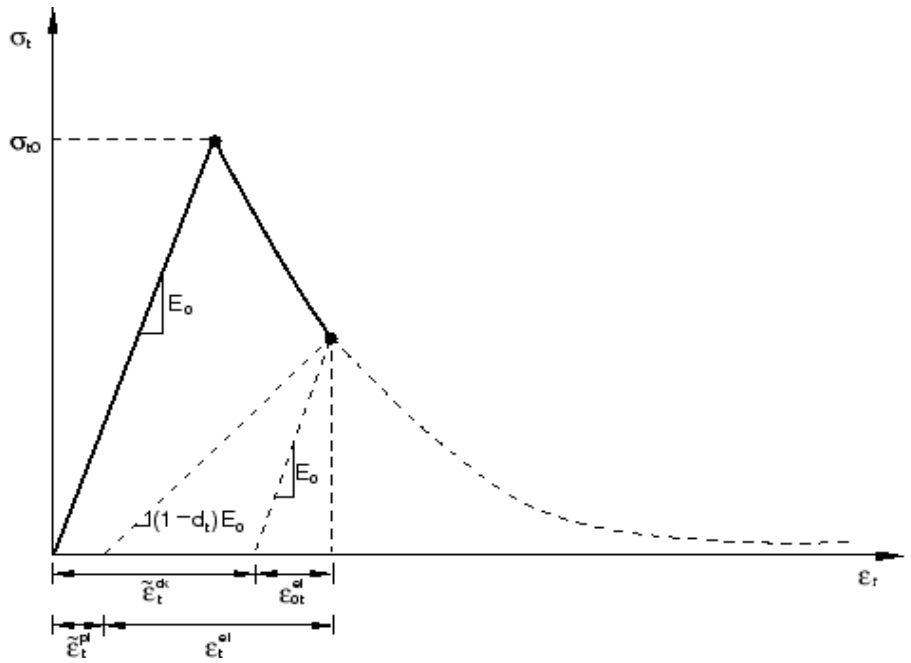

Figure 7.6: Tension stiffening model, stress-cracking strain approach (Abaqus theory manual 2010).

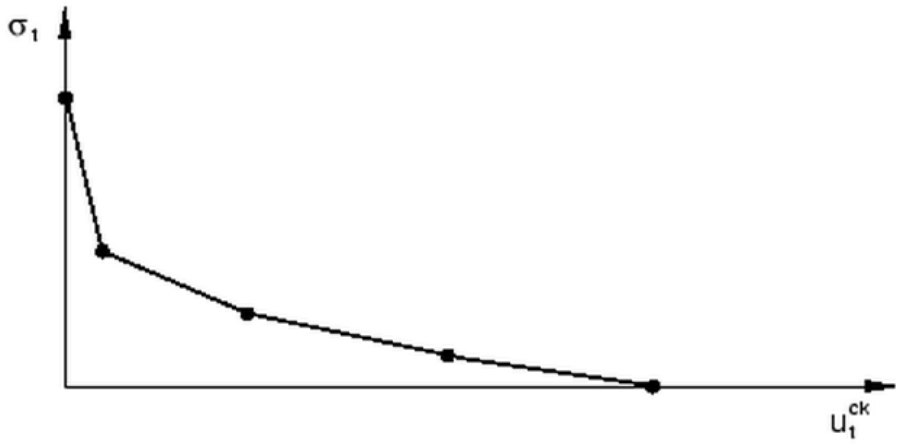

Figure 7.7: Tension stiffening model, stress-displacement approach (Abaqus theory manual 2010).

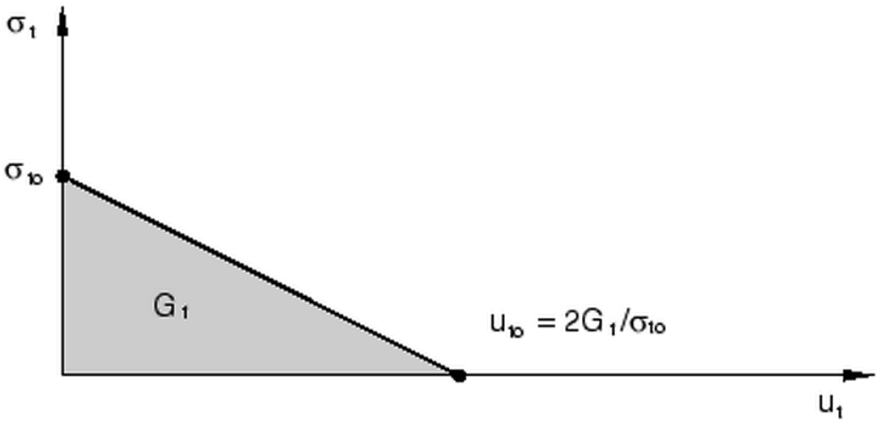

Figure 7.8: Tension stiffening model, stress-fracture energy approach (Abaqus theory manual 2010).

The relationship shown in Figure 7.6 is very similar to the one proposed for the CSC model in Figure 7.1. The stress-strain relationship is defined to be linear elastic until the value of failure tensile stress, σ_{t0}, is reached. The failure stress corresponds to the onset of microcracking in the concrete. The post-failure behaviour is given as a function of cracking tensile strain, $\tilde{\varepsilon}_t^{ck}$. The formations of microcracks are represented macroscopically with a softening stress-cracking strain response. The cracking strain is defined as the total tensile strain, ε_t, minus the tensile elastic strain, ε_{0t}^{el}, corresponding to undamaged material and described in Equations 7.7 and 7.8.

$$\tilde{\varepsilon}_t^{ck} = \varepsilon_t - \varepsilon_{0t}^{el} \quad \text{Equation 7.7}$$

$$\varepsilon_{0t}^{el} = \frac{\sigma_t}{E_0} \quad \text{Equation 7.8}$$

where $\tilde{\varepsilon}_t^{ck}$ = cracking tensile strain,

ε_t = total tensile strain,

ε_{0t}^{el} = elastic tensile strain,

σ_t = tensile stress, and

E_0 = initial modulus of elasticity.

Furthermore, when the concrete specimen is unloaded from any point on the strain stiffening branch, the model assumes that the elastic stiffness of the material is either damaged or degraded. The degradation of the elastic stiffness, E, and the tensile degradation variable, d_t, are characterized in the model in Equations 7.9 and 7.10, respectively.

$$d_t = 1 - \frac{\sigma_t}{\bar{\sigma}_t} \quad \text{Equation 7.9}$$

$$E = (1 - d_t)E_0 \quad \text{Equation 7.10}$$

where $0 \le d_t \le 1$

E = degraded elastic stiffness value,

d_t = tensile degradation variable, and

$\bar{\sigma}_t$ = effective tensile stress.

The damage variable takes the values from zero (representing the undamaged material) to one (representing the total loss of strength). The degradation parameter is defined from experimental test data from uniaxial tensile tests using Equation 7.9. The tension stiffening data in this model is provided in terms of cracking tensile strain, $\tilde{\varepsilon}_t^{ck}$. However, Abaqus converts the cracking strain values to plastic strain using the relationship in Equation 7.11.

$$\tilde{\varepsilon}_t^{pl} = \tilde{\varepsilon}_t^{ck} - \frac{d_t}{(1-d_t)}\frac{\sigma_t}{E_o}$$ Equation 7.11

The damage state in tension, using the stress-strain approach, is characterised based on Equation 7.11. Evolution of the yield surface and microcracking in the concrete is controlled by this variable. Once the values of plastic strain are negative or decreasing, Abaqus will run an error message and terminates the analysis. This indicates that the tensile damage curve provided in the input data is incorrect. Furthermore, in the absence of damage degradation in the model, the plastic strain values are assumed to be equal to the cracking strain.

Similar to the CSC model, the tensile stress-strain approach in the CDP model is efficient for concrete structures with heavy reinforcement when cracks are evenly distributed. However, with little or no reinforcement in the concrete, this approach could result in mesh sensitivity and convergence problems. This may lead to mesh refinement and lead to narrow crack bands which can cause instability in the analysis. Therefore, Abaqus recommends that the tension stiffening behaviour should be represented in terms of either the stress-displacement or the stress-fracture energy responses for modelling concrete members with no or very little reinforcement.

Figure 7.7 shows the stress-displacement response, which is very similar to the method described in CSC model except more than one value for the displacement is required here. The stress-cracking displacement response in Figure 7.7 is determined using Equation 7.12.

$$u_t^{ck} = u_1 - u_{0t}^{el}$$ Equation 7.12

where u_t^{ck} = cracking displacement,

u_1 = total displacement, and

u_{0t}^{el} = displacement at elastic strain.

The advantages of using the stress-displacement approach in this model are the same as those reported for the CSC model. Alternatively, the fracture energy value can be specified directly as a material property for the tension stiffening behaviour in the model. The relationship shown in Figure 7.8 is converted from the area under a stress–displacement response. This is based on the definition of fracture energy for concrete which assumes a linear loss of strength after cracking. The cracking displacement at which complete loss of strength takes place is determined using Equation 7.13.

$$u_{t0} = \frac{2G_f}{\sigma_{t0}} \qquad \text{Equation 7.13}$$

where u_{t0} = cracking displacement at loss of strength,

G_f = fracture energy, and

σ_{t0} = failure tensile stress.

Abaqus recommends some typical values of, G_f, for different types of concrete ranging from low to high compressive strength. However, UHPFRC is not included. It is evident that the material response varies between the two forms of tension stiffening presented in Figures 7.7 and 7.8 for the same material and either method could be used. The former method appears to be more suitable for UHPFRC, since the post-peak failure response of the material model is similar to the tension softening behaviour of the UHPFRC. Therefore, the presented FE results for CDP model in this study are based on the stress-displacement response as shown in Figure 7.7.

Similar to the stress-strain method in tension stiffening, damage degradation requires for the stress-displacement approaches in CDP model. This is based on the same principle described in Equations 7.9 and 7.10, except displacement values are used instead of strains. The tensile cracking displacement, u_t^{ck}, values are converted to plastic displacement, u_t^{pl} to simulate the post-failure behaviour using the relationship in Equation 7.14.

$$u_t^{pl} = u_t^{ck} - \frac{d_t}{(1-d_t)}\frac{\sigma_t}{E_o}$$ Equation 7.14

where u_t^{pl} = cracking displacement at failure, and

l_0 = the specimen length is assumed to be one unit length and equal to1.

For compressive behaviour, the response is similar to the one defined for CSC model. The behaviour is assumed to be linear until the formation of the first crack. The post-cracking response is modelled by stress hardening up until the maximum compressive strength, σ_{cu}, and this is followed by compressive strain softening as shown in Figure 7.9.

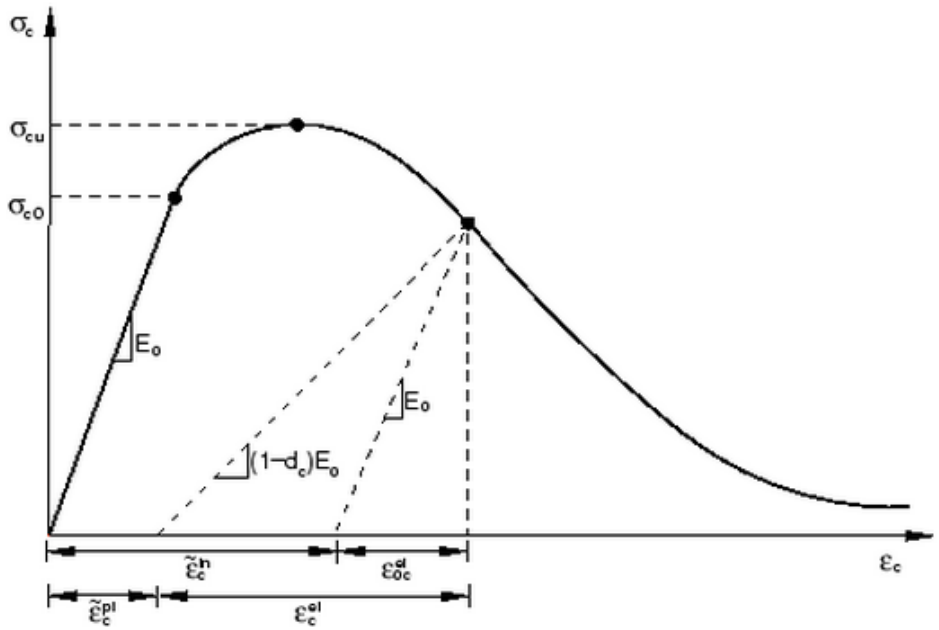

Figure 7.9: Compression hardening model (Abaqus theory manual 2010)

Unlike the tensile behaviour, the hardening response for compressive behaviour is given in terms of compressive inelastic strain, $\tilde{\varepsilon}_c^{in}$, instead of compressive plastic strain, $\tilde{\varepsilon}_c^{pl}$. The inelastic compressive strain is determined from total compressive strain, ε_c, and the elastic compressive strain, ε_{0c}^{el}, using Equations 7.13 and 7.14.

$$\tilde{\varepsilon}_c^{in} = \varepsilon_c - \varepsilon_{0c}^{el}$$ Equation 7.15

$$\varepsilon_{0c}^{el} = \frac{\sigma_c}{E_0}$$ Equation 7.16

where $\tilde{\varepsilon}_c^{in}$ = compressive inelastic strain,

ε_c = compressive total strain,

ε_{0c}^{el} = compressive elastic strain, and

σ_c = compressive stress

From Figure 7.9, it can be seen that when the concrete is unloaded from any point beyond the elastic stage, the unloading response represents the weakening behaviour of the concrete. Similarly for the tensile behaviour, the elastic stiffness of the material is assumed to be damaged (or degraded). The degradation of the compressive elastic stiffness is characterized in the model by Equations 7.17 and 7.18.

$$d_c = 1 - \frac{\sigma_c}{\bar{\sigma}_c}$$ Equation 7.17

$$E = (1 - d_c)E_0$$ Equation 7.18

where $0 \le d_c \le 1$

d_c = compressive degradation variable, and

$\bar{\sigma}_c$ = effective compressive stress.

The unloading data in the model is provided in terms of, $d_c - \tilde{\varepsilon}_c^{in}$. However, Abaqus converts the compressive inelastic strain, $\tilde{\varepsilon}_c^{in}$, values to compressive plastic strain, $\tilde{\varepsilon}_c^{pl}$, using the relationship described in Equation 7.19.

$$\tilde{\varepsilon}_c^{pl} = \tilde{\varepsilon}_c^{ck} - \frac{d_c}{(1 - d_c)} \frac{\sigma_c}{E_o}$$ Equation 7.19

where $\tilde{\varepsilon}_c^{pl}$ = compressive plastic strain, and

$\tilde{\varepsilon}_c^{pl} = \tilde{\varepsilon}_c^{in}$ (in the absence of compressive damage).

The stiffness degradation is defined for both tension and compression and these variables are important in the CDP model. However, experimental observation for most quasi-brittle materials, including concrete, reports that the compressive stiffness is recovered upon crack closure as the load changes from tension to compression (Abaqus theory manual 2010). However, the tensile stiffness is not recovered as the load changes from compression to tension once the crushing of microcracks has developed. Therefore, Abaqus reports that the tensile damage degradation variable is more influential than the compressive one. Since the FE simulations completed in this study focuses on the tensile failure behaviours of beam and slab specimens only, the compression damage degradation variable was unused and is therefore not included in the material properties. However, when included, the FE results were not affected. Furthermore, the failure surface which governs the plastic response of the concrete in this model is the same as those reported for CSC model in Figure 7.4.

In addition to the compression and tension characteristic curves and their respective damage parameters, the CDP model also contains a set of parameters to further control the properties of the material model. These parameters are:

- The dilation angle in degrees (φ), the default value is set between 20-40 degrees,
- Flow potential eccentricity (ε), the default value is set as 0.1,
- Ratio of initial equibiaxial compressive yield stress to initial uniaxial compressive yield stress (f_{b0} / f_{co}), the default value is set as 1.16,
- Ratio of the second stress invariant on the tensile meridian to that on the compressive meridian (K), the default value is set as 0.6, and
- A viscosity parameter (μ) that defines visco-plastic regularization and the default value is set as 0 (Chen and Graybeal 2012).

The dilation angle was reported to be important for concrete at high confining pressure and when failure is controlled by compressive crushing. Lower values of this variable in the model were reported to result in brittle failure behaviour, while higher values will result in more ductile failure behaviour. Acceptable values of the dilation angle for

flexural tests were reported to be in range of 20 to 40 degrees for normal concrete (Malm 2009). In this study, the value of the dilation angle was set to be 40 degrees and no significant variation was observed when the value was modified. The other three parameters were set at their default values as recommended for normal concrete.

Based on the theory described above, the CDP model also appears to be suitable for UHPFRC since the strain hardening and softening behaviour of the concrete in both compression and tension are considered. Therefore, the CDP model was also used to simulate the behaviour of the concrete in this study. The material properties used in the model is presented in Tables 7.1 and 7.2. Further theoretical background on this model can be found in the following references (Hillerborg et al. 1976, Lubliner et al. 1989, Lee and Fenves 1998, Abaqus theory manual 2010).

7.1.1.3 Brittle cracking model (BC)

The brittle cracking concrete model is designed for the analysis of reinforced concrete structures such as beams, trusses, shells and solids. This model assumes that the compressive behaviour is insignificant and is always linear elastic. It is designed for applications where behaviour is dominated by tensile brittle cracking such as plain concrete. It can also be used for modelling materials such as ceramics or brittle rocks. The model includes consideration of the anisotropy induced by cracking. The linear elastic properties of the material must be defined to simulate the behaviour of the material prior to cracking. The BC model is used in Abaqus/Explicit.

It is evident the BC model is not suitable for materials with ductile behaviour such as UHPFRC. Therefore, this model was not used for the concrete in this thesis. Furthermore, the model was not used for simulating the behaviour of the UHPC beam specimens reported in Chapter 5. This is because the flexural behaviour of those specimens was believed to have been damaged due to the curing condition. Therefore, no further discussion regarding the theory of this model is included here.

7.4 Finite Element Modelling Procedures

This section presents details of the finite element simulation procedures for modelling the beam and slab specimens cured at 90 ^{o}C temperature. The models were created in Abaqus/Standard versions 6.10-2 and 6.12-3. There are no major differences between both versions of the software. The CSC and CDP models were run for both types of specimens. While the material definition between both models are slightly different as described earlier, other variables in the simulations such as element type, boundary conditions, loading configuration were kept the same for both models for consistency reasons.

7.4.1 Creating the model

Initially, the beam and slab specimens (phase 3) were created using 3D models. However, for computational efficiency reasons, 2D and axisymmetric models were used for the beam and slab specimens, respectively. Results from the 2D and axisymmetric models were compared to those of the 3D models and no significant differences were seen. Figures 7.10 and 7.11, shows the 3D models of a beam and slab specimen against their equivalent 2D and axisymmetric models, respectively.

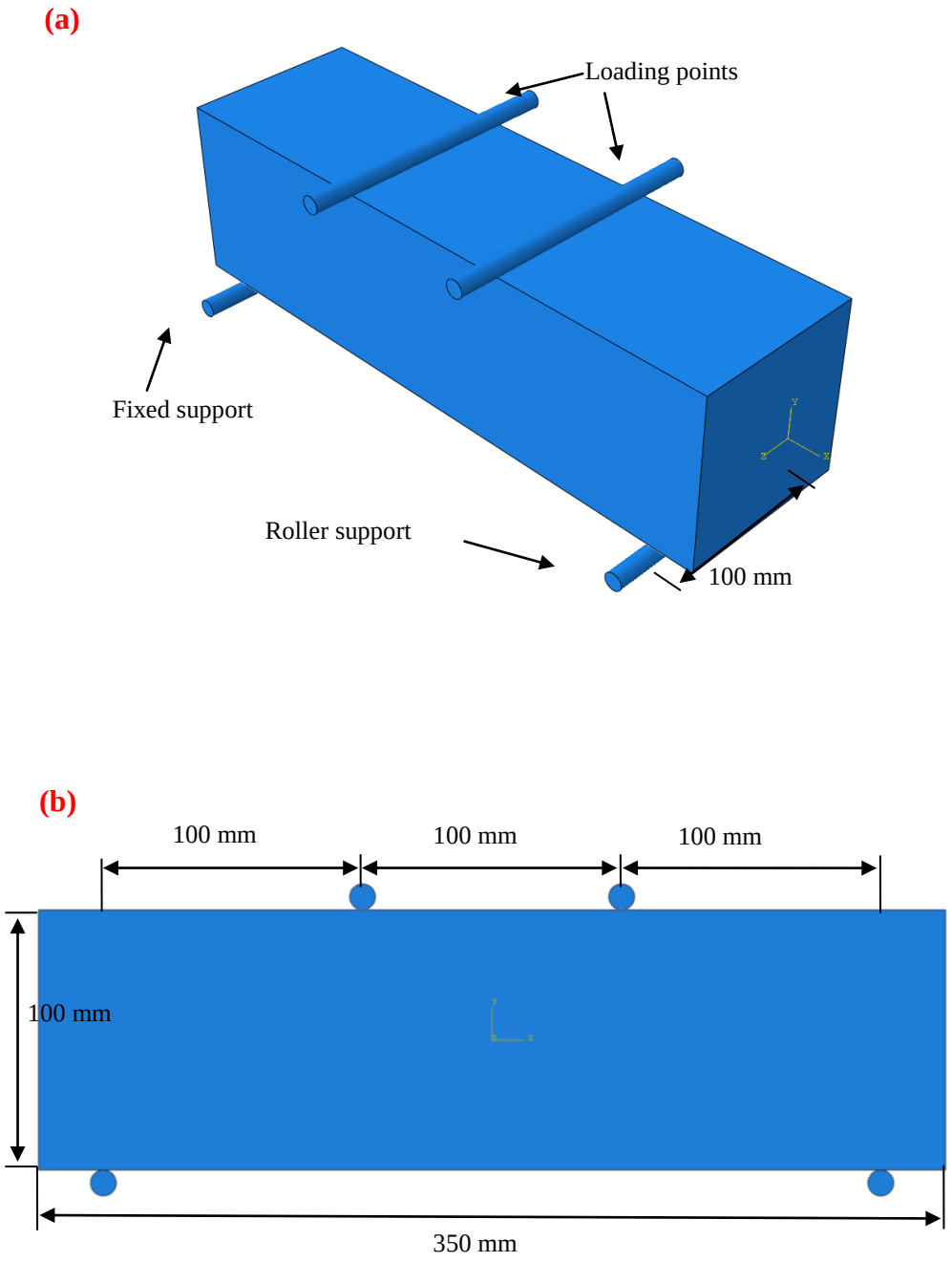

Figure 7.10: Beam specimen of 350 mm length in: (a) 3D model, and (b) 2D model.

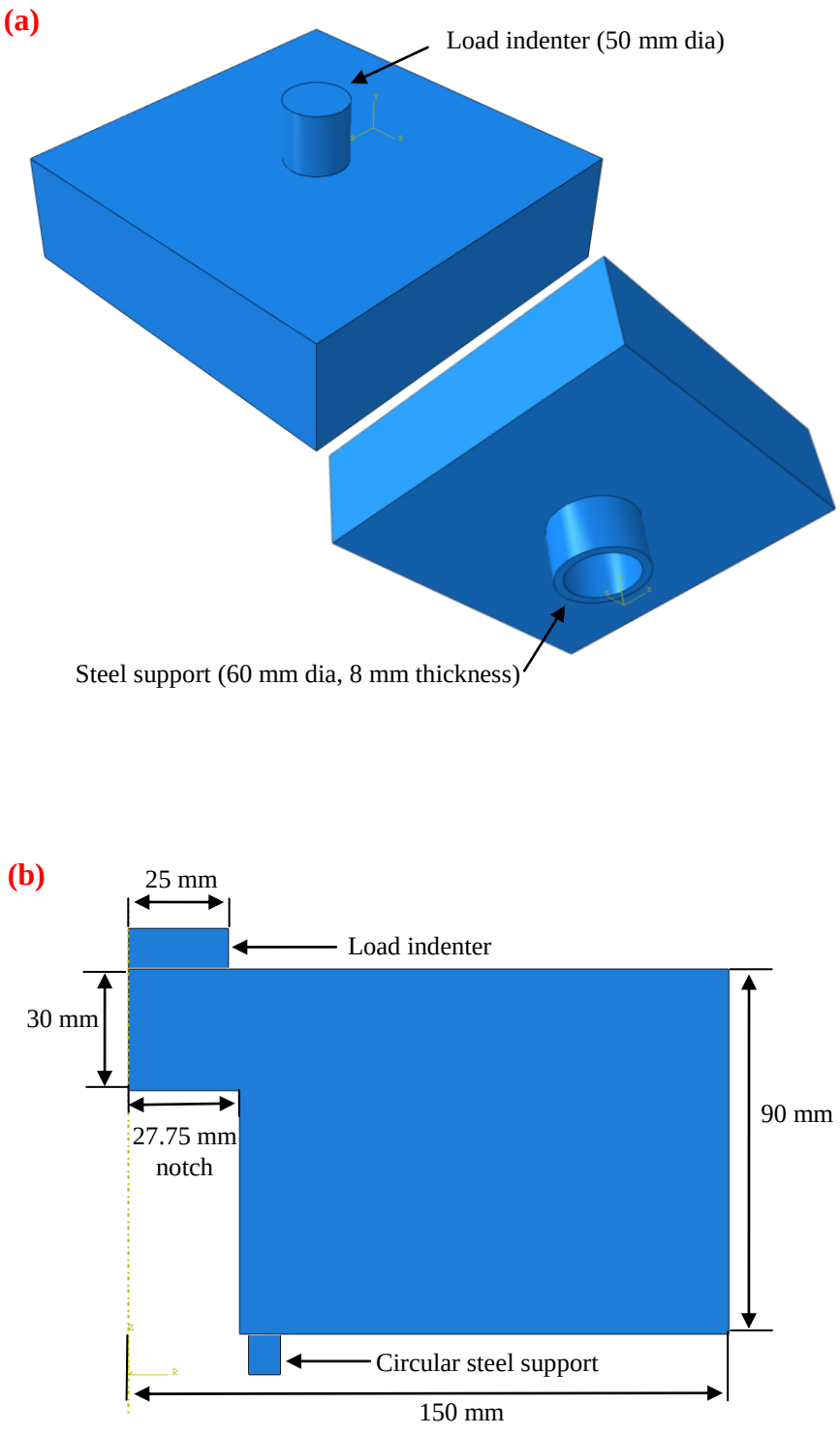

Figure 7.11: Slab specimen with a notch diameter of 55.5 mm in: (a) 3D model, and (b) Axisymmetric model.

Since failure of the beam specimens occurred in two directions (X and Y), it is apparent that no difference can be seen between the 3D and 2D models in Figure 7.10. Furthermore, for the slab specimens, the punching shear failure occurred in truncated shape radiating from the edge of the load indenter to the notches, as shown in Figures 6.15 and 6.23. Form both figures; it is evident that failure had concentrated in a small area of the slab specimens and all the areas beyond the notches were not contributing to the punching shear capacity of the section. Therefore, the slab specimens can be modelled as a circular geometry and the dead weight of the section can be excluded in the simulation. The axisymmetric model for the slab simulations were chosen since the geometry of the failure area, the supports, and the loading indenter were all circular. Therefore, in all the modelling, only a plane through the components of the test setups and specimens were required to model. The FE procedures presented hereinafter are for the 2D and axisymmetric models only.

In addition, the random distribution of a large number of fibres in the concrete was not modelled, as the fibre-matrix interaction would be required for every fibre in the concrete and this is not feasible. Therefore, the UHPFRC was modelled as a homogenous material and the physical presence of fibres in the concrete was ignored.

7.4.2 Material properties input

Most of the input material properties of the concrete were obtained from the constitutive material model proposed in Section 3.6.3 or directly from the direct test results presented in Chapters 3 and 4. For both models, the values of density, elastic modulus, Poisson's ratio and compression hardening were the same, see Table 7.1. However, the values of tension stiffening for both models were slightly different to each other as shown in Table 7.1. The values of the six additional perimeters for the CSC and five additional perimeters for the CDP were set to their default values as discussed earlier, see Table 7.2 (Abaqus theory manual 2010, Chen and Graybeal 2012).

Table 7.1. Material properties for the CSC and CDP models for UHPFRC finite element modelling.

Density (kg/m^3)			2440
Concrete elasticity			
Elastic modulus (GPa)			45.0
Poisson's ratio			0.21
Concrete compression hardening			
Compressive stress (MPa)			Strain
135.0			0.000000
138.0			0.000100
141.0			0.000200
144.0			0.000300
147.0			0.000400
150.0			0.000500
Concrete tension stiffening (CSC)			
Displacement at failure (mm)			6.20
Concrete tension stiffening (CDP)			
Tensile stress (MPa)	Deflection (mm)	Damage variable	Deflection (mm)
8.5	0.00	0.000	0.00
8.0	0.20	0.059	0.20
7.5	0.42	0.118	0.42
7.0	0.68	0.176	0.68
6.5	0.93	0.235	0.93
6.0	1.20	0.294	1.20
5.5	1.45	0.353	1.45
5.0	1.70	0.412	1.70
4.5	2.00	0.471	2.00
4.0	2.30	0.529	2.30
3.5	2.75	0.588	2.75
3.0	3.10	0.647	3.10
2.5	3.55	0.706	3.55
2.0	4.10	0.765	4.10
1.5	4.65	0.824	4.65
1.0	5.20	0.882	5.20
0.5	5.70	0.941	5.70
0.4	5.80	0.953	5.80
0.01	6.20	0.999	6.20

For both models, the concrete tension stiffening was defined using the stress-displacement approach. This is because this method was reported to be numerically stable for members with no steel reinforcement and is also recommended by the Abaqus

manual (Abaqus theory manual 2010). Furthermore, the tension damage degradation values were determined using Equation 7.9.

Table 7. 2: Additional parameters for the CSC and CDP models for UHPFRC finite element modelling.

The parameters for CSC model	
Failure ratio	
Ratio 1	1.16
Ratio 2	0.056
Ratio 3	1.28
Ratio 4	0.33
Shear retention	
Rho-close	1.0
Eps-max	0.1
The parameters for CDP model	
Dilation angle (degrees)	40
Eccentricity	0.1
f_{b0} / f_{co}	1.16
K	0.60
Viscosity parameter	0.0

For any FE modelling, there are recommendations (Abaqus theory manual 2010) to convert the nominal stress-strain to true stress-strain data where the cross-sectional change factor is taken into account by using the instantaneous cross-section at each increment. However, when this was converted, no significant differences in the FE results were seen. Therefore, the material properties used in the modelling were obtained from the constitutive material model proposed in Section 3.6.3 and are of the nominal stress-strain values.

Furthermore, the validity of the material properties of the concrete presented in Tables 7.1 and 7.2 was checked by simulating the load-deflection response of a dog bone specimen. The agreement between the FE predictions and experimental results at peak strength was approximately 98% at various curing ages, see Figure 7.12. From the figure below and the results presented in Chapter 5, it is evident that UHPFRC reaches its maximum compressive and tensile strengths within 7 days. Therefore, only one set of

material input data was used for the modelling to simulate the structural behaviour of the concrete at the ages of 7, 14, 28 and 58 days.

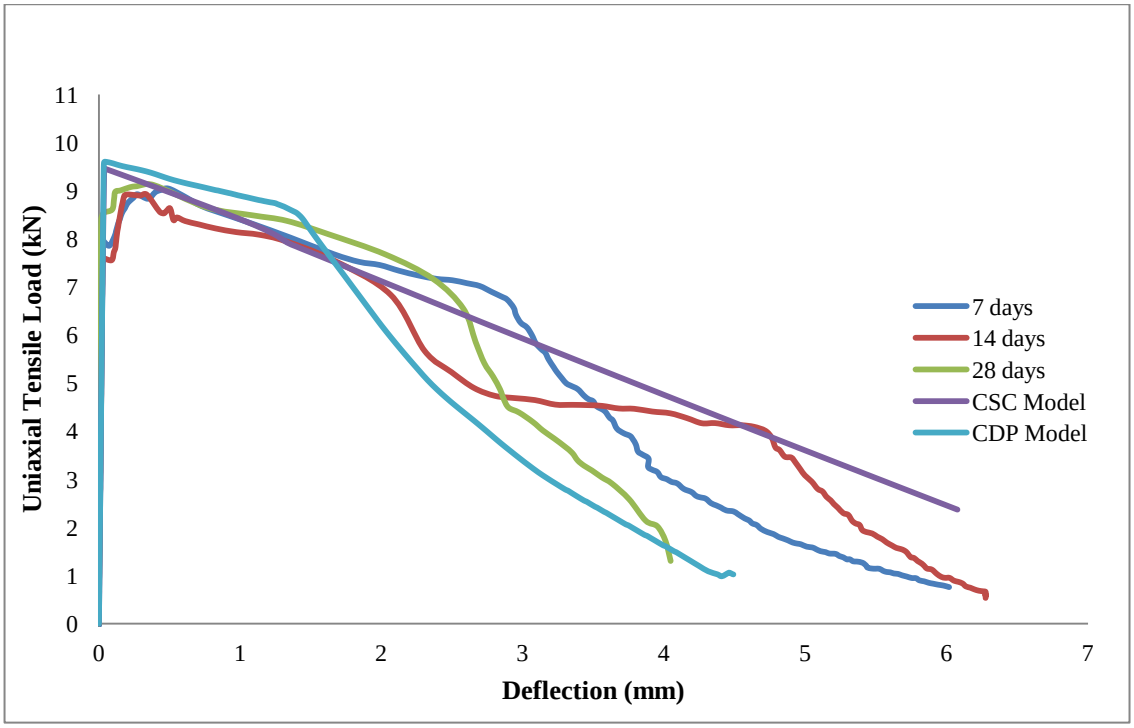

Figure 7.12: Comparison of experimental and FE simulation load-deflection response for doge bone specimens at different ages.

7.4.3 Boundary and loading configurations

In Abaqus, the global coordinate system (X, Y, Z) or (1,2,3) are available and based on these coordinates models are created and set to boundary conditions as required. To replicate the exact boundary and loading configurations of the experimental work, the exact geometry of the steel supports and load indenters were created in each model. The material properties of these steel entities were set to 8000 kg/m^3, 200 GPa and 0.3 for the values of density, modulus of elasticity and Poisson's ratio, respectively.

The boundary conditions for the beam specimens were fixed at one support in all directions, while the other support was restricted only in the vertical direction (Y axis), allowing movements in the horizontal direction (X axis) when required. For the slab specimens, the circular steel ring (support) was fixed at the bottom in all directions, while the edge of the specimen and load indenter along the axisymmetric line were

restricted in the horizontal direction and all the other sides were free to rotate in every direction.

The experimental investigations for the beam and slab specimens were conducted in a displacement control testing manner. Therefore, displacement boundary conditions were used to simulate the loading conditions. This was implemented by assigning displacement control in the vertical direction at the positions of applied load in each model. The interaction between the supports, load indenters and the specimens were created by defining various contacts. The assignment of the boundary conditions and load configurations are shown in Figure 7.13.

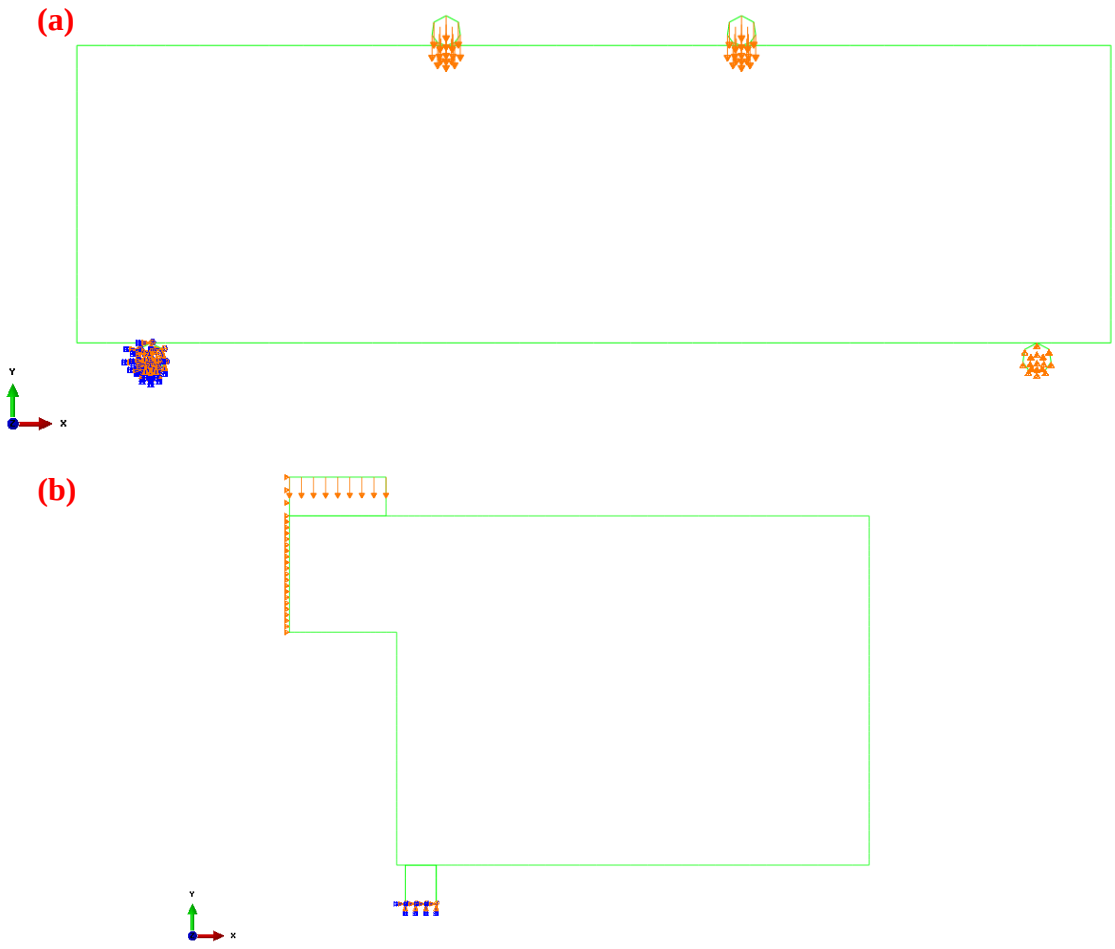

Figure 7.13: The boundary and load configurations for: (a) The 2D model of the 350 mm length beam, and (b) The axisymmetric model of the 55.5 mm notch diameter slab.

In addition, the reaction force and deflection values were acquired from the boundary conditions and a node below the applied load, respectively. These results were used to simulate the load-deflection response during the analysis.

7.4.4 Interaction

Contact pair interaction between the supports, load indenters and the specimens were created using surface-to-surface interactions. The contact properties between the supports and the specimens were set to hard contacts allowing separation after initial contact, the separation option was used to allow rotation of the specimen when required. Furthermore, tangential behaviour frictionless contact was also assigned. This type allows slipping between the specimen and support when required.

Similarly, the contact properties between the load indenters and the specimens were also set to hard contacts but separation was not allowed. This is because the load indenters were intact with the specimens at all times during the experiments. The tangential behaviour frictionless contact was also defined for the case of slipping between the load indenter and the specimen when required.

7.4.5 Element

In Abaqus element library, a wide range of element types ranging from brick, shell, contact to beam are available. Each type is designed for various analyses depending on the type of the model and application.

For the 2D model, plane stress elements are recommended when the thickness of a body is small relative to its lateral dimensions (Abaqus theory manual 2010). Therefore, the 4-node bilinear plane stress quadrilateral, incompatible mode element (CPS4I) type was used for the beam specimens. By default, 4-node bilinear plane stress quadrilateral, reduced integration, hourglass control (CPS4R) type is usually assigned. The latter type has been reported to be unsuitable for bending problems in which excessive deformation may occur before failure. In this study, both types were used and the former one appeared to provide results with better accuracy. In Section 7.5.4, a detailed discussion regarding both element types is presented.

For the slab specimens, the 4-node bilinear axisymmetric quadrilateral incompatible mode element type (CAX4I) was chosen over the default element type of 4-node bilinear axisymmetric quadrilateral, reduced integration, hourglass control (CAX4R) for axisymmetric models. The axisymmetric bilinear elements type is recommended for modelling bodies of revolution under axially symmetric loading conditions, thus, suitable for modelling the slab specimens. The incompatible mode element type was also used here for the same reasons which will be discussed later in this chapter.

In all the FE simulations, excessive aspect ratio was avoided; the ratio of 1 was always used where possible. However, due to having a number of partitions in each model, at times the aspect ratio was increased to about 1.3 and this value was never exceeded. In this study, for any FE analysis with an aspect ratio higher than 1.1, the results are clearly identified. It is worth mentioning that Abaqus by default allows the limit of aspect ratio to up to 10.

In addition, at the points of applying loads and supports, small element sizes were always used, see Figure 7.14. This was assumed that the numerical results will improve as the sizes of the elements are reduced. In Section 7.5.4, mesh dependency analysis was carried out to study the effect of various element sizes on the accuracy of the simulations.

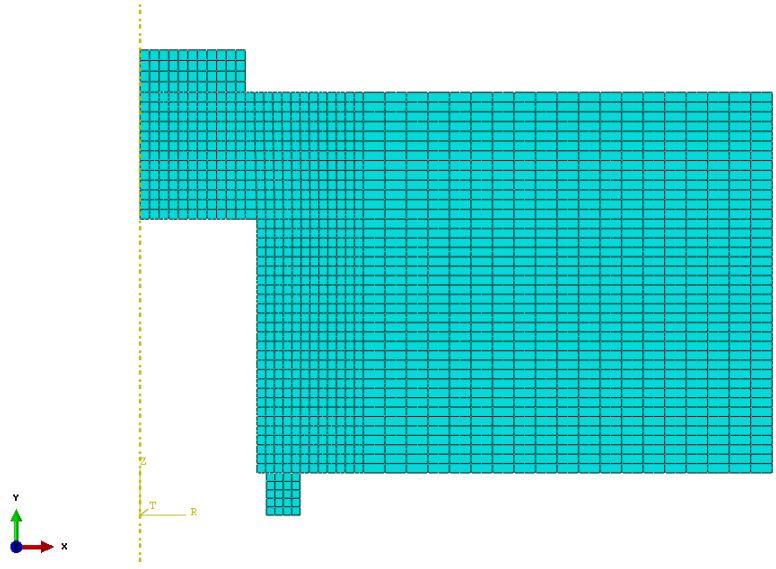

Figure 7.14: Different mesh sizes for the axisymmetric slab model with a notch diameter of 55.5 mm.

7.4.6 Output

The post-processing in ABAQUS is read in visualization mode in which contour plots, animations, *XY* plots, and tabular outputs of the simulations can be obtained. For both models used here, the propagation of cracks is not physically supported. Alternatively, various stress contours can be plotted and used to show stress concentration in the models. Another suitable option in the visualization mode is the capability of transforming the axisymmetric models into full 3D models after the analysis has completed. This can provide better visualisation mode of the models. Furthermore, from the output, the load-deflection response were generated for each model and compared to the results obtained from the experimental tests.

7.5 Results and Discussion

This section presents the results of finite element simulations of beam and slab specimens subjected to flexural and shear loads. Results obtained from both CSC and CDP models are compared to the experimental test results presented in Chapters 4, 5 and 6. The simulations presented here are valid only for UHPFRC specimens cured at 90 ^{o}C curing temperature.

7.5.1 Beam specimens

The load-deflection response of two different beam sizes of 100x100x350 mm and 100x100x500 mm in width, depth and length, respectively, were predicted at various curing ages. In Figure 7.15 to 7.18, the experimental load-deflection response of the beam specimens are compared to the FE simulations. Results obtained from the CSC model simulation are in good agreement with the experimental test results up until peak load. However, in the post-failure region, results from this model increasingly deviate from the experimental test results and exhibits greater stiffness than was observed experimentally. From the same figures, results obtained from the CDP model accurately replicates the experimental test results of all the beam specimens, regardless of the curing age and size, in both elastic and plastic regions.

The predictions of both models in the elastic region and up until the peak load are in close agreement to the experimental results and each other. This is because their different damage plasticity models are not activated yet. However, beyond the peak load, the CSC model appears to be inefficient for UHPFRC. It must be noted, in the CSC simulations, severe convergence problems were experienced for the same element sizes used for the CDP model. In order for the FE simulation to converge to a unique solution, a coarser mesh size had to be used with the CSC model simulations throughout this study. For instance, the element sizes for the CSC and CDP simulations for the beam specimens were 12.5 mm and 6 mm, respectively. The difference in mesh sizes between both models is believed to have resulted in some of the poor accuracy of post-peak failure prediction of the CSC simulations. Furthermore, the CSC model is specifically developed for concrete members with heavy reinforcement compared to the CDP model. Therefore, the results obtained here, highlights the limitation of this model for UHPFRC.

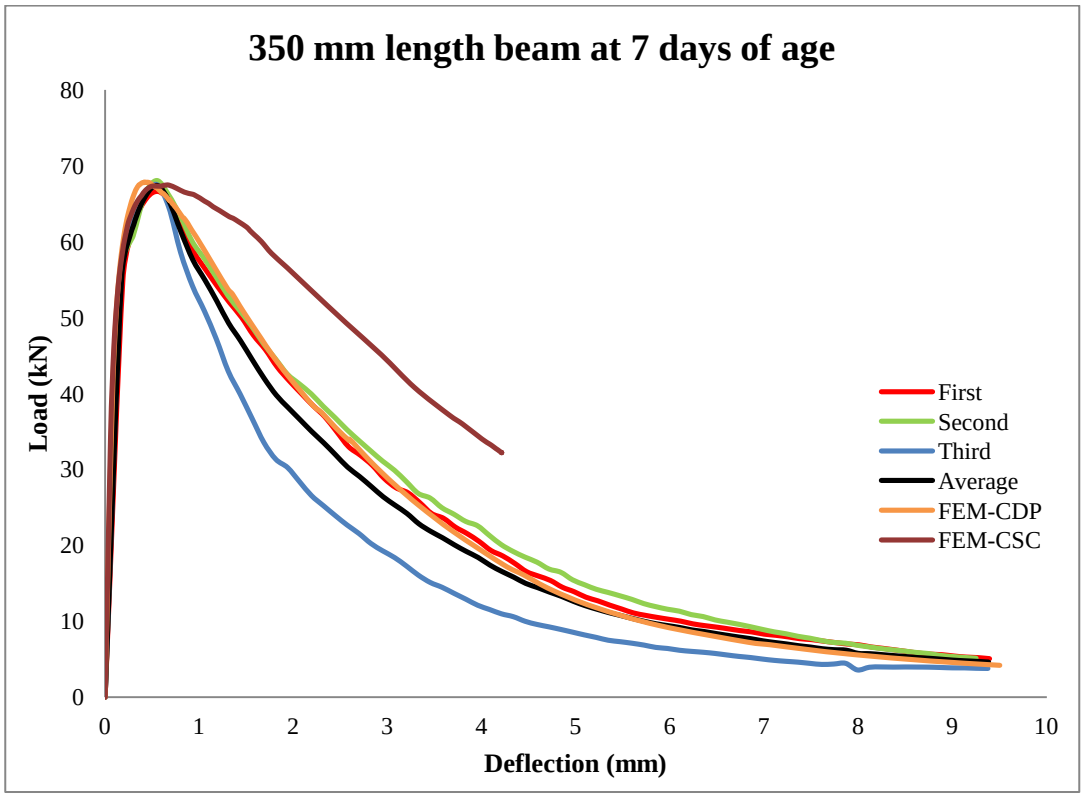

Figure 7.15: Load- deflection response for UHPFRC beam specimens.

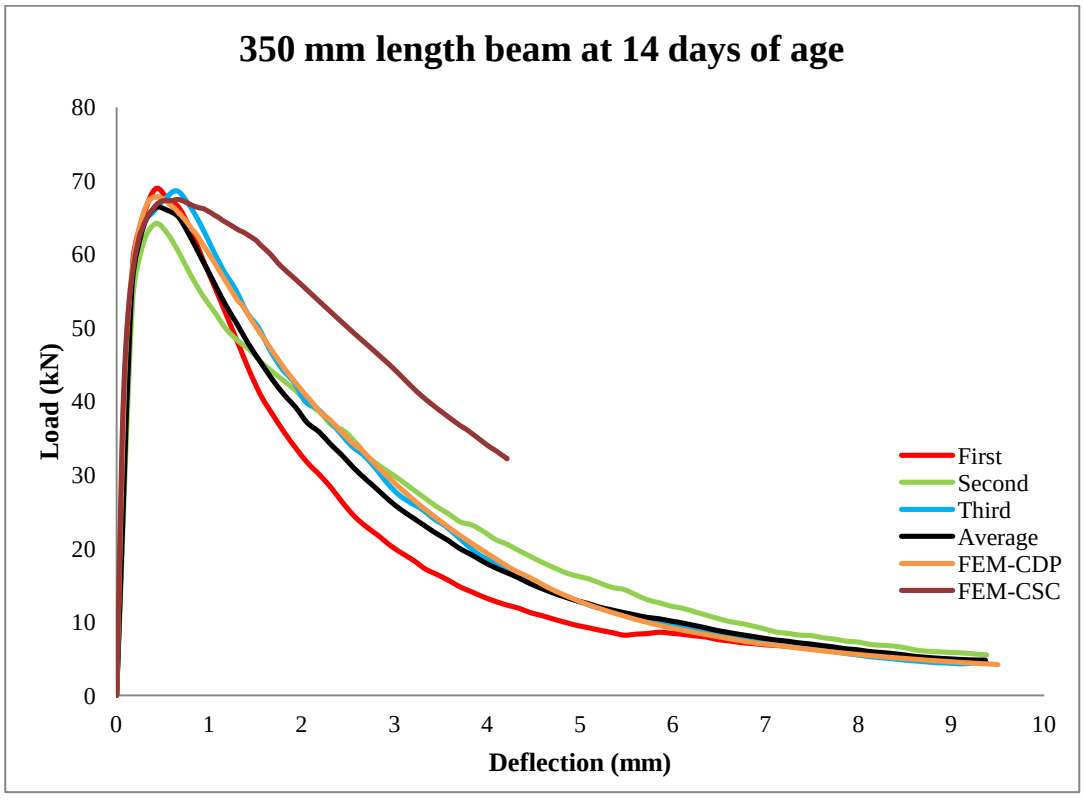

Figure 7.16: Load- deflection response for UHPFRC beam specimens.

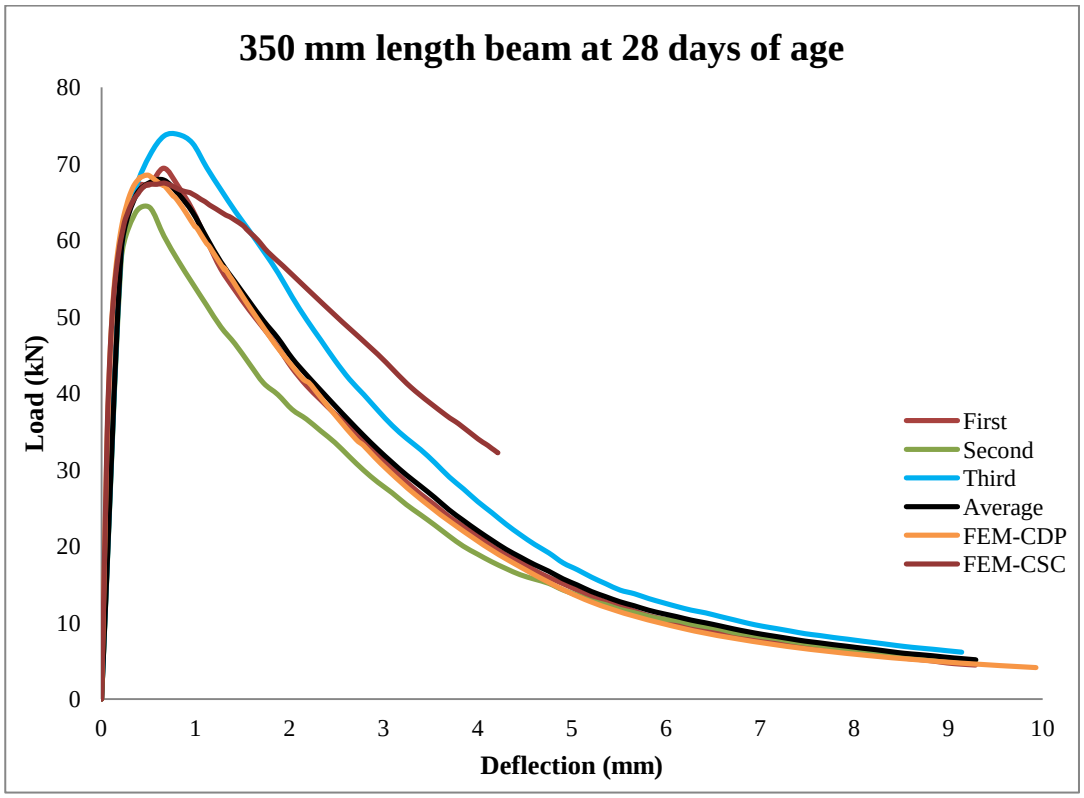

Figure 7.17: Load- deflection response for UHPFRC beam specimens.

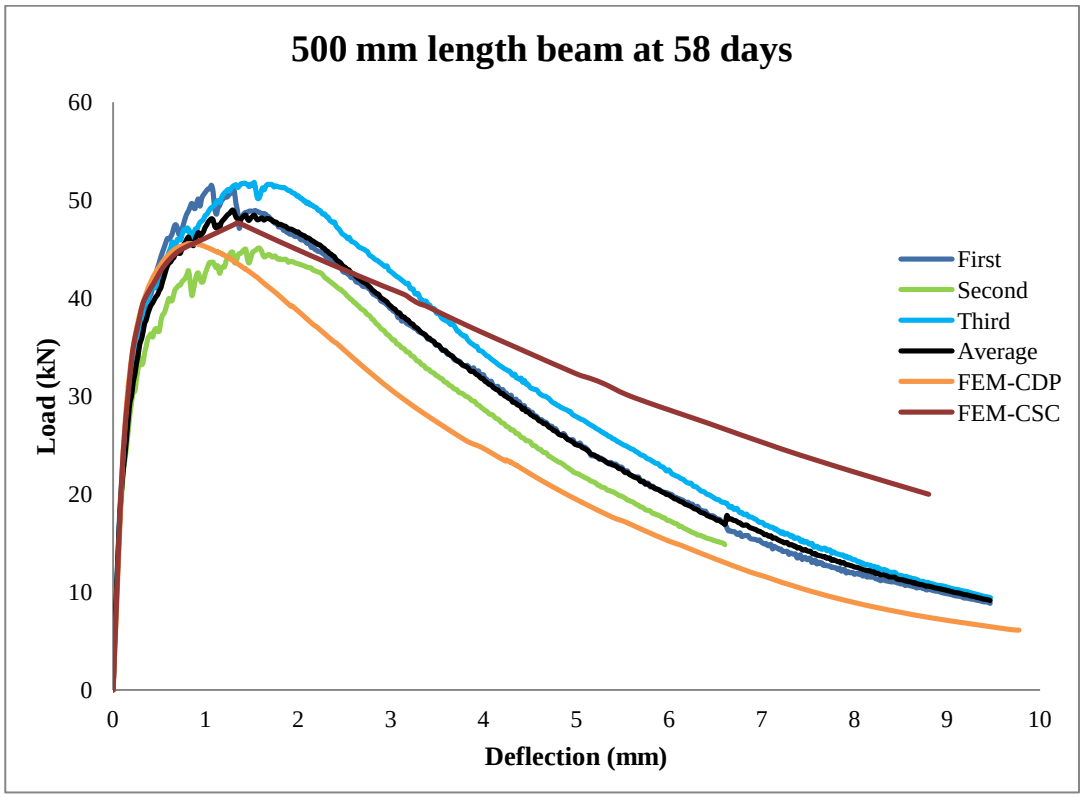

Figure 7.18: Load- deflection response for UHPFRC beam specimens.

In Table 7.3, the values of ultimate flexural load, P_u, and corresponding deflection, δ_u, of the experimental test results and the simulations are presented. Both models predict the values of failure load with good accuracy, with errors of not more than 7%. However, the accuracy for the deflection values is reduced considerably, with errors up to 50%. This appears to be large; however, such discrepancy in predicting very small deflection values (0.415 to 1.291 mm) can be expected. Furthermore, similar variations in deflection values between the three experimental specimens tested for each testing age were also observed. This is due to the random distribution of fibres in the concrete in which the deflection values are highly dependent on. Therefore, the deflection values obtained from the FE simulations are considered to be acceptable.

Table 7.3: Experimental and FE results of maximum loads and corresponding deflections for beam specimens.

	Experiment		CSC		CDP		Error (CSC)		Error (CDP)	
Age (days)	P_u (kN)	δ_u (mm)	P_u (kN)	δ_u (mm)	P_u (kN)	δ_u (mm)	Load (%)	Deflection (%)	Load (%)	Deflection (%)
7	67.40	0.554	67.02	0.623	67.86	0.417	0.56	12.45	0.68	24.73
14	66.32	0.415	67.02	0.623	67.86	0.417	1.06	50.12	2.32	0.48
28	67.87	0.662	67.02	0.623	67.86	0.417	1.25	5.89	0.01	37.01
58	49.00	1.291	47.69	1.346	45.55	0.929	2.67	4.26	7.04	28.04

Since UHPFRC exhibits high ductility behaviour, the von Mises yield criterion in the FE simulations was used to study stress distribution of the models. In Figure 7.149, the von Mises stress contours for both different size beam specimens are illustrated based on the CDP model. From this figure, it is evident that maximum stress occurs at regions where bending moments are ultimate. Furthermore, failure of the specimens did occur in similar positions to those shown in the FE simulation, see Figure 7.20.

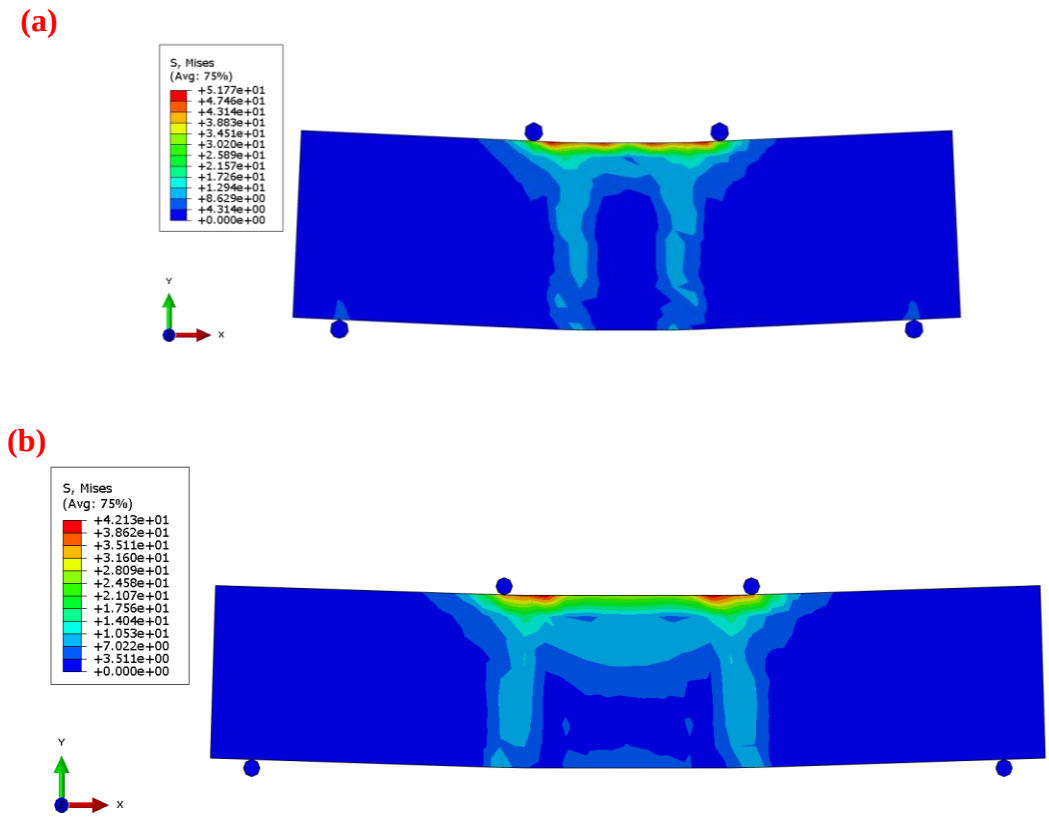

Figure 7.19: Von Mises stress distribution, in MPa, for beam specimens of: (a) 350 mm length, and (b) 500 mm length.

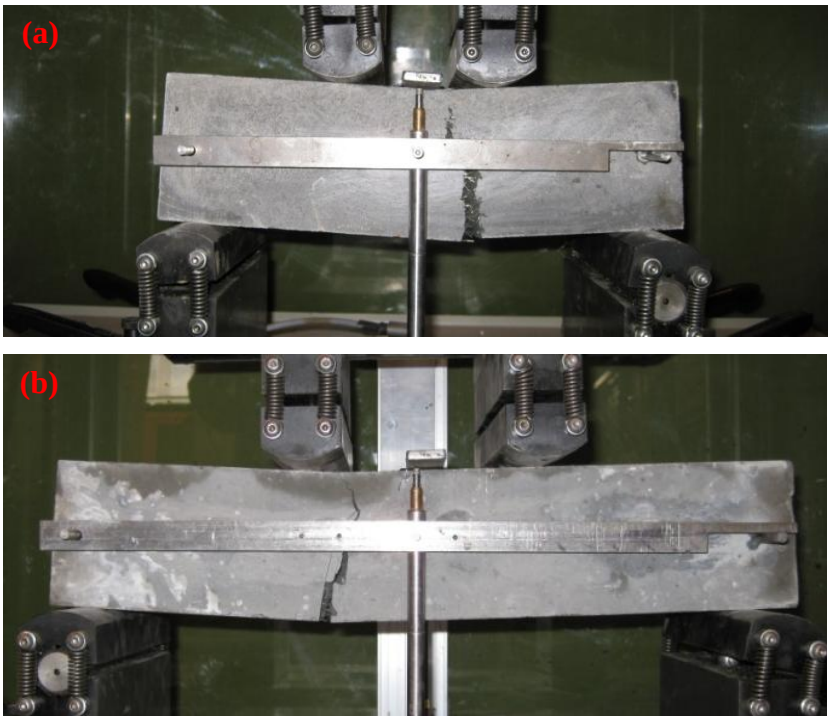

Figure 7.20: Failure mode for beam specimens of: (a) 350 mm length, and (b) 500 mm length.

7.5.2 Slab specimens

From the FE results obtained for the beam specimens, the suitability of CSC model for UHPFRC appeared to be limited. Attempts were made of using this model to predict the load-deflection response for the slab specimens. However, the simulation experienced convergence problems and finding a solution with acceptable element sizes were not possible. Therefore, FE simulations based on the CSC model is not included here. All the FE results shown for the slab predictions are based on the CDP model only.

In Figures 7.21 to 7.26, the experimental load-deflection responses for slab specimens with various notch diameters are compared to the FE simulations. In these figures, the FE simulations have predicted the behaviour of the experimental test results up until ultimate load with good accuracy. In general, the initial modulus of elasticity of the FE results is greater than those obtained in experimental tests. This is due to the concrete crushing behaviour that the slab specimens experienced in the beginning of each test. However, this behaviour was not modelled in the FE simulations. The concrete crushing was more pronounced for the slab tests with smaller notch diameters, those shown in Figures 7.21 and 7.22.

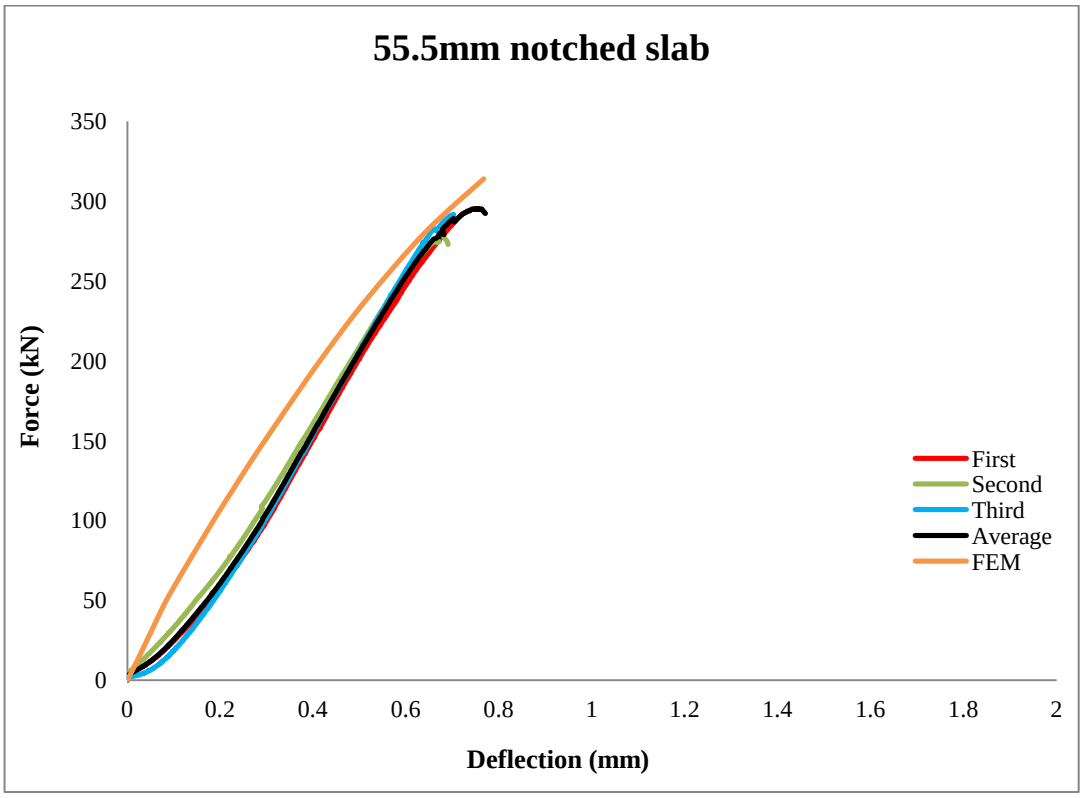

Figure 7.21: Load- deflection response for UHPFRC slab specimens.

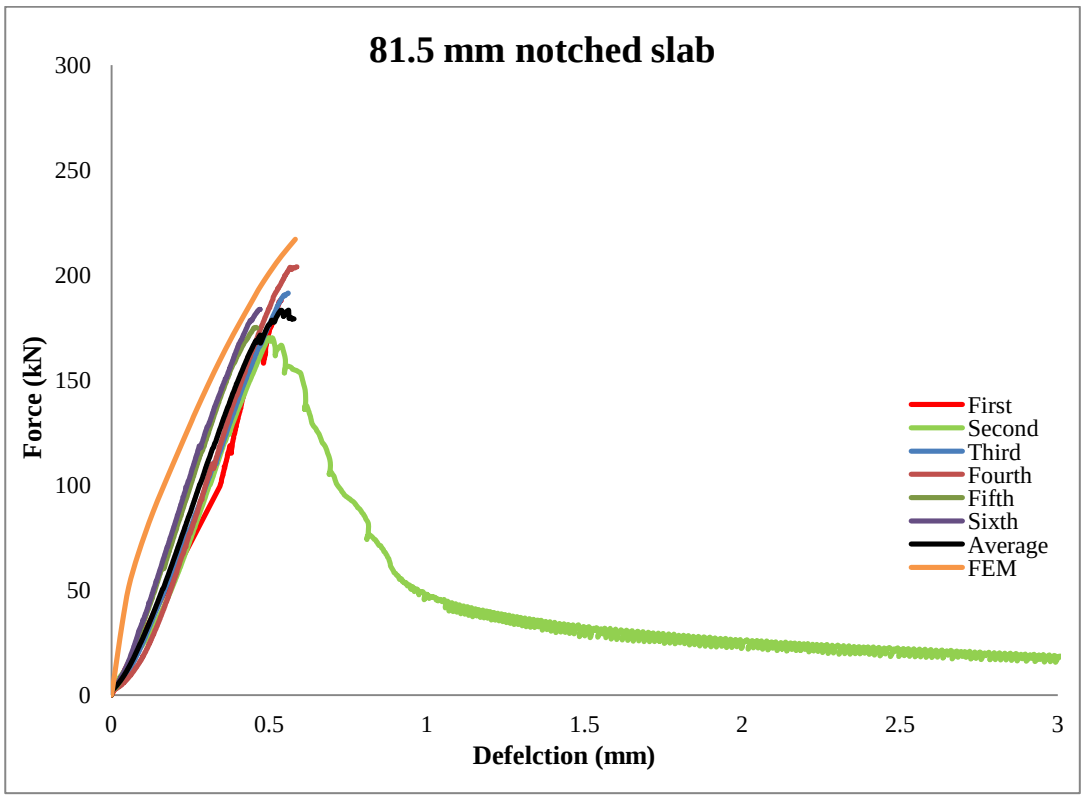

Figure 7.22: Load- deflection response for UHPFRC slab specimens.

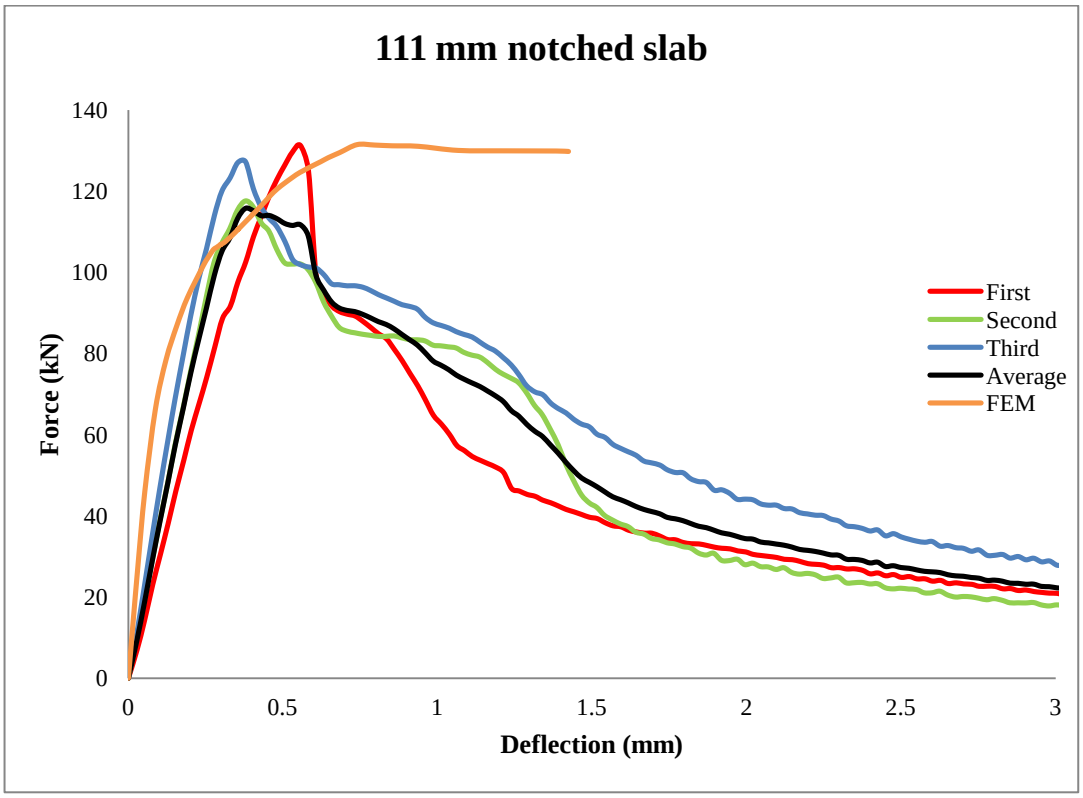

Figure 7.23: Load- deflection response for UHPFRC slab specimens.

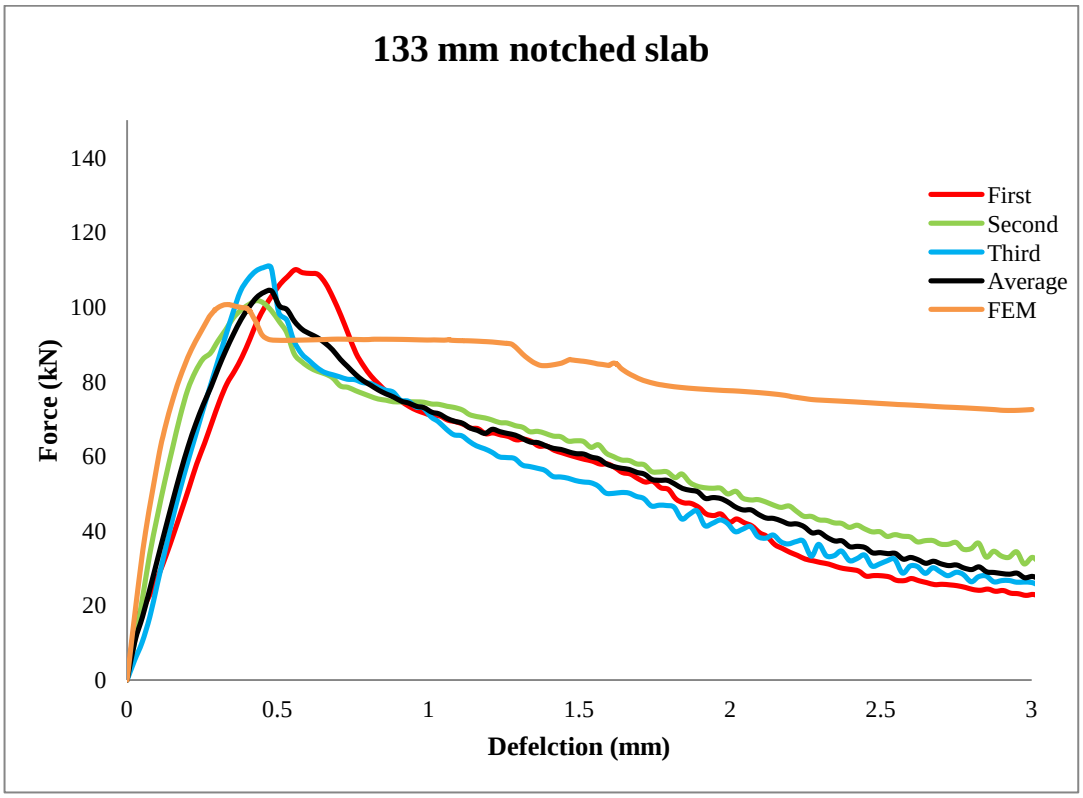

Figure 7.24: Load- deflection response for UHPFRC slab specimens.

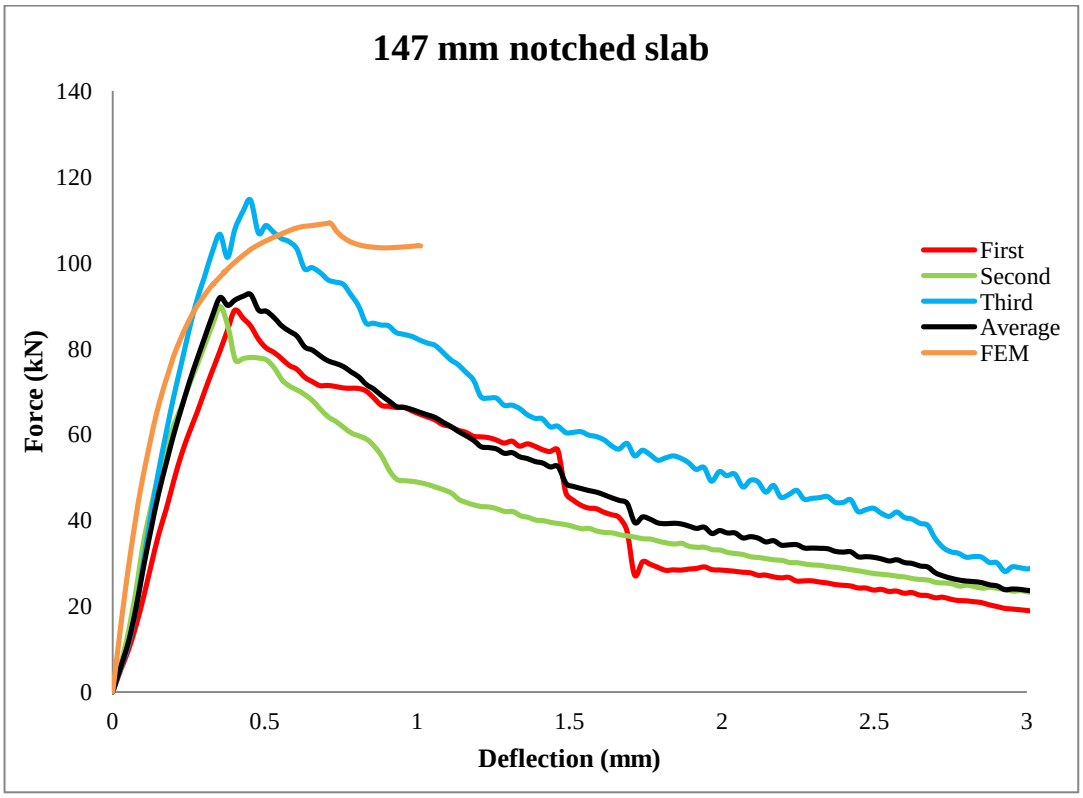

Figure 7.25: Load-displacement response for UHPFRC slab specimens.

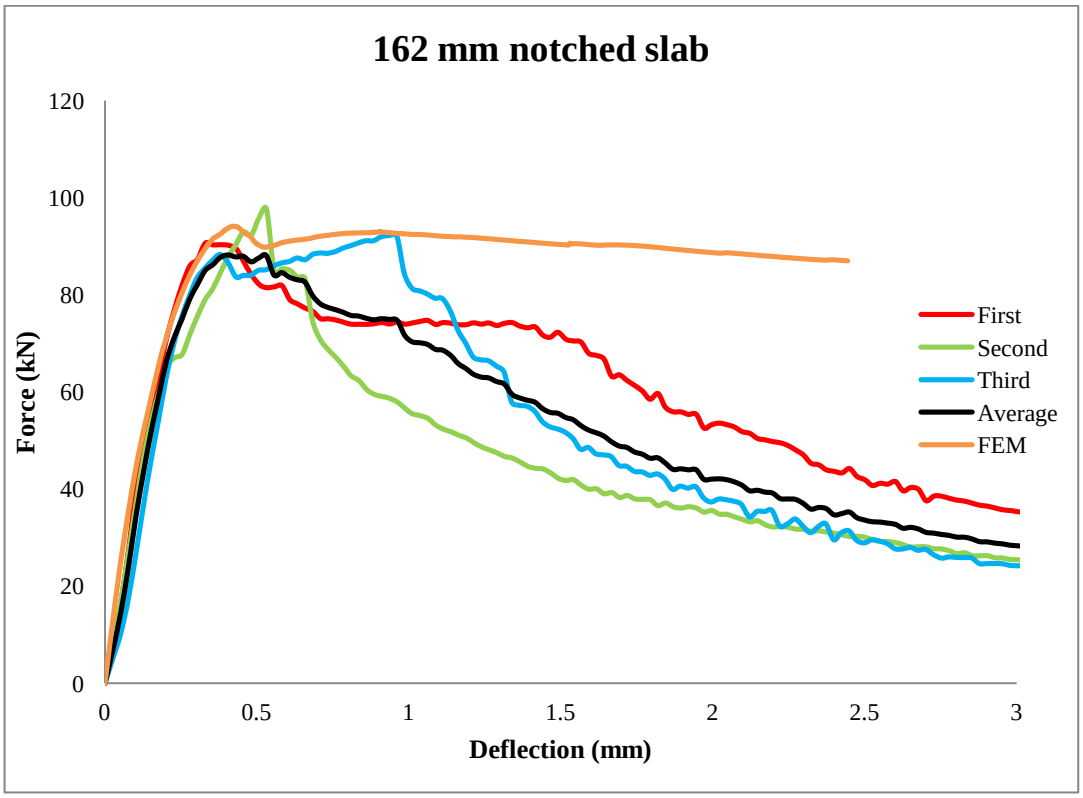

Figure 7.26: Load- deflection response for UHPFRC slab specimens.

Unlike the beam predictions, the CDP model was not able to simulate the post-peak behaviour of the slab tests with an acceptable degree of accuracy; in particular, for tests that exhibited ductile behaviour, see Figures 7.23 to 7.26. This is believed to be due to the complexity of the failure mechanism of the slabs and nature of the test setup, which the FE simulations cannot take these into account as accurately as those for the beam tests. For instance, the FE simulations for the slab specimens assume failure occurs when the principal shear stress exceeds the tensile strength of the material and with an angle equal to the punching shear angle of each test. This might be the case, however, the effect of randomly distributed fibres diagonally bridging along the failure lines are not considered in the simulations which certainly influences the post-peak behaviour predictions. While, the FE simulations for the beam tests assumes failure occurs due to principal bending stress along the X direction with no failure angles, which is a more straightforward prediction. Therefore, the absence of fibres in the FE beam simulations could not be as influential as those of the slabs.

In addition, in the slab tests, the specimens are supported in two directions, the failure mechanism is complicated and the influence of bending stress might not be completely eliminated. The influence of flexural stress in this test cannot be ruled out even when no signs were observed. This is because the test has been developed only and limited test results are available. Thus, uncertainty involved with this test is still high. However, in the beam tests, the specimens are supported in one direction only, and the failure mechanism is straight forward. Thus, better accuracy with the CDP model simulations can be seen for the beams compared to the slab specimens.

Furthermore, the material parameters presented in Table 7.2 for both models, are based on default values recommended for normal concrete. Using these values for UHPFRC FE simulations could have influenced the accuracy of the results. Therefore, for more accurate simulations, the correct values of these parameters for the concrete are vital. Due to the limitation of this study, no experimental work was conducted to identify these parameters.

In Table 7.4, the ultimate punching shear load carried by the slab specimens, V_{rd}, and corresponding deflection, δ_{rd}, for the experimental test results and the simulations are presented. From this table, the predicted ultimate load values are in good agreement with the test results, with errors of approximately 18%. However, the predicted deflection values are generally greater than the test results, with errors of approximately 95%. Such discrepancy may appear large; however, with such small deflections at high failure loads, this can be taken as acceptable, similar to the FE simulations for the beam specimens.

It must be noted, FE simulation for slab specimens with notch diameters of 179 mm and 194 mm did not converge to a unique solution with acceptable element size, i.e. not smaller than 30 mm. Thus, in this study, simulations for these test results are not included.

Table 7.4: Experimental and FE results of maximum loads and corresponding deflections for slab specimens.

Notch diameter (mm)	Experimental		FEA		Error	
	V_{rd} (kN)	δ_{rd} (mm)	V_{rd} (kN)	δ_{rd} (mm)	Load (%)	Deflection (%)
55.5	294.86	0.762	313.76	0.767	6.41	0.66
81.5	183.26	0.561	217.07	0.583	18.45	3.92
111	115.79	0.379	131.49	0.740	13.56	95.25
133	104.18	0.479	100.63	0.331	3.41	30.90
147	92.58	0.453	109.32	0.710	18.08	56.73
162	88.27	0.405	94.03	0.434	6.53	7.16

The von Mises stress distribution at failure for the slab specimens is shown in Figure 7.27. In this figure, a good resemblance between the stress contour of the FE simulations and truncated cone failure shaped of the slab specimens reported in Figures 6.15 and 6.22 can be seen. In Figure 7.27, maximum stress occurs in the region of the applied load and propagates to the edge of the notches, this agrees well with the failure behaviour of the slab specimens reported in Chapter 6. Furthermore, a 3D model of the slab specimen with a notch diameter of 55.5 mm is shown in Figure 7.28. This model

was transformed from the axisymmetric model in the visualisation mode, which illustrates the validity of using the axisymmetric model in this study.

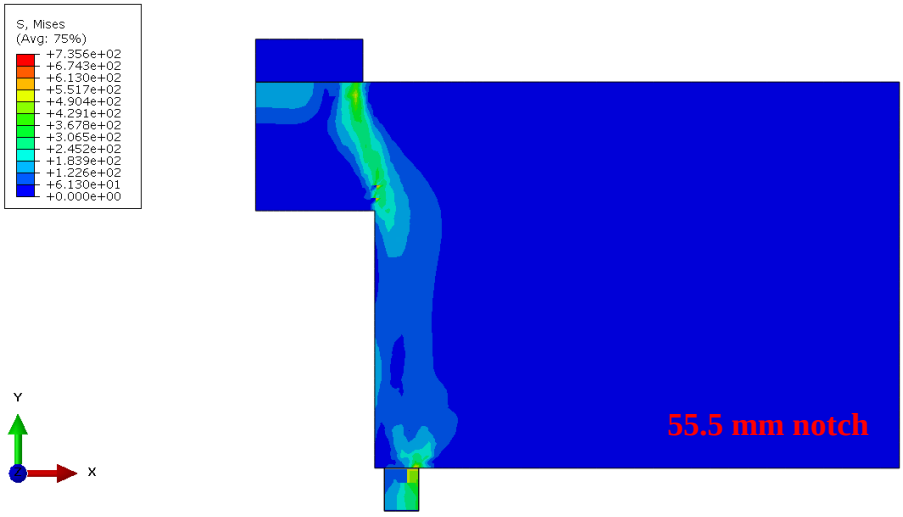

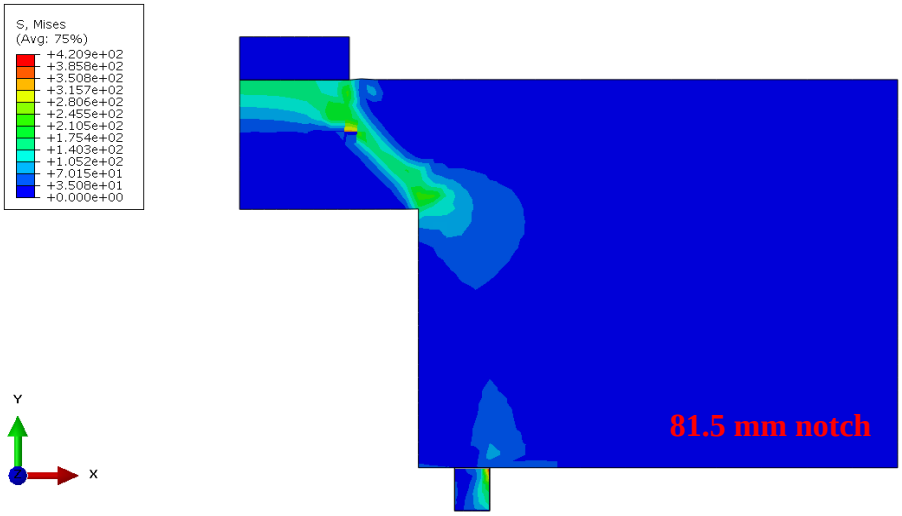

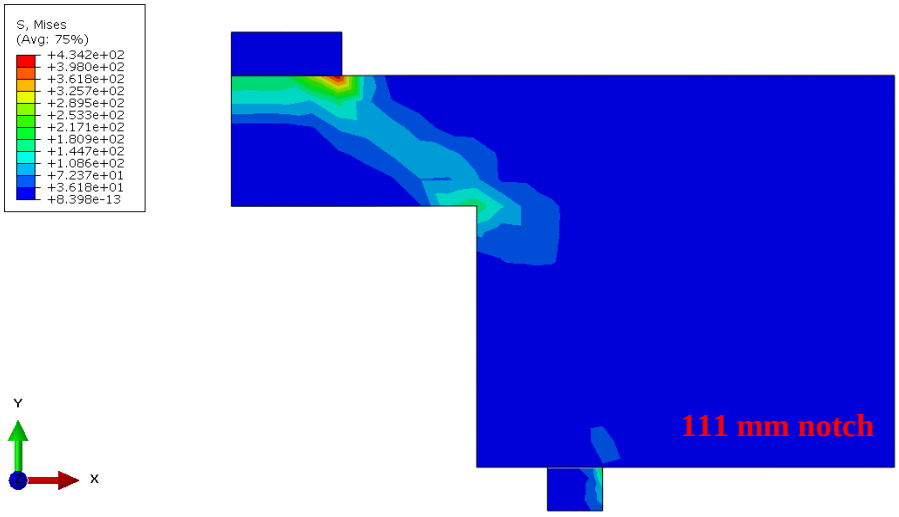

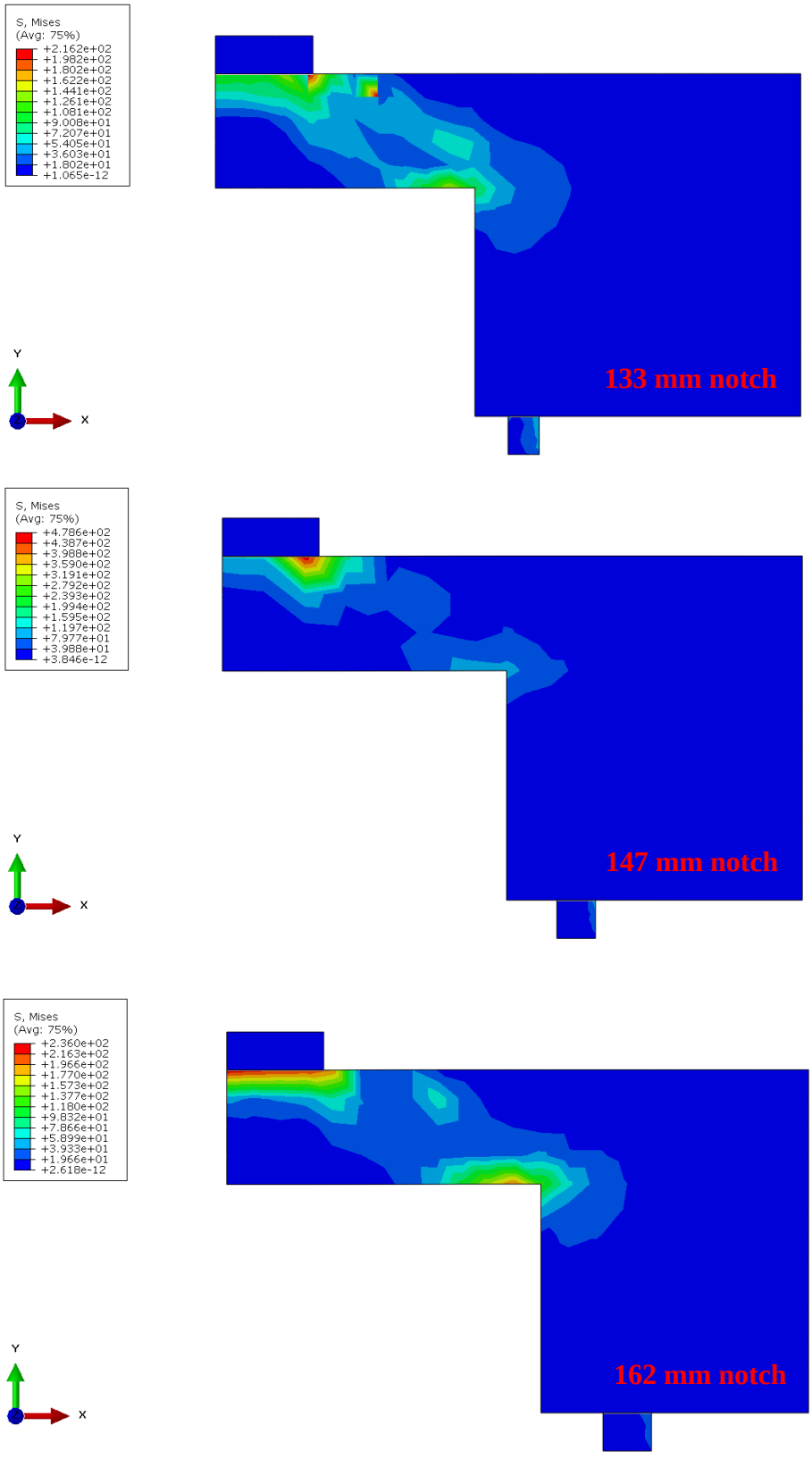

Figure 7.27: Von Mises stress distribution, in MPa, for UHPFRC slab specimens with various notch diameters.

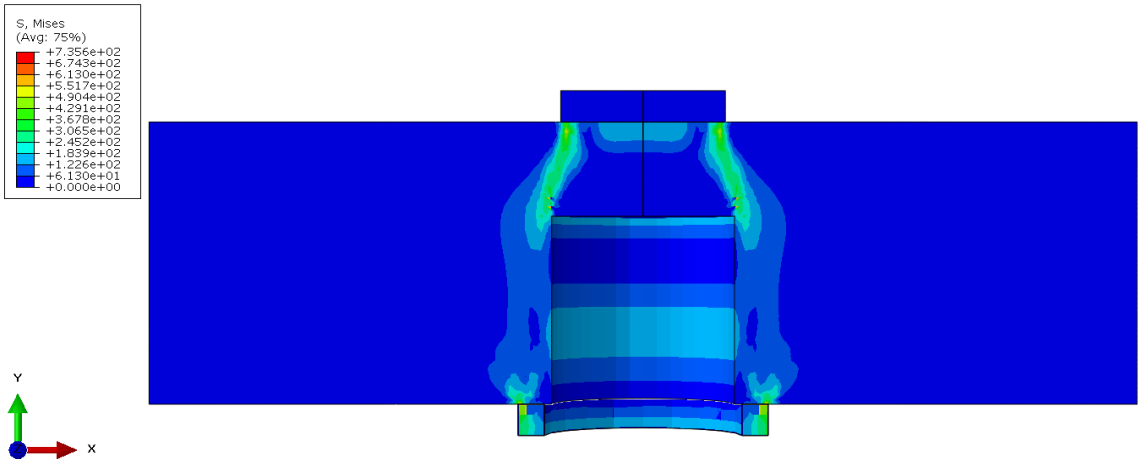

Figure 7.28: A 3D von Mises stress distribution, in MPa, for UHPFRC slab specimens with a notch diameter of 55.5 mm.

From the FE results presented for the beam and slab specimens, it appears that the CSC model is limited for UHPFRC, while the CDP model provides better accuracy. The limitation of both models for this concrete and, in particular, the CSC model is due to the complexity of the material behaviour of UHPFRC which cannot be taken into account fully in the simulation. For instance, the nonlinear stress-strain behaviour of the concrete in compression and tension compared to that of normal concrete, which both models are not designed for. Another factor could be due to the absence of progressive cracking of the concrete after the formation of microcracks and the subsequent crack interface behaviour in the models. Furthermore, the physical absence of steel fibres in the concrete within the fibres-matrix, so that interface effects such as dowel action, fibre pull-out, or fibre failure are not included in either model. Therefore, it is evident that both models require improvement to take the aforementioned problems discussed above before they can be used in predicting the full structural behaviour of this concrete.

7.5.3 Incompatible mode element type

The FE simulations presented here were based on incompatible mode element types, CPS4I and CAX4I for the 2D and axisymmetric models, respectively. These types were chosen to improve the accuracy of the predictions and minimise convergence problems during the simulations. It must be noted that, by default, Abaqus selects first order reduced integration (CPS4R and CAX4R) of these element types for computational

reasons. This is because reduced integration uses lower-order integration, only one point, to find the element stiffness. Therefore, it uses less computational time compared to fully integrated and incompatible mode types at four integration points. However, the reduced integration element type has serious drawbacks when is used for bending behaviour simulations. It results in mesh instability, commonly referred to as "hour-glassing". The hour-glassing behaviour often makes this type of element unusable when the element experiences excessive bending and should be avoided for bending problems. An alternative to the reduced integrated type is the fully integrated (CPS4 and CAX4) which do not suffer from hour-glassing and uses more integration points. However, this type also suffers from an effect known as " shear locking" when is used for bending problems (Abaqus theory manual 2010). Abaqus reports that the numerical formulation of fully integrated first order element types in bending problems gives rise to shear strains that do not really exist; this is known as "parasitic shear". Therefore, this type becomes too stiff in the simulations and should also be avoided for bending problems. Due to the problems involved with fully and reduced integrated first order element types, the FE simulations resulted in poor accuracy and often experienced convergence problems. However, when incompatible element types were used, the accuracy of the results was improved and convergence problems were minimised. This is because incompatible element types use full integration, at four points, and are specially designed for bending simulation problems. The hour-glassing and shear locking behaviours do not exist with this type. The problems described above for reduced and fully integrated first order element types are common for bending problems in almost every FE packages such as MSC Nastran, Ansys and Abaqus (Sun 2006, Abaqus theory manual 2010).

To investigate the suitability and accuracy of the incompatible mode, reduced integrated and fully integrated (CPS4I, CPS4R and CPS4) element types for predicting the bending behaviour of UHPFRC beams, the load-deflection response for the 350 mm length beam specimens at 28 days are predicted in Figure 7.30, using all of the three element types in CDP model.

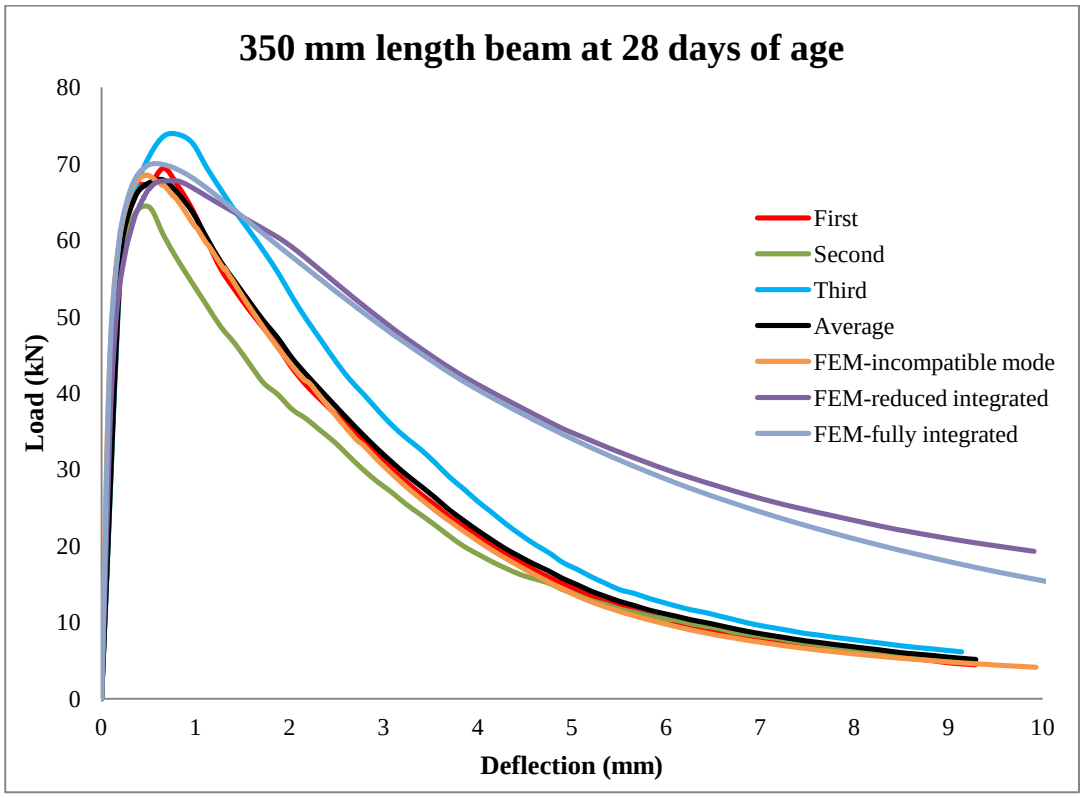

Figure 7.29: FE simulation against experimental test results using different element types.

It is evident that the CPS4R and CPS4 types have overestimated the post-peak failure of the experimental test results, while the CPS4I type has increased the accuracy considerably. This validates the discussion presented above. Alternatively, the second-order reduced-integrated element type can be used instead of incompatible element in the FE simulation. However, the computational time for this type are expensive and usually provides results of similar accuracy to those reported for the incompatible mode elements type. Therefore, all the FE results presented in this study were based on CPS4I and CAX4I element types unless reported otherwise.

7.5.4 Mesh dependency

To ensure that the FE results were not subject to mesh dependency, a mesh refinement analysis was performed. In general, small element sizes were always adopted in regions where maximum bending moment and punching shear failure was imminent, as shown in Figure 7.14. For each model, various element sizes ranging from 30 to 4 mm were

used and accuracy of the simulations was compared to experimental test results. In Figure 7.30, mesh sensitivity analysis for improving the accuracy of the FE results at ultimate load for the slab specimen with a notch diameter of 162 mm against experimental test results are presented.

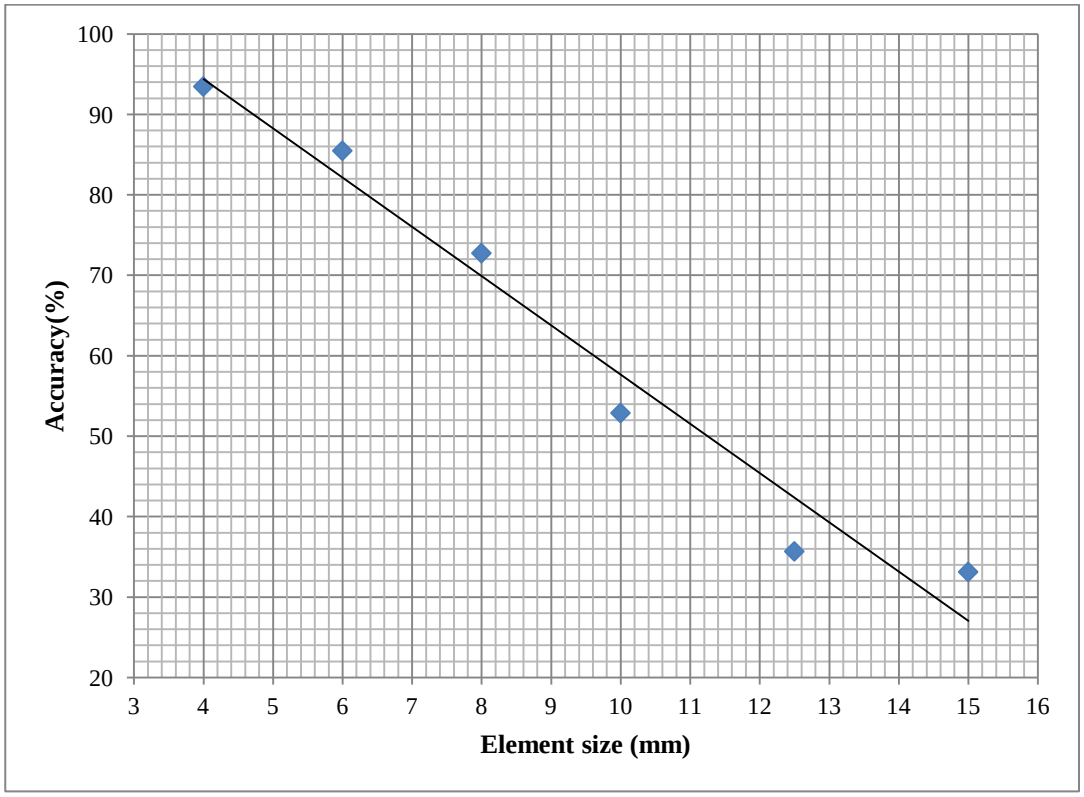

Figure 7.30: improvement in accuracy of FE results with various element sizes for slab specimen with a notch diameter of 162 mm.

The improvements in accuracy were seen as the sizes of elements were reduced. However, improvement for element sizes of 6 mm and below were not significant. In general, the accuracy of the FE results obtained from element sizes of 6 mm and below was approximately 80% and above. Minimal differences between the results of 6 mm and 2 mm element sizes were found. Furthermore, for element sizes of 2 mm and below, the computational time increased significantly and at some point convergence problems occurred. Therefore, in this study, a balance had to be struck between accuracy and computational efficiency. For every model, the mesh was refined until a solution was found and convergence occurred with minimum problems. For all the FE results based

on CDP model presented in this thesis, the size of the elements ranged from 2 to 6 mm with aspect ratio of 1.0 to 1.1.

7.6 Summary

The purpose of the numerical study presented in this study was to examine the efficiency and limitation of two FE material models (the concrete smeared cracking (CSC) and the concrete damaged plasticity (CDP)) in predicting the flexural and shear behaviour of UHPFRC beam and slab specimens. Both models were originally developed for reinforced concrete members. However, with some modifications, they were adapted here for UHPFRC. In the FE simulation, the concrete was modelled as a homogenous material and the physical presence of fibres were not feasible to model, and was ignored.

From the FE results, the suitability of the CSC model was found to be limited for UHPFRC. This model experienced severe convergence problems and provided results with poor accuracy, in particular, for predicting the post-peak behaviour of the concrete. This is because the model is primarily designed for reinforced concrete members. However, the suitability of the CDP model appeared to be more promising. The simulations from the CDP model replicated the load-deflection responses of the beam specimens in bending up until failure and the slab specimens in punching shear up until the peak strength. The CDP model was not capable of accurately predicting the post-peak response of the slab tests at the current modelling stage. The absence of randomly distributed fibres and crack propagation in the FE simulation with the complexity of punching shear failure is believed to have played a significant role in the poor prediction. Furthermore, a good correlation between the stress distribution contours obtained from the CDP model and the failure mechanism of the tested beam and slab specimens were observed. Overall, the CDP model appears to be promising for UHPFRC; nevertheless, improvement of this model is required before it can be used for predicting the full linear and nonlinear behaviour of the concrete.

It must be noted, the FE simulations often suffered from severe convergence difficulties. This was a significant issue encountered when first-order continuum reduced and fully integrated element types were used. These element types should be avoided for

UHPFRC or any other materials with high ductility behaviour in bending problems, as they are overly stiff, exhibit slow convergence, and provide poor accuracy results. However, to overcome these problems, first-order continuum incompatible mode element types can be used. This type reduces convergence problems and improves accuracy of bending problem simulations considerably. Furthermore, to ensure that the FE results were not subject to mesh dependency, mesh sensitivity analysis was carried out using incompatible mode element type in CDP model. Element sizes of 6 mm and smaller, appeared to predict the maximum flexural and punching shear loads of the concrete with good accuracy, 80% and above. Insignificant accuracy differences between the results of 6 mm and 2 mm element sizes were found.

In most design cases, the maximum load carrying capacity and corresponding deflection of a structural member are the main parameters required. The FE simulation based on CDP model was shown to predict both parameters of UHPFRC beam and slab specimens with an acceptable degree of accuracy. This is an important numerical finding for this concrete in structural design, in particular, for members where the ultimate flexural and punching shear loads are of concern. Finally, the good correlation between the FE simulation and experimental test data can be used to validate the accuracy of the experimental test setups designed in this thesis for the material characterisation and structural behaviour investigation of UHPFRC.

Chapter VIII: UHPFRC for Highway Bridge Applications

8.1 Introduction

The structural use of UHPFRC for highway bridge applications is still limited considering its superior properties. The main obstacles restricting the widespread use of this concrete in construction are:

- The high initial cost,
- Industry's reluctance to adopt a new material whose properties are perceived not fully understood, and
- The lack of recognised design standards.

The studies conducted in this research and presented in Chapters 3 to 7 have investigated various aspects of the first two obstacles shown above. In this chapter, the overall suitability of UHPFRC for highway bridge applications is assessed based on the findings of this thesis.

8.2 High Initial Cost

The high cost of the constituents combined with the method of manufacturing makes UHPFRC significantly expensive compared to normal concrete. The high content of cement, silica sand, superplasticisers and steel fibre in the mix contributes to the high initial cost considerably. A tonne of steel fibre costs approximately £3000-3500 and only 1% of steel fibres by volume in the mix were reported to cost more than the entire cement content (Kim et al. 2008). This means the cost of UHPFRC's raw materials are in a range of 3 to 5 times higher than normal concrete. Options to use cheaper type of fibres are available; however, to maintain the improved mechanical properties of the concrete, the fibre type and content is recommended to be steel and of 2% by volume in the mix. Therefore, the manufacturing method could be a good option in reducing the current price of the concrete.

The current production process of UHPFRC contributes significantly to the high initial cost. Storing UHPFRC members for at least 48 hours at high curing temperatures of 90 ^{o}C in factories is very expensive. This process contributes to the cost to increase by approximately 3 to 4 times compared to its cast in-situ normal applications. In total, the costs of UHPFRC precast members are approximately 10 to 15 times more expensive than normal concrete on a volumetric basis. Therefore, finding possible ways to reduce the cost of the concrete in the manufacturing process could be a good solution to minimise the cost of the concrete when it is used in large structures, i.e. cast in-situ highway bridge applications.

The investigation presented in Chapter 5 focused on the suitability of UHPFRC for cast in-situ applications. The results showed compressive strength gains for the 10, 20 and 30 ^{o}C cured UHPFRC specimens were much greater than conventional concrete at very early ages. The compressive strength gain at these curing temperatures after 2 days, were approximately 22, 63 and 84 MPa, respectively. Moreover, compressive strength for the concrete after 1 day for the 20 and 30 ^{o}C curing temperatures were 22 and 53 MPa, respectively. This early age strength gain of UHPFRC with ambient temperatures is considered to be of special importance. In particular, for cast in-situ UHPFRC highway bridge structures in stripping of formwork and opening the structure to traffic or allowing follow-on construction as early as 1 day after casting. It is desirable to develop concrete with sufficient strength within a short period of time; however, it is not a design requirement for concrete members to exhibit a compressive strength of 160 MPa within the first day of construction. Therefore, if construction allows 24 hours for casting, cast in-situ UHPFRC is possible in hot climates and is a good choice to minimise the cost of the concrete in construction. It must be noted that the three lower curing temperatures exhibited similar or even higher compressive and tensile flexural strengths compared to those cured at 90 ^{o}C after 2 months.

The significance of using the concrete in cast in-situ applications can reduce the current cost by 30%. It must be noted that this comparison was derived based on volumetric usage of the concrete when used in cast in-situ compared to precast concrete. Generally, precast concrete results in waste reduction. However, the waste that potentially occurs

during cast in-situ application of the concrete was not considered in the price comparison. Reducing the cost by this much may not appear convincing since the cost of the concrete at this stage is still 6 to 9 times higher than normal concrete. However, the high compressive and tensile flexural strength gains of the concrete at early ages, i.e. 7 days, can also be exploited in reducing member sizes compared to normal strength concrete. This can result in lower volumetric usage of UHPFRC and an overall lower material cost in the structure.

In general, large amounts of data were obtained in this study. The strength development of the UHPFRC at temperatures similar to typical site conditions were shown to be acceptable within 1 day after casting and matched those of precast production after 2 months. Considering the low maintenance costs of UHPFRC structures combined with high compressive and tensile flexural strengths with no conventional reinforcement requirement in members at lower cost than before, makes the concrete more economically competitive against normal concrete highway bridge structures.

8.3 Mechanical Properties

Despite a large number of research studies available on UHPFRC, the full structural behaviour, in particular, the punching shear behaviour is not fully understood. The lack of knowledge on punching shear capacity of UHPFRC is down to unavailability of appropriate test methods since the concrete behaves differently compared to normal concrete. This has also resulted in limited numerical modelling. Therefore, detailed studies on UHPFRC's punching shear behaviour for highway bridge applications are essential.

In Chapters 5 and 6 of this thesis, experimental investigations on the flexural and shear behaviours of the concrete were carried out. The results obtained here were validated using numerical modelling in Chapter 7. Furthermore, for implementation of the numerical modelling, material properties were required. Therefore, material characterisations were carried out in Chapters 3 and 4.

The flexural and shear behaviour of UHPFRC have been discussed extensively in this thesis. Form the flexural test results, specimens cured at the three lower curing temperatures appeared to exhibit similar strength and better ductility than those cured at 90 ^{o}C with time. Furthermore, the flexural failure behaviour of the concrete without conventional reinforcement was very similar to that of reinforced concrete members. Such findings are significant for cast in-situ application of this concrete, since flexural members can now be designed with no reinforcement, smaller cross section and much lower cost than ever realised before.

In addition, the results obtained from the punching shear tests of the UHPFRC notched slabs with no shear reinforcement were significant. The failure behaviour for UHPFRC slabs with basic control perimeters of equal and greater than 1.02d were reported to be ductile, similar to its flexural failure. The basic control perimeter for the concrete was shown to be reduced by half compared to normal concrete. These behaviours are beneficial for concrete members where punching shear failure is imminent and the option of heavy shear reinforcement is limited such as thin UHPFRC highway bridge decks.. Furthermore, a punching shear test was developed and proved to be suitable for the determination of this essential parameter of the concrete. The experimental investigation carried out here provides significant insight into the punching shear capacity of UHPFRC slabs. The results illustrate some of the advantages of using UHPFRC compared to normal concrete in highway bridge designs such as improvement in ductility, the ability of undergo significant deflection after peak strength and high load carrying capacity.

In the numerical modelling, an existing material model (CDP) was modified and used to simulate the structural behaviour of UHPFRC in both flexure and shear. The results obtained here were validated against experimental results obtained in Chapters 4, 5 and 6 and found with good agreement. The accuracy of the prediction shows the reliability and efficiency of the model in predicting the maximum flexural and shear load carrying capacity of the concrete, with errors no more than 20%. This finding is significant since in most design cases, the maximum load carrying capacity of a structural member is the main parameter required. Therefore, the CDP model can possibly be exploited for

predicting the failure load of UHPFRC members in highway bridge or any other applications.

The results reported in Chapters 3 and 4 provided full material characterisation of the concrete with a high degree of reliability. In particular, discovering an easy and cost effective non-destructive testing method such as UPV for future maintenance checks of UHPFRC highway bridge application is significant. The test methods developed and identified in here are crucial for the future development of this concrete in construction.

8.4 Summary

In this study, some of the factors restricting the use of UHPFRC in highway bridge applications were investigated. The high initial cost of the concrete was shown to be reduced when the current manufacturing process is changed from precast to cast in-situ construction. Furthermore, various test methods were developed and identified for the determination of the material and mechanical properties of the concrete. The applicability of these test methods were confirmed from the repeatability of the test results and validated using numerical modelling. The findings reported here provide significant insight on the excellent structural behaviour of UHPFRC for highway bridge applications at a lower cost than stated in the literature.

Chapter IX: Conclusions and Recommendations

9.1 Introduction

The main aim of this research was to highlight the suitability of ultra high performance fibre reinforced concrete (UHPFRC) for highway bridge applications. This has been achieved by conducting extensive experimental and numerical studies on various aspects of the concrete ranging from strength and cost to choice of construction method (cast in-situ applications).

The experimental study was carried out in two phases. In the first phase, the material properties of a specific UHPFRC mix, which was previously developed at the University of Liverpool (Le 2008), were obtained and used for implementation of numerical studies. The material properties were determined using various existing static and dynamic test methods. Furthermore, a number of new test methods were developed and used in this phase. Subsequently, numerical investigations were conducted using the well known finite element software, Abaqus, to predict the structural behaviour of UHPFRC beam and slab members in flexure and shear. The second phase of the experimental study focused primarily on the structural behaviour of beams and slabs members analysed in the numerical models. In this study, important findings on the flexural and shear behaviour of the concrete were obtained. The findings reported here can be applied in the structural design of UHPFRC highway bridge applications.

9.2 Conclusions

In this section, all the findings reported in this research are presented. For clarity, the conclusions have been separated into 5 sections, each focusing on the findings reported in Chapters 3 to 7.

9.2.1 Material characterisation

In this study, conventional test methods developed for normal concrete such as tensile splitting, flexural and compression tests were applied to define the stress-strain relationship of UHPFRC and UHPC in both tension and compression. The influence of

steel fibre content and age on these properties was also studied. The following conclusions were found:

- The existing test methods for normal concrete were found unreliable in determining the stress-strain relationship of UHPFRC in both tension and compression. In particular, for capturing the post-cracking behaviour of the concrete.

- In this study, uniaxial tensile and compressive test methods were developed and used successfully to determine the stress-strain relationships of the concretes. The consistency of the test results showed the reliability of both test methods.

- The influence of steel fibre content in UHPFRC on ductility and strength was found to be significant. Fibre content in the concrete contributed to the considerable ductility improvement in both tension and compression after the formation of microcracks and even beyond maximum strength. Furthermore, significant enhancement in the tensile strength and corresponding strain was also reported. The maximum tensile strength and corresponding strain for the concrete compared to those of UHPC were approximately 170 to 200% and 700% to 1700%, respectively. However, fibre content showed little effect on the compressive strength and modulus of elasticity of the concrete.

- The UHPC concrete exhibited brittle behaviour in both tension and compression and its failure mechanism was very sudden. The absence of fibres on the compressive strength and modulus of elasticity of this concrete was found to be insignificant, while its tensile behaviour was affected considerably.

- A circular shaped defect phenomenon on the surface of the failed UHPC specimens was observed, in particular, with the cylinder and beam specimens. This defect phenomenon was believed to have occurred due to the curing temperature of 90 ^{o}C and resulted in considerable loss of strength. Further studies regarding this are presented in Chapter 5.

- Both concretes have gained their maximum strength within 7 days and little improvement in strength and ductility was reported beyond this age.

- From the tests results reported here, a stress-strain relationship for this specific mix of UHPFRC was determined. This relationship is important and required for formulating and calibrating any potential constitutive material model for design purposes or FE modelling for the concrete.

9.2.2 Non-destructive testing

In this study, the potential use of two non-destructive testing methods to determine the values of the modulus of elasticity and Poisson's ratio of UHPFRC has been investigated. These methods are the ultrasonic pulse velocity (UPV) and resonant frequency testing techniques that are developed for normal concrete. Furthermore, reliability of a few empirical relationships to predict the modulus of elasticity of the concrete from its compressive strength was also studied. The results of the non-destructive testing methods and empirical relationships were validated against results from static compression tests and the following conclusions were found:

- Conventional compression transducers with a frequency of 2MHz used in the ultrasonic pulse velocity approach produced comparable results to static test values, with errors less than 10%. This method is potentially useful to study the elastic properties of this type of concrete.

- The resonant frequency testing technique is an alternative to the UPV method and can produce results with an acceptable degree of accuracy, with errors less than 14%. However, empirical relationships that exist for this method improves the results to errors of just 2%. This method of testing appears to be promising for UHPFRC; however, it is limited to laboratory specimen testing only. The size and shape of tested specimens are required to be cylinders or beams.

- Results from the empirical equations indicated good agreement compared to the static test results with errors less than 11%. However, the accuracy of these equations has to be studied on a larger number of test results.

- For the values of the Poisson's ratio, both non-destructive testing techniques were also in good agreement to the static test, with errors less than 14%.

- The results obtained here demonstrate the necessity of high frequency transducers in the UPV testing technique for UHPFRC. Furthermore, faster pulse velocities were also recorded for the concrete when compared to normal concrete test results reported by (Qixian and Bungey 1996). The requirements for high frequency transducers and results of higher pulse velocities for UHPFRC are linked to the steel fibre content and high density of the matrix.

- From the results reported, it is evident that the dynamic test results were satisfactory and comparable to the static tests results. The reliability of both non-destructive testing methods for UHPFRC was found to be acceptable, in particular, the UPV testing method. This method is easy to use, portable and appears to be the most reliable non-destructive testing method for this concrete. The findings reported here suggest that the UPV testing method can now be used with high certainty for the determination of the elastic properties of existing UHPFRC structures. One beneficial application can possibly be the periodic maintenance check of UHPFRC highway bridge structures.

9.2.3 UHPFRC cast in-situ application

In this study, extensive experimental work was carried out to investigate the suitability of UHPFRC for cast in-situ applications. This was done by studying the influence of various curing temperatures (10, 20, 30 and 90 ^{o}C) on the development of the compressive strength, first and maximum flexural loads and flexural toughness of UHPFRC and UHPC from an early age up to 360 days. The three lower curing temperatures were chosen to represent conditions that are likely to be encountered for cast in-situ applications, while the 90 ^{o}C curing temperature is currently used in the

precast production of UHPFRC components. The UHPC concrete was included to further investigate the effect of 90 ^{o}C curing temperature on the circular shaped phenomenon reported for the tensile tests in Chapter 3. Furthermore, a simple durability check for UHPFRC specimens cured at the different curing temperatures was also conducted. From this study, the following conclusions were found:

- For UHPFRC, the curing temperature was found to have a significant effect on the rate of compressive strength development. However, the effect varied depending on the curing time and temperature. The 90 ^{o}C curing temperature resulted in high early age strength development and ultimate strength within 5 days after casting. While the 10, 20 and 30 ^{o}C curing temperatures have provided sufficient compressive strength within 5 days and the strength development continued up until 360 days, matching the same or even higher strengths than those for the 90 ^{o}C cured specimens. Similar results due to the curing temperatures were reported for the UHPC specimens in compression.

- Flexural tensile behaviour for UHPFRC at early age was found to be dependent on the curing temperature. Generally, higher curing temperatures resulted in higher tensile flexural strengths and flexural toughness development with age. However, from 28 days onwards, better flexural behaviours were reported for the 30 ^{o}C cured specimens than those cured at 90 ^{o}C.

- The 90 ^{o}C curing temperature appeared to have an adverse effect on the flexural behaviours of both concretes, more specifically the UHPFRC first cracking flexural load and UHPC maximum flexural load. The tensile flexural strength and toughness development of the three lower curing temperatures for the UHPC specimens were found to be higher than those cured at 90 ^{o}C. Such findings were striking and had not been reported previously in the literature. Similar results from the tensile tests reported in Chapter 3 were also observed.

- To further investigate the poor flexural behaviour for the 90 ^{o}C cured specimens in both concretes, the failure surfaces of the UHPC specimens at all the different

curing temperatures were checked and a phenomenon with the 90 ^{o}C cured specimens was reported. This phenomenon appeared to be a significant defect in the concrete and have occurred due to thermal expansion of incorporated water in the core of the specimen due to the high temperature curing. As a result, hydraulic loading have formed microscopic areas of fracture and have caused loss of tensile flexural strength. This behaviour was limited to the 90 ^{o}C cured concretes and was more pronounced with the UHPC test results than those of UHPFRC. This finding is in contrast to the views reported in the literature stating that 90 ^{o}C curing temperature improves all the mechanical properties of the concrete.

- The flexural toughness of UHPFRC appeared to be highly dependent on the fibre content in the mix rather than curing temperatures. The toughness values reported for this concrete were 100 to 875 times larger than those of UHPC. This is a clear indication of improved ductility behaviour of UHPFRC due to its steel fibre content compared to conventional concrete. However, UHPFRC specimens of the lower curing temperatures appeared to have resulted in higher deflection values at first cracking and maximum flexural loads than those cured at 90 ^{o}C. Such behaviour is important in structural design and can be exploited in UHPFRC cast in-situ applications.

- The reliability of a relationship proposed in the AFGC recommendation for predicating the tensile strength of UHPFRC from its first cracking load in flexural test was investigated. Results reported for the uniaxial tensile strength in Chapter 3 were compared to the values obtained from this relationship and errors in a range of 15 to 20 % were observed. The accuracy might not seem poor, however, since the first cracking load was found to be influenced significantly by the 90 ^{o}C curing regime and this has not being considered in the relationship. The validity of the equation appears questionable.

- From visual inspection the durability of UHPFRC appeared to be significantly improved due to the high packing density of the composite and the steel fibre content was well protected in the concrete.

- The findings reported here, indicate cast in-situ applications of UHPFRC in warm climates, i.e. 30 ^{o}C exhibits approximately 70% of the compressive and tensile flexural strengths of precast components of the concrete within 7 days and even similar strength within 28 days. This shows the suitability of UHPFRC in cast in-situ applications if the construction programme allows the component to wait a little longer before being subject to design loading. Since the high cost of UHPFRC precast members are mainly determined due to energy consumption, storage and time during production, the findings reported here could have significant beneficial cost and environmental impact consequences. It also shows the suitability of the concrete for cast in-situ highway bridge applications at a lower material cost.

9.2.4 Punching shear strength

Studying the punching shear capacity of UHPFRC has been the subject of a number of studies in the literature. However, difficulties in determining this parameter were reported due to the occurrence of flexural failure prior to punching shear during testing. Therefore, in this study, an extensive experimental programme was carried out to develop a suitable test method to study the punching shear strength of UHPFRC slab specimens with minimal flexural influence. Results obtained in this study were used to investigate the relationship between punching shear load and angle, failure mode, failure behaviour and the value of the basic control perimeter of UHPFRC slab specimens under a high concentrated load. From this study, the following conclusions were found:

- A test method was designed and used successfully to study the punching shear strength of the concrete using notched slab specimens. The proposed test method incorporated a predefined shear notch in the slab specimens and used circular steel ring supports for boundary conditions. The shear notches and supporting

arrangement resulted in punching shear failure of the specimens with little or no flexural influence.

- As expected, the ultimate punching shear load was found to increase with greater punching shear angle with the exception of two test results. This behaviour is known as shear support enhancement, in which the punching shear capacity of the concrete increases proportionally with the increase of the punching shear angle due to extra enhancement from the compression struts of the concrete. The punching shear load was found to be the smallest at a punching shear angle of 28.2^{o} (basic control perimeter of approximately 2d). This is in close agreement to what has been reported for normal concrete (BS EN 1992-1-1 2004).

- The failure mode for each test were examined and the results showed that all the slabs had failed with a truncated cone shaped in the tensile side and a stub punching in the loaded side due to the load indenter. Such a failure mode is similar to typical punching shear failure reported for normal concrete (Mosley et al. 2007), and validates the accuracy of the test developed in this study.

- The failure behaviour for the slab specimens with punching shear angles equal and greater than 62^{o} (basic control perimeter of 0.53d and smaller) were found brittle, similar to a typical punching shear failure for normal concrete. However, the failure behaviour changed to a ductile mode for specimens with punching shear angles equal and smaller than 45^{o} (basic control perimeter of 1.02 and greater), similar to the flexural beam failure tests reported in Chapter 5. The improved ductile behaviour of these tests was provided by the fibre bridging effect along the shear failure planes in the concrete. As a result, the slab specimens could undergo greater deflection after the maximum load was attained. Such behaviour is a preferred failure mechanism for slabs in concrete designs.

- The findings reported on the ductile behaviour of the punching shear failure of UHPFRC slabs with no shear reinforcement are significant. The result illustrates

a reduction of the basic control perimeter of UHPFRC slabs by half compared to what has been specified in EC2 for conventional concrete.

- The improved ductile behaviour of the concrete in punching shear with its high tensile strength can be exploited to limit shear reinforcement in UHPFRC slab members to 1d. This behaviour is beneficial in the design of structures where punching shear failure is imminent and the option of heavy shear reinforcement is limited in the member such as thin UHPFRC highway bridge decks.

- In the literature, a number of empirical questions are proposed to predict the punching shear capacity of UHPFRC. However, these equations could not be verified here since the parameters investigated in this study were not considered in the equations. This study has shown that for any models to predict the punching shear strength of UHPFRC, the crack fibre bridging effect, and the punching shear angle are vital parameters that should be considered.

- The experimental investigation undertaken in this research program provides significant insight into the punching shear capacity of UHPFRC slabs. The results illustrate some of the advantages of using UHPFRC compared to normal concrete in highway bridge designs such as improvement in ductility, the ability of undergo significant deflection after peak strength and a reduction of the basic control perimeter by half (1d).

9.2.5 Finite element modelling for UHPFRC

In this study, a numerical investigation using Abaqus was carried out to examine the efficiency and limitation of two FE material models (the concrete smeared cracking (CSC) and the concrete damaged plasticity (CDP)) for predicting the flexural and shear behaviour of various UHPFRC specimens. Both models are originally developed for reinforced concrete members. However, with some modifications they were adapted here for UHPFRC. In the FE study, the concrete was modelled as a homogenous material and the physical presences of fibres were not feasible to model, and were ignored. In this study, the following findings were reported:

- The suitability of the CSC model was found to be limited for UHPFRC. This model experienced severe convergence problems and provided results with poor accuracy, in particular, for predicting the post-peak behaviour of the concrete. This is because the model is primarily designed for reinforced concrete members.

- The suitability of the CDP model appeared to be more promising. Results obtained from this model replicated the load-deflection responses of beam specimens in bending until failure and the slab specimens in punching shear up until the peak strength. This model was not capable of accurately predicting the post-peak response of the slab tests at the current modelling stage. The absence of randomly distributed fibres and crack propagation in the FE simulation with the complexity of punching shear failure is believed to have played a significant role in the poor prediction of the post-peak response.

- Good correlation between the stress distribution contour obtained in the CDP model and the failure mechanism of the beam and slab specimens reported in Chapters 4, 5 and 6 were observed. From the results obtained here, the CDP model appears to be promising for UHPFRC. However, improvement in this model is required for more accurate predictions.

- During the analysis, the FE simulations often suffered from severe convergence difficulties when first-order continuum reduced and fully integrated element types were used. These types of elements should be avoided for UHPFRC or any other materials with high ductility behaviour in bending problems, as they are overly stiff, exhibit slow convergence and provide poor accuracy results. However, first-order continuum incompatible mode element type was found to minimise these problems. This type is recommended to be used for UHPFRC since it reduces convergence problems and improves accuracy in bending problem simulations.

- From mesh sensitivity analyses, element sizes of 6 mm and below was found to predict the experimental test results with good accuracy, 80% and above.

Minimal accuracy differences between the results of 6 mm and 2 mm element sizes were found for this concrete.

- In most design cases, the maximum load carrying capacity and corresponding deflection of a structural member are the main parameters required. The FE simulation based on CDP model was shown to predict both parameters of UHPFRC beam and slab specimens with an acceptable degree of accuracy. This is an important numerical finding for this concrete in structural design, in particular, for members where the ultimate flexural and punching shear loads are of great concerns.

- Finally, the good correlation between the FE simulation and experimental test data validates the accuracy of the experimental test setups designed in this thesis for material characterisation and the structural behaviour investigation of UHPFRC.

9.3 Recommendations for Future Work

Due to the timeframe and resource limitations of this study, it was not possible to investigate a number of potential topics. These are recommended below for future research:

- To confirm the reliability of the non-destructive test methods described here, further studies are recommended for a range of UHPFRC mixes containing different volumes of steel fibres, possibly higher volume than 2%.

- The defect phenomenon and hypothesis reported in Chapters 3 and 5 are in contrast to what have been reported in the literature. Therefore, further studies to investigate the cause of the defect and loss of tensile flexural strength due to 90 ^{o}C curing temperature would be of great interest.

- The validity of the relationship proposed in the AFGC recommendation to determine the tensile strength of UHPFRC from the first cracking load in flexural

test needs to be verified. This is because the first cracking load is highly influenced by the curing regime and this parameter has not been considered in the relationship.

- Further experimental investigations on larger scale UHPFRC slabs with various thicknesses using the punching shear test developed in this study are required for future applications of this concrete in highway bridge structures when punching shear capacity is of great concerns.

- Further experimental studies on the punching shear behaviour of the concrete cured at ambient temperature is required to highlight the punching shear capacity of the concrete in cast in-situ application.

- From the punching shear test, it was evident that the punching shear capacity of the concrete is highly dependent on the crack fibre bridging effect and basic control perimeter (angle of punching shear). Therefore, any model to predict the punching shear capacity of UHPFRC should consider both parameters.

  The CDP model in Abaqus appears to predict the flexural and shear behaviour of UHPFRC members with an acceptable degree of accuracy. However, further improvement of this model, i.e. modelling the fibre content and crack propagations, are required before they can be used in predicting the full linear and nonlinear behaviours of the concrete with better accuracy.

References

Aarup, B. 2007. CRC–Applications of fibre reinforced high performance concrete. Concrete Plant International CPI**,** 1-10.

Abaqus theory manual 2010. Dassault Systèmes Simulia Corp, Providence, RI, USA.

ACI Committee 308 2001. (Reapproved 2008):Guide to curing concrete reported by ACI committee 308. American Concrete Institute, 31.

ACI Committee 318 2011. Building code requirements for structural concrete (ACI 318-11). American Concrete Institute, 509.

ACI Committee 363 1997. (Reapproved 1997):State-of-the-art report on high-strength concrete (ACI 363-92). American Concrete Institute, 55.

Acker, P. & Behloul, M. 2004. Ductal® technology: A large spectrum of properties, a wide range of applications. Proceedings of the International Symposium on Ultra High Performance Concrete. Kassel, Germany. Kassel University Press GmbH, 11-23.

Ahlborn, T. M.Peuse, E. J. & Misson, D. L. 2008. Ultra-high performance concrete for Michigan bridges material performance–Phase I. Center for Structural Durability Michigan Tech Transportation Institute, 190.

Ahlborn, T. M. & Steinberg, E. P. 2012. An overview of UHPC effort through the north American working group. Proceedings of Hipermat 2012, 3rd International Symposium on UHPC and Nanotechnology for High Performance Construction Materials. Kassel, Germany. Kassel University Press GmbH, 43-50.

Aitcin, P. C. 2000. Cements of yesterday and today: Concrete of tomorrow. Cement and Concrete Research, 30**,** 1349-59.

Aitcin, P. C.Delagrave, Y. & Beck, R. 2000. A 100-m high prefabricated concrete pole: why not? Institute of Electrical and Electronics Engineers**,** 365-74.

Alexander, K. & Taplin, J. H. 1962. Concrete strength, paste strength, cement hydration and the maturity rule. Australian journal of applied science, 13**,** 277-84.

Alexanderson, J. 1973. Strength losses in heat curing-causes and countermeasures. Behavior of Concrete Under Temperature Extremes**,** 91-108.

Alford, N. & Birchall, J. 1985. The properties and potential applications of macro-defect-free cement. Proceedings of the Symposium on Very High Strength Cement-based Materials. Materials Research Society, 265-76.

Allos, A. E. & Martin, L. H. 1981. Factors affecting Poisson's ratio for concrete. Building and environment, 16**,** 1-9.

An, V. V. T. & Ludwig, H.-M. 2012. Proportioning optimization of uhpc containing rice husk ash and Ground Granulated Blast Furnace Slag. Proceedings of Hipermat 2012, 3rd International Symposium on UHPC and Nanotechnology for High Performance Construction Materials. Kassel, Germany Kassel University Press GmbH, 196-205.

Andrade, M.Frias, M. & Aarup, B. 1996. Durability of ultra-high strength concrete: Compact reinforced composite. BHP96 Fourth International Symposium on Utilisation on High Strength/High Performance Concrete. Paris, France. 529-34.

Ashour, S. A.Hasanain, G. I. S. & Wafa, F. F. 1992. Shear behavior of high-strength fiber reinforced concrete beams. ACI Structural Journal, 89**,** 176-84.

ASTM C78-10 2010. Standard test method for flexural strength of concrete (using simple beam with third-point loading). American Society for Testing and Materials Standards, 4.

ASTM C215-08 2008. Standard test method for fundamental transverse, longitudinal, and torsional frequencies of concrete specimens. American Society for Testing and Materials Standards, 7.

ASTM C293-94 1994. Standard test method for flexural strength of concrete (using simple beam with center-point loading). American Society for Testing and Materials Standards, 3.

ASTM C469-02 2002. Standard test method for static modulus of elasticity and Poisson's ratio of concrete in compression. American Society for Testing and Materials Standards, 5.

ASTM C496-96 1996. Standard test method for splitting tensile strength of cylindrical concrete specimens. American Society for Testing and Materials Standards, 4.

ASTM C597-09 2009. Standard test method for pulse velocity through concrete. American Society for Testing and Materials Standards, 4.

ASTM C1018-97 1997. Standard test for flexural toughness and first-crack strenght of fiber reinforced concrete (using beam with thrid point loading). American Society for Testing and Materials Standards, 8.

ASTM C1550-03 2003. Standard test method for flexural toughness of fiber reinforced concrete (using centrally loaded round panel). American Society for Testing and Materials Standards, 9.

Bache H, H. 1981. Densified cement/ultra-fine particle-based materials. Second International Conference on Superplasticizers in Concrete. Ottawa, Canada**,** 1-35.

Bache H, H. 1987. Introduction to compact reinforced composite. Nordic concrete research**,** 19-33.

Banthia, N. & Mindess, S. 1996. Impact resistance of steel fiber reinforced concrete. ACI Materials Journal, 93**,** 472-79.

Barnett, S.Lataste, J.-F.Parry, T.Millard, S. & Soutsos, M. 2010. Assessment of fibre orientation in ultra high performance fibre reinforced concrete and its effect on flexural strength. Materials and Structures, 43**,** 1009-23.

Barnett, S. J.Soutsos, M. N.Millard, S. G. & Bungey, J. H. 2006. Strength development of mortars containing ground granulated blast-furnace slag: Effect of curing

temperature and determination of apparent activation energies. Cement and Concrete Research, 36**,** 434-40.

Bayard, O. & Plé, O. 2003. Fracture mechanics of reactive powder concrete: material modelling and experimental investigations. Engineering Fracture Mechanics, 70**,** 839-51.

Bayasi, Z. 1992. Effects of fly ash on silica fume concrete. Concrete International, 14**,** 52-54.

Behloul, M. & Batoz, J. 2008. Ductal® applications over the last Olympiad. Proceedings of the Second International Symposium on Ultra High Performance Concrete. Kassel, Germany. Kassel University Press GmbH, 855-62.

Behloul, M.Ricciotti, R.Ricciotti, R. F.Pallot, P. & Leboeuf, J. 2008. Ductal® Pont du Diable footbridge, France. International fib symposium. Amsterdam, Holland. Taylor & Francis Ltd, 335-40.

Benson, S. & Karihaloo, B. 2005a. CARDIFRC®-Development and mechanical properties. Part I: Development and workability. Magazine of Concrete Research**,** 347-52.

Benson, S. D. P. & Karihaloo, B. L. 2005b. CARDIFRC®-Development and mechanical properties. Part III: Uniaxial tensile response and other mechanical properties. Magazine of Concrete Research**,** 433–43.

BFUP AFGC 2002. Ultra high performance fibre-reinforced concretes. Interim recommendations. AFGC/SETRA working group 142.

Bierwagen, D.Abu-Hawash, A.Moore, B. & Keierleber, B. 2009. Ultra-high performance concrete in Iowa. HPC Bridge Views**,** 1-13.

Birchall, J.Howard, A. & Kendall, K. 1981. Flexural strength and porosity of cements. Nature**,** 388-90.

Blais, P. Y. & Couture, M. 1999. Precast, prestressed pedestrian bridge-world's first reactive powder concrete structure. PCI Journal, 44**,** 60-71.

Bonneau, O. 1997. Mechanical properties and durability of two industrial reactive powder concretes. ACI Materials Journal, 94**,** 286-90.

Bonneau, O.Poulin, C.Dugat, J.Richard, P. & Aitcin, P. C. 1996. Reactive powder concretes: From theory to practice. Concrete International-Design and Construction, 18**,** 47-49.

Bonneau, O.Vernet, C.Moranville, M. & Aïtcin, P.-C. 2000. Characterization of the granular packing and percolation threshold of reactive powder concrete. Cement and Concrete Research, 30**,** 1861-67.

Brühwiler, E. & Denarié, E. 2008. Rehabilitation of concrete structures using ultra-high performance fibre reinforced concrete. Proceeding of the Second International Symposium on Ultra High Performance Concrete. Kassel, Germany. Kassel University Press GmbH, 895-902.

BS 1881-121 1983. Testing concrete-Part 121: Method for determination of static modulus of elasticity in compression. British Standards Institution, 12.

BS 1881-203 1986. Testing concrete-Part 203: Recommendations for measurement of velocity of ultrasonic pulses in concrete. British Standards Institution, 24.

BS 1881-209 1990. Testing concrete-Part 209: Recommendations for the measurement of dynamic modulus of elasticity. British Standards Institution, 10.

BS EN 1992-1-1 2004. Eurocode 2: Design of concrete structures-Part 1-1: General rules and rules for buildings. British Standards Institution, 230.

BS EN 12390-3 2009. Testing hardened concrete-Part 3: compressive strength of test specimens. British Standards Institution, 22.

BS EN 12390-5 2009. Testing hardened concrete-Part 5: Flexural strength of test specimens. British Standards Institution, 14.

BS EN 12390-6 2009. Testing hardened concrete-Part 6: Splitting tensile strength of test specimens. British Standards Institution, 14.

BS EN 12504-4 2004. Testing concrete-Part 4: Determination of ultrasonic pulse velocity. British Standards Institution, 18.

BS EN 14651:2005+A1:2007 2008. Test method for metallic fibre concrete. Measuring the flexural tensile strength (limit of proportionality (LOP), residual). British Standards Institution, 20.

Bungey, J. H.Millard, S. G. & Grantham, M. 2006. Testing of concrete in structures. Taylor & Francis, 4th Edition**,** 352.

C. N. C ELECTRONICS LTD 1989. Pundit manual for use with the portable ultrasonic non-destructive digital indicating tester. *In:* HOLMES ROAD, L. (ed.).

Carpinteri, A. & Chiaia, B. 2002. Embrittlement and decrease of apparent strength in large-sized concrete structures. Sadhana, 27**,** 425-48.

Chan, Y.-W. & Chu, S.-H. 2004. Effect of silica fume on steel fiber bond characteristics in reactive powder concrete. Cement and Concrete Research, 34**,** 1167-72.

Chanvillard, G. & Rigaud, S. 2003. Complete characterization of tensile properties of ductal UHPFRC according to the French recommendations. RILEM Publications SARL, 21-34.

Chen, L. & Graybeal, B. 2012. Modeling structural performance of ultrahigh performance concrete I-girders. Journal of Bridge Engineering, 17**,** 754-64.

Chen, L. & Graybeal, B. A. 2010. Finite element analysis of ultra-high performance concrete: Modeling structural performance of an AASHTO type II girder and a 2nd generation Pi-girder. 198.

Cheng, M. Y.Parra-Montesinos, G. J. & Shield, C. K. 2010. Shear strength and drift capacity of fiber-reinforced concrete slab-column connections subjected to biaxial displacements. JOURNAL OF STRUCTURAL ENGINEERING, 136**,** 1078-88.

Cheyrezy, M. 1999. Structural applications of RPC. Concrete, 33**,** 20-23.

Cheyrezy, M.Maret, V. & Frouin, L. 1995. Microstructural analysis of RPC (reactive powder concrete). Cement and Concrete Research, 25**,** 1491-1500.

Collepardi, S.Coppola, L.Troli, R. & Collepardi, M. 1997. Mechanical properties of modified reactive powder concrete. ACI Special Publications, 173**,** 1-22.

Cousins, T.Roberts-Wollmann, C. & Sotelino, E. 2008. UHPC deck panels for rapid bridge construction and long term durability. Proceedings of the International Symposium on Ultra High Performance Concrete. Kassel, Germany. Kassel University Press GmbH, 699-705.

Crisfield, M. 1986. Snap-through and snap-back response in concrete structures and the dangers of under-integration. International Journal for Numerical Methods in Engineering, 22**,** 751-67.

de Graft-Johnson, J. W. S. & Bawa, N. S. 1969. Effect of mix proportion, water-cement ratio, age and curing conditions on the dynamic modulus of elasticity of concrete. Building Science, 3**,** 171-77.

De Larrard, F.Belloc, A.Renwez, S. & Boulay, C. 1994. Is the cube test suitable for high performance concrete? Materials and Structures, 27**,** 580-83.

di Prisco, M.Lamperti, M.Lapolla, S. & Khurana, R. 2008. HPFRCC thin plates for precast roofing. 675-82.

Dils, J.De Schutter, G.Boel, V. & Braem, E. 2012. Influence of vacuum mixing on the mechanical properties of UHPC. Proceedings of Hipermat 2012, 3rd International Symposium on UHPC and Nanotechnology for High Performance Construction Materials. Kassel, Germany. Kassel University Press GmbH, 241-48.

Dowd, W. & Dauriac, C. E. 1996. Reactive powder concrete. The Construction Specifier, 49**,** 47-52.

Dugat, J.Roux, N. & Bernier, G. 1996. Mechanical properties of reactive powder concretes. Materials and Structures, 29**,** 233-40.

El-Ashkar, N. H. & Kurtis, K. E. 2006. A new, simple, practical method to characterize toughness of fiber-reinforced cement-based composites. ACI Materials Journal, 103**,** 33-44.

Fall, M.Célestin, J. C.Pokharel, M. & Touré, M. 2010. A contribution to understanding the effects of curing temperature on the mechanical properties of mine cemented tailings backfill. Engineering Geology, 114**,** 397-413.

Fehling ESchmidt MBunje K & Schreiber W 2004. Ultra high performance composite bridge across the river Fulda in Kassel. Proceedings of the International Symposium on Ultra High Performance Concrete. Kassel, Germany. Kassel University Press GmbH, 69-75.

Ferrara, L.Bamonte, P.Caverzan, A.Musa, A. & Sanal, I. 2012. A comprehensive methodology to test the performance of Steel Fibre Reinforced Self-Compacting Concrete (SFR-SCC). Construction and Building Materials, 37**,** 406-424.

Freyssinet, M. E. 1936. Cement and Concrete Manufacture. 71.

Ghafari, E.Costa, H.Júlio, E.Portugal, A. & Durães, L. 2012. Optimization of UHPC by adding nanomaterials. Proceedings of Hipermat 2012, 3rd International Symposium on UHPC and Nanotechnology for High Performance Construction Materials. Kassel, Germany. Kassel University Press GmbH, 71-78.

Glaubitt, A. & Middendorf, B. 2008. Non-destructive ultrasonic testing methods for quality control of UHPC. FEHLING, E., SCHMIDT, M. & STÜRWALD, S., eds. Proceedings of the Second International Symposium on Ultra High Performance Concrete Kassel, Germany. Kassel University Press GmbH, 319-26.

Gowripalan, N. & Gilbert, R. 2000. Design guidelines for ductal prestressed concrete beams. School of Civil and Environmental Engineering,The University of New South Wales, 53.

Graybeal, B. 2007a. Analysis of an ultra-high performance concrete two-way ribbed bridge deck slab. TECHBRIEF. FHWA-HRT-07-055, FHWA, US Department of Transportation, 4.

Graybeal, B. 2008. UHPC in the U.S. highway transportation system. FEHLING, E., SCHMIDT, M. & STÜRWALD, S., eds. Proceedings of the Second International Symposium on Ultra High Performance Concrete. Kassel University, Germany. Kassel University Press GmbH, 11-17.

Graybeal, B. A. 2005. Characterization of the behavior of ultra-high performance concrete. PhD, University of Maryland**,** 360.

Graybeal, B. A. 2006. Material property characterization of ultra-high performance concrete. Federal Highway Administration, 186.

Graybeal, B. A. 2007b. Compressive behavior of ultra-high-performance fiber-reinforced concrete. ACI Materials Journal, 4**,** 146-52.

Grohmann, M. & Zimmermann, G. 2008. UHPC free form design with pneumatic formwork. Proceeding of the Second International Symposium on Ultra High Performance Concrete. Kassel, Germany. Kassel University Press GmbH, 871-78.

Gunes, O.Yesilmen, S.Gunes, B. & Ulm, F. J. 2012. Use of UHPC in bridge structures: Material modeling and design. Advances in Materials Science and Engineering, 2012**,** 1-12.

Habel, K. 2004. Structural behaviour of elements combining ultra-high performance fibre reinforced concretes (UHPFRC) and reinforced concrete. PhD, École Polytechnique Federale De Lausanne**,** 196.

Habel, K.Charron, J. P.Braike, S.Hooton, R. D.Gauvreau, P. & Massicotte, B. 2008. Ultra-high performance fibre reinforced concrete mix design in central Canada. Canadian Journal of Civil Engineering, 35**,** 217-24.

Habel, K.Viviani, M.Denarié, E. & Brühwiler, E. 2006. Development of the mechanical properties of an ultra-high performance fiber reinforced concrete (UHPFRC). Cement and Concrete Research, 36**,** 1362-70.

Hajar, Z.Lecointre, D.Simon, A. & Petitjean, J. 2004. Design and construction of the world first ultra-high performance concrete road bridges. Proceedings of the International Symposium on Ultra High Performance Concrete. Kassel, Germany. Kassel University Press GmbH, 39-48.

Hansen, B. 2009. ASCE's infrastructure report card gives nation a D, estimate cost at $2.2 Trillion. ASCE News, 34**,** 1-4.

Harajli, M. H.Maalouf, D. & Khatib, H. 1995. Effect of fibers on the punching shear strength of slab-column connections. Cement and Concrete Composites, 17**,** 161-70.

Harris, D. K. 2004. Characterization of punching shear capacity of thin UHPC plates. PhD Virginia Polytechnic Institute and State University**,** 146.

Harris, D. K. & Roberts-Wollmann, C. L. 2008. Characterization of punching shear capacity of thin ultra-high performance concrete slabs. Proceedings of the International Symposium on Ultra High Performance Concrete. Kassel, Germany. Kassel University Press GmbH, 727-34.

Hassan, A. M. T. & Jones, S. W. 2012. Non-destructive testing of ultra high performance fibre reinforced concrete (UHPFRC): A feasibility study for using ultrasonic and resonant frequency testing techniques. Construction and Building Materials, 35**,** 361-67.

Hassan, A. M. T.Jones, S. W. & Mahmud, G. H. 2012. Experimental test methods to determine the uniaxial tensile and compressive behaviour of ultra high performance fibre reinforced concrete (UHPFRC). Construction and Building Materials, 37**,** 874-82.

Higashiyama, H.Ota, A. & Mizukoshi, M. 2011. Design equation for punching shear capacity of SFRC slabs. International Journal of Concrete Structures and Materials, 5**,** 35-42.

Hillerborg, A.Modéer, M. & Petersson, P. E. 1976. Analysis of crack formation and crack growth in concrete by means of fracture mechanics and finite elements. Cement and Concrete Research, 6**,** 773-81.

Hirschi, T. & Wombacher, F. 2008. Influence of different superplasticizers on UHPC. Proceeding of the Second International Symposium on Ultra High Performance Concrete. Kassel, Germany. kassel university press GmbH, 77-84.

Hjorth, L.Alford, N. M. N.Mangabhai, R.Hirsch, P.Moir, G.Jefferis, S.Blundell, R.Kelly, A.Defosse, C. & Sing, K. 1983. Development and application of high-density cement-based materials [and discussion]. Philosophical Transactions of the Royal Society of London. Series A, Mathematical and Physical Sciences, 310**,** 167-73.

Holschemacher, K.Mueller, T. & Ribakov, Y. 2010. Effect of steel fibres on mechanical properties of high-strength concrete. Materials & Design, 31**,** 2604-15.

Hong, K. N.Kang, S. T.Kim, S. W.Park, J. J. & Han, S. H. 2010. Material properties of air-cured ultra-high-performance steel-fiber-reinforced concrete at early ages. International Journal of the Physical Sciences, 5(17)**,** 2622-34.

Imam, M.Vandewalle, L.Mortelmans, F. & Van Gemert, D. 1997. Shear domain of fibre-reinforced high-strength concrete beams. Engineering Structures, 19**,** 738-47.

Jin, X. & Li, Z. 2001. Dynamic property determination for early-age concrete. ACI Materials Journal, 98**,** 365-70.

Joh, C.Hwang, H.Choi, E.Park, J. J. & Kim, B.-S. 2008. Punching shear strength estimation of UHPC slabs. Proceedings of the International Symposium on Ultra High Performance Concrete. Kassel, Germany. Kassel University Press GmbH, 719-26.

Jones, R. 1962. Non-destructive testing of concrete. Cambridge University Press, 1st Edition**,** 103.

JSCE-SF4 1984. Method of test for flexural strength and flexural toughness of steel fibre reinforced concrete. Japanese Society of Civil Engineers, 4.

JSCE-USC 2006. Guideline for concrete NO.9: Recommendations for design and construction of ultra high strength fiber reinforced concrete structures. 106.

Kamen, A.Denarie, E. & Bruhwiler, E. 2007. Thermal effects on physico-mechanical properties of ultra-high-performance fiber-reinforced concrete. ACI Materials Journal, 104**,** 415-23.

Kang, S.-T. & Kim, J.-K. 2011. The relation between fiber orientation and tensile behavior in an ultra high performance fiber reinforced cementitious composites (UHPFRCC). Cement and Concrete Research, 41**,** 1001-14.

Kang, S. T.Lee, B. Y.Kim, J.-K. & Kim, Y. Y. 2011. The effect of fibre distribution characteristics on the flexural strength of steel fibre-reinforced ultra high strength concrete. Construction and Building Materials, 25**,** 2450-57.

Kim, D.Naaman, A. E. & El-Tawil, S. 2008. High tensile strength strain hardening FRC composites with less than 2% fiber content. Proceeding of the Second International Symposium on Ultra High Performance Concrete. Kassel, Germany. Kassel University Press GmbH, 169-76.

Kowald, T.Trettin, R.Dorbaum, N.Stadler, T. & Jian, X. 2008. Influence of carbon nanotubes on the micromechanical properties of a model system for ultra-high performance concrete. Proceeding of the Second International Symposium on Ultra High Performance Concrete. Kassel, Germany. Kassel University Press GmbH, 129-34.

Kupfer, H. B. & Gerstle, K. H. 1973. Behavior of concrete under biaxial stresses. Journal of the Engineering Mechanics Division, 99**,** 853-866.

Kwak, Y. K.Eberhard, M. O.Kim, W. S. & Kim, J. 2002. Shear strength of steel fiber-reinforced concrete beams without stirrups. ACI Structural Journal, 99**,** 530-38.

Lafarge. 2012. *Ductal® -structural elements.* *http://www.ductal-lafarge.com/wps/portal/ductal/1-About_Ductal* [Online]. [Accessed 10-09-2012].

Lafarge March 2009. Ductal® in evidence. 8.

Lappa, E. S. 2007. High strength fibre reinforced concrete: static and fatigue behaviour in bending. PhD, Delft University of Technology**,** 236.

Le, T. 2008. Ultra high performance fibre reinforced concrete paving flags. PhD, University of Liverpool**,** 387.

Le, T.Soutsos, M.Millard, S. & Barnett, S. 2007. UHPFRC–Optimisation of mix proportions. Proceedings of Concrete Platform, Belfast Queen's University of Belfast 339–48.

Le, T.Soutsos, M.Millard, S. & Kang, K. 2008. Structural behaviour of a UHPFRC flag pavement. Second International Symposium on Ultra High Performance Concrete. 663-70.

Lee, J. & Fenves, G. 1998. Plastic-damage model for cyclic loading of concrete structures. Journal of Engineering Mechanics, 124**,** 892-900.

Leung, C. K. Y. 2009. Selective use of high performance cementitious composites in concrete structures. Key Engineering Materials, 400**,** 27-36.

Leung, C. K. Y. & Pheeraphan, T. 1995. Microwave curing of Portland cement concrete: experimental results and feasibility for practical applications. Construction and Building Materials, 9**,** 67-73.

Li, V. C. & Leung, C. K. Y. 1992. Steady-state and multiple cracking of short random fiber composites. Journal of Engineering Mechanics, 118**,** 2246-64.

Li, Z.Li, F.Chang, T. P. & Mai, Y.-W. 1998. Uniaxial tensile behavior of concrete reinforced with randomly distributed short fibers. ACI Materials Journal, 95**,** 564-74.

Lohaus. LGrünberg. JLindschulte. N & Kromminga. S 2012. Experimental analysis and numerical simulation of ultra-high-performance concrete tube columns with a steel sheetwrapping for large sized truss structures. Proceedings of Hipermat 2012, 3rd International Symposium on UHPC and Nanotechnology for High Performance Construction Materials. Kassel, Germany. Kassel University Press GmbH, 741-48.

Lu, X. & Hsu, C.-T. T. 2006. Behavior of high strength concrete with and without steel fiber reinforcement in triaxial compression. Cement and Concrete Research, 36**,** 1679-85.

Lubliner, J.Oliver, J.Oller, S. & Oñate, E. 1989. A plastic-damage model for concrete. International Journal of Solids and Structures, 25**,** 299-326.

Ma, J.Dehn, F.Tue, N.Orgass, M. & Schmidt, D. 2004. Comparative investigations on ultra-high performance concrete with and without coarse aggregates. Proceedings of the International Symposium on Ultra High Performance Concrete. Kassel, Germany. Kassel University Press GmbH, 205-12.

Mahmud, G.Yang, Z. & Hassan, A. 2012. An investigation on size effect for ultra high performance steel fibre reinforced concrete (UHPSFRC) beams using finite element method. the 20th Annual Conference on Computational Mechanics in Engineering. Manchester, UK. University of Manchester, 47-50.

Majdzadeh, F. 2003. Fracture toughness of hybrid fiber reinforced self-compacting concrete. MSc, University of British Columbia**,** 147.

Malhotra, V. M. & Carino, N. J. 2004. Handbook on nondestructive testing of concrete. MALHOTRA, V. M. & CARINO, N. J. (eds.). CRC Press, 2nd Edition**,** 384.

Mallat, A. & Alliche, A. 2011. A modified tensile test to study the behaviour of cementitious materials. Strain, 47**,** 499-504.

Malm, R. 2009. Predicting shear type crack initiation and growth in concrete with non-linear finite element method. PhD, Linköping University**,** 64.

Mansur, M.Ong, K. & Paramasivam, P. 1986. Shear strength of fibrous concrete beams without stirrups. Journal of Strucutural Engineering, 112**,** 2066-79.

Matsubara, N.Ohno, T.Sakai, G.Watanabe, Y.Ishii, S. & Ashida, M. 2008. Application of a new type of ultra high strength fiber reinforced concrete to a prestressed concrete bridge. Proceedings of the Second International Symposium on Ultra High Performance Concrete. Kassel, Germany. Kassel University Press GmbH, 787-94.

Maya, L. F.Fernández Ruiz, M.Muttoni, A. & Foster, S. J. 2012. Punching shear strength of steel fibre reinforced concrete slabs. Engineering Structures, 40**,** 83-94.

Mesbah, H. A.Lachemi, M. & Aitcin, P. C. 2002. Determination of elastic properties of high-performance concrete at early ages. ACI Materials Journal, 99**,** 37-41.

Millard, S. G.Molyneaux, T. C. K.Barnett, S. J. & Gao, X. 2009. Dynamic enhancement of blast-resistant ultra high performance fibre reinforced concrete under flexural and shear loading. International Journal of Impact Engineering, 37**,** 405-13.

Moreillon, L.Nseir, J. & Suter, R. 2012. Shear and flexural strength of thin UHPC slabs. Proceedings of Hipermat 2012, 3rd International Symposium on UHPC and Nanotechnology for High Performance Construction Materials. Kassel, Germany. Kassel University Press GmbH, 748-56.

Morris, A. D. & Garrett, G. G. 1981. A comparative study of the static and fatigue behaviour of plain and steel fibre reinforced mortar in compression and direct tension. International Journal of Cement Composites and Lightweight Concrete, 3**,** 73-91.

Mosley, W. H.Bungey, J. H. & Hulse, R. 2007. Reinforced concrete design to Eurocode 2. Palgrave MacMillan. 6th Edition**,** 408.

Mu, B. & Meyer, C. 2003. Bending and punching shear strength of fiber-reinforced glass concrete slabs. ACI Materials Journal-American Concrete Institute, 100**,** 127-32.

Muttoni, A. 2008. Punching shear strength of reinforced concrete slabs without transverse reinforcement. ACI Structural Journal, 105**,** 440-50.

Naaman, A. E. & Wille, K. 2012. The Path to ultra-high performance fiber reinforced concrete (UHP-FRC): Five decades of progress. Proceedings of Hipermat 2012, 3rd International Symposium on UHPC and Nanotechnology for High Performance Construction Materials. Kassel, Germany. Kassel University Press GmbH, 3-13.

Narayanan, R. & Darwish, I. 1987. Use of steel fibers as shear reinforcement. ACI Structural Journal, 84**,** 216-27.

Neville, A. M. 2012. Properties of concrete. Prentice Hall, 5th Edition**,** 846.

Nguyen-Minh, L.Rovňák, M.Tran-Quoc, T. & Nguyenkim, K. 2011. Punching shear resistance of steel fiber reinforced concrete flat slabs. Procedia Engineering, 14**,** 1830-37.

Nielsen, C. V. 1998. Triaxial behavior of high-strength concrete and mortar. ACI Materials Journal, 95**,** 144-51.

Nilson, A. H.Darwin, D. & Dolan, C. W. 2003. Design of concrete structures. McGraw Hill, 13th Edition**,** 779.

Odler, I.Yudenfreund, M.Skalny, J. & Brunauer, S. 1972. Hardened portland cement pastes of low porosity III. Degree of hydration. Expansion of paste. Total porosity. Cement and Concrete Research, 2**,** 463-80.

Orange, G.Dugat, J. & Acker, P. 2000. Ductal®: New ultra high performance concretes. Damage resistance and micromechanical analysis. Fifth International RILEM Symposium on Fibre-Reinforced Concrete (FRC). 781-90.

Park HUlm F-J & Chuang E 2003. Model-based optimization of ultra high performance concrete highway bridge girders. Massachusetts Institute of Technology, 139.

Park, S. Y.Cho, K.Cho, J. R.Kim, S. T. & Kim, B.-S. 2012. Structural performance of prestressed UHPC ribbed deck for cable-stayed bridge. Proceedings of Hipermat

2012, 3rd International Symposium on UHPC and Nanotechnology for High Performance Construction Materials. Kassel, Germany Kassel University Press GmbH, 873-80.

Perry, V. & Seibert, P. 2012. Field cast UHPC connections for precast bridge elements and systems. Proceedings of Hipermat 2012, 3rd International Symposium on UHPC and Nanotechnology for High Performance Construction Materials. Kassel, Germany. Kassel University Press GmbH, 669-78.

Portland cement association. *Innovative concrete bridge wins quality initiative structure award-* http://www.cement.org/exec2/05-04-09.htm [Online]. [Accessed 28-12-2012].

QAGOMA. 2010. *Martin Boyce-Installation of 'We are shipwrecked & landlocked' 2008–10-* http://www.flickr.com/photos/queenslandartgallery/5215698413/in/set-72157625396634508 [Online]. [Accessed 08-09-2012].

Qixian, L. & Bungey, J. H. 1996. Using compression wave ultrasonic transducers to measure the velocity of surface waves and hence determine dynamic modulus of elasticity for concrete. Construction and Building Materials, 10**,** 237-42.

Rangan, B. V. 1998. High-performance high-strength concrete: Design recommendations. Concrete international, 20**,** 63-68.

Rebentrost, M. & Wight, G. 2008a. Behaviour and resistance of ultra high performance concrete to blast effect. Proceeding of the Second International Symposium on Ultra High Performance Concrete. Kassel, Germany. Kassel University Press GmbH, 735-42.

Rebentrost, M. & Wight, G. 2008b. Experience and applications of ultra-high performance concrete in Asia. Proceedings of the Second International Symposium on Ultra High Performance Concrete. Kassel, Germany. Kassel University Press GmbH, 19-30.

Reineck, K. & Greiner, S. 2004. Tests on ultra-high performance fibre reinforced concrete designing hot-water tanks and UHPFRC-shells. 361-74.

Richard, P. & Cheyrezy, M. 1995. Composition of reactive powder concretes. Cement and Concrete Research, 25**,** 1501-11.

Richard, P. & Cheyrezy, M. H. 1994. Reactive powder concretes with high ductility and 200 - 800 Mpa compressive strength. American Concrete Institute, 144**,** 507-18.

RILEM TC 162-TDF 2002. Test and design methods for steel fibre reinforced concrete: Bending test. Materials and Structures, 35**,** 579-82.

Rossi, P. 1997. High performance multimodal fiber reinforced cement composites (HPMFRCC): The LCPC experience. ACI Materials Journal, 94**,** 478-83.

Rossi, P. 2000. Ultra-high performance fibre reinforced concretes (UHPFRC): an overview. In Proceeding Fifth RILEM Symposium on Fibre-Reinforced Concretes (FRC) - BEFIB' 2000. 87-100.

Rossi, P. 2005. Development of new cement composite materials for construction. Proceedings of the Institution of Mechanical Engineers, Part L: Journal of Materials Design and Applications, 219**,** 67-74.

Roux, N.Andrade, C. & Sanjuan, M. 1996. Experimental study of durability of reactive powder concretes. Journal of Materials in Civil Engineering, 8**,** 1-6.

Roy, D. M.Gouda, G. R. & Bobrowsky, A. 1972. Very high strength cement pastes prepared by hot pressing and other high pressure techniques. Cement and Concrete Research, 2**,** 349-66.

Şahin, Y. & Köksal, F. 2011. The influences of matrix and steel fibre tensile strengths on the fracture energy of high-strength concrete. Construction and Building Materials, 25**,** 1801-06.

Said, I. 1996. Mechanical properties of high-performance concrete. ACI Materials Journal, 93**,** 416-26.

Saito, M. 1983. Direct tensile fatigue of concrete by the use of friction grips. ACI Journal Proceedings. ACI, 431-38.

Samaris 2005. Report D22, full scale application of UHPFRC for the rehabilitation of bridges – from the lab to the field. European project 5th FWP/SAMARIS, 77.

Schachinger, I.Hilbig, H. & Stengel, T. 2008. Effect of curing temperature at an early age on the long-term strength development of UHPC. Proceedings of the International Symposium on Ultra High Performance Concrete. Kassel, Germany. Kassel University Press GmbH, 205-12.

Schachinger, I.Schubert, J. & Mazanec, O. 2004. Effect of mixing and placement methods on fresh and hardened ultra high performance concrete (UHPC). Proceedings of the International Symposium on Ultra High Performance Concrete. Kassel, Germany. Kassel University Press GmbH, 575-86.

Schmidt, C. & Schmidt, M. 2012. "Whitetopping" of asphalt and concrete pavements with thin layers of ultra-high-performance concrete - construction and economic efficiency. Proceedings of Hipermat 2012, 3rd International Symposium on UHPC and Nanotechnology for High Performance Construction Materials. Kassel, Germany. Kassel University Press GmbH, 921-27.

Schmidt, M. 2012. Sustainable building with ultra-high-performance concrete (UHPC)– coordinated research program in Germany. Proceedings of Hipermat 2012, 3rd International Symposium on UHPC and Nanotechnology for High Performance Construction Materials. Kassel, Germany. Kassel University Press GmbH, 17-24.

Schmidt, M. & Fehling, E. 2002. Ultra-high-performance concrete: Research, development and application in Europe. 32.

Schmidt, M.Fehling, E.Teichmann, T.Bunje, K. & Bornemann, R. 2003. Ultra-high performance concrete: Perspective for the precast concrete industry. Concrete Precasting Plant and Technology, 69**,** 16-29.

Schnellenbach-Held. M & Prager. M 2012. Numerical study on the shear behavior of micro-reinforced UHPC beams. Proceedings of Hipermat 2012, 3rd International Symposium on UHPC and Nanotechnology for High Performance

Construction Materials. Kassel, Germany. Kassel University Press GmbH, 469-76.

Semioli, W. J. 2001. The new concrete technology. Concrete international, 23**,** 75-79.

Shaaban, A. & Gesund, H. 1993. Splitting tensile strength of steel fiber reinforced concrete cylinders consolidated by rodding or vibrating. ACI Materials Journal, 90**,** 366-69.

Shaaban, A. M. & Gesund, H. 1994. Punching shear strength of steel fiber reinforced concrete flat plates. ACI Structural Journal 406-14.

Shah, A. A. & Ribakov, Y. 2011. Recent trends in steel fibered high-strength concrete. Materials & Design, 32**,** 4122-51.

Simeonov, P. & Ahmad, S. 1995. Effect of transition zone on the elastic behavior of cement-based composites. Cement and Concrete Research, 25**,** 165-76.

Smallsmalls. 2007. *Toll gate* - *http://www.flickr.com/photos/smallsmalls/2908944533/in/datetaken/* [Online]. [Accessed 01-09-2012].

Song, P. S. & Hwang, S. 2004. Mechanical properties of high-strength steel fiber-reinforced concrete. Construction and Building Materials, 18**,** 669-73.

Spasojević, A. 2008. Structural implications of ultra-high performance fibre-reinforced concrete in bridge design. PhD, École Polytechnique Federale De Lausanne**,** 285.

Spasojevic, A.Redaelli, D. & Muttoni, A. 2009. Thin UHPFRC slabs without conventional reinforcement as light-weight structural elements. Fib Symposium London. London**,** 1-8.

Stengel, T. & Schießl, P. 2008. Sustainable construction with UHPC–from life cycle inventory data collection to environmental impact assessment. Proceeding of the Second International Symposium on Ultra High Performance Concrete. Kassel, Germany. Kassel University Press GmbH, 461-68.

Sun, E. Q. 2006. Shear locking and hourglassing in msc nastran, abaqus, and ansys. Msc software users meeting. 1-9.

Swamy, N. & Rigby, G. 1971. Dynamic properties of hardened paste, mortar and concrete. Materials and Structures, 4**,** 13-40.

Tan, K. H. & Paramasivam, P. 1994. Punching shear strength of steel fiber reinforced concrete slabs. Journal of Materials in Civil Engineering, 6**,** 240-53.

Theodorakopoulos, D. & Swamy, N. 1993. Contribution of steel fibers to the strength characteristics of lightweight concrete slab-column connections failing in punching shear. ACI Structural Journal, 90**,** 342-55.

Thibaux, T. 2008. Strengthening of Huisne bridge using ultra-high-performance fibre-reinforced concrete. International fib symposium. Amsterdam, Holland. Taylor & Francis Ltd, 331-34.

Tue, N.Schneider, H.Simsch, G. & Schmidt, D. 2004. Bearing capacity of stub columns made of NSC, HSC and UHPC confined by a steel tube. Proceedings of the International Symposium on Ultra High Performance Concrete. Kassel, Germany. Kassel University Press GmbH, 339-50.

U.S. Geological Survey. 1989. *Loma Prieta, California Earthquake: http://gallery.usgs.gov/sets/1989_Loma_Prieta,_California_Earthquake/list/_/5* [Online]. [Accessed 24-12-2012].

Ulm, F. & Acker, P. 2008. Nanoengineering UHPC materials and structures. Proceeding of the Second International Symposium on Ultra High Performance Concrete. Kassel, Germany. Kassel University Press GmbH, 3-9.

Vergoossen, R. 2008. Tailor made bridge design with ultra-high-performance concretes. Tailor Made Concrete Structures. London**,** 1067-68.

Vicenzino, E.PERRY, V. H.CHOW, T. S.CULHAM, G. & ZAKARIASEN, D. 2005. First use of UHPFRC in thin precast concrete roof shell for Canadian LRT station. PCI journal, 50**,** 50-67.

Voo, J.Foster, S. J.Gilbert, R. I. & Gowripalan, N. 2001. Design of disturbed regions in reactive powder concrete bridge girders. High Performance Materials in Bridges: Proceedings of the International Conference. Hawaii, USA. ASCE, 117-27.

Voort, T. L. V.Suleiman, M. T. & Sritharan, S. 2008. Design and performance verification of UHPC piles for deep foundations (final report of project entitled use of ultra-high performance concrete in geotechnical and substructure applications). Center for Transportation Research and Education, Iowa State University, 224.

Wang, Y.Li, V. C. & Backer, S. 1990. Experimental determination of tensile behavior of fiber reinforced concrete. ACI Materials Journal, 87**,** 461-68.

Washer, G.Fuchs, P.Graybeal, B. A. & Hartmann, J. L. 2004. Ultrasonic testing of reactive powder concrete. Ultrasonics, Ferroelectrics and Frequency Control, IEEE Transactions on, 51**,** 193-201.

Washer, G.Fuchs, P.Rezai, A. & Ghasemi, H. 2005. Ultrasonic measurement of the elastic properties of ultra-high performance concrete (UHPC). PETER J. SHULL, ANDREW L. GYEKENYESI & AFTAB A. MUFTI, eds. Nondestructive Evaluation and Health Monitoring of Aerospace Materials, Composites, and Civil Infrastructure IV. San Diego, CA, USA. SPIE, 416-22.

Wille, K.Naaman, A.El-Tawil, S. & Parra-Montesinos, G. 2012. Ultra-high performance concrete and fiber reinforced concrete: Achieving strength and ductility without heat curing. Materials and Structures, 45**,** 309-24.

Xiangming, Z.Joel, S.Stuart, W. & Olayinka, O. 2012. Effects of PFA and GGBS on early age engineering properties of portland cement systems. Advanced Concrete Technology, 10**,** 74-85.

Xing, F.Huang, L. D.Cao, Z. L. & Deng, L. P. 2005. Study on preparation technique for low-cost green reactive powder concrete. Key Engineering Materials, 302**,** 405-10.

Yang, S. & Diao, B. 2009. Influence of curing regime on the ductility of ultra-high performance fiber reinforced concrete (UHPFRC). ASCE**,** 2621-27.

Yang, S. L.Millard, S. G.Soutsos, M. N.Barnett, S. J. & Le, T. T. 2009. Influence of aggregate and curing regime on the mechanical properties of ultra-high performance fibre reinforced concrete (UHPFRC). Construction and Building Materials, 23**,** 2291-98.

Yazici, H. 2007. The effect of curing conditions on compressive strength of ultra high strength concrete with high volume mineral admixtures. Building and environment, 42**,** 2083-89.

Yudenfreund, M.Odler, I. & Brunauer, S. 1972. Hardened portland cement pastes of low porosity I. Materials and experimental methods. Cement and Concrete Research, 2**,** 313-30.

Zanni, H.Cheyrezy, M.Maret, V.Philippot, S. & Nieto, P. 1996. Investigation of hydration and pozzolanic reaction in reactive powder concrete (RPC) using ^{29}Si NMR. Cement and Concrete Research, 26**,** 93-100.